Technical Report

TR-14-23

System design and full-scale testing of the Dome Plug for KBS-3V deposition tunnels

Main report

Pär Grahm, Svensk Kärnbränslehantering AB

Richard Malm, Daniel Eriksson, Sweco Energuide AB

December 2015

Svensk Kärnbränslehantering AB
Swedish Nuclear Fuel
and Waste Management Co

Box 250, SE-101 24 Stockholm
Phone +46 8 459 84 00

ISSN 1404-0344
SKB TR-14-23
ID 1373163
December 2015

System design and full-scale testing of the Dome Plug for KBS-3V deposition tunnels

Main report

Pär Grahm, Svensk Kärnbränslehantering AB

Richard Malm, Daniel Eriksson, Sweco Energuide AB

Keywords: Dome plug, Deposition tunnel end plug, Bentonite seal, Backfill transition zone, Filter, Gravel, Concrete dome, B200, KBP1004, DOMPLU.

A pdf version of this document can be downloaded from www.skb.se.

Preface

This report summarizes four years of system design development for the KBS-3V deposition tunnel plugs, carried out in cooperation between SKB and Posiva Oy. The report summarizes the main events of the work in the full-scale test of the Dome plug.

The formal name of the project is “System design of Dome Plug” (KBP1004). Significant resources have been involved in this project. The main project team consisted of the following people:

SKB:	Pär Grahm (Project leader), Patrik Hagman , Karin Nilsson, Anna Blomqvist, Behnaz Aghili, Pär Viberg, Mats Lundquist, Gunnar Ramqvist, Stefan Grandin Svärdh, Mikael Hedin.
Posiva Oy:	Petri Koho (Project partner), Petri Korkeakoski, Sanna Mustonen.
NCC:	Hans Wimelius, Jonas Magnusson, Alexandre Mathern, Lars-Olof Dahlström, Christina Claeson-Jonsson.
Clay Technology:	Lennart Börgesson, Torbjörn Sandén, Mattias Åkesson, Linus Andersson, Viktor Jensen.
KTH:	Richard Malm, Stefan Trillkott, Claes Kullberg.
SWECO:	Richard Malm, Daniel Eriksson.
Palmer Engineering:	Sten Palmer (Technical supervisor).
Vattenfall Teknik:	Tobias Gasch.
Uppländska berg:	Rickard Karlzén.

The project activities have been multifaceted and thus results have been reported in various background reports. In this main report, it is clearly stated in each chapter which background report provides the basis for the summary. However, some activities have not been published as separate reports, therefore the documentation from these activities has been incorporated directly into this main report.

Acknowledgements

The work reported on in this document is the result of a joint project supported by Posiva and SKB. Posiva is acknowledged with much appreciation for their cofinancing, support, contributions and valuable expert comments in scientific details.

The research leading to these results has received funding from the European Union’s European Atomic Energy Community’s (Euratom) Seventh Framework Programme FP7/2007-2013 under grant agreement no 323273, the DOPAS project.

Sammanfattning

Denna rapport sammanfattar fyra års teknikutveckling av pluggsystemet som ska försegla deponeringstunnlarna i Kärnbränsleförvaret. Arbetet har utförts som ett samarbetsprojekt mellan Svensk Kärnbränslehantering AB (SKB) och Posiva Oy, baserat på KBS-3V-förvarets referensdesign för deponering av kärnbränsle. Utvecklingen och verifieringen av pluggsystemet har i detta projekt genomförts med analytiska och numeriska beräkningar, laboratorieexperiment och skalförsök. Den primära aktiviteten i detta projekt har emellertid varit att testa pluggsystemet i fullskala (DOMPLU-experimentet) under realistiska hydrogeologiska förhållanden vid Äspölaboratoriet.

Instrumentering, utvärdering och rapportering av DOMPLU-projektet har ingått som en del av DOPAS-projektet (*Full-Scale Demonstration of Plugs and Seals*). DOPAS är ett EU-projekt som delvis finansieras av *Euratom Seventh Framework Programme* samt av europeiska kärnavfallsorganisationer, i vilket laboratorieförsök, fullskaleförsök och utvärderingar av pluggar för geologiska förvar har genomförts.

Fullskaleförsöket DOMPLU baseras på nuvarande referensdesign för pluggning av deponeringstunnlar. Jämfört mot tidigare fullskaleförsök som SKB har genomfört så representerar DOMPLU en detaljerad iteration av designen snarare än en fundamental förändring. Nuvarande referensutformning och pluggutformning av DOMPLU är snarlik, med undantag för vissa modifikationer som utvecklats i syfte att utvärdera nya material som kan komma att inkluderas i referensutformningen i framtiden.

Ett av de viktigaste resultaten från detta fullskaleförsök var att visa att det gick att bygga pluggsystemet på ett ändamålsenligt sätt. Detta inkluderade verifiering av praktiska aspekter så som logistik och hantering av parallella aktiviteter i tunnelmiljön. Det visades i fullskaleförsöket även att det är möjligt att utforma en oarmerad betongkupol av låg-pH betongreceptet B200 som uppfyller funktionskraven. En avancerad kylprocedur användes framgångsrikt i syfte att reducera inducerade spänningar i betongkupolen under hydratationen och i syfte att skapa en termisk förspänning i betongkupolen efter kontaktinjektering.

Ett annat grundläggande syfte med experimentet var att mäta pluggens vattentätande förmåga genom att utsätta den för ett högt vattentryck. Under försöket så uppstod problem med vattenflykt från experimentet, dels via sprickor i berget och dels läckage via givarkablage. Detta medförde att vattentrycket inte kunde ökas som det var tänkt till 7 MPa (70 bar) utan trycket bibehölls istället vid 4 MPa (40 bar) i åtta månader.

I slutet av september 2014 var det uppmätta läckaget förbi pluggen 0,043 l/min (motsvarande 2,6 liter per timme) vid 4 MPa vattentryck. Läckaget har tydligt minskat efter att det uppstod och kommer troligvis att fortsätta följa denna trend. Resultaten visar att vattentrycket på betongkupolen minskar medan vattentrycket uppströms bentonittätningen är konstant. Denna observation, tillsammans med mätningar av relativ fuktighet och totaltryck visar att bentonittätningen blir mer och mer vattentät. Följaktligen förutses det att läckaget förbi pluggen kommer fortsätta att minska.

Summary

This report summarizes four years of system design development for the deposition tunnel end plugs, carried out in cooperation between Swedish Nuclear Fuel and Waste Management Co (SKB) and Posiva Oy, according to the KBS-3V reference disposal concept. System design development has included verification of the plug system by analytical and numerical calculations, laboratory examinations and scale tests. The main activity though, has been to test a dome plug system in full scale (The DOMPLU experiment) with representative hydrogeological conditions at the Äspö Hard Rock Laboratory (Äspö HRL).

Monitoring, evaluation and technical reporting of DOMPLU have been part of the Full-Scale Demonstration of Plugs and Seals (DOPAS) Project. The DOPAS project is a European Commission (EC) programme of work jointly funded by the Euratom Seventh Framework Programme and European nuclear waste management organizations, in which full-scale experiments, laboratory tests and performance assessments studies of plugs and seals for geological repositories are being carried out.

The current SKB reference design and DOMPLU design are broadly similar, with the exception of a few modifications intended to test the performance of new materials planned to be introduced in the future as part of SKB's revised reference design for a deposition tunnel plug. DOMPLU therefore represents a more detailed iteration of the basic design rather than a fundamental change to the earlier plug experiments undertaken by SKB.

One of the main outcomes from the full-scale test is demonstrating that it is feasible to build the dome plug system. This included verification of practical aspects such as logistics and arranging of parallel activities. It was also shown that it is possible to use an unreinforced concrete dome plug consisting of low-pH concrete mix B200 that satisfy the design requirements. An advanced cooling scheme was successfully used to reduce the induced stresses in the concrete dome during hydration and to cause a thermal pre-stress after contact grouting.

Another crucial purpose of the experiment was to measure the water sealing function of the plug by subjecting it to a high water pressure. During the trial there were issues related to water escape, partly through a fracture in the rock and partly via sensor cabling. This resulted in an operational limit for the water pressure at 4 MPa (40 bar), although the original plan was to pressurize the plug to 7 MPa (70 bar). The pressure on the concrete dome was maintained at 4 MPa for eight months.

By the end of September 2014 the measured leakage past the plug was 0.043 l/min (corresponding to 2.6 litres per hour) when the hydraulic head across the plug was 4 MPa. The measured leakage rate has clearly been decreasing with time and may continue to follow this trend. The results show that the water pressure on the concrete dome is decreasing while the water pressure upstream of the bentonite seal is constant. This observation, together with measurements of relative humidity and total pressure, shows that the bentonite seal is becoming more and more watertight. Subsequently, the leakage past the plug is expected to continue decreasing.

Contents

1 Introduction

This report summarizes four years of system design development for the deposition tunnel end plugs for the KBS-3V reference disposal concept (see Section 1.1.1), carried out in cooperation between SKB and Posiva Oy. The system design development has included verification of the plug design by analytical and numerical calculations, laboratory experiments and scale tests. The main activity though, has been to test a plug system at full scale (The DOMPLU test) under realistic hydro-geological conditions at the Äspö Hard Rock Laboratory (Äspö HRL).

Monitoring, evaluation and technical reporting of DOMPLU has been part of the The Full-Scale Demonstration of Plugs and Seals (DOPAS) Project. The DOPAS project is an European Commission (EC) programme of work jointly funded by the Euratom Seventh Framework Programme and European nuclear waste management organizations, in which full-scale experiments, laboratory tests and performance assessments studies of plugs and seals for geological repositories are being carried out.

In this Chapter, the background to the conceptual design of the reference KBS-3V deposition tunnel end plug is described. This includes a description of the main safety functions of deposition tunnel plugs and how these are met by the conceptual design on a component-by-component basis. This is followed by a review of design basis development and the objectives for the DOMPLU test. Finally, the purpose of this report is explained which basically is to summarize all activities that have been carried out within the plug system design development including an evaluation of the full-scale test DOMPLU.

1.1 Background

The KBS-3V method is proposed by SKB for the disposal of spent fuel packaged in copper canisters with cast iron inserts in a crystalline host rock. The long-term safety principles are based on isolation and containment of radioactive waste through the choice of a stable geological environment at depth and the use of a multi-barrier system consisting of engineered barriers (canister, buffer, backfill, and closure) and the host rock. The canisters are emplaced in vertical holes, containing pre-compacted blocks of bentonite buffer, below horizontal deposition tunnels. The deposition tunnels are backfilled with bentonite blocks and pellets, and closed with a deposition tunnel plug, see Figure 1-1.

In the KBS-3 method, high reliance is placed on physical containment of the radionuclides by the canister whereas the key function of the buffer and the deposition tunnel backfill is to protect the canister. The principal role of the deposition tunnel plug is to confine the backfill in place during ongoing repository operations in other areas; this is achieved through use of a strong, dome-shaped concrete plug. The repository main tunnel system and caverns in the central area will be open during the expected operation of about 100 years. As the function of deposition tunnel plugs is related to operational activities, the designed service life of this structure is 100 years.

After all canisters have been emplaced and deposition tunnels backfilled and plugged, the rest of the repository will be backfilled and sealed from the underground level to the surface.

Owing to the potential for water flow to erode the bentonite buffer in the deposition holes, the water flux across the plug must be low. The initial requirement on water tightness is achieved by contact grouting of the concrete dome which is completed approximately 100 days subsequent to casting. The plug design includes a filter that drains water past the structure in order to delay the pressurisation of the plug until the concrete has cured and developed sufficient strength. To assure that low hydraulic conductivity is provided for the full service life of 100 years, a watertight seal composed of swelling bentonite is also used in the reference design. The timescale for saturation and swelling of the bentonite seal depends on the rate of groundwater flow. After the bentonite seal has saturated, the leakage requirement on the concrete dome is redundant and the main purpose of the concrete dome is to act as support and carry the loads of the water and swelling pressure from the deposition tunnel.

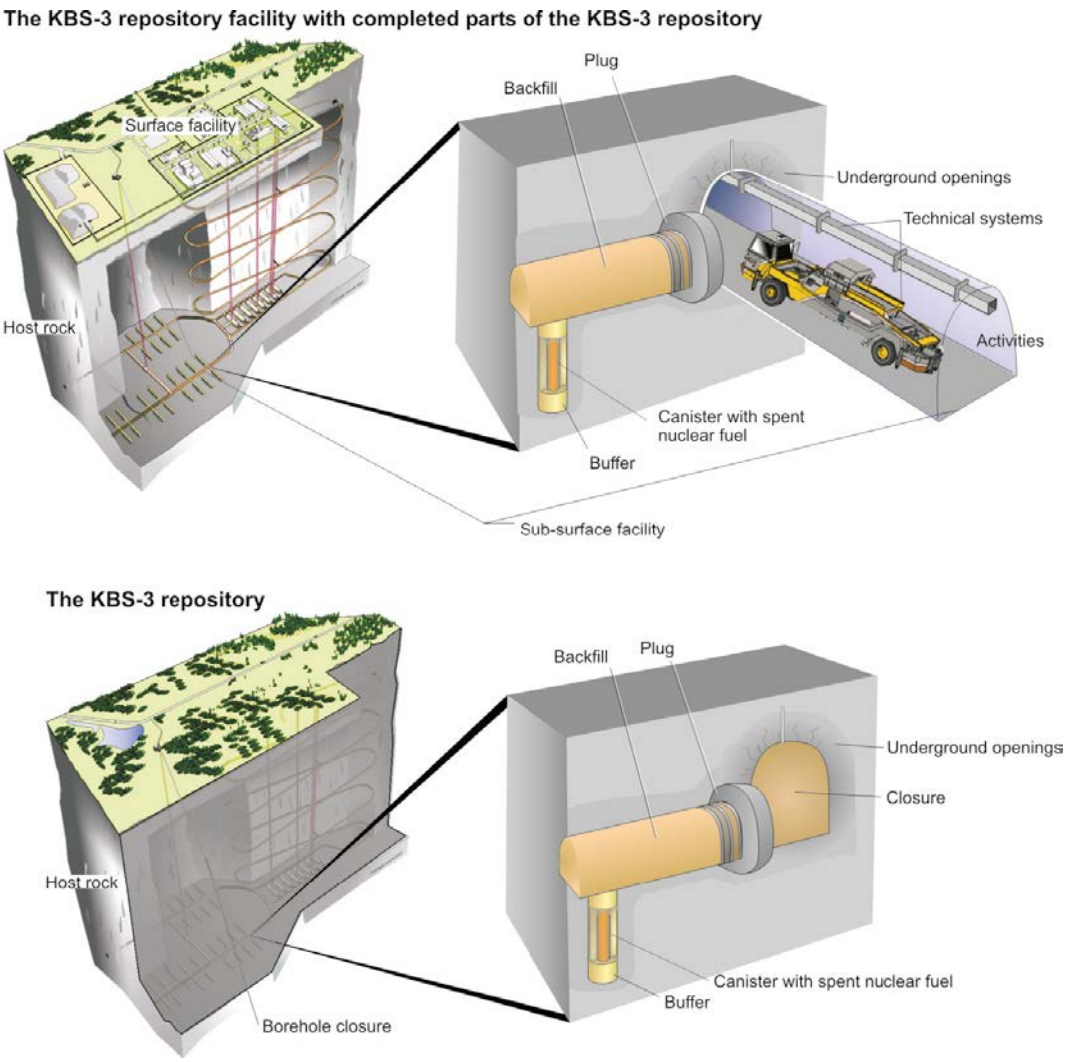

Figure 1-1. *The KBS-3 repository facility and the KBS-3 repository. The KBS-3 repository is constructed within the KBS-3 repository facility. (SKB 2010a.)*

Moreover, the method needed in order to provide a low hydraulic conductivity across the deposition tunnel plug largely depends on the specific rock conditions at the plug location. The function of the bentonite seal is supportive to accommodate a range of rock conditions.

In Sweden, a site has been selected at Forsmark for final disposal of spent nuclear fuel from the Swedish nuclear power plants. The spent fuel repository will be located approximately 470 m below the ground surface in crystalline rock. A license application for disposal of spent fuel, based on the KBS-3V method, was submitted in March 2011.

1.1.1 Development of the design basis for deposition tunnel plugs

The design basis for deposition tunnel plugs has been under development for many decades, driven by the learning gained from more detailed knowledge on the repository site conditions and from full-scale experiments and laboratory tests in Sweden and elsewhere. These experiments have been undertaken in collaboration with Posiva and have also contributed into the development of the reference deposition tunnel plug in the Posiva disposal concept.

The need for a plug at the entrance to a deposition tunnel was recognized at an early stage of the Swedish programme as a means of maintaining the backfill in place and having a compartment which has a higher water head than the open galleries in the repository. Different designs have been tested in previous full-scale experiments, including:

- The Stripa mine tunnel plugging experiment in the 1980s.
- The Äspö HRL Backfill and Plug Test in the 1990s.
- The Äspö HRL Prototype Repository in the 2000s.

A first test of a simple design of a concrete plug was tested in the Stripa mine in Sweden as part of the Tunnel Plugging Experiment in the 1980s. An O-ring of bentonite was introduced into the design after this experiment, and was tested in the Backfill and Plug Test at the Äspö HRL in the late 1990s and early 2000s. The O-ring did not perform as intended, as leakage of water was found to be quite high. Subsequent to these experiments, the Prototype Repository, incorporating two identical plugs, was built at the Äspö HRL, beginning in 2001. Unlike previous experiments, both concrete plugs were cast with self-compacting concrete (SCC).

As part of the ESDRED project, a low-pH shotcrete plug was tested for KBS-3H horizontal emplacement of disposal containers. Significant water leakage was observed at the bottom of the plug and thus the concept was changed to use welded steel plugs and relying on effective contact grouting. Two steel plugs for KBS-3H have thereafter been built at Äspö HRL. These tests have had good results with low rates of leakage across the plugs.

Another experiment from which valuable experience has been utilized in the design of the KBS-3V deposition tunnel plug is the Canadian Tunnel Seal Experiment (TSX). The TSX include a concrete bulkhead made of unreinforced low-heat high-performance concrete (LHHPC) and a bulkhead composed of highly compacted sand-bentonite blocks. According to Martino et al. (2006) the TSX showed it is possible to construct functional clay and concrete bulkheads that will limit axial water flow. The average measured flow at 4 MPa hydraulic pressure in the tunnel was 1ml/min for the clay bulkhead and 10 ml/min for the concrete bulkhead. The clay bulkhead provided an effective barrier to water transport and demonstrated the ability to close off existing flow paths and to self-seal. The TSX also highlighted the importance of keeping joints and interfaces to a minimum and the effectiveness of contact grouting to reduce seepage between the concrete bulkhead and rock.

A further full-scale sealing trial that involved SKB, Posiva and other international partners that provides useful information on plugging is ongoing in Canada (Enhanced Sealing Project). The ESP involved installation of a full-scale seal constructed using concrete and bentonite components in a shaft excavated in granitic rock (REF) and although the details of the geometry differ from that of a tunnel plug, it has further demonstrated the effectiveness of a composite design approach. The ESP consists of an instrumented, full-scale shaft seal, designed to permanently seal the access shaft to Atomic Energy of Canada Limited's (AECL's) URL. The seal consists of two concrete segments that sandwich a bentonite-clay-based unit limiting the mixing of deeper saline groundwater with shallower less-saline groundwater on a hydraulically active fracture zone. The monitoring results are indicative of a system where the clay is effectively isolating the regions above and below the fracture feature. (Dixon et al. 2012).

Following on from the previous full-scale tests and design development projects, a reference conceptual design of the deposition tunnel plug was compiled (SKB 2010b), see Section 1.1.2. Since then an additional iteration of the deposition tunnel plug has been undertaken. In the main report from this phase of work (Malm 2012), the conceptual design was further defined and included design of the unreinforced low-pH concrete dome plug with respect to loads acting on the concrete dome from a swelling bentonite seal.

Based on the fact that the plug design developed and reported on by Malm (2012), deviates from previously tested plugs, it is needed to be tested in order to verify that it works under expected field conditions. In the process to develop the design of the plug, numerical and analytical calculations have been important tools to support the design development for all components in the plug design. Another important part of the verification process is that material tests have to be performed to determine the behaviour of each of the different components and regions of the plug system. These laboratory tests are designed to either test different functions of the plug system or performed to obtain material properties that is needed in the numerical analyses. Moreover, it was conceived that a full-scale test will give valuable input on evaluating the water-tightness of the plug and will support the development of construction procedures for application during implementation. Prior to performing the full-scale test, updated numerical analyses are performed to make predictions of expected behaviour of the full-scale test.

1.1.2 Reference design of the Deposition tunnel plug

Deposition tunnel plugs in the Swedish repository have only a short-term functional requirement. Their purpose is to support the performance of long-term safety barriers in the operational/pre-closure phase. The functions of deposition tunnel plugs during the operational period of the repository (up to 100 years) are to:

- Confine the backfill in the deposition tunnel.
- Support saturation of the backfill.
- Provide a barrier against water flow that may cause harmful erosion of the bentonite in buffer and backfill.

During the course of the project another safety function of the plug, gas tightness, was also identified:

- Provide a barrier against air and vapour transports, to and from the deposition tunnel.

The current SKB reference conceptual design for a deposition tunnel plug is described in SKB's *Design, production and initial state of the backfill and plug in deposition tunnels* report (SKB 2010b), and includes the following components, see Figure 1-2:

- Concrete Plug: The concrete plug is a dome-shaped structure made of low-pH reinforced concrete. It contains pipes for auxiliary equipment such as air ventilation pipes, cooling pipes, and grouting tubes. The cooling pipes are used to avoid internal cracking due to cement hydration and to pre-stress the concrete dome before contact grouting. The function of the concrete plug is to resist deformation and to keep the watertight seal, filter and backfill in place.
- Bentonite seal: The seal is made of bentonite blocks and pellets in a similar configuration to the backfill. It is 710 mm thick. The functions of the seal are:
  - To seal water leakage paths through small cracks in the concrete plug or between the concrete and the rock surface.
  - To reduce the water pressure acting on the concrete dome so that no unfavourable water pressure is applied in the interface between the rock and the concrete, and so that the water pressure within the backfilled deposition tunnel is equalized.
  - To prevent air and vapour transports across the plug.

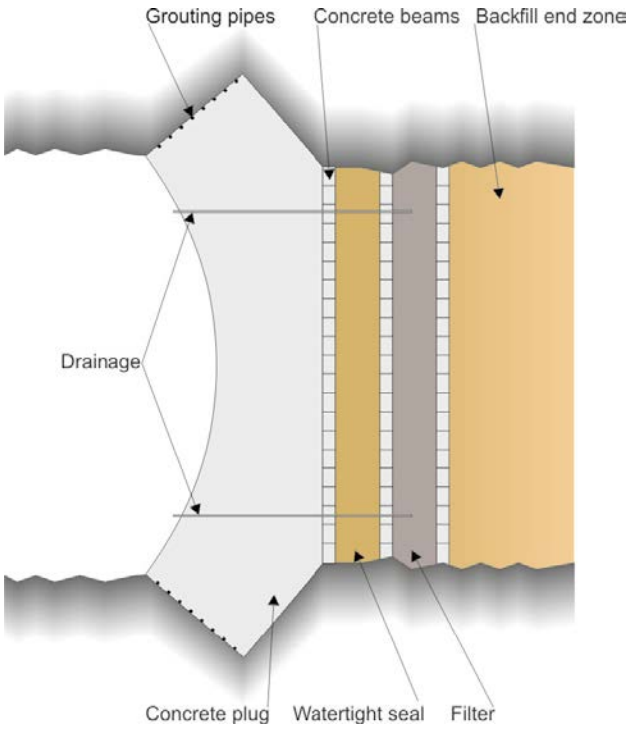

Figure 1-2. *Schematic section of the reference design of the plug (SKB 2010b).*

- Filter: The filter is made of sand or gravel. Its function is to collect groundwater leaking from the backfilled deposition tunnel and, if required, drain it via the drainage pipes, so that no water pressure is applied on the concrete plug before it has cured and gained full strength. The filter will also facilitate saturation of the bentonite seal.
- Backfill Transition Zone (TZ): The part of the backfill closest to the plug in which the density is reduced to lower the swelling pressure loads on the plug. The design of backfill TZ has been further elaborated by Börgesson et al. (2015a, e.g. Chapter 1, Figure 1-1).
- Concrete beams (Delimiters): The beams are made of pre-manufactured, low-pH reinforced concrete. Their function is to facilitate the construction works. The beams in the outer delimiter (towards the concrete plug) are covered with a thin layer of shotcrete to prevent the concrete slurry from mixing with the bentonite during casting of the concrete plug. The function of the outer delimiter is to keep the watertight seal in place during installation, also acting as an inner formwork for the concrete dome. The inner delimiter (towards the deposition tunnel) shall keep the backfill in place during installation. The middle delimiter shall keep the filter in place during installation.
- Drainage pipes: The drainage pipes are made of steel or titanium and are required during plug construction to drain the water collected in the filter and transport it out of the deposition tunnel. This will limit water pressure on the concrete dome until it has cured and gained full strength. In dry tunnel conditions, the drainage pipes can be used for water injection into the filter for an artificial wetting of the bentonite seal. This contributes to achieving the requirements on gas- and water tightness. During the operational phase, pressure in the plug system can be controlled by the aid of valves.
- Grouting pipes: The grouting pipes are made of steel and may be isolated by geotextile to prevent blocking during pouring. They shall be grouted when the concrete has reached a certain level of strength and shrinkage. The grout shall seal the contact area between the concrete plug and rock, thereby reducing the potential for water leakage in this part of the plug. The grout also contributes to keeping the concrete dome under compression.

1.1.3 Terminology

Different terms are present in various reports when describing tunnel plugging and sealing concepts and designs. For the sake of clarity, a short list of the terms or abbreviated text used in this report is presented in Table 1-1.

Table 1-1. Terminology used in this report.

Structural component full name:	or in abbreviated form
Plug System – *or* Plug Structure.	Plug
Spherical Concrete Dome Structure.	Concrete Dome – *or* dome
Slot excavation.	Slot
Material Zone Delimiter.	Delimiter
Bentonite Seal.	Seal
Filter Zone.	Filter – *or* gravel filter
Backfill Transition Zone – *or* Backfill end zone.	Transition zone – *or* Backfill TZ

Position of each structural plug component is provided by Figure 1-3.

The tunnel inclination is 1 % and thus the terminology “upstream” and “downstream” is used in this report. The upstream side of the plug system is towards the backfill, i.e. in direction towards the tunnel face of the deposition tunnel (left side in Figure 1-3). Consequently, the downstream side is the direction towards the leakage measurement weir and main tunnel (right side in Figure 1-3).

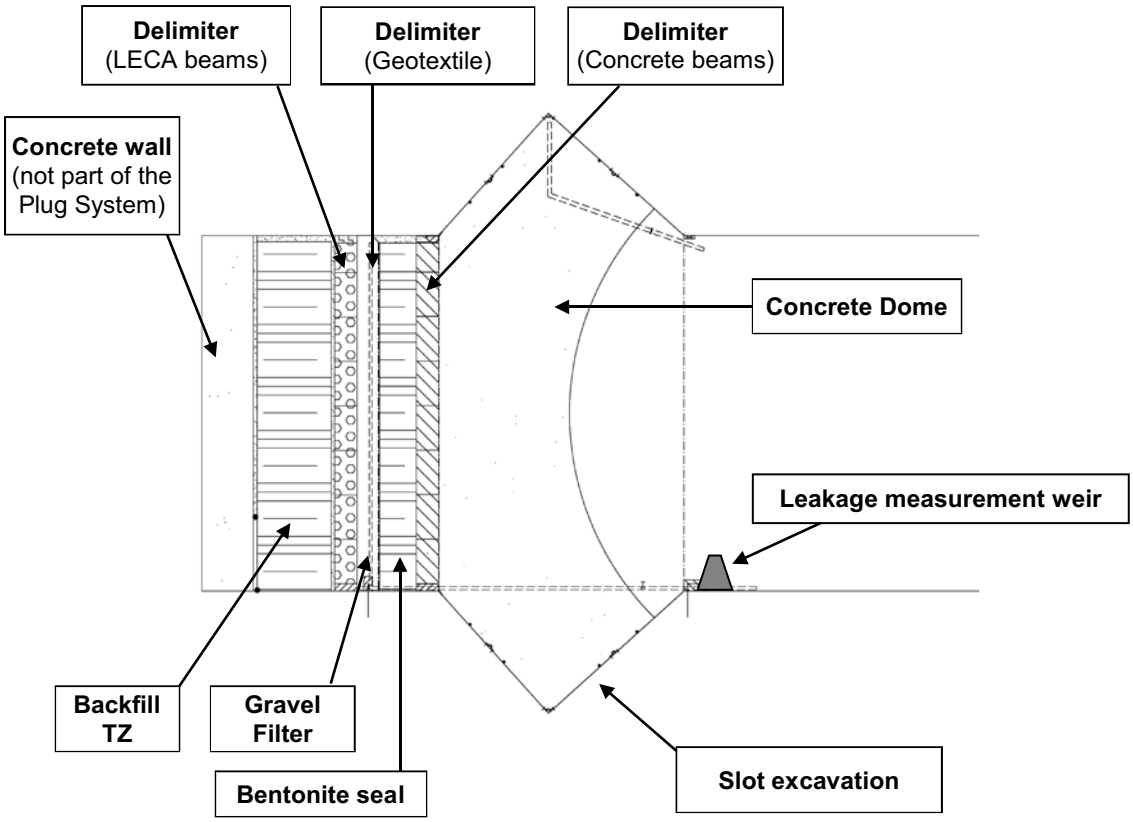

Figure 1-3. *Illustration of the structural components that make up the Plug System. Note that the concrete wall is not a plug system component but a structural part of the DOMPLU experiment.*

1.2 Objectives of the system design

The objective of system design development (i.e. this project) is to ensure, so far as is possible at the design stage, that the modified reference configuration for the dome plug provides a structure that works as intended. By testing the design through a full-scale demonstration, it is intended that the method is shown to be feasible and performance is predictable.

The result of the project will facilitate an updating of the production report for backfill and plugs in deposition tunnels, to be included in the PSAR for the Swedish Spent Fuel Repository.

To meet the overall objectives on the system design, the project was organized in the following five sub-projects, see Figure 1-4.

Project administrative work and technical reporting as well as operations, monitoring and evaluation of DOMPLU were part of the EC FP7 DOPAS project. All other activities associated with the plug test were outside of DOPAS and were part of SKB's project "System design of dome plug for deposition tunnels" (Project No. KBP1004).

The system design development, installation and monitoring activities of the full-scale test are summarised in the present report. Several background reports have also been produced by the project. These are used as references to this report, see Table 1-2.

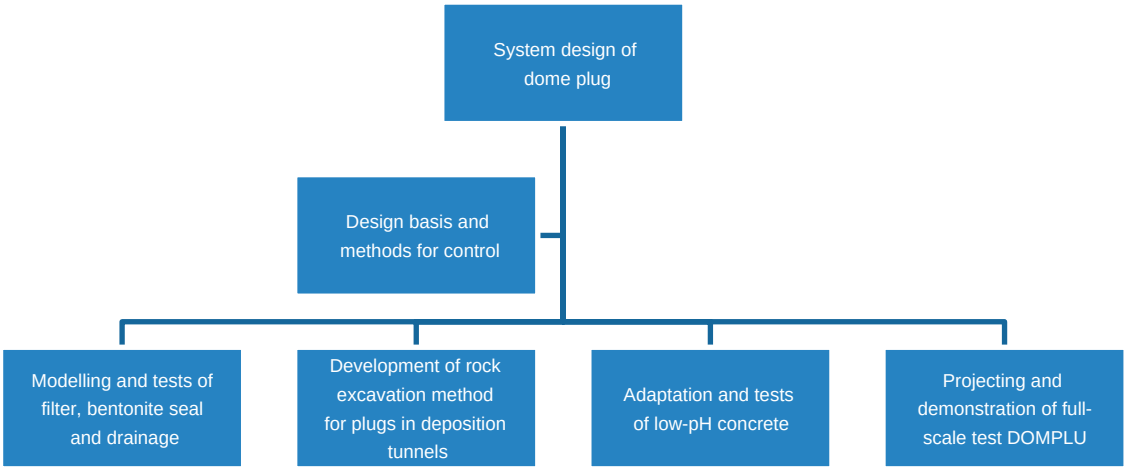

Figure 1-4. *Organizational chart of the project System design of dome plug (Project no. KBP1004).*

Table 1-2. Public reports produced by the project "System design of dome plug".

Full title	Report no.	Reference
End plug for deposition tunnels – Preparatory modelling and tests of the sealing and draining components.	SKB R-14-25	Börgesson et al. (2015a)
System design of Dome Plug. Experiences from full-scale wire sawing of a slot abutment for the KBS-3V deposition tunnel plug.	SKB R-14-24	Grahm and Karlzén (2015)
System design of Dome plug. Experience of low-pH concrete mix B200. Material properties from laboratory tests and full-scale castings.	SKB P-14-26	Magnusson and Mathern (2015)
Creep properties at high stress levels of concrete for deposition tunnel plugs.	SKB P-13-37	Flansbjer and Magnusson (2014a)
Mechanical properties of rock-concrete interface at the concrete plug.	SKB P-13-38	Flansbjer and Magnusson (2014b)
Instrumentation and Evaluation of the Concrete Dome Plug DOMPLU.	KTH TRITA-BKN Report 147	Malm (2014)

1.3 Purpose and objectives of the full-scale test

In addition to enhancement of the design basis for the deposition tunnel plug, there were specific goals associated with the DOMPLU experiment:

- To finalize the details of the reference design.
- To demonstrate the feasibility of plug installation.
- To validate requirements on construction methods.
- To demonstrate that the plug works as intended under realistic conditions, up to the reference design total pressure of 7 MPa.
- Develop a method for leakage measurement and use it to determine a leakage rate across the deposition tunnel plug. Evaluate whether a low enough hydraulic conductivity can be achieved (< 0.1 l/min as discussed in Section 2.1).
- To improve testing and quality control during repository construction.

1.4 Purpose and content of the report

The objectives of this report are to:

- Summarize results from the dome plug system design development project undertaken by SKB and Posiva from 2011 to 2014, and
- present results and an evaluation of the full-scale test DOMPLU.

1.4.1 Limitations

With regard to the second objective of the report, DOMPLU results are summarized for the time period 2013-03-13 (the casting day of the concrete dome) until 2014-09-30, which is the date used for data freeze of the technical reporting. However, the experiment will continue to operate for at least two more years because of the long times required for bentonite saturation and concrete creep and shrinkage. This further evolution will be evaluated separately and reported before the experiment is ended.

Investigations concerning requirements related to leakage and erosion of buffer are not included in the plug system development project but the DOMPLU test will contribute in developing specifications for control of water flow around a plug structure.

Since gas tightness was identified as an additional requirement during the course of the project this has not been specifically evaluated.

Development work and experiences associated with rock excavation, modelling and laboratory examinations of bentonite seal and filter components, low-pH concrete tests and installation of monitoring system are reported elsewhere. Consequently, this report provides the main conclusions in these areas and references to supporting reports (Table 1-2) are provided where relevant.

There were several practical considerations that resulted in DOMPLU differing in minor aspects from what would potentially be required in a repository. The main deviations were:

- A requirement was not set for using low-pH concrete for support plinths, measuring weir and injection grout. Therefore verification of pH of leakage water is not covered by the project. In addition, development of low-pH injection grout for contact grouting of the concrete dome was not part of this project.
- Undertaking getting component materials approved for use in a final repository has not been a part of the project.
- The crystalline rock in the Äspö HRL is more fractured, and as a consequence has a higher hydraulic conductivity, than the rock in the planned repository at Forsmark. In general the rock quality at the Forsmark site is considered to be superior, which may affect tunnel plug performance. Differences in properties between these two sites have been described in Malm (2012).

1.4.2 Contents of the report

The outline of this report is as follows.

In Chapter 1, *Introduction*, a description of the background to the report, the SKB reference design and the objectives of this project and this report are provided.

Chapter 2, *The full-scale test DOMPLU*, presents the design of the DOMPLU plug and the differences between the plug tested in the full-scale test and the reference design plug.

In Chapter 3, *Geology and rock excavation*, the excavation method developed to excavate the horseshoe shaped experiment tunnel and also the method to excavate the slot that constitute the abutment for the concrete dome are presented.

Chapter 4, *Development of bentonite seal and filter*, presents the design of the filter and bentonite seal section including the material tests that have been performed In this chapter, a 1:20 scale model test of the DOMPLU test is also presented.

Chapter 5, *Testing of the concrete B200 mix*, presents all additional tests and their results that have been performed within this project on the concrete mix. These tests include shrinkage, creep, strength development and bond strength.

Chapter 6, *Civil works – installation of the plug*, summarizes the installation of the whole plug system and presents the activities undertaken during the installation of each component.

In Chapter 7, *Monitoring of the full-scale test*, presents the instrumentation used to monitor backfill, bentonite seal and concrete dome in the full-scale test. In addition, the pressurization system is presented together with the cable lead-through installations and the system for monitoring the leakage.

Chapter 8, *Numerical analyses*, presents the hydro-mechanical analyses performed to evaluate the filter and bentonite seal. In addition, the thermal and structural analyses performed to evaluate the behaviour of the concrete dome are also presented.

In Chapter 9, *Results from the full-scale test*, the results of the full-scale test obtained from field measurements and numerical analyses are presented.

Chapter 10, *Conclusions and experiences*, summarizes the experiences, findings and conclusions from this project and the full-scale test in particular. In this chapter, recommendations for further work are also presented.

As mentioned in the preface, for each chapter a reference is given to which background report provides the basis for the summary. In Table 1-3, a dedication is given to co-authors responsible for a specific section of this report.

Table 1-3. Acknowledgement to co-authors of specific sections in this report.

Chapter	Description
5.3	The section regarding on site concrete testing has been written by Carsten Vogt at Projektengagemang.
7.1	The section regarding sensors installed in the backfill and the bentonite seal has been written by Torbjörn Sandén and Reza Goudarzi at Clay Technology.
8.1	The section regarding hydro-mechanical modelling of the backfill, filter and bentonite seal has been written by Mattias Åkesson at Clay Technology AB.
8.2	The section regarding the thermal and structural models for the concrete dome has been written by Tobias Gasch at Vattenfall Teknik.
9.1	The section regarding results from the backfill and bentonite seal measurements is partly written by Sandén, Goudarzi and Åkesson at Clay Technology AB.

2 The full-scale test DOMPLU

In the previous chapter, the reference conceptual design of the deposition tunnel plug has been described. In this chapter, the principles of a developed design basis for the full-scale test DOMPLU are described together with proposed modifications to the reference design. This is followed by a discussion of the DOMPLU design and the principles of a quality assurance program for plugs.

2.1 Development of the design basis for DOMPLU

The DOMPLU experiment is based closely on the reference conceptual design of the SKB deposition tunnel plug, as described by SKB (2010b) in the licence application for the KBS-3V repository. Accordingly, DOMPLU represents a full-scale test of the deposition tunnel plug that is currently expected to be used in the Spent Fuel Repository. The reference design and its requirements have been further elaborated by Malm (2012) and these fundamentals were used as the principal basis for DOMPLU. A few further modifications were introduced during the system design phase, intended to test the performance of new materials planned to be introduced as part of a slightly revised reference design. A further description of the revisions is provided in Section 2.2.

There are two driving forces for the demonstration of plugging and sealing technology in SKB's programme; firstly to decrease uncertainties in the description of the initial state of the deposition tunnel plugs, and also to decrease uncertainties in the performance of deposition tunnel plugs over their 100 years functional life. The reference design of the SKB plug will be updated and modified based on DOMPLU outcomes, and a new design basis will be published for inclusion in the Preliminary Safety Analysis Report (PSAR) which is fundamental for the construction licence of the facility. The update on the new design basis is required in order to capture any learning from the DOMPLU experiment and quantify any uncertain requirements (e.g. specific flow rates through the concrete plug).

Development of the DOMPLU experimental objectives has been driven by the need of defining water flux and plug production requirements on the reference design of the deposition tunnel plug. In addition to this, material specifications have been modified with respect to long-term safety driven requirements, e.g. the change from conventional concrete to low-pH concrete and exclusion of steel reinforcement. None of the previous full-scale concrete plugs have been subjected to the expected hydraulic and swelling pressure of bentonite conditions expected in a repository. The requirements of the plug system have also changed over time as knowledge has increased and this has meant that materials currently envisaged in the DOMPLU design are not the same as were used in earlier studies.

The design basis for the deposition tunnel plug provided by SKB (2010b) was thus further developed for DOMPLU by the project team. Potentially modified requirements on certain areas are discussed throughout the report as part of the system design. A summary (not a comprehensive list) of the design criteria elaborated for the DOMPLU structure is as follows:

- Siting and how to choose the specific plug location (characterization):
  - The strength and properties of the rock in the area of the recess with the concrete dome have to be suitable for construction and for performance of the plug during the repository operation period. This means that long or water bearing fractures should not be present at the plug location in order to prevent leakage of water past the plug.
- Rock excavation method:
  - This requires that the rock surfaces connecting the concrete dome abutment are so far as possible free from EDZ (excavation damaged zone) and to be smooth for a minimalized bond with the young concrete. The rock excavation method recommended is wire-sawing.
- Functional requirements:
  - During its operational lifetime of 100 years, the plug system shall limit groundwater flow in the deposition tunnel to prevent piping and subsequent erosion of bentonite material.

According to Börgesson et al. (2015b) a leakage rate less than 0.1 l/min past the plug is acceptable to the buffer for all combinations of inflow rates into deposition holes and tunnel if the inflow rate to deposition holes is less than 10 % of the inflow into the tunnel. At a plug leakage higher than 0.1 l/min there may be too large erosion damages in the backfill. Thus the water tightness requirement for the deposition tunnel plug is suggested to < 0.1 l/min.

- Geometrical conditions:
  - These include tunnel dimension prerequisites and local requirements on the concrete dome geometry and the shape of the excavated slot. Cut pictures from construction drawings are provided by Appendix 1.
- Material properties for all plug components:
  - These criteria include the choice of filter material, bentonite seal, the delimiters, concrete dome, drainage pipes, cooling pipes, and grouting pipes. Low-pH concrete based on the B200 mix (Vogt et al. 2009) is used for the low-pH concrete components, including the concrete dome.
- Load cases:
  - For the hydraulic pressure, a nominal design value of 5 MPa is used.
  - For the swelling pressure, 4 MPa is assumed based on Malm (2012). However, a resulting swelling pressure of approximately 2 MPa is expected to be applied to the plug as a result of the design decision to introduce a backfill transition zone (i.e. a safety factor of 2 is applied for the load from swelling pressure). The backfill TZ reduces swelling pressure from ~ 6-10 MPa to ~ 2 MPa. Consequently, 2 MPa is also used as the design value for the bentonite seal.
- Design of the experiment set-up including decisions on data to be recorded by the monitoring system, the water pressurization system and the leakage control system. These are described in Chapter 7.

2.2 Modifications to the reference conceptual design applied in DOMPLU

DOMPLU represents a detailed iteration of the reference design rather than a fundamental change. A schematic illustration of DOMPLU is provided in Figure 2-1. The current SKB reference design and DOMPLU design are broadly similar, with the exception of a few modifications intended to test the performance of new materials planned to potentially be introduced as the reference design in the future, or to facilitate experiment implementation. Such modifications include:

- The use of unreinforced concrete instead of reinforced concrete for the concrete dome. This has been previously analysed by Dahlström et al. (2009) and Malm (2012).
- In DOMPLU, the backfill end zone is redefined as a backfill transition zone where the swelling pressure from tunnel backfill is reduced to a level that is similar to the sought swelling pressure of the bentonite seal (about 2 MPa). In Malm (2012, Section 3.3.2) the design load for swelling pressure acting on the concrete dome is stated to be 4 MPa with a safety factor of two to ensure the highest safety class in construction. Hence a swelling pressure of 2 MPa is the expected load on the concrete dome (in addition to the design load of 5 MPa from hydrostatic pressure). According to Börgesson et al. (2015a) the swelling pressure in the backfill can reach considerably higher than 2 MPa and this has called for the development of a transition zone. Another purpose of introducing a transition zone is to reduce displacement of other plug system components. In DOMPLU, a backfill transition zone of 100 cm is included. It consists of bentonite blocks with low density and bentonite pellets that allows for swelling pressures generated some distance from the plug (simulated by injected water in DOMPLU) to be dissipated by the frictional forces of the fill material against the rock wall.
- In DOMPLU, the innermost delimiter is considered to be part of the filter. Instead concrete beams, porous LECA beams and gravel with high permeability are used. The LECA beams facilitate inflow to the filter. The filter thickness is 600 mm, made up of 300 mm of gravel (with aggregate size of 2–4 mm) and 300 mm of LECA beams, compared to a thickness of 700 mm, which is specified in the reference design for the filter.

- The middle delimiter between the filter and the watertight seal is composed of a geotextile instead of concrete beams. The purpose of introducing a geotextile instead of concrete beams in DOMPLU is to simplify installation and improve wetting of the bentonite seal.
- The outer delimiter is composed of low-pH concrete beams as for the reference design. In addition, a double geotextile layer is introduced between this delimiter and the concrete dome to prevent adhesion of the delimiter to the concrete dome, and therefore avoid potential cracking of the concrete dome during shrinkage.
- Cooling pipes are specified to be made of copper. This is a material easy to work with, likely to be approved for future use and common for similar applications.
- Grouting tubes are made of cross-cut 50 mm plastic drainage tubes. This is a new promising design of injection tubes, but has never been tested by SKB before.
- The thickness of the watertight seal is 500 mm in DOMPLU, which is considered sufficient for the timescales of the experiment, compared to 710 mm in the reference design.
- The installed dry density of the gravel ("macadam") filter is 1400 kg/m^3 in DOMPLU while a value of 1900 kg/m^3 is considered in the reference design. In the reference design compaction of the filter was presumed, but this turned out to be impractical and not useful for the grading chosen of the filter material. The result is of course a larger compression of the filter by the swelling pressure, which has to be taken into account in the design of the transition zone.

The design of filter, drainage and bentonite seal components for DOMPLU is based on numerical simulations and tests, presented by Börgesson et al. (2015a). These findings are summarized in Chapter 4 of this report. The design of the concrete dome is based on the results found by Dahlström et al. (2009) and Malm (2012).

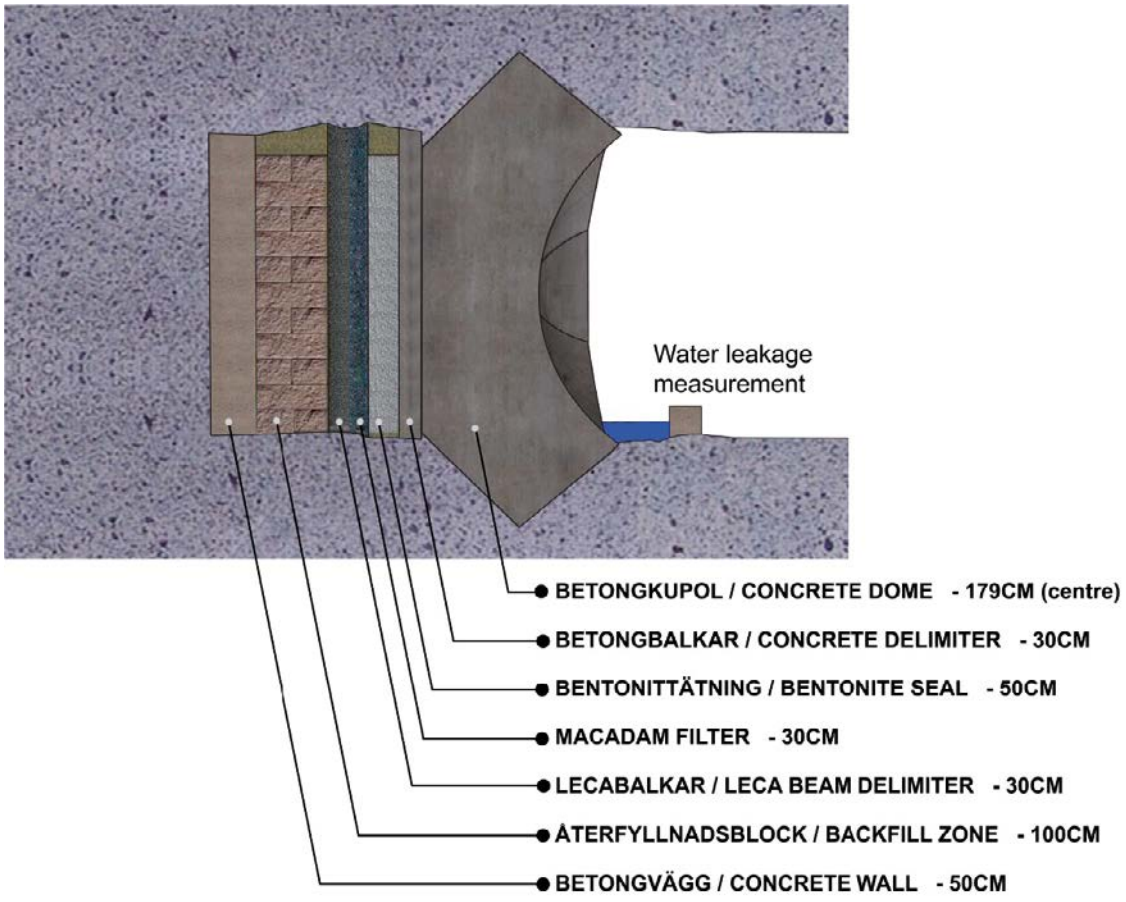

Figure 2-1. *Schematic section of the DOMPLU full-scale test.*

2.3 Discussion of DOMPLU design

One main purpose of the DOMPLU design is to accurately simulate to the KBS-3V reference conceptual plug design and to demonstrate that it is possible to fulfil requirements required as part of SKB's licence application for the Spent Fuel Repository at Forsmark.

DOMPLU is a demonstration of the initial state of the deposition tunnel plug. This initial state is the starting point for safety analysis. Consequently, verification of the plug structure's conformity to the design basis is vital for the accuracy of the safety case and also for the safety during operations.

DOMPLU addresses the "short term" period and, thus, addresses requirements applicable to the design and construction phases of the deposition tunnel plug. DOMPLU also tests the initial operation and performance of the plug under the full hydrostatic pressure and the backfill swelling pressure. The initial plan for the experiment was to pressurize the filter to 7 MPa of water pressure, and that this pressure would be maintained for a period of two years. A pressure of 7 MPa corresponds to the design load for the dome plug and would represent the sum of the hydraulic and swelling pressures under full water saturation and hydrostatic head. However, reassessment of the DOMPLU system during preliminary testing resulted in a reduced applied water pressure of 4 MPa, the reasons for this are provided in more detail Section 9.3. Despite this reduction in field pressure, a water pressure equal to 4 MPa is a more realistic case for comparison to the repository state since it is close to the hydrostatic head at the anticipated repository depth. At the end of the operational phase of DOMPLU, i.e. just before dismantling the DOMPLU, the plan is to perform a short-term load test on the plug by applying possibly up to 10 MPa of total pressure.

The main uncertainty in the DOMPLU design is whether a leakage rate through the plug of less than 0.1 l/min is a realistic requirement. The DOMPLU results will therefore be used to help realistically quantify achievable rates through the plug during the operational period of the final repository.

The reference conceptual design of the plug will be updated and modified based on DOMPLU outcomes. This may include consideration of the materials and installation processes for each component of the plug. The update on the new design is required to capture any learning from the DOMPLU experiment.

2.4 Quality assurance program

Deposition tunnel plugs are not classified as having a direct barrier function but a secondary safety class based on *Impact on barrier function* (SKB 2010a). The plugs may have impact on the properties of buffer, backfill and closure and since the plugs are left in place during closure. Their properties must therefore be known in order to assess and evaluate the safety of the final repository.

Quality plans will be established for the engineered barriers, underground openings and other parts of the KBS-3 repository. The quality plans shall specify the procedures and associated resources that will be applied, and shall describe who is responsible for the activities and when they must be undertaken. The quality plans provide a concise picture of all quality controlling and quality assuring activities. They will include the activities carried out before the production is initiated as well as the activities during the production until the initial state defined for each component of the system is achieved.

Learnings from DOMPLU will be used to further develop the quality plan for plugs. In many cases established procedures for quality assurance are already available as conventional standards. SKB intends to apply conventional procedures as far as possible and reasonable, e.g. for qualification of measuring equipment for inspection of weight, dimensions and placement, and for inspection of construction materials such as steel and concrete.

Specifically for DOMPLU, quality assurance of examinations and filed investigations carried out at Äspö HRL follow the established SKB procedure of Activity plans. The DOMPLU full-scale test contains several activities which to a varying degree make examinations that generate primary data. Reviewed and approved data are stored in the SICADA database to assure quality of the source material. On the basis of these, data is to be supplied as support and reference for calculations and reports of the project.

3 Geology and rock excavation

In crystalline rocks there is a potential for both the host rock and the excavation damaged zone (EDZ) to provide groundwater flow paths that could bypass the plug. Therefore, the plugs must be keyed into the host rock by a so-called slot excavation. The slot is also designed to facilitate transfer of the forces from the plug to the rock. Criteria to determine the suitability of the plug location must be established in advance of the decision on slot position.

In this Chapter, the general requirements and the method used in choosing the location of the full-scale test DOMPLU are described. Furthermore, a brief summary of the excavation of the experiment tunnel is presented, followed by a review of the performed excavation of the DOMPLU slot by wire-sawing. The information provided in this chapter is primarily based on the report by Grahm and Karlzen (2015).

3.1 Plug location and rock conditions

During initial planning of the project, a set of requirements was developed in order to find a feasible test site for DOMPLU. It was decided that a purpose-built experiment tunnel should be exclusively reserved for DOMPLU since sensitive monitoring and high water pressure would be used. The feasibility of the experiment tunnel location was to be tested by characterization of the core from a single pilot borehole followed by high-pressure water injection tests in the borehole.

3.1.1 DOMPLU rock requirements

A general design premise for deposition tunnels plugs is that the strength and properties of the rock in the plug location shall be suitable for construction of the slot abutment for the concrete dome and anchoring of temporary structures such as concrete beams and formwork.

To facilitate pressurisation and to obtain conditions similar to what is expected to be present in a final repository, the DOMPLU experiment needed to be placed as deep as possible in the Äspö HRL. DOMPLU was therefore located in the crystalline rock at level −450 m, where a groundwater pressure of about 3.0 MPa could be expected. The tunnel geometry needed to conform to the reference KBS-3V deposition tunnel (SKB 2010c) excavated by drilling and smooth-blasting techniques. The result is a horseshoe-shaped tunnel contour according to principle dimensions provided in Figure 3-1.

Initial surveys proposed an extension of the existing Äspö HRL main tunnel TASJ. Thereafter, the experiment tunnel, named TAS01, could be excavated almost parallel to the major principal stress direction (σ_1), see Figure 3-2. The proposed tunnel direction for TAS01 accounts for a favourable tangential stress. However, the experiment tunnel is also nearly parallel to the orientation of the main water-bearing fractures in the Äspö HRL which may be less suitable from the aspect of achieving a watertight plug.

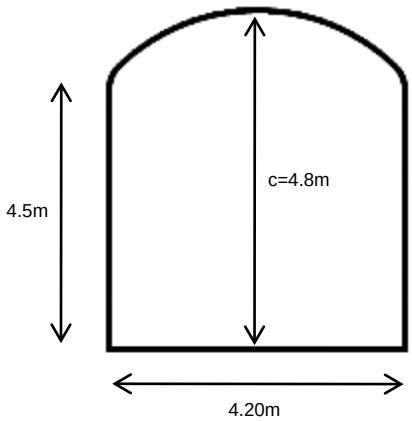

Figure 3-1. *Principle tunnel dimensions of a KBS-3V deposition tunnel.*

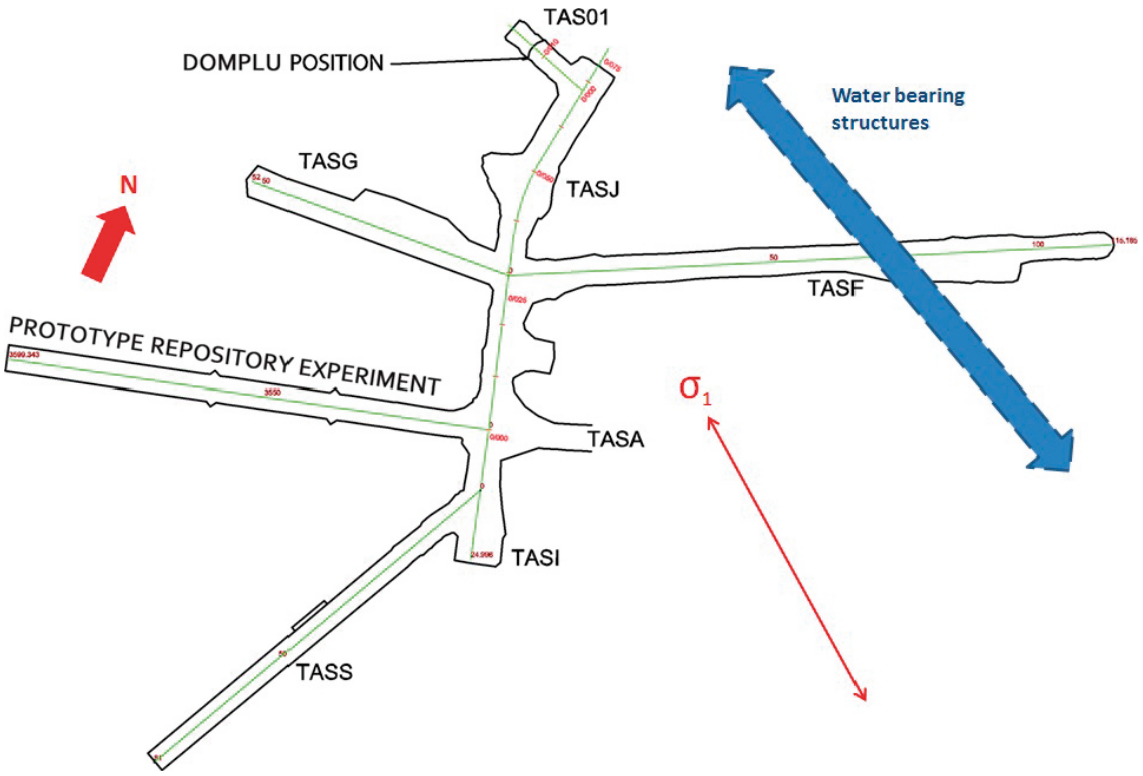

Figure 3-2. *Layout of Äspö HRL at level −450 m and the location of the DOMPLU full-scale plug test site TAS01. The major principal stress direction (σ_1) and the main direction for the water bearing structures have been marked in the figure.*

The set of key requirements on the experiment tunnel included:

1. A need to find an area with no continuous fractures longer than the tunnel diameter. This requirement was applied for the full length of the plug system, i.e. from the downstream side of the concrete dome to the upstream side of the backfill transition zone (a total of 6.5 m). A preference for an absence of such fractures for the entire length of the experiment niche was also stated in the design basis.
2. In the plug system position any visible fracture longer than 1.0 m was undesirable and, in particular, no water-bearing fractures are allowed.
3. Any fractures with an angle of incidence less than 30° against the tunnel axis were to be avoided in the location of the concrete dome. Such cracks can cause stability failure and split wedges from the slot.

The reasons for these requirements are to obtain the desired boundary conditions for DOMPLU and reduce potential risk to the successful completion of the project.

Although the above-listed tunnel requirements were identified prior to tunnel excavation, the actual presence of fractures in the area was largely unknown and so the tunnel length that needed to be excavated could not be fully predicted in advance. To ensure rock stability, the minimum distance from the tunnel entrance to the front slot abutment of concrete dome was set to 7 m, while the length of DOMPLU itself was designed to 6.5 m. The shortest possible test tunnel was consequently 13.5 m if ideal conditions existed. Anticipating challenges in finding a suitable length of suitable rock in the identified area, the length of the first pilot borehole was set to 30 m.

For the purposes of conducting DOMPLU in the tunnel selected, there was recognition that at least some rock reinforcement might be needed. In order to avoid interference of this reinforcement with DOMPLU, it was specified that no rock bolting was allowed for the DOMPLU test area itself. Beyond this location, conventional rock reinforcement was accepted for use in the region between the tunnel entrance and to within 1.0 m of the front of the DOMPLU slot.

3.1.2 DOMPLU site investigation

As discussed in Section 3.1.1 the suitability of the plug location must be determined in advance of a decision on the plug's position. This task was thoroughly planned and investigation data was evaluated before excavation of the DOMPLU test tunnel TAS01.

To prepare the tunnel excavation and to decide on the plug location, a 30 m pilot hole (named KJ0068A01) was drilled for the purposes of core and borehole mapping and conduct of high-pressure water injection tests (up to 10 MPa). Figure 3-3 shows a photo of the core box containing one third (the first 10 metres) of the borehole.

According to the mapping of the borehole, the most suitable geological section for DOMPLU construction is between approximately 7–11 m depth from the original tunnel face. This region corresponds to the three lowest core-sections shown in Figure 3-3. This rock section is a medium-grained, massive, fresh and almost fracture-free Ävrö granodiorite (rock code 501056). Only one open (broken) fracture was observed at position 8.7 m of the core (left-side of second core segment from bottom of Figure 3-3).

Stepwise hydraulic injection tests in the pilot borehole were performed by Geosigma. The measurements began with conventional water injection tests, HWIC, to obtain information about which parts of the hole that could pose potential section to install the plug. There were a total of four injection tests with a section length of 5 meters, and one section with a length of 4.95 m. All sections were below the imposed lower measuring limit (1.7E–9 m^2/s) for the equipment. Subsequently, high-pressure tests were done in three sections, each with a section length of 3.86 m due to the specifically developed equipment. These measurements were made in steps with increasing injection pressure until the injection pressure of about 10 MPa was obtained. Flows measured at the lower pressure stages were around the flowmeter lower measuring limit. The tightest section appears to be 9.42 to 13.28 m with a transmissivity of about 1E–13 m^2/s, which corresponds to a rock without fractures.

Based on the examined hydrogeological conditions, a decision was made to place the slot for the concrete dome between 7.2 m (downstream) and 10.4 m (upstream) from the original tunnel face. Since the total length of DOMPLU – including bentonite seal, filter section and backfill – was designed as a 6.5 m long installation and the length of the slot excavation is approximately 3.2 m, the total tunnel length that needed to be excavated for TAS01 was determined to be 13.7 metres.

Figure 3-3. *Photo of the core box for pilot hole KJ0068A01, section 0–10 m (wet core).*

3.2 Excavation of the experiment tunnel

The reference method for excavation of deposition tunnels is drilling and smooth-blasting techniques. Experience shows that when proper control of drilling and blasting procedures is applied, tunnels with acceptable excavation damaged zone (EDZ) and geometry can be constructed (SKB 2010c). For the DOMPLU experiment tunnel, it was decided to attempt to reduce further the magnitude of the EDZ through careful blasting in a two-step excavation method. This method is described below.

The reference method for sealing the deposition tunnels is grouting the rock beyond the excavation face, i.e. pre-grouting, using low-pH cement (SKB 2010c). Based on the very low transmissivity levels in the pilot borehole injection tests, it was decided to avoid pre-grouting of the rock before DOMPLU test tunnel excavation. This decision was supported by a risk assessment that showed that the rock area could be damaged significantly by drilling and grouting around the test tunnel.

Before each round of blasting, all holes needed for charging are drilled. The lookout angle for the drill-holes is assumed to be ≤ 25 cm. A blast round is normally performed as one activity, i.e. all drillholes are blasted at the same time. For DOMPLU test tunnel, the desire to reduce the EDZ to the maximum possible extent prompted a need for a slightly modified blasting technique. Accordingly, the excavation method was adapted into a two-step method of careful blasting as illustrated in Figure 3-4.

In step one, all holes were drilled and then the holes in the centre (light-blue, orange and light-green in Figure 3-4) were charged and blasted. As a result of this first blast, a pilot tunnel for TAS01 was blasted and thereafter cleared of rock. In step two, the perimeter drillholes (blue and dark-green in Figure 3-4) were charged for a lower-energy explosive effect, and the remaining peripheral rock (approximately 30 to 40 cm) was then blasted. Each round of careful blasting for TAS01 was at most 4.0 m in length. In total four rounds were needed to expand the tunnel length to just short of 14 metres.

The extent of the EDZ in the finished TAS01 tunnel was not verified by direct measure but by using this careful blasting method, it is believed that the risk of generating any continuous EDZ-fractures has been minimized. As a consequence, the test tunnel was considered to provide good conditions for the experiment.

The remaining perimeter rock prior to the blasting of the third excavation round can be seen in Figure 3-5. The presence of the half-barrel of essentially all of the outermost blasting boreholes used in tunnel excavation is generally taken as evidence of a low energy excavation with little rock damage (EDZ) in the rock radially-outward.

The tunnel excavation and detailed tunnel mapping activities were carried out by another project (The Äspö HRL Expansion Project in 2012). The completed test tunnel TAS01 was handed over to this project in late April 2012.

The fully extended test tunnel is shown in Figure 3-6.

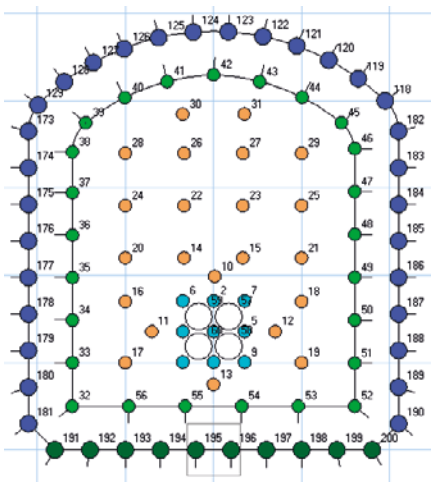

Drillhole Type	No. of drillholes	Drillhole dist. (m)	Burden (m)	Charge
Contour	30	0.4	0.5	According to construction documents
Helpers	19	0.5	0.6	
Stope	13	0.7	0.7	
Stope	9	0.7	0.7	
Sole	6	0.6	0.5	
Bottom	10	0.4	0.5	
Wedge	9			
Sum	**96**			

Figure 3-4. *Drill and charge plan for DOMPLU test tunnel TAS01.*

Figure 3-5. *Photo of the test tunnel TAS01 during ongoing excavation of the third round. The perimeter boreholes to be used for separate charging and blasting of the peripheral tunnel contour are visible.*

Figure 3-6. *Photo of the completed test tunnel TAS01. Geodetic survey is ongoing to mark out positions of the plug components.*

3.3 Wire-sawing of slot abutment for the concrete dome

The abutment for the concrete dome plug was excavated by the use of wire-sawing. To facilitate excavation by wire-sawing, the slot had been designed as an octagon with a symmetric borehole pattern and with established borehole angles. Before full-scale sawing of DOMPLU, the technique was developed and demonstrated at full-scale for a partial section of the slot. In this pre-study test, two rock segments out of the total eight required for a slot were excavated at Äspö HRL, level −460 m (Grahm and Karlzén 2015).

Besides an efficient production rate, the goals for wire-sawing are to strive for an EDZ-free rock abutment and also to produce a smooth rock surface for casing of the concrete dome. A smooth surface is preferred in order for the concrete dome to release from the rock during its early shrinkage and during the controlled cooling procedure. Release of the concrete dome helps to prevent high initial tensile stresses during autogenous shrinking of the concrete and supports successful grouting of the interface between the dome and the rock.

Based on the pre-study test experience, the proposed wire-sawing strategy for DOMPLU included:

- An initial drilling campaign of all the necessary boreholes, i.e. both holes for wire sawing and for the concluding blasting of free-sawn rock.
- Erection of a worker protection scaffold including steel mesh for the roof and walls.
- While scaffolding and mesh installation is progressing, the wire sawing equipment establish on site.
- When the sawing has been completed, blasting of the free-sawn rock segments is done simultaneously with blasting of the safety scaffolding bearing structure.

During the progress of full-scale slot excavation, one adjustment to the originally planned method for wire-sawing was needed. This change is described in detail by Grahm and Karlzén (2015) and is briefly presented in Section 3.3.2. In Section 3.3.1, the results of the revised wire-sawing sequence used for the slot excavation of DOMPLU is summarized.

Figure 3-7 illustrates the basic sequence of activities needed to excavate a partial section of the octagonal slot by dragging the wire along the rock web between two neighbouring boreholes (known as blind cuts).

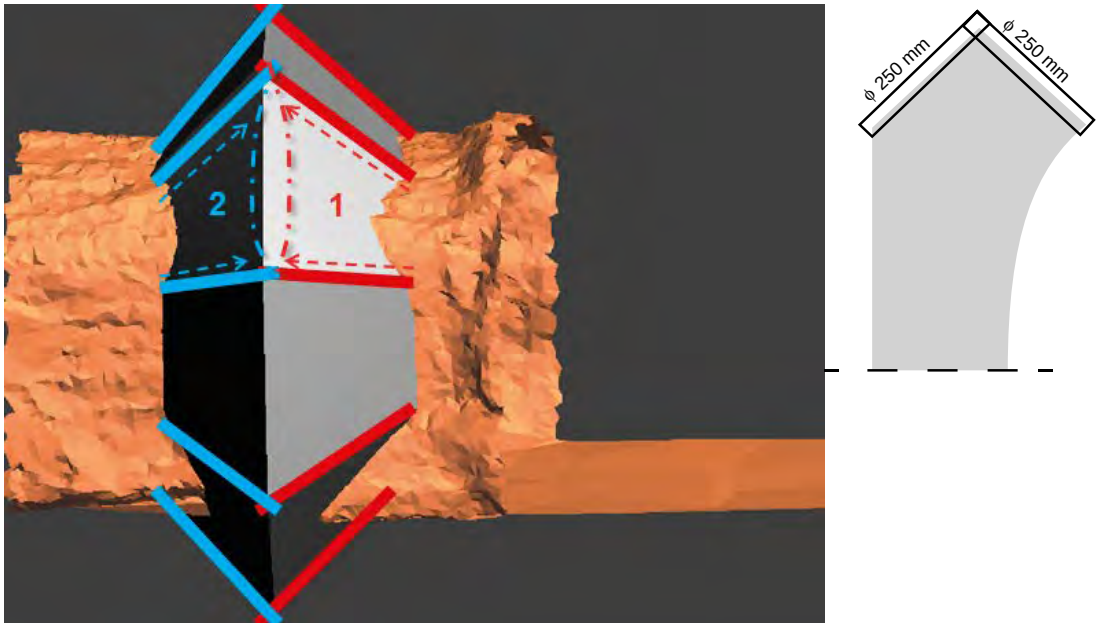

Figure 3-7. *a) Principle for drilling and wire-sawing of the slot by blind cuts. b) Diameter of the boreholes for emplacement of tower and pulley for the wire.*

3.3.1 Improved excavation sequence

The following sequence was used to complete the wire-sawing of the slot:

1. Core drilling of ⌀250 mm holes from the downstream side at each corner of the octagon (eight holes in total) to a predetermined depth ending 300–500 mm past the specified intersection point (as illustrated by red lines in Figure 3-7). The reason for making the holes deeper than absolutely necessary is to ensure that it is possible to break the cores loose and to provide sufficient space for the wire pulley in the bottom of the hole.
2. Core drilling of ⌀250 mm holes from the upstream side at each corner of the octagon (eight holes in total). These drill holes are drilled until they intersect and pass the ⌀250 mm holes from the downstream side (as illustrated by blue lines in Figure 3-7).
3. Small-diameter holes of ⌀38 mm, to be used for blasting of free-sawn rock segments, are drilled in the same angle as the octagon design which corresponds to the cut-line. The holes are drilled with a respect distance of 70 cm to the resulting slot surfaces in order to diminish damage. Five holes are drilled in the three uppermost segments and three holes are drilled in the remaining five segments respectively, see Figure 3-8. The aim of these holes is just to facilitate block breaking for an easy removal and not to generate any special size fraction.
4. To protect the workers from potentially falling rocks, it is necessary to erect a steel beam structure. This safety scaffolding was specially developed for the DOMPLU test and dimensioned so it would be able to support the big rock segments cut free by the wire-sawing. The mass of each segment of rock cut by the wire sawing was up to 10 000 kg. Design details of the scaffolding are presented by Grahm and Karlzén (2015). Photos of the protecting steel structure are presented in Figure 3-9.
5. Wire-sawing begins with the bottom segment on downstream side, by inserting guide pulleys into the two adjacent 250 mm holes. A blind cut is then performed between them as the wire is pushed onto the rock when the wire-sawing machine moves backward on its rail, see Figure 3-10. The sawing sequence continues upwards and ends with the roof section. In total, eight cuts on the downstream side were completed.
6. Wire-sawing continues on the upstream side of the slot. The wire is realigned in the same manner as previously with the difference that pulleys to turn the wire are now also mounted in the steel beam structure on the back wall (i.e. the blue beams that are visible in Figure 3-9a). The reason for this arrangement is lack of space in the short test tunnel. In a full deposition tunnel, sawing equipment can also be placed on the upstream side of the slot.
7. Blasting of rock segments and safety scaffolding structure is done in one activity where the load bearing beams are detonated just some milliseconds before the rock. The tunnel is then cleared and remaining rock fragments in the slot are mechanically removed.

Figure 3-11 includes a photo of the excavated slot abutment for the concrete dome.

3.3.2 Adjustment of the wire sawing method from original plans

Initially, the plan was to drill all wire sawing holes on the upstream side of the slot with a small-diameter (⌀46 mm). These holes were intended to be used for threading the wire out to the upstream side immediately after a performed blind cut from downstream side. Thence pulling cuts would be used for sawing upstream side of the slot.

Previous tests had showed that pulling cuts resulted in surfaces that are more planar compared to blind cutting. Furthermore, drilling of small-diameter holes is favourable compared to ⌀250 mm. However, in the full-scale sawing, it proved problematic to thread the wire through the small holes. Once threading was accomplished, it was then problematic to start sawing without a wire breaking. The reason for this later issue is related to rock creep-movements making the diamond wire stick at the innermost part of the slot. This potential issue was recognized during pre-study tests but it was initially expected that a rapid installation and start to sawing would be enough to avoid this complication. However, within just 45 minutes of installation the wire was unrecoverably stuck in the borehole.

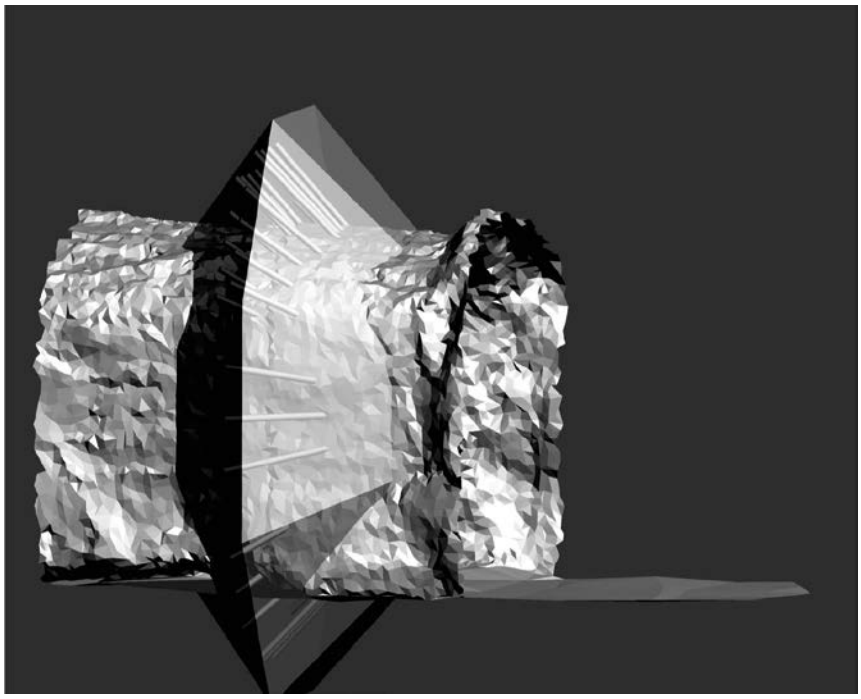

Figure 3-8. *Theoretical model showing the laser scanned tunnel and the design pattern of drill holes for blasting, performed from the downstream side of the slot.*

a) b)

Figure 3-9. *a) Photo of the erected safety scaffolding including a tunnel mesh to protect workers from falling rocks b) Detail of the scaffolding with two of the ⌀250 mm boreholes visible.*

Figure 3-10. *Wire-sawing equipment moving on rails in TAS01.*

Figure 3-11. *TAS01 with the excavated slot abutment for the concrete dome.*

After several attempts to make the small diameter borehole installations work, revision of the procedure was made and all ⌀46 mm boreholes were reamed to ⌀250 mm. Thereafter sawing continued with blind cuts also being used for the upstream side of the slot, as described in Section 3.3.1.

The remedial reaming of the boreholes, added about 10 days to the excavation schedule. Therefore, although originally planned to take 40 days, the sawing required 50 days to be completed. Daily working shifts were used. This time does not include stand-down times required for building the platforms for the drilling machines, scaffolding and geodetic surveying.

3.3.3 Evaluation of performed cuts

After the rock was removed and the octagonal slot had been cleaned, laser scanning was performed to measure deviations on the surfaces compared to the theoretical geometry. The results show that in general, the resulting excavation surface is a bit deeper than the theoretic plane in the centre-bottom of almost every cut. It was noted that when the first cut (from downstream side) for each segment was made, the following cut (from upstream side) is closer to the target depth. This is likely an effect of released stresses in the rock as a result of the nearby cuts. More information can be found in Grahm and Karlzén (2015).

In Figure 3-12, a 3D-model composed of data from the 16 laser scanned slot surfaces has been incorporated in the laser scanned model of experiment tunnel TAS01.

An evaluation of the small surface nonconformities showed that there is no risk for reduced stability of the concrete dome. Calculations confirm that the octagonal shape of the slot is tolerant of small deviations.

A recommendation for future development of slot excavation by wire-sawing is to find a way to release rock tensions before cutting begins. Perhaps a few extra boreholes can be introduced to solve this issue. A possible solution could also be to change the order of sawing and begin with the sides of the slot instead of the bottom segments.

According to Grahm and Karlzén (2015) another experience from the full-scale excavation is that it will be possible to implement more productive ways to drill holes for the guide pulleys. Moreover the productivity can be increased with improved methods for drill rig positioning and use of specially adapted platforms.

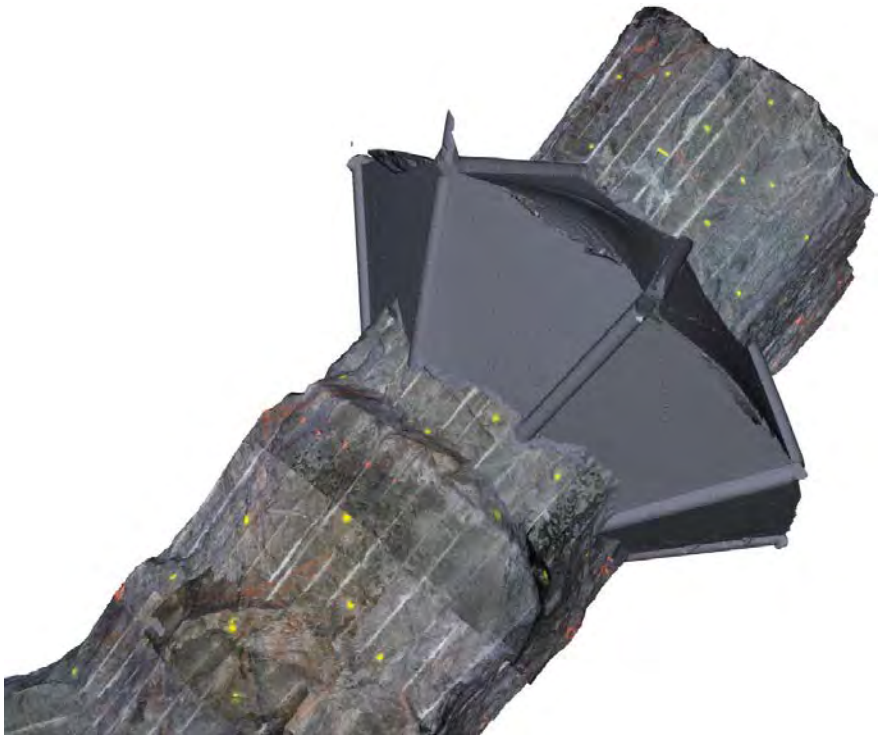

Figure 3-12. *3D-visualization, composed of data from laser scanning of TAS01 and the excavated slot abutment (seen from above).*

3.4 Monitoring niche

In conjunction with excavation of TAS01, an existing niche in the main tunnel TASJ was expanded to accommodate the pressurization system and a water tank for supply of water. See further information in Section 7.3. Room was also dedicated for a data cabinet that collect the signals from sensors in backfill, filter and bentonite seal.

Three lead-through boreholes (⌀200 mm) were drilled from the monitoring niche towards the central backfill section of DOMPLU as illustrated by Figure 3-13. The holes are placed in a vertical line and each hole is about 21 m long. One of the boreholes (the bottom one) was dedicated to the five water inlet pipes coming from the pressurisation system. The other two boreholes were used to feed-out sensor cables to the data cabinet from backfill, filter and bentonite seal.

The main reason for expansion of a niche in TASJ is that the lead-through boreholes must have a sufficient respect distance, about 2 m, to the excavated slot abutment, see Figure 3-14.

The lead-through cable installation is further described in Section 7.4.

3.5 Water inflow to the experiment tunnel

Before plug installation commenced, as is described in Chapter 6, coarse groundwater inflow measurements to the plug location of TAS01 were carried out. Firstly, measurement was carried out on the upstream side of the excavated slot towards the concrete back-wall which can be seen in the centre of Figure 3-11. A temporary weir was used to prevent water from entering into the slot section. The tunnel floor was then completely drained by the use of a wet vacuum machine. After three full days this procedure was repeated and the collected water by the machine was recorded. Secondly, water was collected in the slot section in a similar way. The inflow measurement results are summarised in Table 3-1.

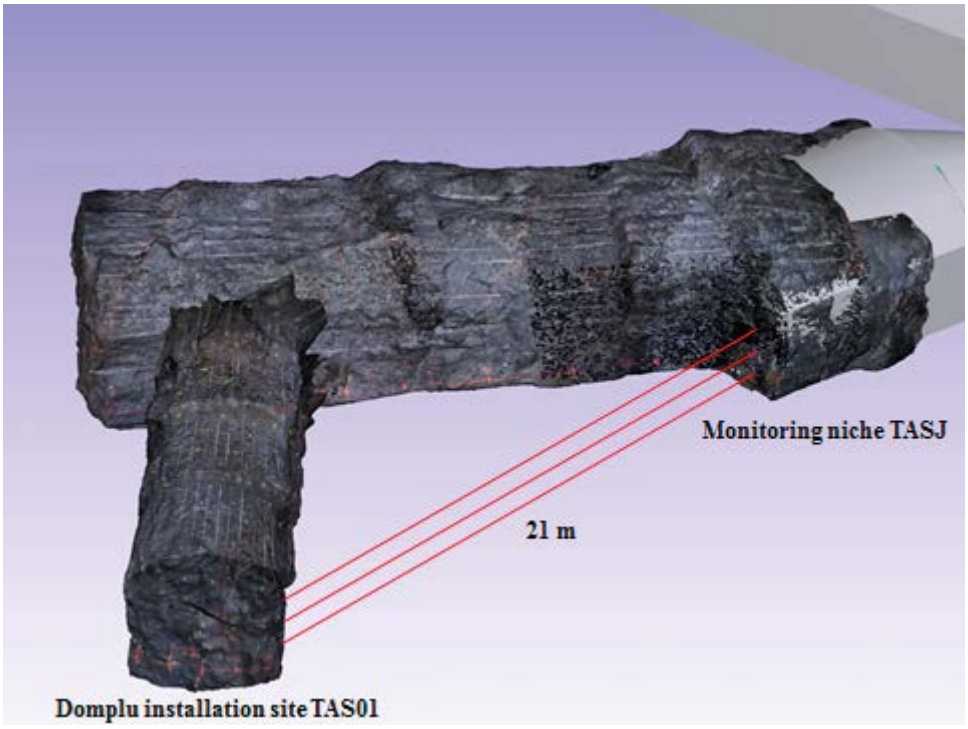

Figure 3-13. *Illustration of the lead-through boreholes between the monitoring niche in TASJ and the DOMPLU backfill section in TAS01.*

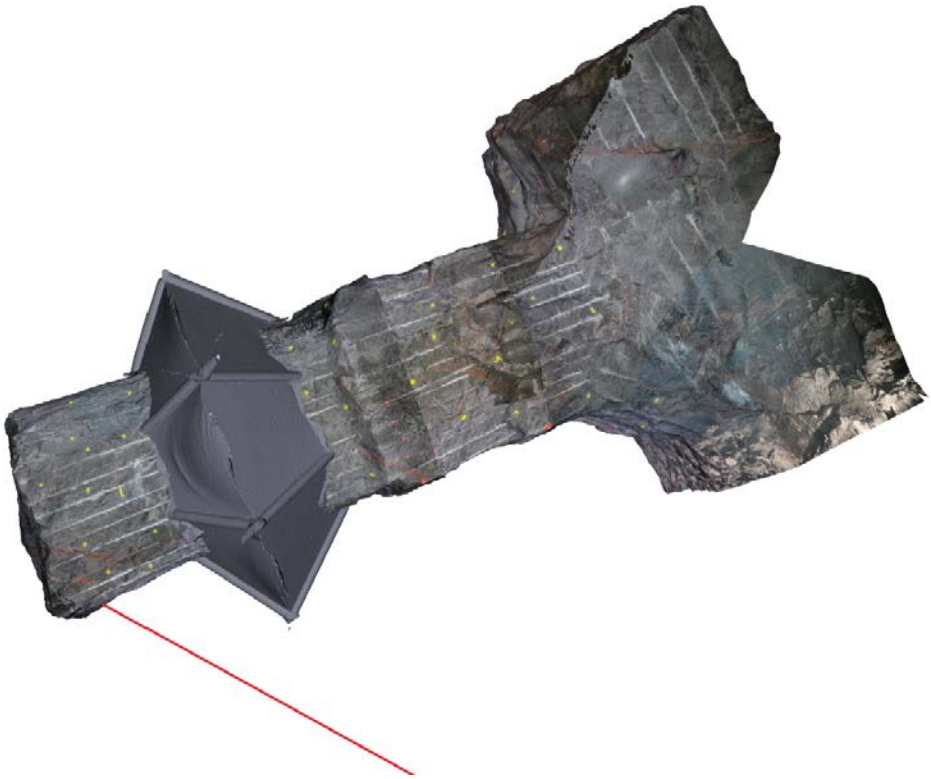

Figure 3-14. *Experiment tunnel TAS01 with the excavated slot, seen from above. Red line indicates the approximate position of the lead-through boreholes in relation to the slot.*

Table 3-1. Groundwater inflow measurements to TAS01 before start of plug installation.

Section	Start	Stop	Total volume (l)	l/min
Back-wall to slot	January 11, 2013, 11:30 am.	January 14, 2013, 10.55 am.	122	0.028
Slot	January 14, 2013, 11:00 am.	January 15, 2013, 09:00 am.	79	0.059

As can be noted from the results there was an evident inflow especially to the slot section despite the promising dry results of the pilot-borehole investigations. This water mainly originates from two of the large diameter drill holes for the guide pulleys, as can be seen as darker fields of wet rock in the photo provided by Figure 3-11. These holes (on the top left and on the right side in Figure 3-11) unfortunately intersect water bearing fractures. Consequently the assumed rock requirement to not allow any water bearing fractures at the DOMPLU location could not be fulfilled. This had been a recognized project risk since the rock at Äspö HRL is much fractured in general and in this way not similar to the good quality rock expected at the deposition area in the Spent Fuel Repository in Forsmark.

As understood from Table 3-1 the measured total inflow over the 6.5 m tunnel section for DOMPLU was 0.087 l/min. Extrapolated to a 300 m deposition tunnel this environment would correspond to a total inflow to the filter of approximately 4 l/min. The maximum accepted water inflow rate to a deposition tunnel is at present set to 5 l/min and this rate was suggested to later be tested for the DOMPLU filter, see further information in Sections 4.2.6 and 9.1.1.

4 Development of bentonite seal and filter

The two main components of the plug system, apart from the concrete dome, are i) the bentonite seal, which will severely limit water flow through the concrete dome and, especially, between the dome and the rock wall; and ii) the permeable filter, which will enable drainage from the tunnel and/or water injection during the hydration of the bentonite seal. The present chapter describes the work associated with the design and testing of the sealing and drainage components to be used in the full-scale test DOMPLU.

In addition to the full-scale test, extensive studies have been performed within the scope of this project regarding the properties for the sealing material as well as the draining filter. These results are presented in detail in the report by Börgesson et al. (2015a) and this chapter summarizes the main developments and conclusions from that research. From this work on the design and testing of the sealing and drainage components to be used in the full-scale test DOMPLU a greater confidence and understanding of system evolution and performance has been developed.

As noted above, the primary requirements of the dome plug are that the water leakage past it is kept small enough to result in a build-up of water pressure inside the plugged volume and to keep water escape from the tunnel at an acceptable level. It is very important that the plug is so tight that the lowest water pressure gradient is moved from the rock/bentonite interface in the tunnel to the plug, since that will give the bentonite time to swell and seal in a non-flow condition. The plug must also be so tight that the water leakage past the plug does not allow for unacceptable erosion of clay from the deposition holes. This is of particular importance during the period before the water pressure in the transport tunnel outside the plug has reached the same level as inside the plugged deposition tunnel.

The concrete dome needs time for hardening and the contact between the dome and the rock must be grouted. Prior to the concrete dome achieving sufficient strength (which requires a period of approximately 3 months) the concrete must be protected from flowing water. This is of particular importance for wet tunnels (tunnels with water inflow rates too high to be stored in the filter and pellet sections and where there is a risk for water reaching the backfill front during the construction of a plug). Such locations will require installation of a drainage system that manages the water coming from the inner parts of the deposition tunnel.

4.1 Material testing

4.1.1 Sealing materials

The present design of a KBS-3V deposition tunnel end plug includes a bentonite seal, positioned behind the cast concrete dome, Figure 1-2. The sealing blocks were originally planned to be placed in a rock section, sawed out by use of wire sawing technique i.e. the surfaces were meant be very smooth with very precise dimensions. With this design the sealing blocks could be positioned tight against the rock surface, requiring that the block density be kept rather low in order to limit swelling pressure to less than 2 MPa (which is a pre-set design parameter). The plug design has however changed with time and in the present design (DOMPLU test at the Äspö HRL) the bentonite sealing blocks are to be placed in a section excavated by blasting, which means that the rock surface is very uneven. This also means that the sealing blocks must be piled on a bentonite pellet flooring fill, used in order to even out the rock surface. This same pellet material will be used along the walls and also against the ceiling. In this design the sealing blocks must therefore have a higher density in order to reach the same average backfill density for the section.

The different kinds of experimental tests that have been performed during this research program by Börgesson et al. (2015a) regarding the sealing material are:

- Compaction properties.
- Strength of blocks.
- Compressibility (Oedometer tests).
- Swelling pressure and hydraulic conductivity.
- Self-sealing of fractures and slots.

Below, the main conclusions from the test program are presented. For further information regarding the test methods used and a more extensive summary of the results see Börgesson et al. (2015a).

Compaction of sealing blocks

In the initial planning of the DOMPLU design, it was intended to use sealing blocks with low density, 1400–1500 kg/m^3, and high initial water content. In order to investigate the compaction properties of such material, block compaction tests were performed in laboratory scale.

The performed tests showed that it is possible to produce blocks of low density and high water content. However, the strength of these kinds of blocks has not been tested since the subsequent design activities focused on blocks with higher density. The compaction pressures needed to reach a density of 1400 to 1500 kg/m^3 are low, between 4 and 12 MPa, depending on the water content. If the water content of the bentonite powder was higher than 30 % some production-related problems were indicated. A summary of the results is shown in Figure 4-1.

Strength of the sealing blocks

The sealing blocks are planned to be installed by use of a vacuum lifting tool, placing the blocks one by one, into position. An important parameter for this block handling is that the strength of the compacted blocks has to be high enough to avoid damage or pieces falling off. The tensile strength of these materials has been investigated by performing beam tests on compacted specimens of differing densities and water contents.

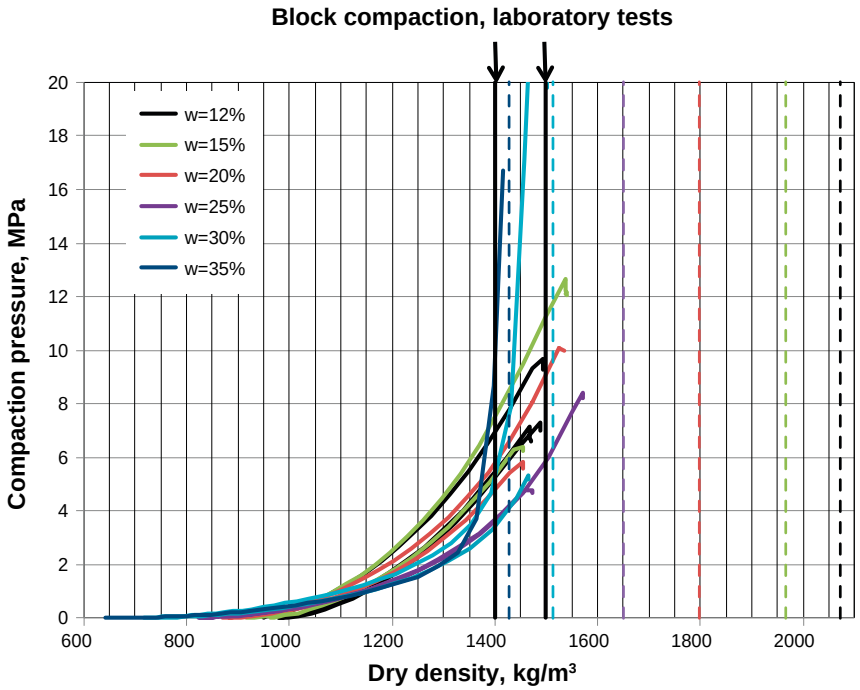

Figure 4-1. *Compaction pressure plotted versus dry density for samples with different initial water content. The two black vertical lines show the target densities (1400 and 1500 kg/m3). The coloured vertical lines show the density where each of the compacted samples theoretically will reach full saturation (if the compaction would continue).*

In order to achieve blocks with this rather low density 1400–1500 kg/m^3 and still keep certain strength it would be necessary to have high water content, around 28 %. However, during the project design phase, the density requirements on the sealing blocks could be increased to 1700 kg/m^3. To achieve blocks with this density and with high strength it was recommended to use a water content of the raw material of 17 %. A summary of the test results is shown in Figure 4-2.

Compression / expansion properties

Knowing the compressibility properties of the sealing blocks is of considerable importance if modeling of the movements of the backfill behind the deposition tunnel end plug is to be accurate. The compressibility of the low density blocks that may be used both for sealing just inside the drift end plug as well as in the transition zone needs to be known in order to control the swelling pressure that will be applied to the plug. This information was determined via oedometer tests where the blocks could be saturated through two filters located at the top and bottom surface of the blocks.

Results from the performed oedometer tests are presented in Börgesson et al. (2015a).

The results from these tests agreed well with what was expected for MX-80 bentonite.

The results from the oedometer tests were used for comparisons with results from numerical models, especially stress paths in the void ratio vs. net stress plane (both axial and radial). The model results showed quite good agreement with the experimental data, which strengthens the confidence in the validity of the used material model.

Swelling pressure and hydraulic conductivity

The tests are described in detail by Börgesson et al. (2015a). The aim of the testing was to investigate whether blocks compacted to a high degree of saturation showed the same properties as blocks with a low degree of saturation. The tests were performed by using a swelling pressure oedometer (Börgesson et al. 2015a, Figure 2-12).

By introducing a predetermined pore pressure gradient over the specimen, via the filters, and measuring the flow of water through the outlet, the hydraulic conductivity of the specimens could be determined. The swelling pressure was measured by a load cell placed between the piston and the upper lid of the testing rig. The specimens were compacted to a specified dry density at different initial water contents before emplacement in the test cells. The tests were made using two different types of water, ordinary tap water and water with 1 % salinity (Na/Ca, 50/50). The salinity is equivalent to the expected formation water at Äspö HRL. The specimens were saturated for approximately 2 weeks before a water pressure was applied in the bottom filter. The applied water pressure was 500 kPa, corresponding to a pressure gradient of 2500.

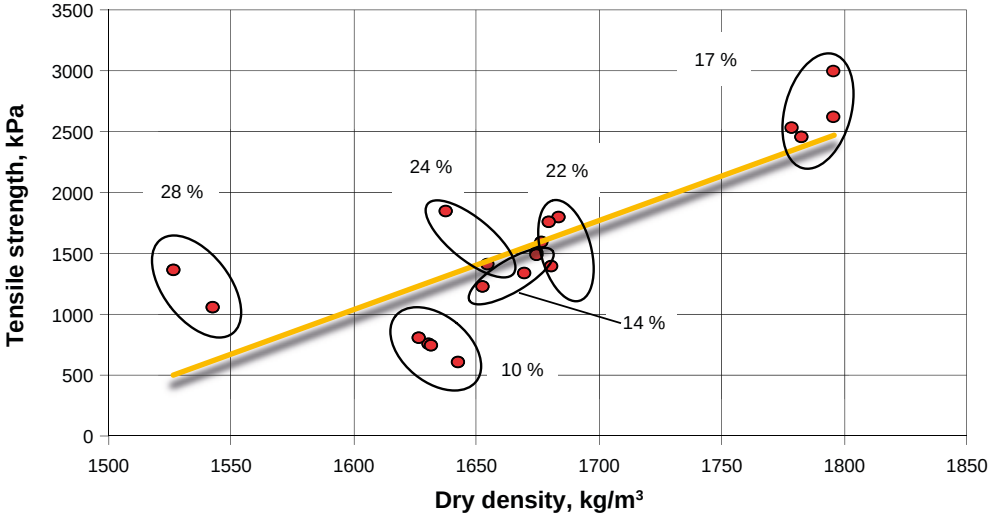

Figure 4-2. *Summary of the strength test results showing the maximum tensile strength at failure for the beam tests plotted as function of the dry density of the specimens prepared using 25 MPa load, from Börgesson et al. (2015a).*

The performed testing showed that there is no significant influence of the water content of the bentonite specimen on its swelling pressure and hydraulic conductivity (k). The swelling pressure obtained by the current study is essentially identical to the reference values and the hydraulic conductivities measured are just slightly lower, which is interpreted as being due to the fact that the higher initial water content gives somewhat more homogenized specimens and hence a slightly lower k-value.

Based on previous studies and a substantial database, the influence of a 1 % salt concentration in the pore-water was not expected to have a substantial effect on the swelling pressure or hydraulic conductivity (Börgesson et al. 2015a), and the new data shown in Figure 4-3 is consistent with these expectations.

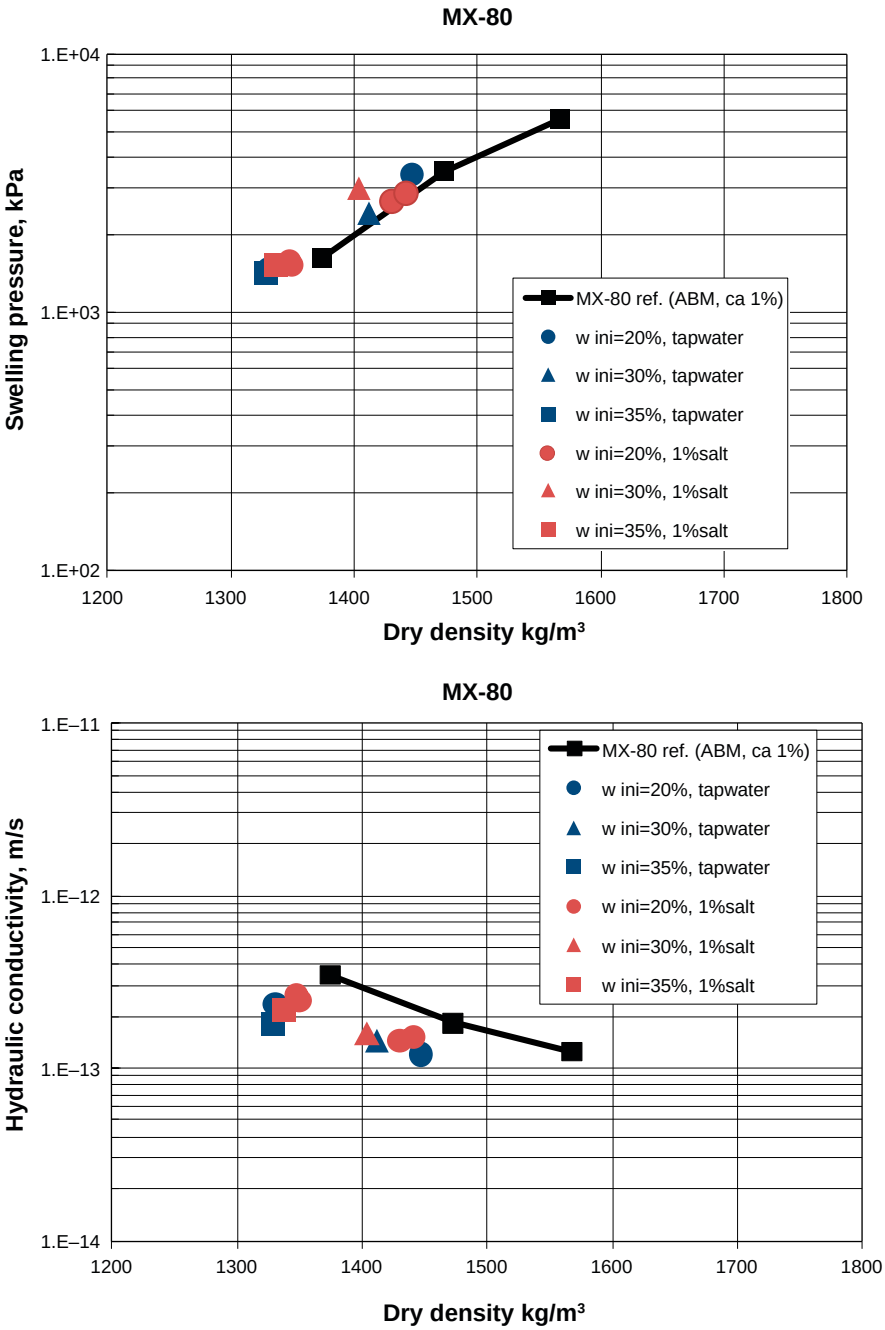

Figure 4-3. *Figures showing the test results. For comparison some results from measurements within the ABM test are also shown in the figures. Upper: Swelling pressure as function of dry density. Lower: Hydraulic conductivity as function of the dry density, from Börgesson et al. (2015a).*

Self-sealing of fractures

Previously completed tests have shown that eroding bentonite from a pellet filling can seal fractures in the rock up to apertures of 0.15 mm (Börgesson et al. 2015a). If the sealing blocks have the same potential to supply material to clog adjacent fractures or gaps, it would be of great significance regarding the demands on the initial tightness of the plug.

The test equipment used was the same as was used in other sealing tests involving bentonite pellets, see Figure 4-4. In these new tests the pellet filling was replaced by compacted bentonite blocks, piled on each other in a cylindrical volume with a diameter of 100 mm, leaving a 2 mm wide gap between bentonite and steel wall. The aperture of the artificial fracture can be adjusted by use of shims of various thicknesses. By monitoring the hydraulic pressure increases required to inject water at a constant rate of 0.01 l/min a measure of the degree of gap closure could be determined.

Three tests were performed in this test series. Two of the tests were performed with bentonite blocks with densities of 1400 and 1500 kg/m^3 and with water contents of 35 % and 30 % respectively i.e. the degree of saturation was very high. The bentonite in these two tests did not manage to seal the artificial fracture (0.01 mm aperture) during the test time. The third test was performed with bentonite blocks having a dry density of 1500 kg/m^3 and with a water content of 13.9 %. In this test the behaviour was quite different. The bentonite sealed quickly and a water pressure could be built up at the inflow end without inducing piping (maximum 2 MPa was applied in this test). One explanation for the observed behaviour might be that the erosion rate is higher for bentonite blocks with low initial water content, which means that the eroding bentonite more quickly can move into and seal the artificial slot. However, there is some doubt if the sealing took place in the cylindrical tube containing the blocks or in the artificial slot. The full results are provided by Börgesson et al. (2015a).

The number of tests that have been performed is limited and the results are not clear. Together with the results from earlier performed tests where eroding bentonite pellets have been tested there are nevertheless indications that eroding bentonite will contribute to the sealing of a plug.

Sealing of initial slots

The bentonite seal inside the plug is planned to consist of compacted blocks, piled on each other to a wall. The floor will be evened out by use of bentonite pellets and the gaps between blocks and rock will also be filled up with bentonite pellets. The time for the bentonite blocks to swell and seal the initial gaps between them is of high interest for the function of the plug. In order to study this behaviour a series of specially designed tests have been performed.

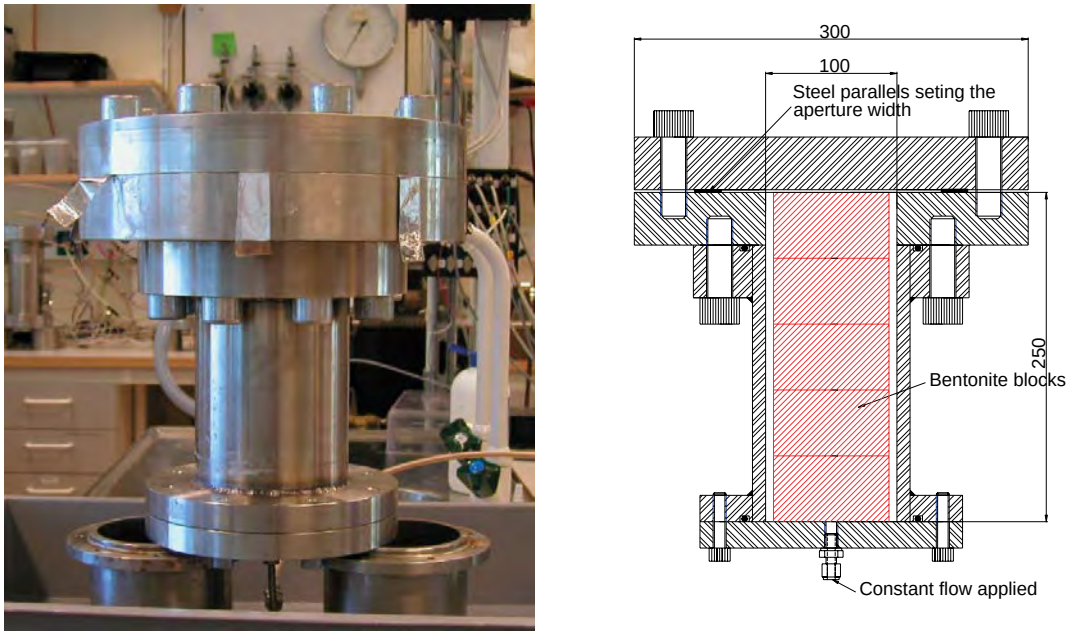

Figure 4-4. *Left: Photo of the test equipment. Right: Schematic showing the test equipment.*

In these tests, bentonite blocks with different initial densities and different initial water contents were allowed to swell and expectantly seal a slot with a width of either 2 or 4 mm, see Figure 4-5. During the tests, one week for most of the tests, the axial and radial pressure build up under low or no applied hydraulic head, but with access to water at the specimen base, was monitored.

The results from the tests performed by Börgesson et al. (2015a) showed, as expected, that the slot width is of great importance. In the tests performed with 2 mm slot, the radial pressure build up was much faster compared to the tests with 4 mm slot. Another observation was that the initial water content of the bentonite block also influenced the results. The time for swelling and filling up the slot with bentonite and start of pressure build-up at the contact between the bentonite and the cell walls took longer for the samples with high initial water contents (and high degree of saturation).

Two of the samples were, after one week of homogenization exposed to a stepwise increasing water pressure. After 800 and 2000 hours respectively, both samples could withstand very high water pressures (3.7 and 5 MPa respectively) applied at their base, without exhibiting piping or channelled flow along their length. These hydraulic pressures were much higher than the swelling pressure of these specimens. The explanation for this is probably that the bentonite in the former slot forms an arch within the test cell, which can withstand very high pressures. The same phenomena have been observed in many tests were bentonite pellets have been used (Sandén et al. 2008).

4.1.2 Filter material

During the course of the project described in this document, different filter designs were discussed and the approach selected was to exclude two of the delimiters (concrete beams) present in the original conceptual design, Section 1.1.3. The concrete beams between the clay seal and the draining material were judged to be unnecessary since the bentonite blocks are stiff enough to prevent the sand in the draining material from interfering with the clay seal if the system of sand, bentonite blocks and concrete beams are placed in parallel as the elevation of the assemblies is raised. The more massive concrete beams between the sand filter and the backfill was replaced by a stiff draining material like LECA or light concrete. Figure 4-6 below, and likewise Figure 2-1, shows the plug with the proposed new design that was subsequently built and tested in DOMPLU. The purpose of the geological and the stiff draining material is to drain the region immediately upstream of the plug, preventing a water pressure build-up prior to the hardening of the cast concrete plug. Use of a geotextile in DOMPLU required that the geotextile, the stiff draining material and the geological draining material needed to undergo performance testing prior to selection of a suitable combination of materials. In total, three types of geological draining materials, two types of stiff draining materials and two types of geotextiles were tested and evaluated by Börgesson et al. (2015a).

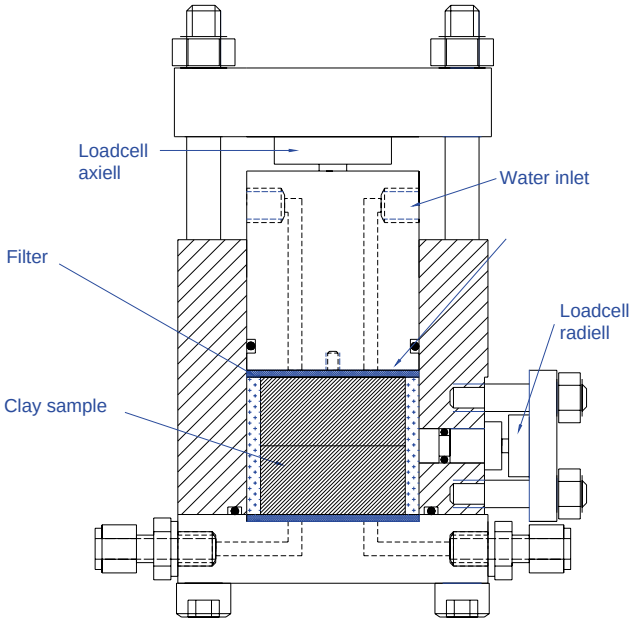

Figure 4-5. *Schematic drawing of the test equipment.*

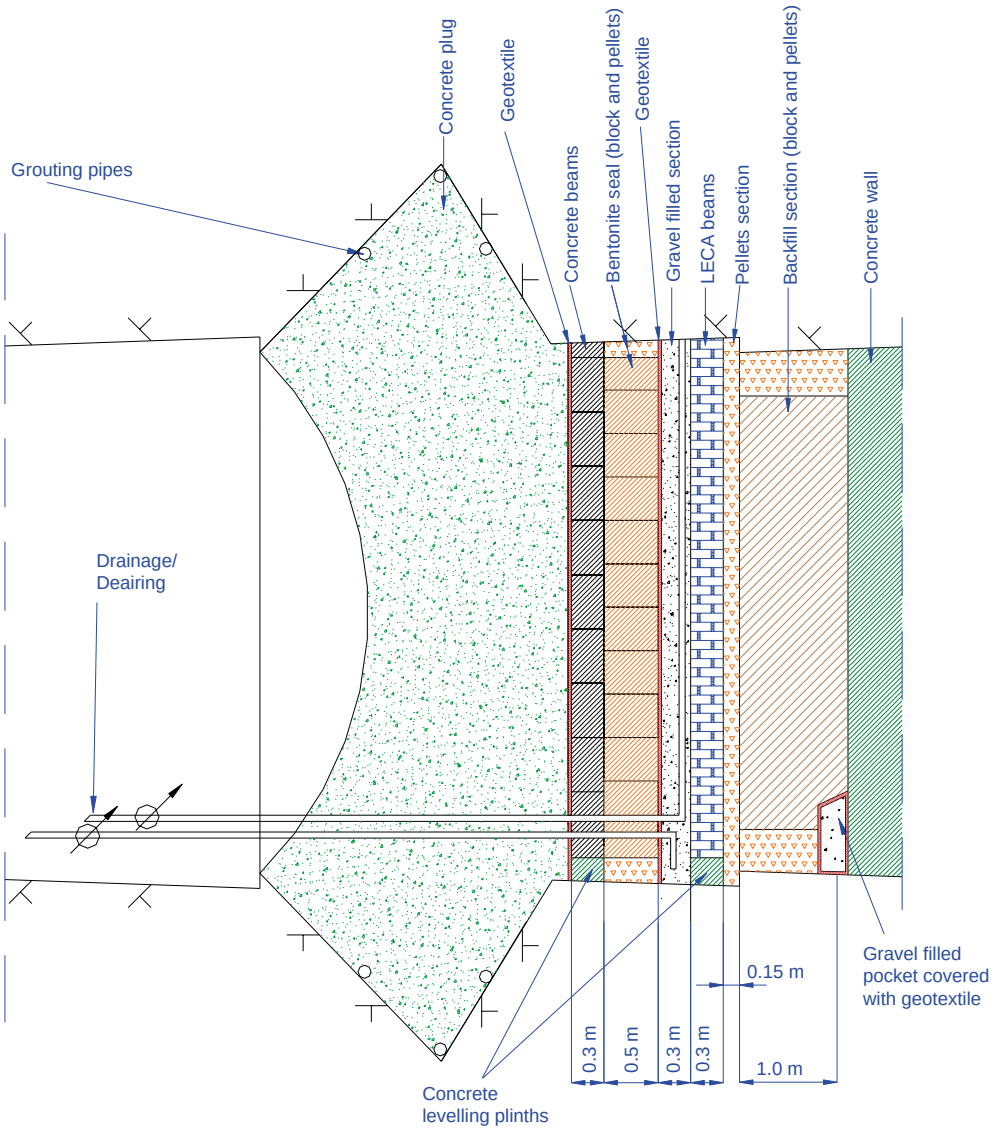

Figure 4-6. *Layout of DOMPLU with its stiff draining material and the geological material that will drain the system to prevent a water pressure build-up on the concrete dome before it has hardened. The bentonite blocks will eventually swell and seal off water flow past the seal. The concrete beams will act as mechanical support.*

The following materials were studied:

Geological draining material – The aim was to investigate three geological (rock) draining materials with different attributes. For example a poorly graded material with high draining ability and a more packable well graded material were suggested. Samples were taken from both a natural sandpit and a stone crusher production site. Three candidates were chosen for detailed evaluation:

- **Natural sand/gravel, 0–4 mm.** A natural sand/gravel material with a grain size distribution 0–4 mm was taken at Skånegrus sandpit in Ilstorp/Sjöbo.
- **MakPak® 0–5 mm.** A combination of gravel < 5mm and stone dust. The product origins from Sydsten AB in Dalby and is described as both packable and draining.
- **Gravel 2–4 mm.** This crushed rock product originates from Sydsten AB, Dalby and was chosen since it was expected to have a very high hydraulic conductivity and also to be self-draining.

Geotextile – Geotextiles were delivered from Svenska Geotech AB in two densities; 1000 and 1200 g/m^2 respectively. The former had a thickness of 5 mm and the latter a thickness of 6 mm. The geotextiles where of needle felted type and made from polypropylene. The product can be used for both material separation and draining purpose and it is also rated as having a high tearing strength.

Stiff draining material – Two types of stiff draining materials were tested:

- **LECA.** Blocks for testing were purchased from Beijer Bygg AB in Lund. These blocks consist of a non-swelling, mechanically stable clay aggregate (LECA) rather than rock aggregate and uses cement as the binding agent. The hydraulic conductivity was expected to be good (high) in this material. During the testing described in this document, a supplier (Nyströms Cement AB in Norrtälje) of LECA-beams with a length up to 6 m was found. The supplier provided some test specimens for additional tests to evaluate their specific product in hydraulic conductivity and compressibility.
- **Light concrete.** Light concrete blocks from Beijer Bygg AB in Lund were purchased for testing. Light concrete consists of cement, sand and limestone and typically has a higher strength but a lower hydraulic conductivity than LECA-blocks.

For the different kinds of materials, several different tests were performed. The test had to be adapted to the tested specimen types. Each test is described by Börgesson et al. (2015a) and is just briefly summarized in coming text. All tests were performed with tap water.

- **Modified Proctor Compaction test (ASTM D1557-12)**. The Proctor compaction test aims to determine the water content of a geological material where the specimen is most packable for a known compactive effort. It was performed by PEAB AB. This test was only made on the geological draining materials.
- **Compressibility (ASTM D4186)**. The compressibility of the specimen was determined using a CRS-test (constant rate of strain). A constant deformation rate was applied to the specimen and load and deformation was logged. The specimen strain (%) was plotted as a function of the vertical stress (kPa). This test was performed on all components.
- **Hydraulic conductivity**. The hydraulic conductivity was tested by applying a constant water head on one side of the specimen and measuring the flow rate through it. The hydraulic conductivity k (m/s) could then be determined assuming applicability of Darcy's law.
- **Clogging test.** To investigate the clogging risks of the draining components a bentonite-water slurry was percolated through the specimen using a constant flow rate. The test was run for 7 days or until the water pressure exceeded the pump capacity of 1 MPa. The result was displayed by transforming the water pressure into hydraulic conductivity and then plotting it as a function of time.

The main conclusions from the performed testing are presented below. A more thorough presentation of the testing and the results is given in Börgesson et al. (2015a). Note that the compressibility and hydraulic conductivity was tested for all materials, while the modified Proctor compaction test was only conducted on the draining geological materials. An important factor for inclusion in the evaluation of the results was the pressure of approximately 2 MPa that the draining materials will be subjected to. The clogging test was performed on all tested materials in order to study if they maintained their ability to drain when exposed to a water flow with a high concentration of bentonite.

Geological draining material

As mentioned above, three different geological draining materials were tested in the study. Initially a modified Proctor compaction test and a CRS-test were performed on the candidates and then the hydraulic conductivity was determined at three different densities. Details regarding the tests completed on the geological draining materials are provided by Börgesson et al. (2015a).

Gravel 2–4 mm was the candidate with the highest hydraulic conductivity. The hydraulic conductivity of gravel 2–4 mm was also very little affected by an increased dry density.

The results from the CRS-tests showed that the MakPak® and natural sand/gravel candidates experienced a significant reduction in hydraulic conductivity as a function of stress for the densities associated with a 2 MPa external confinement. In the hydraulic conductivity tests some significant autogenous settling was observed in MakPak® 0–5 mm and natural sand/gravel 0–4 mm. A special test was performed on gravel 2–4 mm to determine if self-settlement was also an issue for that material but no discernible settling was observed. Gravel 2–4 mm was also superior in its performance in the clogging test. Initially the gravel 2–4 mm material's hydraulic conductivity reduced slightly but over time it seemed to maintain its draining ability.

Details regarding the tests completed on the geological draining materials are provided in Börgesson et al. (2015a).

Geotextile

Two needle-felted geotextile were tested; these are referred to as 1000 g/m^2 and 1200 g/m^2. Firstly a CRS-test was performed and then the hydraulic conductivity was investigated as a function of stress on the geotextiles. Both geotextile qualities behaved similar regarding compressibility and hydraulic conductivity. The hydraulic conductivity was clearly reduced when the stress on the specimen increased. The clogging test indicated that the geotextile's draining ability will be reduced with time and that it should not be used for draining water with eroded bentonite present in it. However it could still function to distribute water if artificial wetting of the system is required.

Stiff draining material

The stiff draining material candidates were lightweight concrete and two LECA products.

The LECA specimens had measured hydraulic conductivity ranging from 1.2×10^{-4} to 1.4×10^{-4} m/s. The compressive strength of the two products examined varied somewhat. The Nyströms LECA had slightly higher compression strength than the Beijer LECA; 2.7–2.8 MPa compared to 2.0–2.5 MPa. However, the test results for the Nyströms LECA differed notably from the manufacturer's specification of a compressive strength of about 4.5 MPa. In the clogging test the LECA showed an initial slight reduction in hydraulic conductivity and its behaviour beyond that indicated that it was likely to be able to maintain its draining ability over an extended time.

The lightweight concrete hydraulic conductivity was determined to be 1.3×10^{-7} m/s. Its compression strength was higher than for LECA, about 5.0–5.5 MPa. In the clogging test the lightweight concrete had an instantaneous pressure buildup in the water supply system and was considered impermeable to the bentonite slurry.

Conclusions

The testing identified gravel, with a grain size of between 2–4 mm as the preferred material for the filter. This candidate is clearly superior in terms of its hydraulic conductivity and also seems to maintain its draining ability when exposed to a water flow with high bentonite content.

The geotextile examined seem to clog when percolated with bentonite-containing water and so should therefore not be used to drain the system. However it could function as a distributer of water if manual wetting of the system is required.

LECA is the superior option for use as a stiff draining material in terms of its hydraulic conductivity and seem to maintain its draining ability when exposed to a water flow with high bentonite content. The main concern is the tested compression strength; laboratory test results did not match the producer's specification. There is however not a current specification regarding this parameter in a tunnel seal. It has been assessed that the strength of the LECA beams should be high enough for the installation process i.e. the beams should be able to withstand the total pressure from behind the beams. There is an obvious risk that they will break later due to the swelling pressure from the bentonite. Pressures high enough to break the beams should not develop in the immediate post-construction period and at later times the consequences of beam breakage will be small if any since the mechanical restraining dome portion of the plug would have cured sufficiently to support the pressures.

4.2 Scale model test

4.2.1 Introduction

As mentioned earlier, the design of the plug system is complex because of its size ~ 5 m length and the number of different components used in its construction. The updated design of the plug shown in Figure 4-6 includes geological and stiff draining materials, a concrete dome plug, a bentonite seal component, concrete beams and a geotextile; all interacting with each other.

As part of a stepwise process of moving towards construction of a full-scale plug and confirming the suitability of proposed materials, a laboratory-scale physical model test was designed and tested. At a radial scale of 1:20, it was used to test the functionality of the components and the overall plug. The

small scale of this test allowed six tests to be undertaken where different components and conditions were imposed. These six laboratory-scale simulation tests were implemented with the following main purposes:

- Demonstrate the function of the draining components (LECA and gravel filter).
- Demonstrate that the bentonite seal can withstand a water pressure of 5MPa without leakage.
- Investigate if a bentonite seal component is needed when using grouted concrete beams.
- Investigate the bentonite sealing function against grouted and non-grouted concrete beams.
- Investigate how the sealing function is influenced by the void space size between the concrete beams.
- Study how fast and how soon a water pressure can be applied to the seal after water filling of the filter.

4.2.2 Experimental design

The goal of this study was to design a tunnel plug test at a scale 1:20. A tunnel with the diameter of 5 meters will then correspond to a model tube with a diameter of 25cm. Geometric constraints made it impractical to scale all the components to 1:20 in axial (length) dimension and therefore the axial scale was set to 1:10 instead. The test equipment used consisted of a steel cylinder with a diameter of 25 cm and its interior walls are chamfered to simulate the tunnel wall friction. Four windows were installed in the cylinder to allow for visual observation of the test. Load cells were also installed in both axial and radial directions to allow for measurement of load and calculation of the total pressure. A total of four 6 mm Swagelok-connections were used for wetting, pressurization and drainage of the system.

The inflow rates used in the test were volumetrically scaled i.e. an inflow rate of 4 l/min in full scale corresponds to 0.001 l/min in the scale test.

The assembled equipment is seen in the upper photograph provided as Figure 4-7. In the uppermost photo the observation windows, the Swagelok connections and the radial pressure transducers are all visible. The chamfered interior of the steel tube (that simulates the deposition tunnel walls) is seen on the lower right. The axial load cells can be seen between the restraint cap and the cell body in the bottom left photo of Figure 4-7.

Figure 4-8 shows a cross section sketch of the test. The axial load cells (1) are held in place by a steel plate (2) in each end of the tube. The steel plates are fixed by screws to hold all components positioned in axial direction. Two radial load cells (3) are placed towards the backfill and two are placed towards the bentonite seal. On both sides inside of the axial load cells there is a PVC plate piston (4). On the backfill side the PVC plate piston is sealed with an O-ring (6) to prevent water leakage in that direction. On the plug side the PVC plate piston has no O-ring. The PVC plate piston diameter is 249 mm (compared to the tube diameter 250 mm) and the slot that emerges represents a non-hardened concrete dome that allows for leakage or piping if exposed to a water pressure build-up. The windows (5) are placed so that bentonite sealing, geotextile, gravel, LECA and backfill can be observed from the outside. The Swagelok connections are placed in the sections marked “I”. Two connections, one at the top and one at the bottom, are placed in contact with the gravel filter for draining and pressurization. The other two are connected at the top and bottom of the backfill to simulate the tunnel flow.

4.2.3 Preparation and installation of components

This section describes the preparation and installation of each component. The test equipment was placed standing up with the concrete plug end downwards. All figures in this section are found in Börgesson et al. (2015a).

Figure 4-9 shows the PVC plate piston that represents the concrete plug. This was the first component to be emplaced in the test equipment.

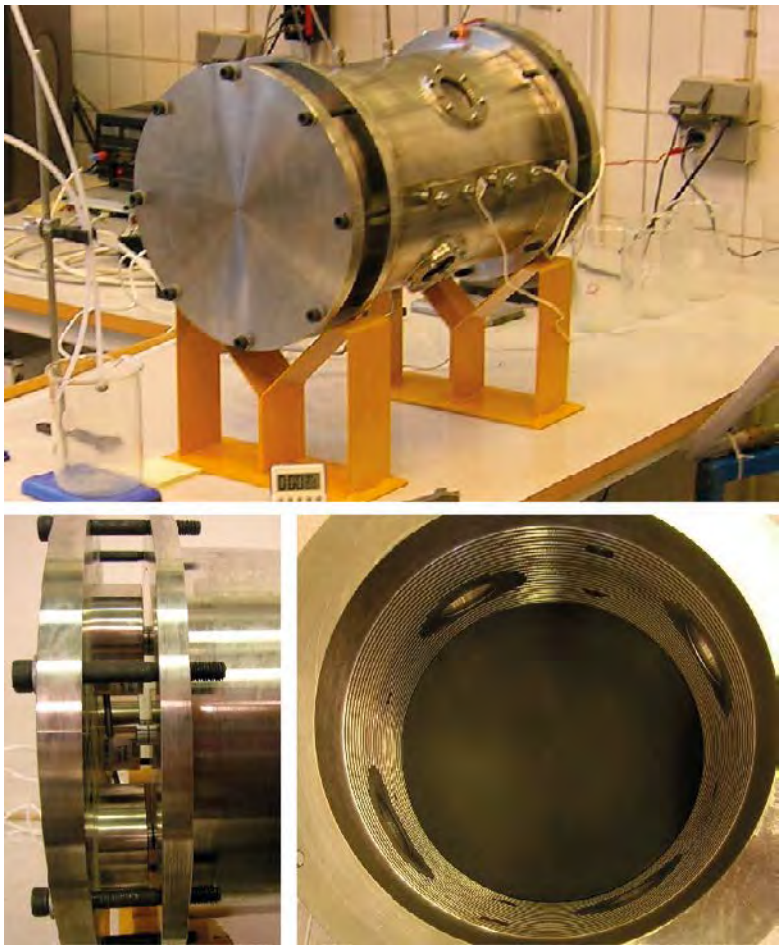

Figure 4-7. *The DOMPLU scale model test equipment, from Börgesson et al. (2015a).*

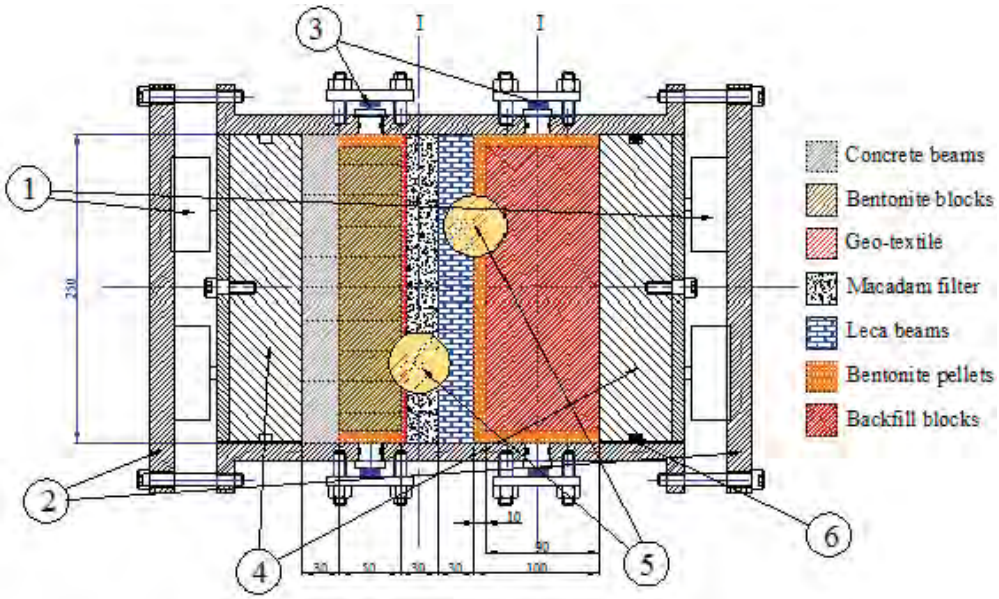

Figure 4-8. *Cross section of the scale model used for testing. The different components are explained by the legend above. The axial load cells (1) are held in place by steel plates (2). Radial load cells (3) are placed on the bentonite sealing and the backfill. There is a PVC plate piston (4) on each side of the components. The PVC plate piston to the left is slightly smaller than the tube and represents a non-hardened concrete dome that allows for leakage. The PVC plate piston to the right is sealed with an O-ring (6) to prevent water from leaking in that direction. On each side of the tube there are two windows (5) showing bentonite sealing, geotextile, gravel (macadam), LECA and backfill. From Börgesson et al. (2015a).*

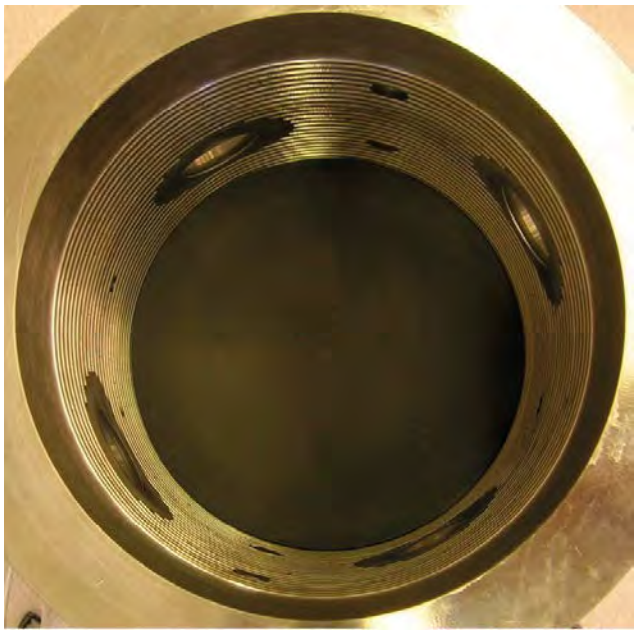

Figure 4-9. *The PVC plate piston that represents the concrete plug was the first component to be emplaced in the test equipment.*

Concrete beams

Concrete was cast as four beams using a standard cement mortar with product name “Weber cementbruk A”. The beams were made approximately 30 mm thick. After hardening, about 48 hours, the beams were carefully shaped to fit the tube. Figure 4-10 shows the beams installed in the test equipment.

Bentonite seal

MX-80 bentonite was used for the manufacturing of sealing blocks. MX-80 is a high-grade sodium bentonite from American Colloid Company (Wyoming, USA) with a montmorillonite content of ~ 80 %. The bentonite seal blocks were cut from a larger block. The sealing component consisted of 16 small blocks and had an assembled diameter of 230 mm and a thickness of 50 mm. The blocks were surrounded by a 10 mm slot filled with MX-80 pellets produced by extrusion technique. Figure 4-11 shows the seal installed in the test equipment. The dry density of the blocks varied slightly (1790–1810 kg/m^3), but this will not influence their performance This block density was used since a number of large blocks were already manufactured and available for use.

Geotextile

The tests of the geotextile described above were performed using materials with two different densities; 1000 and 1200 g/m^2. A needle felted geotextile from Svenska Geotech AB, with a density of 1000 g/m^2, was used in the scale test. Both qualities tested fulfilled the requirements and the 1000 g/m^2 quality was used since the smaller thickness facilitated the handling. However, it was not possible to scale this component in the cell’s axial direction. Figure 4-12 shows the geotextile cut to a diameter of 250 mm and placed in the test equipment.

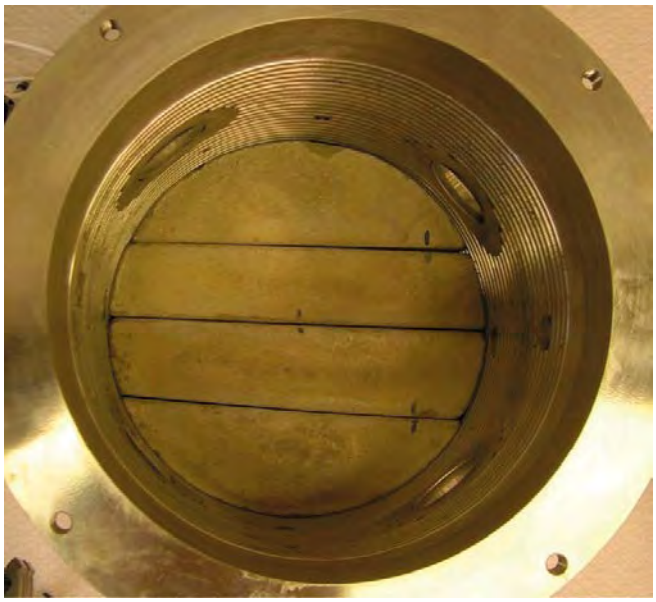

Figure 4-10. *Four concrete beams were cast using a standard cement mortar.*

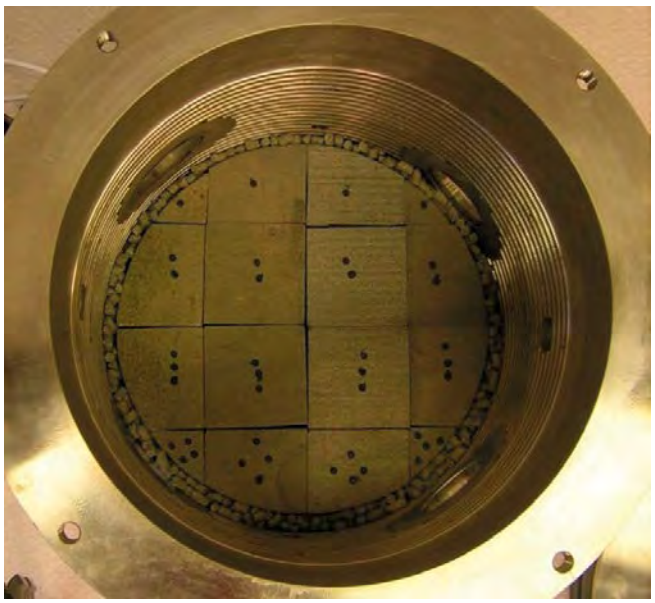

Figure 4-11. *The bentonite sealing was made out of 16 MX-80 blocks and had a diameter of 230 mm and a thickness of 50 mm. The blocks were surrounded by a 10 mm wide, pellet filled slot.*

Gravel filter

A 30 mm thick layer of 2–4 mm gravel (crushed rock from Dalby production site) was placed on top of the geotextile. The gravel was taken from the AB Sydsten production site in Dalby. Figure 4-13 shows the gravel emplaced in the test equipment.

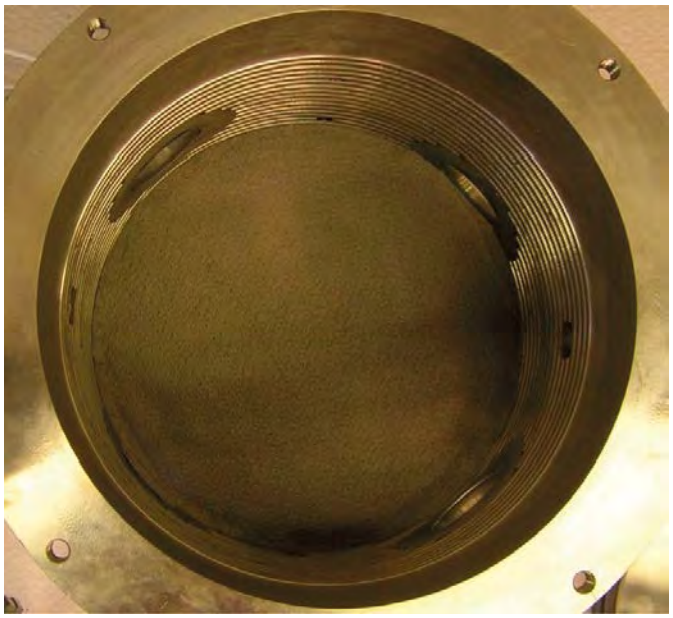

Figure 4-12. *The geotextile cut to a diameter of 250 mm and placed in the test equipment.*

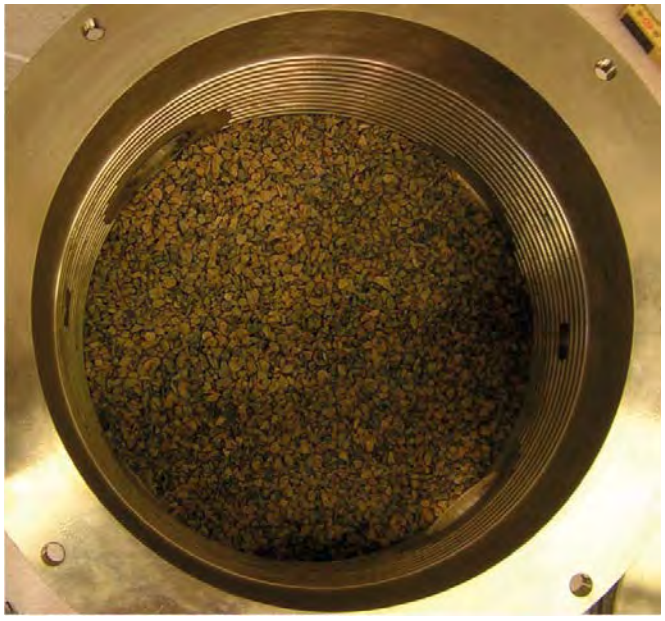

Figure 4-13. *The 30 mm layer of 2–4 mm gravel from AB Sydsten emplaced in the test equipment.*

LECA beam filter

A standard LECA block was cut to produce four beams, each with a thickness of 30 mm. The beams were then carefully shaped to fit the tube. Figure 4-14 shows the LECA beams emplaced in the test equipment.

Bentonite pellets

Due to the dimensional limitations of the pellet layer and slots in this scaled test setup, extruded rod-shaped pellet material was used instead of the more densely compacted pillow-shaped pellets proposed for use in the full-scale construction. The bentonite pellets used in the scale test were manufactured using an extrusion technique where moisture-conditioned MX-80 bentonite was pushed through a matrix. The product is a rod shaped pellet with a diameter of 6 mm and a length

of 16–22 mm. Details on the manufacturing technique can be found in the reports by Dixon et al. (2011) and Andersson and Sandén (2012).

The pellets were used both as a cross sectional layer between the backfill blocks and the LECA beams and to fill the outer slot around the backfill and bentonite sealing blocks (as seen in Figures 4-15 and 4-16).

The small size of the test cell meant that the as-built bentonite pellets were too large for use. Prior to their installation, the pellets were therefore crushed with a rubber hammer and all fines less than 4 mm were separated. This was to reduce the pellet rod length and thereby improve the as-placed pellet density in the relatively thin slots. Figure 4-15 shows the pellet layer between the backfill and the LECA beams.

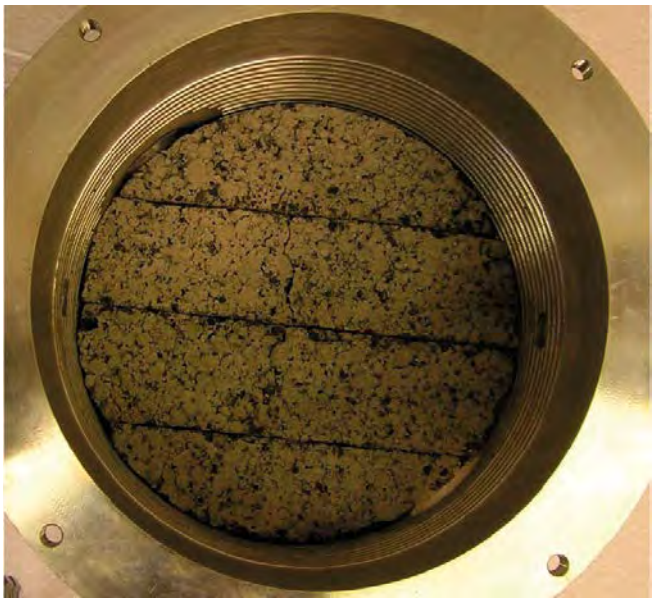

Figure 4-14. *The four 30 mm thick LECA beams emplaced in the test equipment.*

Figure 4-15. *The 10 mm – thick pellet layer between the backfill and the LECA beams. Rod shaped MX-80 bentonite pellets with a diameter of 6 mm were used.*

In this scale-test, the pellet-filled layer was 10 mm thick (Figure 4-15) and the slots between the bentonite seal (Figure 4-11) and the backfill component (Figure 4-16) were of 10 mm dimension, which was considered the smallest acceptable dimension for this scale of test.

Backfill blocks

IBECO bentonite from the island Milos, Greece, was used to manufacture backfill blocks for the scale model test. IBECO is one of the two backfill candidate materials that were investigated by Sandén et al. (2014). The other material investigated came from Ashapura (ASHA), India. At the time for the performance of the scale tests of the plug system, IBECO was believed to be the most promising material. This was, however, later changed to ASHA and this is the reason for why the scale tests were performed with IBECO and later the full scale test with ASHA. The influence of the choice of material for the scale test is believed to be of minor importance for the performance of the tests.

The IBECO material is described by the supplier as a natural calcium bentonite with medium montmorillonite content, i.e. it has not been activated or treated in any other way. The blocks were prepared in the same way as the MX80 bentonite blocks. Two 50 mm thick layers consisting of 16 blocks each were made with a diameter of 230 mm. Figure 4-16 shows the emplaced backfill blocks and the surrounding crushed MX-80 extruded pellets.

Water

All tests except Test 1 were performed with tap water mixed to 1 % salinity by weight ($NaCl/CaCl_2$, 50/50). The salinity is equivalent to the expected formation water at Äspö HRL. Test 1 was performed with tap water.

4.2.4 Test procedure

A detailed description of each test performed can be found in Börgesson et al. (2015a). The procedure used in each test varied slightly but these main phases were included in all six tests:

- **Draining/filling phase**

  A constant rate of inflow from the dosing pump was applied into the backfill through the bottom Swagelok connection. This flow represented a volumetrically scaled deposition tunnel base flow. The draining function of the filter was tested by allowing the flow to run out through the filter bottom Swagelok connection. Finally the system was filled by closing the bottom filter Swagelok connection and keeping the top filter Swagelok connection open for air venting. In some of the tests the filter was instantly filled and the draining was done through the top Swagelok connection. The theoretical available volume in the gravel filter, LECA filter and macro voids in the pellet fillings is 1.49 liters. For a complete saturation of the system an additional 2.44 liters is needed.

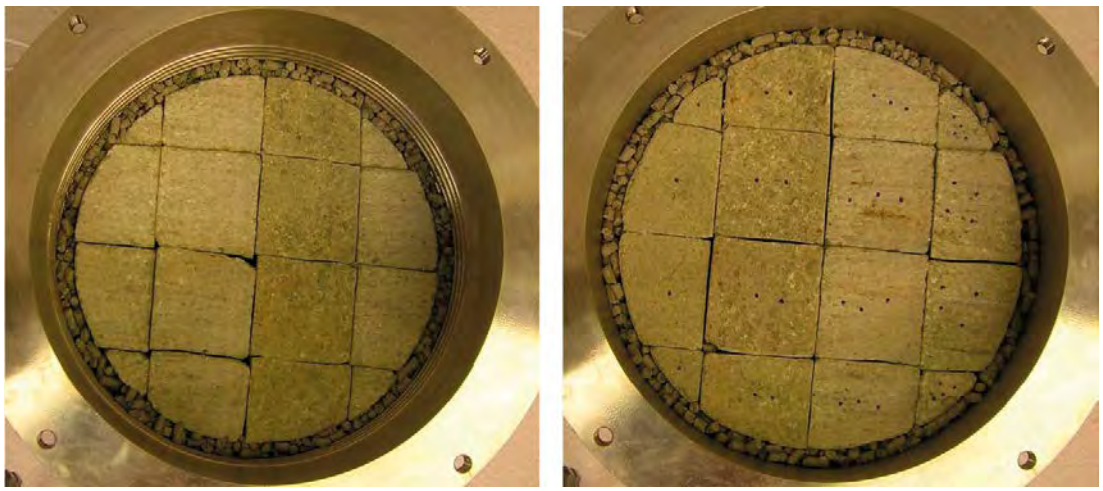

Figure 4-16. *The two 50 mm thick layers of backfill blocks emplaced in the test equipment. The blocks were made of IBECO bentonite from Milos, Greece.*

- **Pressurizing phase**

  In this phase different strategies were tested to pressurize the filter and test the sealing function of the bentonite seal. The GDS (Advanced Pressure/Volume Controller) pressurizing device was used for both constant pressure and pressure elevation steps to test the sealing function of the design.

- **Flow monitoring**

  Water inflow during the drainage period was made with a metering pump giving a constant inflow to the test. The outflows during the drainage period were measured manually by collecting water in a vessel and then weighing it. During the pressurizing period the inflow rate was monitored continuously.

4.2.5 Results from the testing

This section summarises the objectives, results and conclusions from the testing using the scale model. A more thoroughly presentation of the results and conclusions can be found in Börgesson et al. (2015a).

Test 1

In the first test the main goal was to show that all components could be prepared and installed properly in the test equipment and then that the basic design, the test equipment and the data logging system were all working satisfactorily. Tap water was used at a flow rate of 0.001 l/min during the filling and drainage phase.

The main conclusions of Test 1 were that the components could be installed properly and the test equipment and data logging system worked satisfactorily. The draining function of the design was working well and the components were kept in position and were separated from each other as planned. Based on this, testing was extended into the subsequently examined geometries and boundary conditions (Test 2–Test 6).

Test 2

In Test 2 the water flow rate was increased from 0.001 l/min to 0.005 l/min. The test focused on investigating erosion in the draining phase and to make a more extensive density distribution analysis of the bentonite sealing component. It was also the first test performed with 1 % water salinity.

It was shown in Test 2 that the draining function was also working well at 0.005 l/min and with 1 % water salinity. In general, the erosion rate was less than 1g/l in the drainage outflow, which is considered low. The origin of the eroded material is believed to be from the pellet surrounding the backfill blocks. By the time of test dismantling, small amounts of backfill bentonite were found in the filter section. The bentonite intrusion had occurred between the LECA-beams and the windows, probably due to a tiny construction gap.

Test 3

In Test 3, a 0.005 l/min flow rate and 1 % water salinity was used. The main objective in the test was to reach 5 MPa of water pressure across the seal. During the preparation for Test 3, the concrete beams were carefully fitted to minimize the void spaces between them. The largest gaps were measured to be approximately 0.80 mm. The pressure elevation ramping rate was set to 50 kPa/h instead of 100 kPa/h. The filter was filled directly to give the bentonite seal access to water from start. Also the axial expansion of the bentonite seal was measured.

Test 3 reached 5 MPa on day 14. The evaluation suggests that the sealing ability was improved by the smaller void spaces between the concrete beams, by giving the sealing component access to water early and by using a reduced pressure elevation ramping rate. The dry density in the outermost part of the seal was similar to Test 2, but the radial total pressures were surprisingly low by the start of the final ramp. The axial expansion in the seal was about 6–7 mm which corresponds to 12–14 %.

Test 4

The main feature of Test 4 was to use concrete beams that were cast in cement to minimize the void space between them as much as possible. This was investigated in two tests; 4A and 4B.

In Test 4A no bentonite sealing component was installed, only the cement cast concrete beams were used. There was water leakage around the cast concrete beams almost instantly at a water pressure of about 30–35 kPa.

Test 4B was fully prepared with all components and performed according to the normal routine but with a slightly more aggressive approach. The filling and drainage period was only 20 hours. An aggressive pressurization strategy was applied with repeated ramping at 100 kPa/h initiated from test start. After only 3 days, a water pressure of 2 MPa was reached, but leakage then occurred through the seal. After this leakage it was hard to recover the water pressure to the same level as before the start of leakage, but around day 11 the final pressure elevation ramp was initiated. 4.5 MPa water pressure was reached on day 14 and the sealing seemed to have healed again. It is suggested that molding of the concrete beams improves the sealing ability, mainly based on the results from the early part of the test. The short filling and draining period and the 100 kPa/h hydraulic pressure ramping does not seem to favor the sealing function.

Test 5

The strategy of Test 5 was to manually apply the hydraulic pressure steps as larger, instantaneous increments. The test also aimed to provide additional information on the influence of large void spaces between the concrete beams (1–2 mm in the largest gaps).

By 500 kPa hydraulic pressure (6 days of testing), there was leakage through the seal. When compared to Test 4B, which was reaching 2 MPa after 3 days, it was suggested that the difference was related to the large voids between the concrete beams in Test 5. Around day 10 there was a leakage in an observation window at 1500 kPa (no leakage through seal) and the water pressure was lowered and the window was sealed. When quickly raising the water pressure back to 1500 kPa, water leakage started through the seal. It thereby seems important not to increase the water pressure on the seal too quickly, even if it previously could withstand a high water pressure. The radial pressure and dry density of the sealing were in the same order of magnitude as previous tests.

Test 6

Test 6 was performed with a similar manually-applied pressurization method as in Test 5. The void spaces between the concrete beams were somewhat larger than Test 5. The test encountered some complications (a power outage and GDS leakage events), but these are not considered to have affected the results significantly, excepting that all data from the force transducers up to day 21 was lost.

The water pressure was elevated very gradually (50–100 kPa/h) in the beginning but leakage was observed at 300 kPa after less than 3 days of test operation. This is likely because of the large voids between the concrete beams and also a low water uptake in the drainage and filling phase. Only 1.12 liters was taken into the cell in this phase and that is about half the volume taken up in Test 4B and 5. On day 22 of testing, the water pressure reached 5 MPa. After this the test was kept running and the pressure held constant at 5 MPa for an additional 54 days before dismantling. At dismantling it was clearly seen that the bentonite had swelled into the voids between the concrete beams. This indicates that open void spaces can be efficiently filled with bentonite in the homogenization process. Despite the bentonite sealing being below 5 MPa of water pressure for an additional 54 days the density homogenization process does not seem to have progressed any further.

4.2.6 Conclusions from the scale model test

The combined main conclusions from the tests were as follows;

- The test components interacted as desired and the different materials were successfully separated from each other. However, in some tests the LECA-beams were loosely fitted into the equipment and backfill bentonite then managed to intrude into the gravel filter.

- The draining function of the filter worked satisfactorily at both 0.001 and 0.005 l/min.
- The erosion is not considered significant. The amount of eroded material was about 1 g/l or less, which is in the lower region of the erosion prediction model by Sandén and Börgesson (2010).
- The bentonite seal could successfully withstand 5 MPa of water pressure in all tests were it was tested.
- The size of the void spaces between the concrete beams seems to be of importance for the sealing ability. Casting/grouting of the concrete beams to minimize the void spaces seem to improve the sealing function. The bentonite seal is however still crucial for the sealing ability.
- Giving the bentonite seal passive access to water early seems to improve the sealing function significantly.
- In general the 100 kPa/h pressure elevation ramp seems too aggressive. The 50 kPa/h pressure elevation ramp was more successful in raising the pressure without leakage.
- Returning the water pressure to a previously attained higher pressure level must be done carefully to avoid leakage.
- In the tests where 5 MPa of water pressure was reached, the radial total pressure ranged from 750–1400 kPa when the pressure ramping was started (contribution from 500 kPa water pressure included).
- In the tests where 5 MPa of water pressure was reached, the dry densities in the outermost parts of the sealing ranged from 1250–1350 kg/m^3 at time of dismantling.
- The water filling of the filter should be controlled regarding available volume and the volume of the injected water. In one of the tests (Test 6), the injected water volume was approximately 30 % lower than the available volume of the filter and macro voids of the pellet filling, and this seemed to have delayed the bentonite swelling and the following seal.

Recommendations and impact on the full scale test

Based on the conclusions from the scale model testing, a number of important recommendations were suggested for the DOMPLU design including the pressurization program in the field. These recommendations are listed below together with some comments on how they were further handled:

- The draining function of the filter worked well. Thus, drainage of the DOMPLU filter should be tested for the maximum accepted water inflow rate into a deposition tunnel, which at present is set to 5 l/min.
- The erosion during the drainage period should be determined and evaluated to confirm that it is within an acceptable range.
- The size of the void spaces in-between concrete beams and between concrete beams and tunnel wall should be minimized for maximum sealing function. Filling voids with mortar was thus introduced in the delimiter design.
- The filter should be filled up with water early to give the bentonite seal access to water as soon as possible.
- The water pressure elevation should be done carefully to avoid piping through the seal. If the water pressure needs to be reduced for some reason, the re-pressurization needs to be carefully performed as well. It was observed in the scale model tests that a radial swelling pressure of 250 kPa seemed to be necessary for the seal to withstand a ramping of 50 kPa/h that finally reached 5 MPa.

5 Testing of the concrete B200 mix

The results summarized in the report can be divided into four categories: hardened concrete properties; shrinkage; creep; and interaction between concrete and rock. These results will contribute to improve numerical modelling of the structural behaviour of the concrete plug prior to and under loading, in order to analyse among others the effects of the pressure on deformations, cracking and water tightness of the concrete dome plug.

A concrete mix, for a low-pH self-compacting concrete, has been developed specifically for the purpose of use in the Spent Fuel Repository. Details regarding the concrete mix and corresponding material testing is found in Vogt et al. (2009). The mix composition of the low pH concrete, denoted as B200 in Vogt et al. (2009), is as shown in Table 5-1.

Table 5-1. Mix composition of the B200 low pH self-compacting concrete.

Constituent	Amount (kg/m^3)
CEM I 42.5 MH/SR/LA	120
Silica fume (densified)	80
Water	165
Limestone filler L25	369
Sand 0–8 mm (65 % of aggregates)	1037
Gravel 8–16 mm (35 % of aggregates)	558
Glenium 51	6.38
Water/cement	1.375
Water/binder	0.825
Water/powder	0.29

One difference between the concrete mix developed in Vogt et al. (2009), and the concrete mix used for the full-scale test is that a slurry of microsilica has been used in order to improve the workability and the disperse properties of the concrete. The mixing order at the concrete factory is as follows:

- Add silica slurry and water (save approximately 6 liters per batch à 3 m^3 as feed water).
- Add cement, sand and gravel.
- Mix 30 seconds and add limestone filler.
- Add 50 % of Glenium 51 and mix for 60 seconds.
- Add remaining 50 % of Glenium 51 and mix at least 180–240 seconds until the concrete is homogeneous.

Extensive testing has been performed to verify that the concrete mix has the desired material properties. In this chapter, both additional laboratory testing and the concrete testing at casting are presented, in Section 5.2 and Section 5.3 respectively.

5.1 Testing of hardened concrete properties

Testing of the hardened concrete properties has been performed in connection to the concrete casts made on site, at the concrete factory and in laboratories in connection with other tests. This section summarizes all tests performed on the hardened concrete properties. The presentation given in this section is based on a report by Magnusson and Mathern (2015). The purpose of these measurements was primarily to obtain more information regarding the behaviour of the low-pH concrete mix B200. The results from these experiments provide valuable input to the numerical models and for prediction of the behaviour of the concrete dome plug.

Three different large-scale concrete casts were made on site at the Äspö Hard Rock Laboratory. The first cast included a 4 × 2 × 2 m box shaped concrete block, while the second cast consisted of the back-wall of the DOMPLU experimental tunnel. The third and last cast, was the full-scale arc-shaped concrete dome which forms one of the principal components of the plug system. All casts were performed with concrete produced at Swerock's concrete plant in Kalmar according to the mix and mixing order presented above. In addition to these large-scale tests, additional laboratory test series have been performed intended to study isolated effects such as creep and bond between concrete and rock. A summary of the hardened concrete tests is provided in Table 5-2.

Table 5-2. Summary of performed testing and references to relevant documentation.

Test series	Casting conditions	Tested properties	Documentation
4 × 2 × 2 m concrete specimen	Concrete plant / On site	Compression / Splitting	Magnusson and Mathern (2015)
Tunnel back-wall of concrete	Concrete plant / On site	Compression	Magnusson and Mathern (2015)
Dome plug and concrete monolith	Concrete plant / On site	Compression / Splitting/ Elastic modulus	Magnusson and Mathern (2015)
Creep testing	Laboratory	Compression	Flansbjer and Magnusson. (2014a) and Magnusson and Mathern (2015)
Rock-concrete interface testing	Laboratory	Compression / Splitting / Direct tensile test / Fracture energy	Flansbjer and Magnusson (2014b) and Magnusson and Mathern (2015)

5.1.1 On site and factory testing

Concrete specimen

As mentioned above, the first casting performed on site at the Äspö Hard Rock Laboratory was a 4 × 2 × 2 m box shaped concrete block. The main purpose of this large-scale test was to make a practice run regarding a full-scale casting including logistics. In total, three lorry loads of concrete were required to complete the casting. Each lorry load consisted of two separate concrete batches produced at the concrete plant in Kalmar. From each batch of concrete produced, four concrete cubes were cast at the factory; the dimensions of the cubes were 150 × 150 × 150 mm. The compressive and tensile splitting strength of the concrete was then tested at a concrete age of 28 and 90 days. In addition to the concrete cubes cast at the factory, three cubes from each lorry load were cast on site with the same dimensions as in the factory. The first cube was cast immediately on arrival, the second in the middle of the load and the third at the end of the load. After 28 days of curing, the compressive strength of the concrete was tested. The results from the testing are summarized in Table 5-3 and Table 5-4. As it can be seen from the results, the strength from this test is significantly higher than all other experiments, where the cylinder compressive strength after 28 days is 68 MPa compared to about 40 MPa in the other tests. One explanation for this could be that some modifications had been made to the mix where a silica-slurry was used instead which could have improved the dispersion properties.

Table 5-3. Summary of the results from the testing performed at the concrete plant in Kalmar. The values shown are mean values while the standard deviation is given in brackets. From Magnusson and Mathern (2015).

Age [Days]	f_{cm}, cube [MPa]	Density [kg/m^3]	$f_{tm, sp}$ [MPa]	Density [kg/m^3]
28	68.0	2358	5.8	2383
	(13.9)	(35)	(0.7)	(43)
90	86.5	2345	6.4	2362
	(13.1)	(39)	(0.4)	(29)
$f_{90\ days}$ / $f_{28\ days}$	1.27		1.10	

Table 5-4. Summary of the results from the testing performed on site at the Äspö Hard Rock Laboratory. The values shown are mean values while the standard deviation is given in brackets. From Magnusson and Mathern (2015).

Age [Days]	f_{cm}, cube [MPa]	Density [kg/m^3]
28	60.7	2326
	(10.1)	(22)

Concrete back-wall

The back-wall of the tunnel was cast on June 20th, 2012. In total, three lorry loads of concrete were required to complete the casting of the 0.8 m thick concrete wall. The purpose of the concrete back-wall and the civil works performed are described in Section 6.1. In parallel to the casting of the back-wall, four concrete cubes with a dimension of 150 × 150 × 150 mm were cast to test the compressive strength of the concrete. Three of the cubes were cast at the concrete plant, one from each lorry load, and one cube was cast on site at the Äspö Hard Rock Laboratory using the concrete delivered in the third lorry load. All cubes were allowed to cure in water until the testing was performed 28 days later. The purpose of these tests was to verify that the concrete correspond to the expected values. The results from the testing are presented in Table 5-5.

Table 5-5. Summary of test results. Mean values are presented for the concrete plant testing, with standard deviations in brackets. From Magnusson and Mathern (2015).

Concrete plant			Äspö Hard Rock Laboratory	
Age [Days]	f_{cm}, cube [MPa]	Density [kg/m^3]	f_{cm}, cube [MPa]	Density [kg/m^3]
28	40.5	2347	29.5	2390
	(8.4)	(42)	–	–

Concrete dome plug

The concrete dome plug was cast on March 13th, 2013. The total volume required to complete the cast was 93 m^3, which corresponds to 13 lorry loads of concrete. This full-scale casting of the concrete dome is described in Section 6.6. From every two lorry loads, six concrete cubes were cast on site and at the concrete plant in Kalmar, i.e. a total of 12 cubes each with a dimension of 150 × 150 × 150 mm. The cubes were cast for all odd numbered lorry loads, i.e. for seven loads.

The compressive and tensile splitting strength of the concrete were tested after 7, 28 and 90 days at both the concrete plant and the laboratory. The results from the testing are presented and summarized in Table 5-6 and Table 5-7. Note that the presented values are mean values from the seven lorry loads and that the standard deviation is given in brackets.

Table 5-6. Summary of test results from the casting of the concrete dome plug. The values presented are mean values while the standard deviation is given in brackets. From Magnusson and Mathern (2015).

Property	Unit	Specimen	Origin	Age [days]		
				7	28	90
$f_{cm,cube}$	[MPa]	cube 150 × 150 × 150	Concrete plant	17,7 (1,3)	40,3 (2,0)	55,9 (3,0)
$f_{tm,sp,cube}$	[MPa]	cube 150 × 150 × 150	Concrete plant	2,15 (0,1)	4,13 (0,1)	5,09 (0,3)
$f_{cm,cube}$	[MPa]	cube 150 × 150 × 150	Äspö HRL	19,6 (0,9)	42,5 (2,0)	58,0 (3,5)
$f_{tm,sp,cube}$	[MPa]	cube 150 × 150 × 150	Äspö HRL	2,26 (0,1)	4,33 (0,2)	5,56 (0,2)

Table 5-7. Comparison of compressive and tensile splitting strength at different concrete ages. From Magnusson and Mathern (2015).

	Concrete plant		Äspö HRL	
	$f_{cm,cube}$	$f_{tm,sp}$	$f_{cm,cube}$	$f_{tm,sp}$
$f_{7\ days}$ / $f_{28\ days}$	0,44	0,52	0,46	0,52
$f_{28\ days}$ / $f_{28\ days}$	1,00	1,00	1,00	1,00
$f_{90\ days}$ / $f_{28\ days}$	1,39	1,23	1,36	1,28

A comparison of the obtained compressive and tensile splitting strength at the concrete plant and at the Äspö Hard Rock Laboratory is shown in Figure 5-1 and Figure 5-2, respectively. The vertical axis represents the strength obtained from the specimens tested on-site and the horizontal axis represents the strength for specimens tested at the concrete plant. The ideal case, where the tests at both locations show the same strength is illustrated with a red dashed line. The measured strength obtained at an age of 7, 28 and 90 days is shown with squares. Based on the measured values, a trend line has been calculated and is shown as a solid black line.

As can be seen in these two figures, the compressive and tensile splitting strengths do not differ significantly between the two locations of testing. This indicates that the two hour transportation, from the concrete plant in Kalmar to Äspö Hard Rock Laboratory, does not influence the strength of the concrete.

Concrete monolith

In connection to the casting of the concrete dome, a monolith was cast in close proximity to the dome plug using the same type of concrete. The dimensions of the monolith were 2 × 1.4 × 1.5 m. The purpose was to provide a reference concrete sample for measurements of concrete compressive and tensile splitting strength.

At different concrete ages, ranging from 28 to 1095 days, vertical and horizontal concrete cores with a diameter of 100 mm and a length of 1000 mm were drilled from the monolith. Immediately after drilling, the concrete cores were covered in a plastic film. These cores were then cut into specimens with a length of either 100 mm or 200 mm and stored in water with a temperature of 20°C until they were tested.

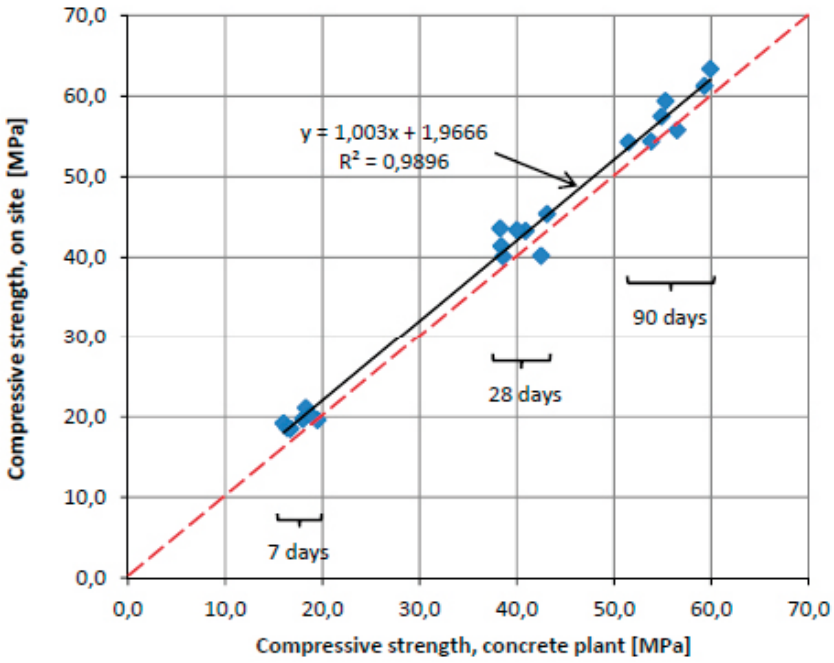

Figure 5-1. *Comparison of compressive strength obtained at the concrete plant and at the Äspö Hard Rock Laboratory. From Magnusson and Mathern (2015).*

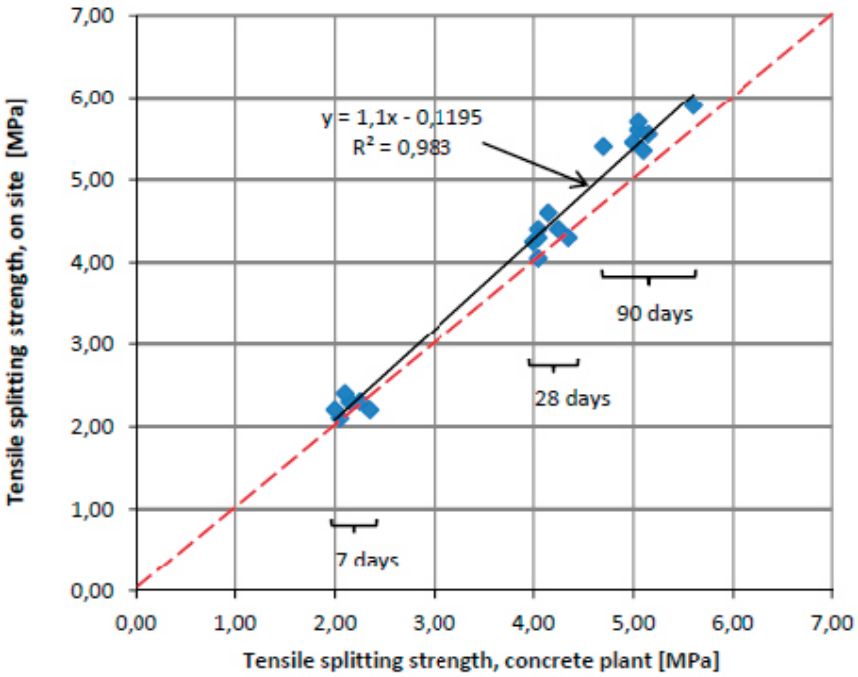

Figure 5-2. *Comparison of tensile splitting strength obtained at the concrete plant and at the Äspö Hard Rock Laboratory. From Magnusson and Mathern (2015).*

The compressive strength was tested for short and long cores drilled in both vertical and horizontal direction while only short horizontal cores were tested to determine the concrete splitting strength. The elastic modulus of the concrete was tested for long cores drilled in both vertical and horizontal direction. The results from the tests are presented in Table 5-8, note that the presented values are mean values based on three specimens.

Table 5-8. Summary of the test results from the drilled cores in the monolith. The values shown are mean values while standard deviations are given in brackets. From Magnusson and Mathern (2015).

Property	Unit	Specimen	Age [days]				
			28	90	135	182	377
$f_{cm,core}$	[MPa]	core ∅100 × 100 (horizontal)	40.2 (1.4)	62.6 (1.9)	64.0 (3.1)	68.9 (2.7)	73.8 (0.9)
$f_{cm,core}$	[MPa]	core ∅100 × 100 (vertical)	40.5 (0.8)	62.0[1)] (1.0)	–	–	74.6 (1.6)
$f_{cm,core}$	[MPa]	core ∅100 × 200 (horizontal)	39.8 (3.1)	58.7 (4.3)	–	–	67.3 (6.1)
$f_{cm,core}$	[MPa]	core ∅100 × 200 (vertical)	41.7 (1.3)	61.9 (1.4)	–	–	73.2 (2.8)
$f_{tm,sp,core}$	[MPa]	core ∅100 × 100 (horizontal)	4.20 (0.15)	5.23 (0.12)	5.23 (0.15)	5.97 (0.15)	6.28 (0.10)
$E_{cm,core}$	[MPa]	core ∅100 × 200 (horizontal)	–	29.8 (2.4)	–	–	30.8 (2.0)
$E_{cm,core}$	[MPa]	core ∅100 × 200 (vertical)	–	30.2 (0.6)	–	–	31.6 (1.5)

1) Based on 4 specimens.

Concluding remarks

Figure 5-3 shows a comparison of the obtained compressive strength of the concrete cubes cast at the concrete plant in Kalmar and on site at the Äspö Hard Rock Laboratory. For those lorry loads where more than one cube was tested, the average value is shown in the figure.

As can be seen in the figure, the obtained compressive strength corresponds well between the two locations of testing. This provides further evidence that the concrete is not affected significantly by the two-hour transportation from the concrete plant to the site.

5.1.2 Laboratory testing

In connection to the creep and the rock-concrete interface tests, discussed in Section 5.2, some hardened concrete properties were also tested. This section describes and summarizes these tests. One purpose of these tests was to take reference samples to make sure that the behaviour of the concrete used corresponded to the expected behaviour. The main purpose was, however, to make sure that the load subjected to the creep samples was in line with the desired stress level and to be able to correlate the development of bond strength with the strength development of concrete.

Hardened concrete properties tested during the creep tests

During the creep testing of the concrete, some hardened compressive concrete property tests were also conducted. The tests performed aimed to determine the stress levels to be used in the creep tests, the strength development with time, the effects of different storage conditions and the stress-strain relationship of the concrete in compression. A more thorough description and presentation of the tests and the results can be found in Flansbjer and Magnusson (2014a) and Magnusson and Mathern (2015).

Two creep test runs were performed with approximately six months in between. The compressive strength of the concrete was tested according to the instructions given in SIS (2009), using both cubes with dimensions of 150 × 150 × 150 mm and cylinders with dimensions of ⌀150 × 300 mm. In the first test run, small cylinders with dimensions ⌀100 × 200 mm were also tested according to the same standard. The elastic modulus in compression was determined according to SIS (2005) using cylinders with dimensions of ⌀150 × 300 mm. All specimens used had been stored in water at a temperature of 20°C prior to testing.

In addition to the specimens above, concrete cylinders with two different sizes were cast in plastic pipes in the same way as the creep specimens. The size of the specimens was either h=2d or h=3d.

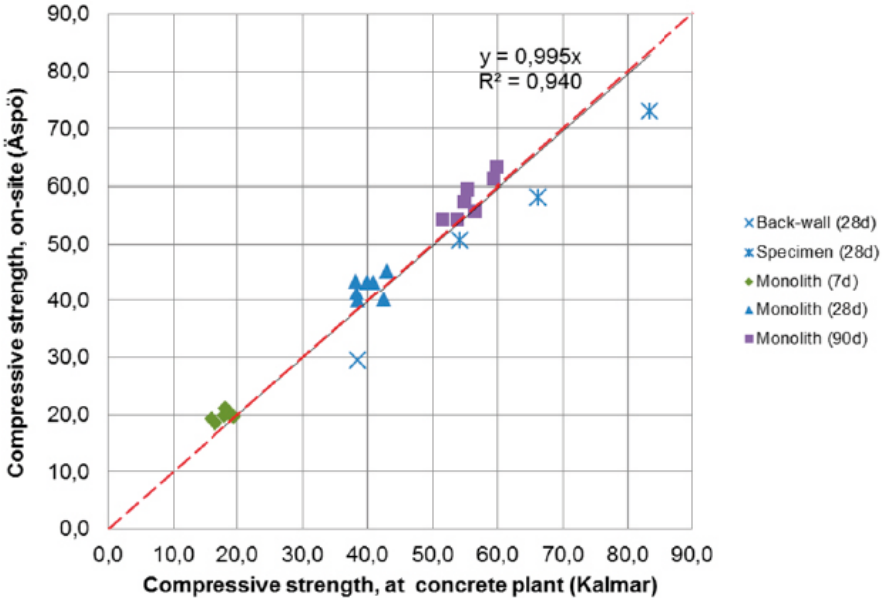

Figure 5-3. *Comparison of tested compressive strength on concrete cubes cast at the concrete plant in Kalmar and on site at the Äspö Hard Rock Laboratory. From Magnusson and Mathern (2015).*

Before testing, the plastic pipes were removed and the specimens were prepared with the same method as used for the creep specimens, see Section 5.2.3. These specimens were used as reference.

The hardened concrete properties from the tests are presented in Table 5-9 and Table 5-10, respectively. The values presented are mean values from the testing while the standard deviations are shown in brackets.

Table 5-9. Results from test run 1 showing mean values and standard deviations in brackets. From Magnusson and Mathern (2015).

Property	Unit	Specimen dim. [mm]	Curing condition	Age [days]				
				90	110[2)]	450	820	1185
$f_{cm,cube}$	[MPa]	150 × 150 × 150	water	76.7 (1.4)	75.4 (1.1)	85.9 (2.0)	85.1 (1.5)	87.2 (1.3)
$f_{cm,cyl}$	[MPa]	⌀150 × 300	water	74.6 (0.5)	–	–	–	–
E_{0m}	[GPa]	⌀150 × 300	water	33.2 (0.6)	–	–	–	–
E_{cm}	[GPa]	⌀150 × 300	water	33.5 (0.6)	–	–	–	–
f_{cm}	[MPa]	⌀100 × 200	water	75.3 (0.2)	–	–	–	–
f_{cm}	[MPa]	⌀100 × 200	sealed pipe[1)]	75.0 (0.5)	–	–	–	–
f_{cm}	[MPa]	⌀100 × 300	sealed pipe[1)]	70.5 (2.3)	–	–	–	–

1) Specimens prepared with the same method as the creep specimens.
2) Concrete age at start of the creep tests.

Table 5-10. Results from test run 2 showing mean values and standard deviations in brackets. From Magnusson and Mathern (2015).

Property	Unit	Specimen dim. [mm]	Curing condition	Age [Days]		
				87	470	820
$f_{cm,cube}$	[MPa]	150 × 150 × 150	water	67.8 (2.1)	86.6 (2.7)	91.1 (0.8)
$f_{cm,cyl}$	[MPa]	⌀150 × 300	water	64.0 (0.2)	–	–
f_{cm}	[MPa]	⌀90 × 180	sealed pipe[1)]	71.3 (0.8)	–	–
f_{cm}	[MPa]	⌀90 × 270	sealed pipe[1)]	68.7 (1.3)	–	–

1) Specimens prepared with the same method as the creep specimens.

The compressive stress-strain behaviour of the concrete was tested using the small cylinders stored in plastic pipes. The second test run also included a more slender cylinder with dimensions ⌀90 × 270 mm in order to investigate whether a higher diameter affects the compressive response. In the testing, the compressive stress, $\sigma_c(\varepsilon_c)$, was compared with the linear elastic response, $E_0\varepsilon_c$, using a ratio η defined as:

$$\eta = \left| \frac{E_0 \varepsilon_c}{\sigma_c(\varepsilon_c)} \right| - 1 \qquad (5\text{-}1)$$

The η ratio describes the deviation of the concrete response in relation to the linear elastic behaviour of the concrete. The results from the testing are presented in Table 5-11.

Table 5-11. Results from the compressive stress-strain behaviour testing of the concrete. (From Magnusson and Mathern 2015).

Specimen dimensions [mm]	Test run	f_{cm} at 90 days [MPa]	E_{0m} at 90 days [GPa]	Mean value $E_0\varepsilon_c$ [MPa]			Mean value $E_0\varepsilon_c/f_0$ [%]		
				η=0,01	η=0,02	η=0,05	η=0,01	η=0,02	η=0,05
∅100 × 200	1	75.0	33.5	42.0	46.7	56.3	56	62	75
∅90 × 180	2	71.3	34.0	33.0	36.5	43.3	46	51	61
∅90 × 270	2	68.7	34.1	37.5	40.4	47.0	55	59	68

Hardened concrete properties tested during the rock-concrete interface tests

Several different hardened concrete properties were tested in connection to the testing of the rock-concrete interface, presented in Section 5.2.1. The properties evaluated were; the compressive strength (f_{cm}), the tensile splitting strength ($f_{ctm,sp}$), the direct tensile strength (f_{ctm}) and the fracture energy (G_{Fm}). The specimens used for the testing were cubes, cylinders and cores drilled from cast concrete blocks. A more thorough description and presentation of the test methods used and the results can be found in Flansbjer and Magnusson (2014b) and Magnusson and Mathern (2015). A summary of the results are given in Table 5-12.

Table 5-12. Results from the testing of hardened concrete properties made in connection with the rock-concrete interface testing. The values shown are mean values while standard deviations are given in brackets. (From Magnusson and Mathern 2015).

Property	Unit	Specimen	Age [days]		
			12	29	90
$f_{cm,cube}$	[MPa]	cube 150 × 150 × 150	–	–	81.9 (2.2)
$f_{cm,cyl}$	[Mpa]	cylinder ∅150 × 300	–	–	78.0 (0.6)
$f_{cm,core}$	[Mpa]	core ∅100 × 100	33.7 (0.5)	55.1 (0.9)	82.2 (1.2)
$f_{tm,sp,core}$	[Mpa]	core ∅100 × 100	3.3 (0.2)	4.3 (0.3)	5.5 (0.4)
$f_{tm,core}$ [1)]	[Mpa]	core ∅65 × 100	–	–	3.2 (0.4)
$f_{tm,core}$ [2)]	[Mpa]	core ∅100 × 100	–	–	3.6 (0.2)
G_{Fm}	[N/m]	core ∅100 × 100	–	–	121 (15)

1) Obtained from core specimens ∅65 × 100 mm with hinged end conditions.

2) Obtained from notched core specimens ∅100 × 100 mm with fixed end conditions.

Development of concrete strength with time

The concrete strength development with time has been and in comparing the results, some deviations between the tests can be observed and several comparisons of test results can be found in Magnusson and Mathern (2015). Figure 5-4 shows a comparison of the obtained compressive strength at the concrete plant and at the Äspö Hard Rock Laboratory from the testing performed during the casting of the dome plug. The results from the drilled cores in the monolith are also included in the comparison. In addition to the measured strengths, the time development of the compressive strength according to Eurocode 2 (SIS 2008) is also included in the figure for comparison.

5.2 Testing of other mechanical concrete properties

5.2.1 Mechanical properties of the rock-concrete interface

The mechanical properties of the interface between the wire sawn rock surface and the concrete plug are important to know for several reasons. The main reason is that the plug is intended to release from the rock surface during concrete curing in order to be able to grout the gap between the plug and the rock.

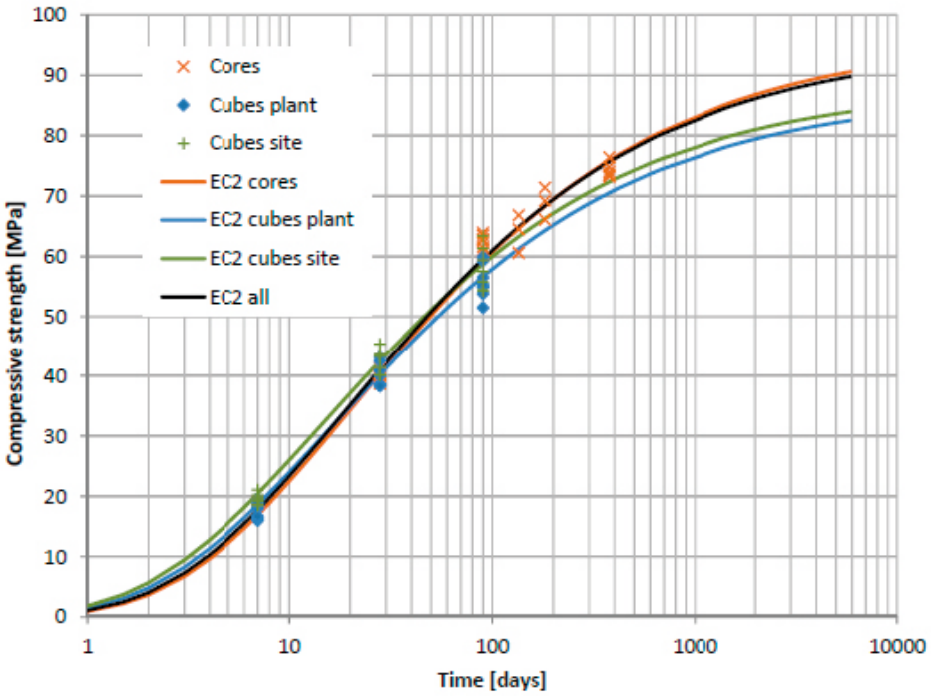

Figure 5-4. *Development of compressive strength with time. Results from the testing done at the concrete plant and at the Äspö Hard Rock Laboratory in connection with the casting of dome plug. Also included are results of testing cores drilled in the monolith. Best fit curves of the strength development according to Eurocode 2 (SIS 2008) are also shown. (From Magnusson and Mathern 2015).*

By doing this, it is possible to improve the water tightness of the plug and thereby reducing the leakage of water through the plug. To predict if the concrete plug releases from the rock surface during the hardening of the concrete or the following cooling period, numerical analyses have been performed. Based on the results from subsequent testing of the interface, the inputs into the numerical models can be improved and hence the accuracy of the predictions of behaviour. This will also allow for determination of which phase of the installation that the plug will release from the rock.

The testing was performed on core-drilled specimens from rock-concrete blocks manufactured in the laboratory of SP Building Technology and Mechanics. Four different properties of the rock-concrete interface were tested; the tensile bond strength, the tensile softening behaviour, the shear strength and the residual shear strength of a broken interface. The testing completed and the results are presented in Flansbjer and Magnusson (2014b). The following sections, describing the test procedure and the results briefly, are based on the aforementioned report.

Test preparations

The rock-concrete blocks were manufactured by casting concrete against a wire sawn rock surface on rock panels delivered from the Äspö laboratory. In total, five rock panels were delivered to the laboratory, they had been wire sawn from two different blocks of rock, denoted Block #1 and #2 (Figure 5-5). The wire sawn surfaces from Block #1 were denoted 1a, 1b, 1c and 1d while the surfaces from block #2 were named 2a and 2b. One of the rock panels from Block #1 had wire sawn surfaces on both sides. All five panels had the following approximate dimensions 800 × 700 × 150 mm.

The concrete mix composition and mixing order were in accordance to the basic specifications for the B200 low pH concrete presented in Vogt et al. (2009). The slump flow value of the concrete was measured to approximately 700 mm, which is within the expected interval according to Vogt et al. (2009). The prepared mix deviated very slightly from the design mix as can be seen in Table 5-13 but were so small that their influence on the cured concrete's properties should be insignificant. The aggregates used in the mix were the same as in the testing of the creep properties of the B200 low pH concrete, see Section 5.2.3.

Figure 5-5. *Delivered rock panels to the SP laboratory from Äspö, from Flansbjer and Magnusson (2014b).*

Table 5-13. Final concrete mix used in the testing of the rock-concrete interface, from Flansbjer and Magnusson (2014b).

Constituents	Supplier	Quantity [kg/m^3]	
		Design mix	Final mix
CEM I 42.5	Cementa	120	120
Silica fume	Elkem	80	80
Water		165	164
Limestone filler Limus 25	Nordkalk	369	368
Sand 0–8 mm	Fogelheim 6:2	1037	1028
Gravel 8–16 mm		558	548
Glenium 51	BASF	6.38	6.0
Water/cement		1.375	1.367
Water/binder		0.825	0.820
Water/powder		0.290	0.289

The rock-concrete blocks were cast in moulds built of plywood (900 × 900 × 250 mm). The moulds were also prepared with plastic foil to prevent moisture loss from the concrete. Before casting, loose materials on the wire sawn rock surface were removed and the surfaces were kept wet for 24 hours prior to casting. The double sided wire sawn rock panel was placed vertically in the mould and the concrete was cast on both sides of the panel (1b and 1c). The other four rock panels were placed horizontally in the mould and the concrete was cast on top of these surfaces (1a, 1d, 2a and 2b). The concrete dome will be bonded, initially, to the rock in the slot and has thereby bond in a circumferential direction. It is desired that the concrete dome releases in the top due to shrinkage and cooling and this is furthered discussed in Section 6.6. By performing these tests and comparing the evolution in bond strength for horizontal and vertical interfaces with the development of tensile strength, it will be possible to judge if it is likely that it releases in the top of the dome or risk of being subjected to cracking prior to loss of bond.

The free concrete surfaces were covered with a wet micro-fibre fabric and sealed with plastic foil immediately after casting. The day after casting, the rock-concrete blocks were sealed by the plastic foil placed in each mould. All blocks were then stored in 20°C until the start of testing. Two plain concrete blocks were also cast to be used for the test of the mechanical concrete properties. The prepared rock-concrete blocks and the plain concrete blocks are illustrated in Figure 5-6.

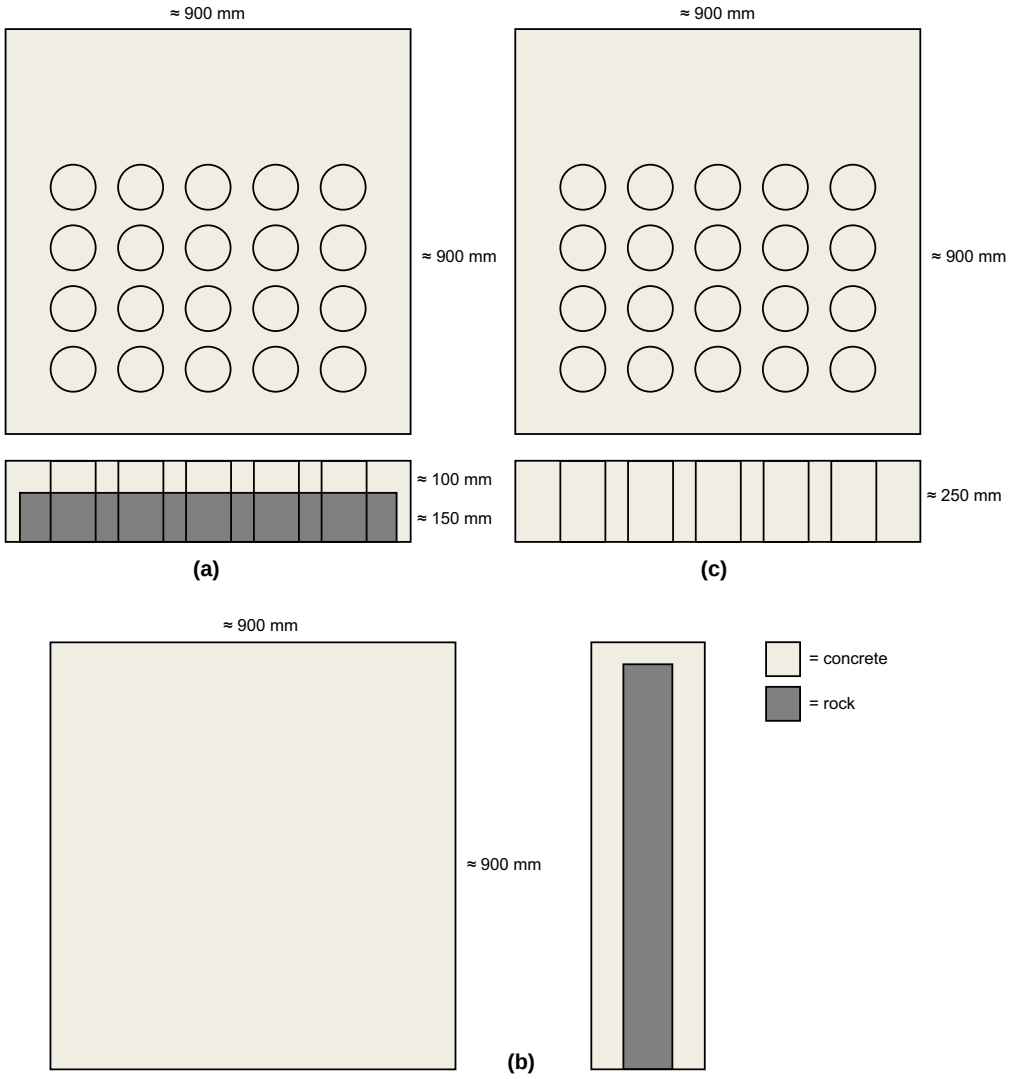

Figure 5-6. *Illustration of the prepared a) horizontal rock-concrete blocks, b) vertical rock-concrete blocks and c) plain concrete blocks. (From Flansbjer and Magnusson 2014b).*

Results from the testing of the concrete-rock interface

The tensile bond strength of the interface between the rock and the concrete was tested at three different concrete ages, 12, 30 and 90 days, with a pull-off test. As explained above, the testing was performed on concrete cast on horizontally- and vertically oriented rock surfaces, called “Horizontal Interface 1a” and “Vertical Interface 1c”, respectively. A summary from the testing is presented in Table 5-14.

Table 5-14. Summary of results from the tensile bond strength testing, the data presented are mean values and standard deviations are provided in brackets. (From Flansbjer and Magnusson 2014b).

Property	Age [days]	Peak tensile stress [MPa]	Tensile bond strength [MPa]
Vertical Interface 1c	12	– [1)]	– [1)]
	30	2.66 (*0.55*)	2.51 (*0.51*)
	91	3.00 (*0.48*)	2.90 (*0.42*)
Horizontal Interface 1a	12	1.45 (*0.04*)	1.48 (–) [2)]
	33	3.31 (*0.29*)	3.37 (*0.14*)
	91	4.25 (*0.23*)	4.38 (*0.28*)

1) Interface failure at drilling – no results.

2) Only one result.

The difference between the peak tensile stress and the tensile bond strength presented in the table above is that the first mean value includes all tests where the failure occurred at the interface or in the concrete. While the second mean value only include the tests where the failure occurred at the interface between the concrete and the rock. The results show that both the peak tensile strength and the tensile bond strength are higher for the horizontally cast concrete. It was also noted that a majority of the vertical test specimens failed at the interface while the horizontal specimens failed in the concrete. These two observations combined imply that the bond strength is higher for the horizontally cast concrete. Lower bond strength for vertical interfaces, is in this case beneficial, since it will increase the likelihood that the concrete dome releases in the top first.

The tensile bond strength as well as the tensile softening behaviour of the interface was tested by direct tensile tests on six specimens at an age of 93–97 days. A summary of the results is given in Table 5-15.

Table 5-15. Summary of results from the direct tensile tests. (From Flansbjer and Magnusson 2014b).

Specimen	Area [cm^2]	Age [days]	Failure mode	Peak tensile stress [MPa]	Tensile bond strength [MPa]	Fracture energy of the interface [N/m]
DTT-RCI-2	77.8	93	Interface	3.6	3.6	25.8
DTT-RCI-3	77.8	93	Interface	3.8	3.8	–
DTT-RCI-4	77.8	93	Interface	3.7	3.7	26.8
DTT-RCI-5	77.8	97	Concrete	4.1	–	–
DTT-RCI-6	77.9	97	Interface	3.9	3.9	–
DTT-RCI-7	77.8	97	Interface	4.0	4.0	–
			Mean	**3.9**	**3.8**	**26.3**
			Std. dev.	**0.2**	**0.1**	**0.7**

As can be seen in the table above, the fracture energy could only be determined for two of the six tested specimens. The reason is that the failure of the interface surface was very brittle and, therefore, it was only possible to evaluate the stress-crack opening relation and fracture energy for two of the tests. Figure 5-7 shows the stress-crack opening relation from the two tests.

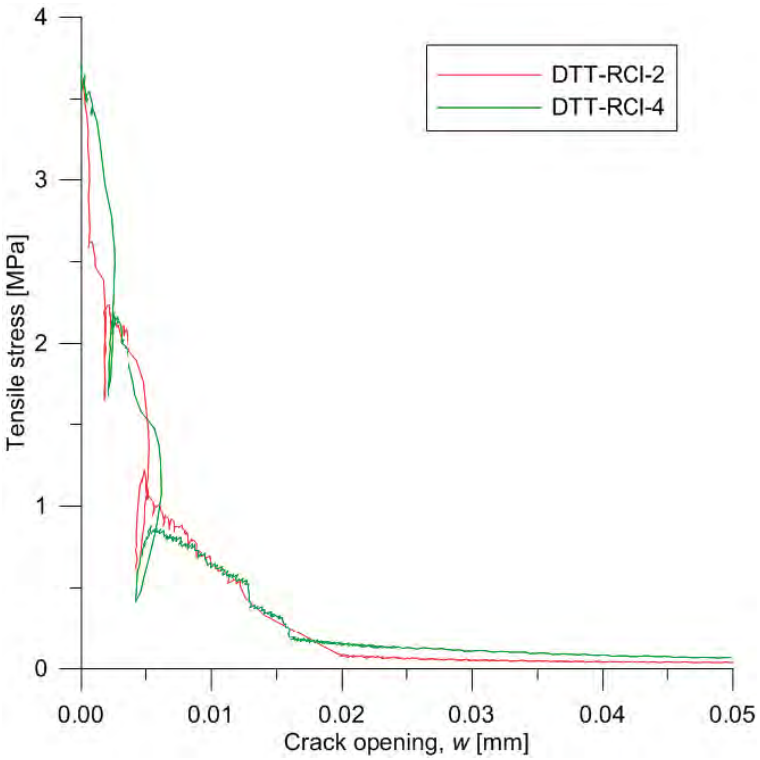

Figure 5-7. *Stress-crack opening relation of the interface for two of the performed direct tensile tests. (From Flansbjer and Magnusson 2014b.)*

Flansbjer and Magnusson (2014b) also concluded that the tensile bond strength between the concrete and the rock was in the same range as the tensile strength of the concrete, see Figure 5-8.

The test program used for the direct shear tests is presented in Table 5-16 as well as a summary of the results from the testing. Note that the cyclic shear loading tests of the broken interface were performed on specimen DST-RCI-7 and 8. Furthermore, the friction coefficient of each broken interface was calculated by dividing the residual shear stress by the applied normal stress on the specimen.

Table 5-16. Summary of the results from the direct shear tests performed and the test program used, from Flansbjer and Magnusson (2014b).

Specimen	Area [cm^2]	Age [days]	Shear seq.[1)]	Normal stress [MPa]	Peak shear stress [MPa]	Res. shear stress [MPa]	Res. shear stress/ Normal	Failure mode[2)]
DST-RCI-1	32.5	91	s	5	11.5	4.3	0.86	b
DST-RCI-2	32.5	91	s	3	11.0	2.4	0.80	b
DST-RCI-3	32.3	90	s	10	15.6	6.0	0.60	c
DST-RCI-4	32.6	90	s	10	15.7	7.1	0.71	c
DST-RCI-7	50.0	90	s	0	6.1	0	–	a
			s1	5	4.8	4.3	0.85	–
			s2	10	8.5	8.2	0.82	–
			s3	30	23.7	22.4	0.75	–
			s4	20	14.7	14.7	0.74	–
			s5	10	7.8	7.8	0.78	–
			s6	30	21.6	21.6	0.72	–
			s7	5	4.1	4.1	0.81	–
DST-RCI-8	50.6	90	s	0	6.2	0	–	a
			s1	5	3.9	3.5	0.70	–
			s2	10	7.2	7.0	0.70	–
			s3	20	14.1	14.0	0.70	–
			s4	30	20.9	20.8	0.69	–
			s5	20	14.3	14.3	0.72	–
			s6	10	7.4	7.4	0.74	–
			s7	5	3.8	3.8	0.76	–

1) Shear sequence: s = shear cycle on intact interface; s# = shear cycle on broken interface.
2) Failure mode: a = in interface; b = mainly in interface; c = inclined failure plane crossing interface.

Figure 5-9 shows the shear stress versus the shear displacement from the testing of the specimens with an intact rock-concrete interface.

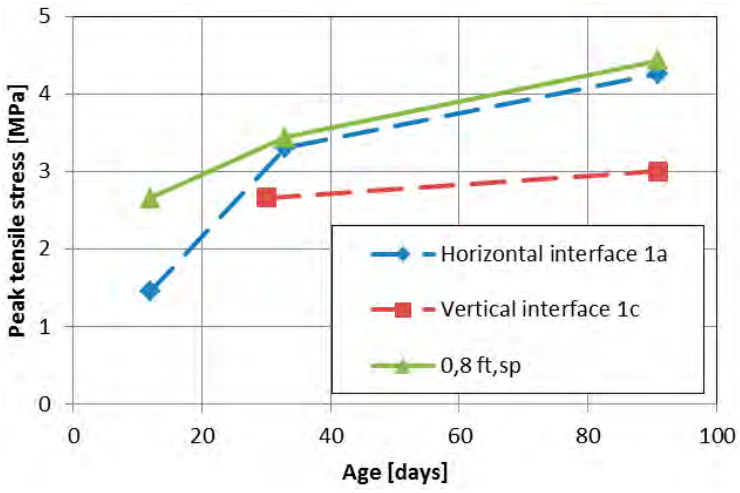

Figure 5-8. *Development of the peak tensile strength at the rock-concrete interface and the concrete tensile strength (assumed as 80 % of the splitting tensile strength). (From Flansbjer and Magnusson 2014b.)*

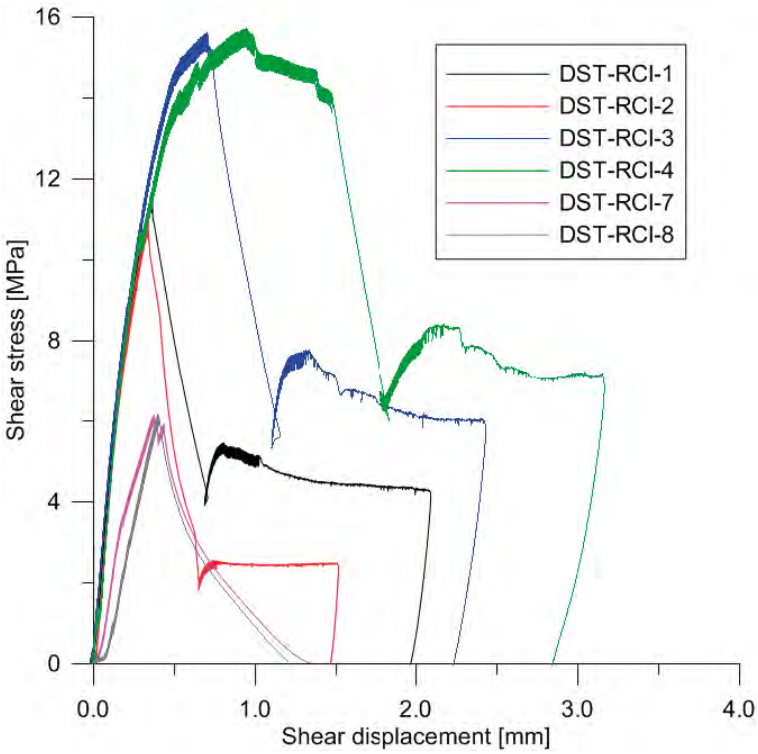

Figure 5-9. *Shear stress vs. shear displacement from the direct shear tests of the rock-concrete interface specimens. (From Flansbjer and Magnusson 2014b.)*

The interface between the rock and the concrete was brittle, this is seen as a first steep drop in Figure 5-9. For the specimens with a normal stress applied, the first drop is followed by another peak and then a plateau corresponding to the residual shear stress in the broken interface.

Figure 5-10 shows the relationship between the peak shear stress, the residual shear stress and the applied normal stress on the specimens.

5.2.2 Shrinkage

The shrinkage of the B200 low-pH concrete has been measured over a three-year period. The initial testing of the shrinkage, presented in Vogt et al. (2009), included three different measuring methods. The first two methods aimed to measure the autogenous shrinkage of the concrete by, (i) measuring the change in volume of the tested specimens with time and (ii) by using a digital dilatometer instead of determining the volume change of the specimens. In the third method used, standard beams with dimensions of 100 × 100 × 400 mm were cast. One day after, the beams were removed from the moulds and half of the beams were sealed with a gas tight butyl tape while the other half was stored, uncovered in air with a relative humidity of 50 %. More information about the testing can be found in Vogt et al. (2009) and Malm (2012).

After the initial shrinkage testing of the low-pH concrete, it was decided to conduct further tests using the third method described above but with three storage options examined. The previous tests showed a significant influence of autogenous shrinkage and therefore additional tests were conducted to obtain further information regarding expected shrinkage. In total, 30 new specimens were cast of which 10 were sealed using the butyl tape, 10 were stored unsealed at 50 % RH and the last 10 were stored in water at a temperature of 20°C. The testing was divided between two different Swedish laboratories, *CBI* and *Clab*. Both laboratories cast 15 concrete beams each and the testing was performed during the same period of time at both laboratories. The results of these shrinkage tests are presented in Figure 5-11 and Figure 5-12.

The results from earlier testing, performed at CBI and presented in Vogt et al. (2009), compares very well with the new test results from specimens cured in similar conditions.

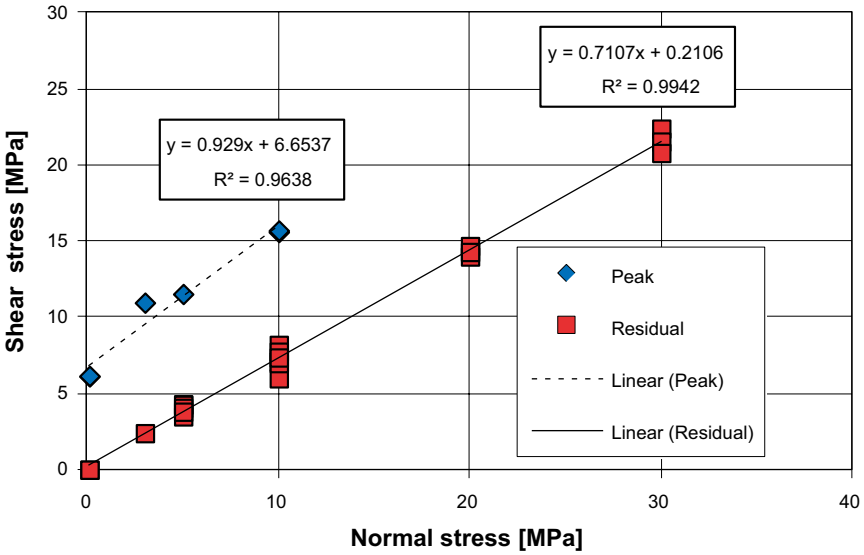

Figure 5-10. *Peak shear stress and residual shear stress vs. normal stress from the direct shear tests on the rock concrete interface specimens. (From Flansbjer and Magnusson 2014b.)*

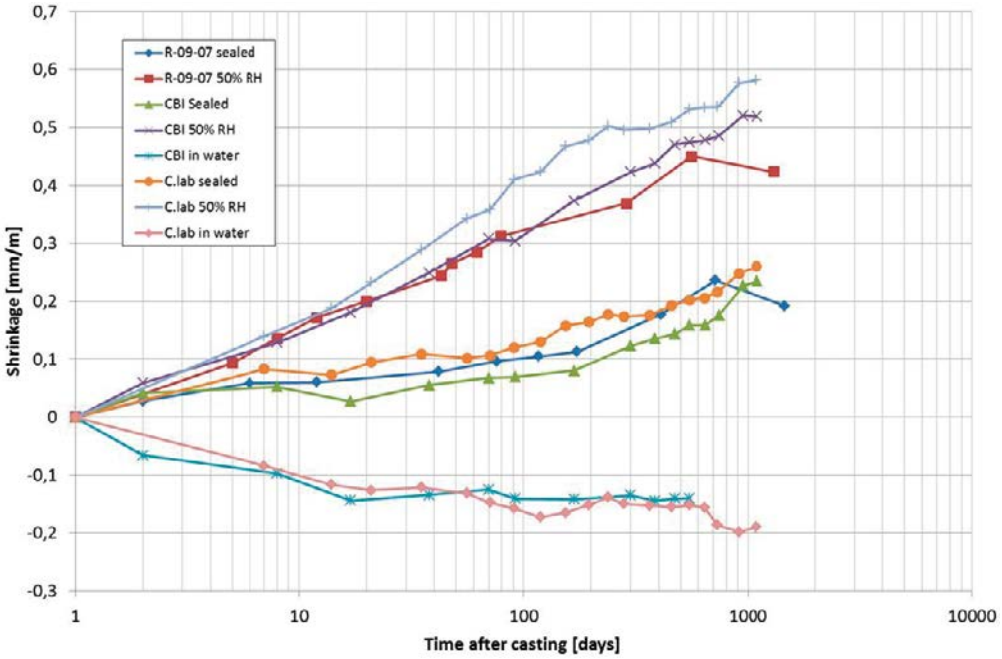

Figure 5-11. *Average shrinkage of the specimens tested at CBI and C.lab. The older results from the testing at CBI, presented in Vogt et al. (2009), are also shown as comparison. (From Magnusson and Mathern 2015.)*

5.2.3 Creep

During the service life of the concrete plug, it will be subjected to high compressive stresses due to the high pressures developed by the swelling bentonite clay in the deposition tunnels. Earlier testing of the creep behaviour of the B200 concrete has focused on linear creep, which assumes that the concrete compressive stresses are within the linear elastic range (Vogt et al. 2009, Malm 2012). In order to improve the confidence in the accuracy of numerical analyses of the plug, new testing of the creep has been initiated for the B200 concrete mix (Flansbjer and Magnusson 2014a). This laboratory study includes testing of the creep behaviour for stress levels in the concrete of 40 %, 50 % and 75 % of the concrete compressive strength. The creep tests began after approximately three months of curing. All concrete cylinders were sealed and loaded in mechanical rigs, where they will remain for three years (the tests are still ongoing). The test method used and results available from Flansbjer and Magnusson (2014a) are more thoroughly described below.

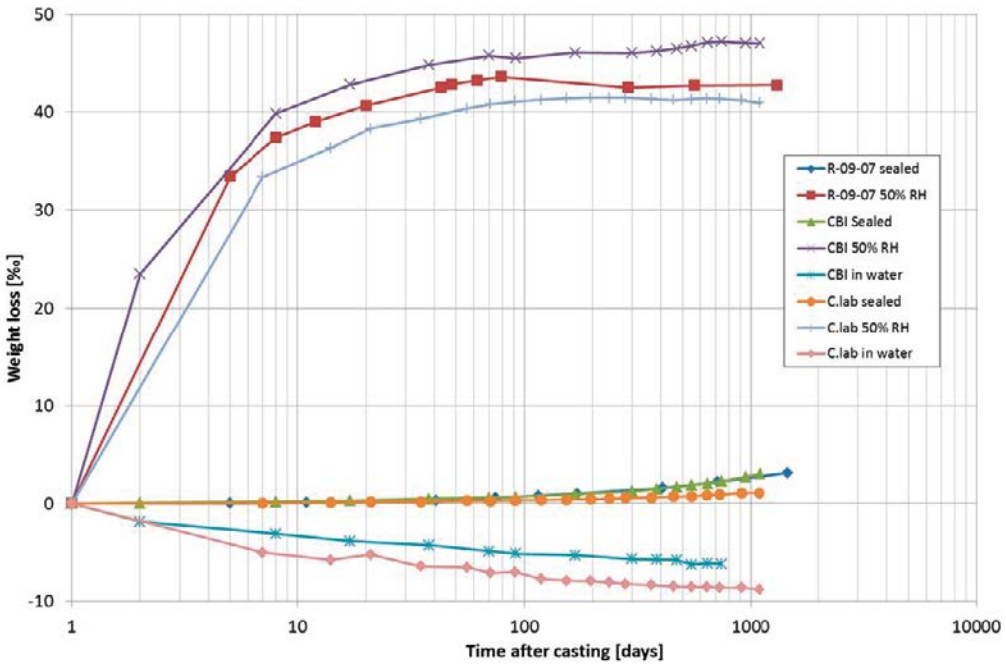

Figure 5-12. *Average weight loss of the specimens tested at CBI and C.lab. The older results from the testing at CBI, presented in Vogt et al. (2009), are also shown as comparison. (From Magnusson and Mathern 2015.)*

Test method

The test method used to determine the creep properties of the concrete is based on the ASTM C512-02 and ISO 1920-9:2009 standards. The cast concrete cylinders were subjected to a sustained longitudinal compressive load and the total deformation of the cylinders was measured. To account for the shrinkage of the concrete, one unloaded control specimen was also cast. The deformation of this control specimen was subtracted from the measured deformation of the loaded cylinders in order to determine the creep of the concrete. All specimens were stored in the same environmental conditions.

Preparations and test specimens

All test specimens were designed as cylinders with a height of three times the diameter of the cylinders. The specimen were cast in plastic pipes with predrilled holes, in which stainless steel gauge studs for strain measurement were placed before the casting. A total of six gauge studs were placed in each specimen, the gauges were placed in pairs along three lines evenly distributed about the perimeter of the cylinders. Each pair of gauge studs was spaced evenly about the mid-height of the cylinders, resulting in a distance of about 200 mm between the studs. An illustration of test specimens and the placement of the studs are shown in Figure 5-13.

The plastic pipes used to cast the concrete cylinders were immediately after casting sealed with plastic foil and other sealant material to prevent moisture from leaving the concrete. After 24 hours, the sealed specimens were moved into a climate chamber with a temperature of 20°C and a relative humidity of 50 %. The specimens were stored in the climate chamber for about 80 days, whereupon the sealing was removed and the specimens were cut to the desired length. At each end of the cut specimens, a steel plate was placed and all cylinders were resealed.

Test procedure

Directly after the predetermined compressive stress was applied on each specimen, the strain and spring deformation were measured. The next measurement on the specimens was made after two and six hours, then daily for one week, weekly until the end of the first month, monthly till the end of the first year and then once every third month. In connection to the measurement of the strain, the stress applied on each specimen was checked and adjusted if needed before the measurement of the strain.

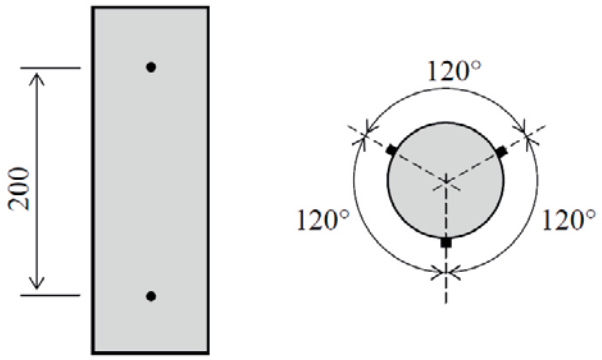

Figure 5-13. *Illustration of the test specimen configuration. The black dots represent the locations at which the gauge studs were placed.*

Concrete material

The concrete used in the creep test was manufactured at CBI, Swedish Cement and Concrete Research Institute, in accordance with the B200 concrete mix given in Table 5-1. In total, two test runs have been performed; the first run was cast on May 25, 2011 and the second on December 19, 2011. The final concrete mix in each of the two test runs has small deviations compared to the design mix. The final concrete composition of each test run is given in Table 5-17.

Table 5-17. Composition of the B200 concrete mix in the first and second test run. (From Flansbjer and Magnusson 2014a).

Constituents	Manufacture	Quantity [kg/m^3]		
		Design mix	Final mix 1	Final mix 2
CEM I 42.5	Cementa	120	120	120
Silica fume	Elkem	80	80	80
Water		165	164	165
Limestone filler Limus 25	Nordkalk	369	368	369
Sand 0–8 mm	Fogelheim 6:2	1037	1028	1032
Gravel 8–16 mm	Fogelheim 6:2	558	548	551
Glenium 51	BASF	6.4	6.0	6.0
Water/cement		1.375	1.367	1.367
Water/binder		0.825	0.820	0.825
Water/powder		0.290	0.289	0.290

The aggregates used in the concrete mix were taken from different parts of Sweden depending on the aggregate size. The natural sand fraction was taken from the same area in Äspö as used in Vogt et al. (2009) while the coarser aggregates were crushed granite taken from the Gothenburg area. The slump flow value for the first and second test run was 680 mm and 690 mm, respectively, which are within the expected interval according to Vogt et al. (2009).

Test program and results

As mentioned above, the creep tests were conducted for three different stress levels on the specimens; 40 %, 50 % and 75 % of the compressive strength. In total, two test runs were performed; in the first run, two of the three stress levels were tested, 40 % and 50 % named TR 1a and TR 1b, respectively. In the second run, the 75 % stress level was applied on the specimens and the test run was named TR 2. The stress level to be applied on each specimen was determined by doing compressive tests on cast standard concrete cylinders from the two runs, more information about these tests can be found in Flansbjer and Magnusson (2014a). In Table 5-18, a summary of the test runs is given; the stress levels are given in relation to the measured compressive strength of the standard cylinders on

which the compressive testing was performed and to the strength of the sealed more slender concrete specimens for the creep test. For each stress level, five specimens were loaded and additional five unloaded specimens were saved to be used as reference.

Table 5-18. Summary of the creep test runs. (From Flansbjer and Magnusson 2014a).

Test run	Specimen #	Specimen dimension [mm]	Age at time of loading, t_0 [days]	Applied stress $\sigma_{cm}(t_0)$[1] [MPa]	$\sigma_{cm}(t_0)/ f_{cm,cyl}$[2] [%]	$\sigma_{cm}(t_0)/ f_{cm}$[3] [%]	$E_{cm}(t_0)$ [GPa]
TR 1a	1–5	∅100 × 300	110	30.0 (0.2)	40.2 (0.3)	42.6 (0.3)	32.9 (0.5)
TR 1b	6–10	∅100 × 300	111	38.5 (0.5)	51.6 (0.6)	54.5 (0.7)	32.7 (0.8)
TR 2	11–15	∅90 × 270	91	49.4 (0.5)	77.3 (0.9)	72.0 (0.9)	28.9 (1.0)

1) σ_{cm}(t0) is the average value of the applied stress σ_c(t0) for the test group.

2) $f_{cm,cyl}$ is the average value of the compressive strength of the standard concrete cylinders ∅150 × 300.

3) f_{cm} is the average compressive strength of the sealed concrete cylinders in the first and second test run.

The creep strain $\varepsilon_{cc}(t,t_0)$ is calculated as the total stress induced strain minus the strain obtained immediately after loading. While the total stress induced strain is calculated as the difference between the average strain values of the loaded specimens and the control specimens.

$$\varepsilon_{cc}(t,t_0) = \varepsilon_{c\sigma}(t,t_0) - \varepsilon_{ci}(t_0) = \varepsilon_c(t) - \varepsilon_{c,control}(t) - \varepsilon_{ci}(t_0) \quad (5\text{-}2)$$

Where $\varepsilon_{c\sigma}(t,t_0)$ is the total stress induced strain, $\varepsilon_{ci}(t_0)$ is the strain immediately after loading, $\varepsilon_c(t)$ is the average strain value of the loaded specimens and $\varepsilon_{c,control}(t)$ is the average strain value of the control specimens.

The creep coefficient was then calculated as the ratio between the total creep strain and the initial strain immediately after loading as:

$$\varphi = \frac{\varepsilon_{cc}(t,t_0)}{\varepsilon_{ci}(t_0)} \quad (5\text{-}3)$$

The mean value of the creep coefficient for the three tested stress levels versus time is shown in Figure 5-14. As seen in the results, the creep curves shows the same behaviour for the three tested stress levels and thereby do not indicate a significant behaviour in creep for higher stress levels, up to approximately 70 % of the compressive strength.

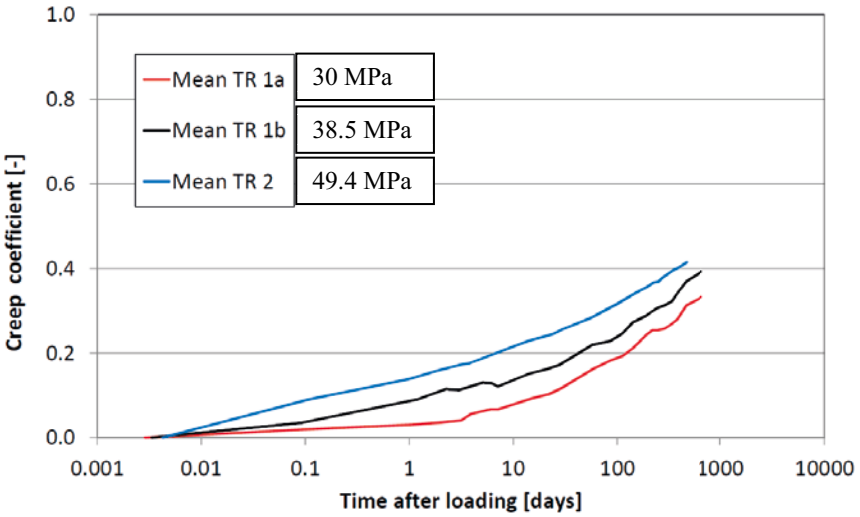

Figure 5-14. *Mean value of the creep coefficient with time for TR 1a, TR 1b and TR2. (From Flansbjer and Magnusson 2014a.)*

5.3 On site testing during casting of the full-scale test

The concrete dome plug was cast using low-pH self-compacted concrete, produced at a batching plant approximately 100 km from the site. The concrete trucks also had to travel down the ramp to the casting site, located at a level –460 m at Äspö hard rock laboratory. Due to the time needed for transportation, the concrete was therefore mixed approximately 2 hours prior to arriving at site.

It is highly important that correct properties are achieved for the fresh concrete, especially when using self-compacting concrete, in order to have a successful pour and casting. Therefore, extensive testing was performed on site for each batch of concrete. In case of insufficient properties, different measures including adjustment of the admixture (superplasticizer) content to rejection of the concrete batch could be used. The following properties of the fresh low pH self-compacted concrete were determined on site according to the following standards:

- Slump flow according to SS-EN 206-9.
- t_{500} according to SS-EN 206-9.
- Air content according to SS-EN 12350-7.
- Density according to SS-EN 12350-7.

In addition, visual inspections of the fresh concrete were also made while taking samples and testing slump flow. Target values for the fresh concrete properties of the low pH self-compacted concrete were defined based on Vogt et al. (2009), as presented in Table 5-19. These values were based on laboratory and factory tests done prior to the casting of the dome plug.

Table 5-19. Target values for fresh concrete properties.

Property	Target value
Temperature	< 20°C
Slump flow	700 ± 30 mm
t_{500}	4 ± 2 sec

If the determined concrete slump flow at arrival did not meet the specifications, the content of the admixture was adjusted according to Table 5-20. The mixture was then retested until acceptable properties were measured.

Table 5-20. Adjustment of admixture, dosages vs. determined slump flow.

Slump flow	Dosage of admixture
440–520 mm	1,0–1,5 l/m^3
530–600 mm	0,5–0,9 l/m^3
610–660 mm[1)]	0,1–0,4 l/m^3 [1)]

1) Extreme care should be taken at slump flow > 600 mm, due to risk of separation.

According to the specifications used at the site, batches were rejected if they had the following characteristics:

- cannot be adjusted to slump flow of at least 650 mm,
- show a paste rim of more than 20 mm when determining the slump flow,
- show obvious signs of separation.

Figure 5-15 and Figure 5-16 show sampling and testing of fresh concrete properties at site. Sampling was done immediately after the concrete truck arrived at site. Before taking samples for testing, the concrete was mixed at high rotation speed for 4 minutes to avoid testing inhomogeneous concrete due to segregation that might have occurred during transport.

Figure 5-15. *Sampling of concrete from a concrete truck (left), measuring slump flow (right).*

Figure 5-16. *Clocking t_{500} while measuring slump flow (left), measuring air content (right).*

The determined fresh concrete properties are summarized in Table 5-21 and presented in graphic form in Figure 5-17 to Figure 5-22. A more detailed table with all measured values can be found in Appendix 2.

The temperature of the fresh low pH self-compact concrete arriving at site varied between 8.9°C and 9.7°C with an average of 9.3°C, see Figure 5-17. The temperature of the fresh concrete met the requirements for all batches and was consistent. The concrete temperature was determined immediately after arrival at site.

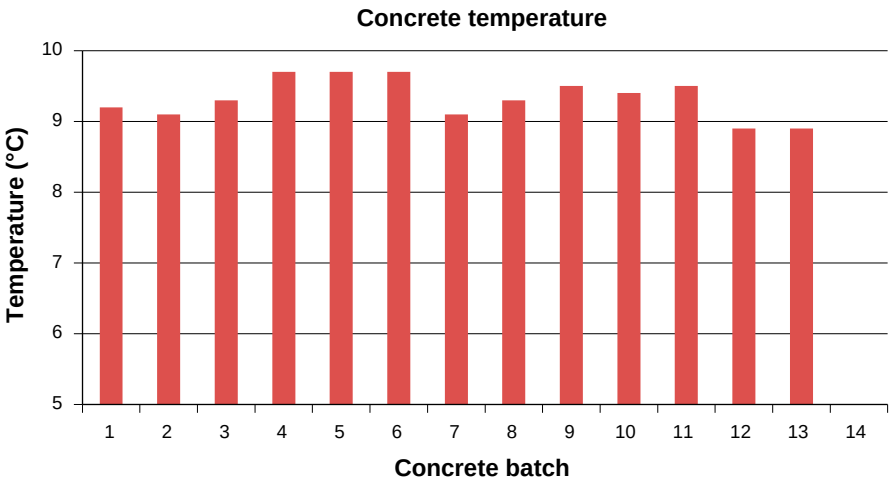

Figure 5-17. *Concrete temperature, determined at arrival without adjustments, for all batches.*

Table 5-21. Results of fresh concrete testing. Temp = fresh concrete temperature, SF = slump flow, Air = air content, Adjust = numbers of required adjustments of admixture.

			At arrival						Final	
Batch no.	arrival time	pump time	Temp °C	SF mm	t_{500} sec	Air %	Density kg/m^3	Adjust. no.	SF mm	t_{500} sec
1	08:47	09:15	9.2	570	3.3	8.5	n.a.	1	680	2.2
2	09:37	10:00	9.1	660	3.0	6.4	2225	0	660	3
3	10:44	11:00	9.3	630	2.5	7.8	2210	1	660	2.6
4	11:20	11:50	9.7	610	2.9	6.0	2240	3	720	n.a.
5	12:03	12:15	9.7	670	5.7	9.0	2180	0	670	5.7
6	12:43	13:00	9.7	570	3.6	8.0	2170	1	700	2.3
7	13:57	14:10	9.1	650	4.0	6.6	2210	0	650	4.0
8	15:11	15:20	9.3	670	3.7	7.2	2190	0	670	3.7
9	15:28	15:45	9.5	680	2.2	7.8	2210	0	680	2.2
10	16:11	16:20	9.4	690	2.3	5.8	2260	0	690	2.3
11	17:02	17:10	9.5	620	2.7	7.2	2180	1	680	2
12	17:51	18:00	8.9	660	2.8	7.8	2190	0	660	2.8
13	18:46	19:00	8.9	640	2.5	7.1	2240	1	720	2.1
14	19:35	n.a.	n.a.	680	3.0	5.5	2240	0	680	3
AVG			**9.3**	**643**	**3.2**	**7.2**	**2210**		**684**	**2.7**
STDEV			**0.3**	**37**	**0.9**	**1.0**	**27**		**19**	**1.0**

The air content of the low pH self-compacted concrete produced for DOMPLU was higher than tested before in laboratory and factory tests. The previous tests had showed an air content of about 2–3 % according to Vogt et al. (2009) and Magnusson and Mathern (2015). The reasons for this difference could not be identified and solved at the time of dome casting, but in agreement with the structural designers, a decision was made to cast the dome plug with concrete with higher-than-planned air content. It was recognized that the mechanical parameters of the hardened low-pH SCC will differ from pretested parameters, but were not judged to be a risk to concrete dome performance in this installation. A sufficiently large number of samples were prepared to determine all relevant concrete properties and re-estimate the as-built characteristics of the dome. The option to using the as-prepared material would have been to terminate the pour, identify the exact reason for the high air content, most likely wait for a delivery of new superplasticizer and try again. According to Magnusson and Mathern (2015) one possible explanation for the high air content could be contamination of the superplasticizer. The risk of swelling of the already installed bentonite in the backfill during this delay was a greater risk to the DOMPLU experiment than a slight change in the concrete's composition.

The air content of the fresh concrete varied between 5.5 % and 8.5 % with an average of 7.2 %, as seen in Figure 5-18. The density of the fresh concrete was between 2170 kg/m^3 and 2260 kg/m^3 with an average of 2210 kg/m^3, see Figure 5-19. The relative low value for the fresh concrete density corresponds to the high air content. The air content was remarkably high for concrete without air entraining agents. One possible explanation for the high air content may be associated with the super-plasticizer used. The batching plant uses another type of superplasticizer for everyday production and the superplasticizer used for the concrete dome plug experiment was ordered specifically for this task. Use of an unfamiliar component might have resulted in separation of the anti-foaming agent (which is a necessary part of any superplasticizer formulation), during manufacturing, transport, handling or storage. Consequently, the use of superplasticizer without the proper content of anti-foaming agent in the mix design may have resulted in higher air content of the low pH SCC.

The slump flow of the low-pH SCC tested directly after arrival and also before pumping the concrete into the form (after necessary adjustments to ensure it met target flow values) is displayed in Figure 5-20. The slump flow at arrival was between 570 mm and 690 mm, with an average of 643 mm. After adjustments, the slump flow was between 660 mm and 720 mm, with an average of 684 mm. With the exception of Batch 2 and Batch 3, the slump flow met the target values of slump flow of 700 mm ± 30 mm. At 660 mm slump, the non-conforming batches were not adjusted due to the risk of over-dosage and separation. The visual inspection of these batches indicated they were a good and stable concrete with sufficient flowability to allow for their successful placement. In addition, these two batches were pumped into the bottom parts of the dome plug where concrete placed on top of them will contribute to their effectiveness in filling.

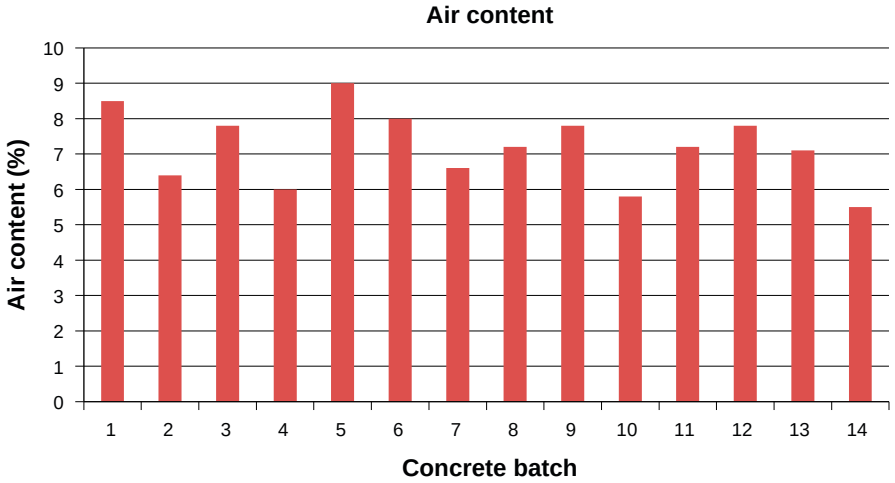

Figure 5-18. *Air content, determined at arrival without adjustments, for all batches.*

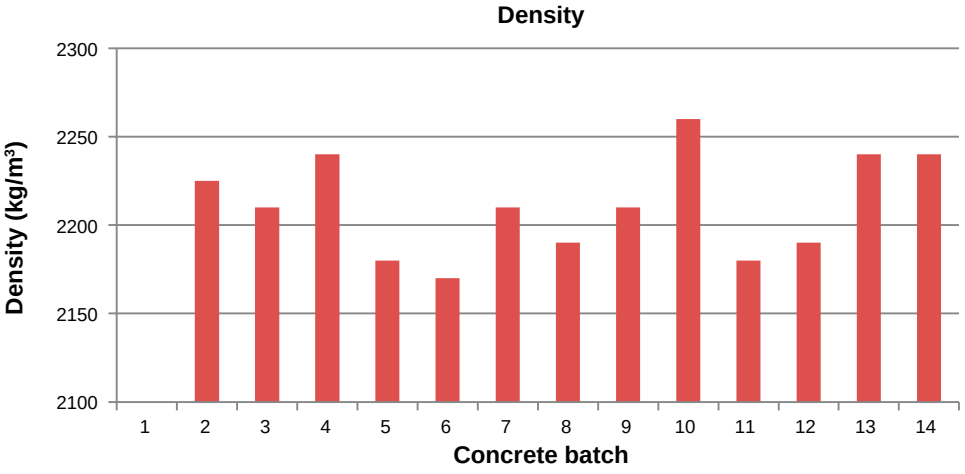

Figure 5-19. *Concrete density, determined at arrival without adjustments, for all batches.*

The viscosity of the low pH self-compacting concrete, measured as t_{500}, tested directly after arrival and after necessary adjustments (before pumping the concrete into the form) is displayed in Figure 5-21. The t_{500} was between 2.3 and 5.7 sec at arrival, with an average of 3.2 sec. After adjustments, t_{500} was between 2.1 sec and 5.7 sec, with an average of 2.7 sec. The viscosity of the low pH self-compacted concrete, measured using t_{500}, satisfied the requirement of 4 sec ± 2 sec. One can also observe that the addition of superplasticizer (with the aim of increasing slump flow) resulted, as expected, in reduced viscosity.

The number of adjustments required to reach the target values for the fresh concrete properties is displayed in Figure 5-22. In general, none or only one adjustment was sufficient, with the exception of Batch 4. In Appendix 2, one can see that, for Batch 4, the slump flow actually decreased with increasing dosage of superplasticizer, which is highly unusual. The visual inspection of the concrete in Batch 4 revealed no problems; the concrete seemed to have a good flowability and was stable. Additionally, being forced to wait for the next batch might have led to the formation of a casting joint in the plug due to stiffening concrete cast earlier. Therefore, the decision was made to use this batch of concrete and re-test slump flow after half of the batch was pumped into the form. The subsequently determined slump flow was 720 mm. Some unidentified problem when initially sampling the concrete is likely to have occurred, as the content of coarse aggregate in the samples seemed high.

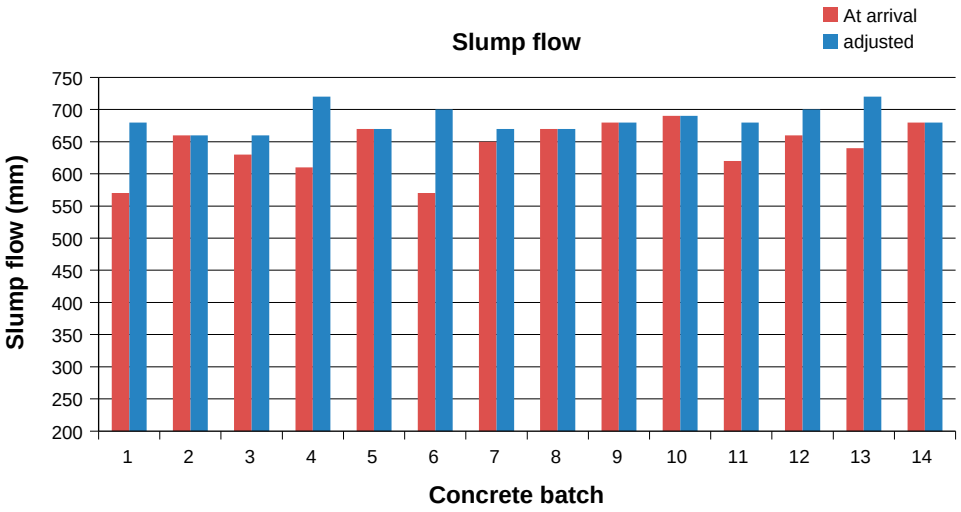

Figure 5-20. *Slump flow, determined at arrival without adjustments and after adjustments, for all batches. In case identical values are presented for one batch, e.g. no.2, no adjustments were done.*

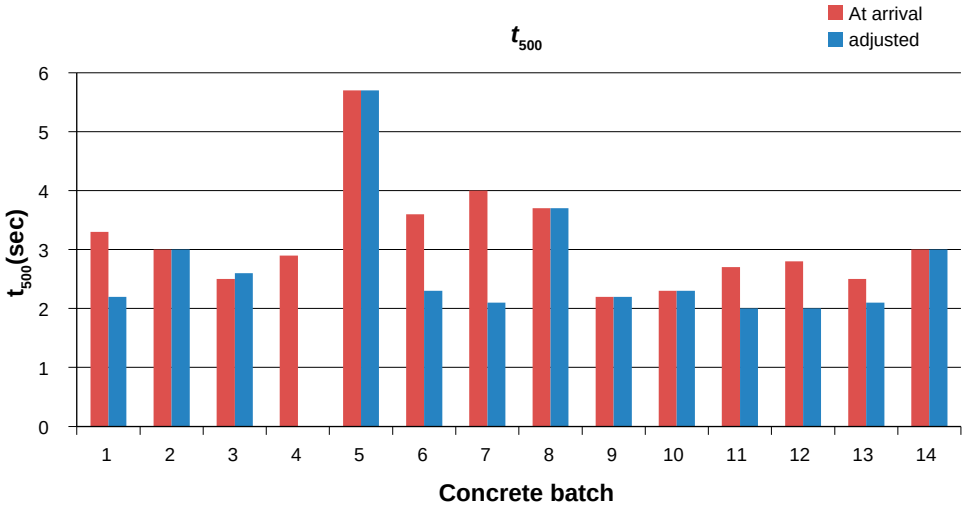

Figure 5-21. *t_{500}, determined at arrival without adjustments and after adjustments, for all batches. In case identical values are presented for one batch, e.g. no.2, no adjustments were done.*

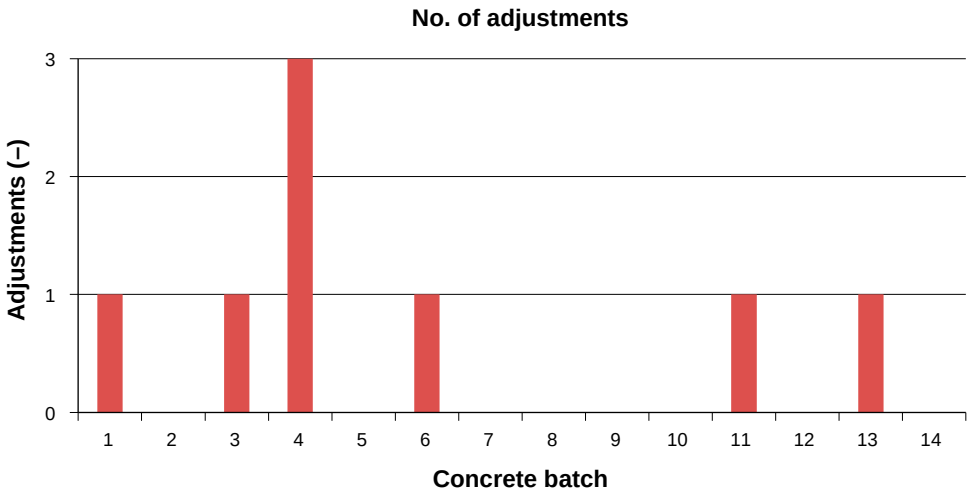

Figure 5-22. *Number of required adjustments for all batches.*

5.3.1 Conclusions from on-site concrete testing during casting

The intensive program of testing fresh concrete properties ensured that concrete of sufficient quality was pumped into the formwork. Some adjustments were required, but the extent was not unlike other sites where self-compacting concrete is used. No concrete batches had to be rejected.

For all but one of the concrete batches, the slump flow was either according to specifications or could be adjusted to satisfy the requirements. For the other batch, the flow of the concrete was judged to be acceptable, despite a slump flow of just 660 mm. This concrete was used in the base of the concrete dome and would have been compacted by the weight of concrete poured on top of it. Batches that had to be adjusted had lower slump flow than required. This is preferred compared to batches being received at site with higher slump flow than required as addition of superplasticizer is a relatively easy process. Had the slump flow been too high, the only options would have been to delay the pouring of the concrete or rejection of the non-compliant batch.

The concrete temperature was consistent with the target properties for fresh concrete.

A higher than anticipated air content was observed in the material produced but this was judged to be an insufficient justification for rejecting the concrete batches delivered. In agreement with the structural designers, a decision was made to cast the dome with concrete with high air content. The mechanical parameters of the hardened low-pH SCC will differ from pretested parameters due to the higher air content.

6 Civil Works, installation of the plug

In this Chapter, the installation of the full-scale test DOMPLU is described component by component. As a final point, most important experiences from the field-work are summarised in Section 6.8.

Prior to the civil work and emplacement of the plug components, excavation of the test tunnel TAS01 and the slot had been finalized, as previously described in Chapter 3. In addition, preparatory works, such as geodetic survey and filling of boreholes in the slot with mortar and injection grout tubes was performed in advance of the plug installation.

Installation of sensors in backfill, filter, bentonite seal and concrete dome was done in conjunction with the installation of each component, but this is described separately in the following Sections 7.1 and 7.2. The water pressurization system is then described in Section 7.3.

The DOMPLU full-scale test set-up is shown in Figure 6-1. The schematic figure includes length-coordinates of the experiment tunnel TAS01. Two components, the concrete back-wall supporting the backfill and the front delimiter supporting the concrete dome, were given fixed coordinates prior to installation. In the figure, all installed components of DOMPLU are illustrated. These are from the upstream side to the downstream side (i.e. from the left to right) in Figure 6-1:

- Concrete back-wall.
- Bentonite backfill.
- Delimiter/Filter part (LECA beams).
- Filter – gravel (fraction 2–4 mm).
- Delimiter (Geotextile).
- Bentonite seal.
- Delimiter (Concrete beams).
- Concrete dome (to be cast in the excavated slot).
- Weir for leakage control.

The installation of the each component is not always done separately; instead some components are installed in parallel as assembly progresses vertically. In this chapter, each component is described in a separate Section, from Section 6.1 Concrete back-wall to Section 6.7 Weir for leakage measurement. Within each section, a short description of the installation procedure of the respective component is included. Due to the parallel installation process, these discussions may be presented with a little overlap.

The installation of the different plug component is described from the upstream to the downstream side, i.e. from left to right in Figure 6-1, and thereby in chronological order as they are installed. The experimental tunnel was scanned with laser scanning before installation. The result from the laser scanning is presented as a tunnel cross section at the location for each component of the plug system. The numbers in the name of each cross section constitute a distance measure in the tunnel direction from the intersection centre point of the main tunnel TASJ. This means that, for instance, the distance between section 0/017.10 and section 0/014.60 is 17.10–14.60 = 2.5 m.

The installation of the plug, from installation of the backfill transition zone to casting of the concrete dome, and including installation of the monitoring system, took about two months in the full-scale test. The installation of the backfill started January 7th 2013 and casting of the concrete dome was finished March 13th 2013. During this period ongoing activities, such as installation of sensors, cable alignment and preparation of lead-through casings were also performed. This time period does not include the time required for excavating the tunnel, excavating the slot abutment, casting the concrete back-wall, drilling lead-through boreholes and other preparations such as concreting of the remaining boreholes from wire-sawing and casting of plinths for LECA delimiter and concrete delimiter.

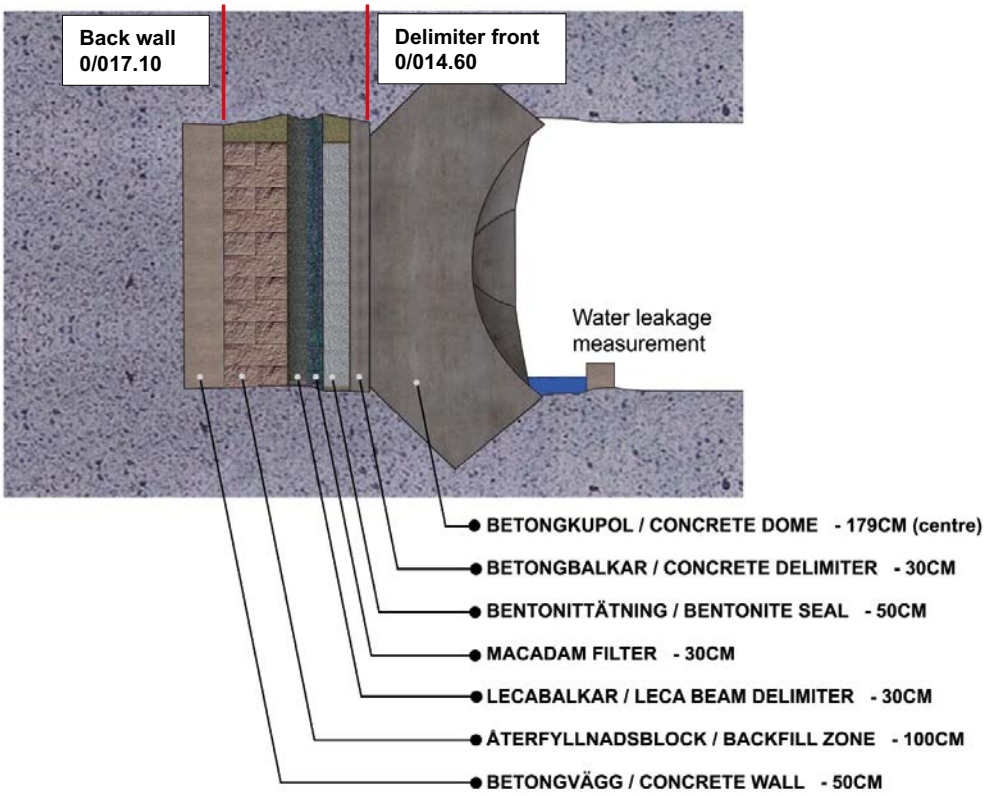

Figure 6-1. *Sketch of the DOMPLU full-scale test in experiment tunnel TAS01, with fixed length-coordinates (Äspö 96) for the front delimiter and for the concrete back wall.*

6.1 Concrete back-wall

On the tunnel face of TAS01, a concrete back-wall was cast consisting of low pH self-compacted concrete B200, see Figure 6-2. It was cast without reinforcement, i.e. the same procedure as for the concrete dome. The reasons for this wall were to achieve a controlled back surface of the tunnel and to get the correct length of tunnel needed for the experiment. The casting of the back-wall was also a practice for the casting of the concrete dome. Temperature sensors were installed inside the concrete back-wall in order to measure the heat generated due to hydration of concrete. In addition, an attempt was made to measure formwork pressure with analogue instruments.

The tunnel cross-section was measured by laser scanning, and plotted for every 20 cm of tunnel length. The nominal tunnel area is 19 m^2 and is illustrated with a blue line in the figure. In Figure 6-3, three scanned cross-sections of the tunnel at the location of the concrete back-wall are presented. In Figure 6-3a, section 0/017.10 is the downstream face of the concrete back-wall (the position of the formwork for the concrete back-wall). Figure 6-3b shows the last scanned section with a full horse-shoe shape; section 0/017.50 (located 40 cm on the upstream side from the face of the concrete back-wall). In Figure 6-3c the scanned tunnel face section is shown, which corresponds to section 0/017.90 (80 cm upstream the back-wall face).

The total amount of used concrete was approximately 17.5 m^3 and the thickness of the concrete wall varied in general, between 0.4 m to 0.8 m, as given from Figure 6-3.

6.1.1 Installation procedure

The back-wall shown in Figure 6-1 was installed using low-pH B200 concrete on June 20th, 2012. The formwork for the concrete back-wall is shown in Figure 6-4. The concrete was pumped into the form successively at one of three connections (positioned at different levels) during the casting procedure. The concrete back-wall was instrumented with three thermocouples measuring the temperature during hydration. The concrete batch was delivered by three lorries and the pouring took about 45 minutes for each lorry load.

Figure 6-2. *Photo of the concrete wall during removal of the formwork subsequent to casting.*

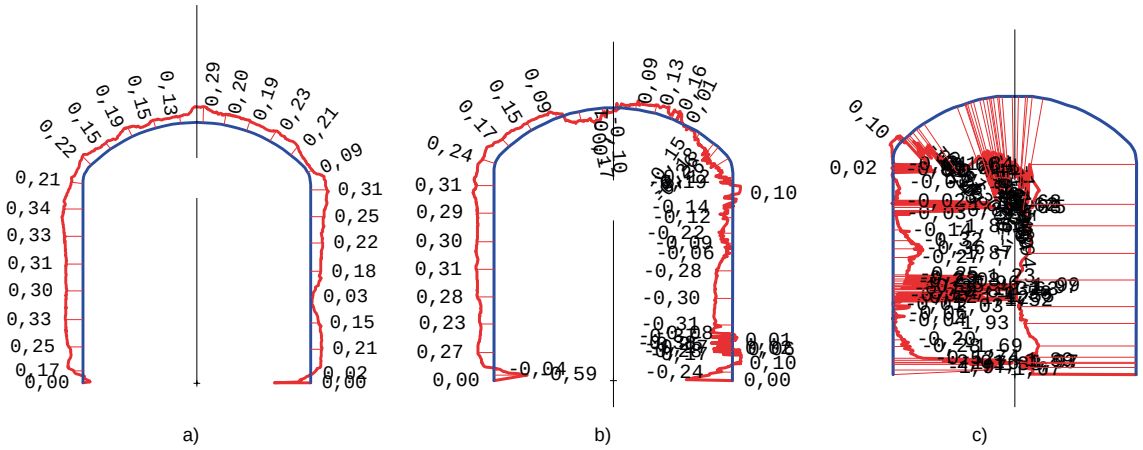

Figure 6-3. *Tunnel cross-section at the concrete wall, a) section 0/017.10 downstream front face of the back-wall, b) section 0/017.50 last horse-shoe shaped section of TAS01, c) section 0/017.90 the tunnel face of TAS01. Figures 6-3b and 6-3c are cluttered by numbers due to measuring contact with the intact rock.*

From each batch of concrete, different material tests were taken:

- Concrete specimen for cube test (described in Section 5.1.1).
- Slump flow measurement at arrival to the site and before starting pumping (described in Section 5.3).

The analogue measurement of formwork pressure showed relatively low pressure, but was only registered at a few fixed time intervals. In addition, one difficulty with the sensors used was that they required an initial pressure in order to measure relevant data and this initial pressure had to be deducted from the obtained results. One conclusion from this casting was that more instrumentation with continuous sampling is required to obtain valid data regarding the pressure on the formwork of the concrete dome.

The formwork was detached 3 weeks subsequent to casting and part of the cast back-wall can be seen in Figures 3-11, 6-7a and 6-9.

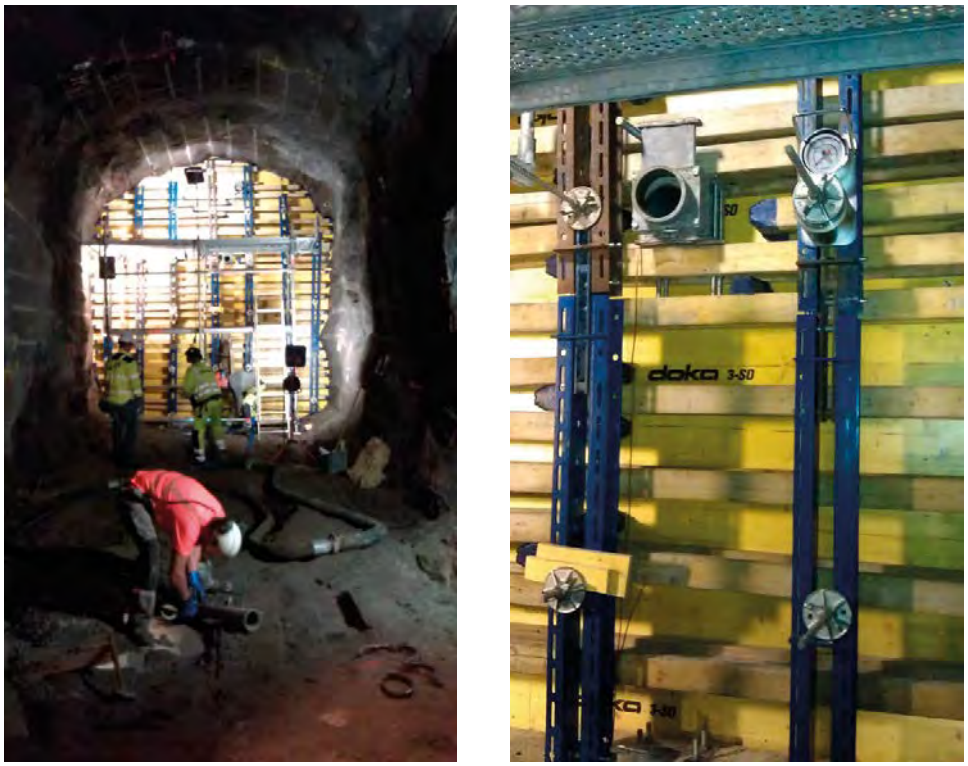

a) b)

Figure 6-4. *a) Complete formwork for the concrete back-wall. b) Formwork detail including analogue pressure gauge.*

6.2 Backfill transition zone

In the configuration used in the DOMPLU test setup, a small gravel pocket was placed on floor level directly in front of the concrete back-wall. This is not included in the reference design and is only part of the full-scale test for experiment operational reasons. It makes it possible to inject water behind the backfill and is thus used for both wetting of the backfill and pressurizing in the DOMPLU test. Further information about the water pressurization system is provided in Section 7.3.

The backfill blocks used for DOMPLU were manufactured of bentonite from Ashapura, India. This was one of the two backfill candidate materials (the other bentonite came from IBECO, Greece) that had been investigated within the project System Design of Backfill, see also Section 4.2.2.

These backfill blocks for the transition zone had been manufactured in brick size (300 × 150 × 75 mm) and could thus be easily stacked by hand. The total length of the backfill section included in the full-scale test was 100 cm. The blocks were arranged as seen in the photo provided by Figure 6-5. The slot between the bentonite blocks and the rock was manually filled with bentonite pellets. The design of the backfill TZ for DOMPLU also included 15 cm pellets between the backfill blocks and the LECA-filter.

The cross-section of the tunnel, at the location of the backfill TZ is illustrated in Figure 6-6. The tunnel cross-section was measured with laser scanning, and is here shown for the two sections closest to the front and end of the backfill. The nominal tunnel area is 18.8 m^2 and is illustrated with a blue line in the figure while the excavated tunnel area, illustrated by the red line, was significantly larger at these sections. In Figure 6-6a), section 0/016.10 is presented which is the downstream face of the backfill (the section closest to the filter). Figure 6-6b) shows section 0/016.90, which is near the upstream face of the backfill (the section closest to the concrete back-wall).

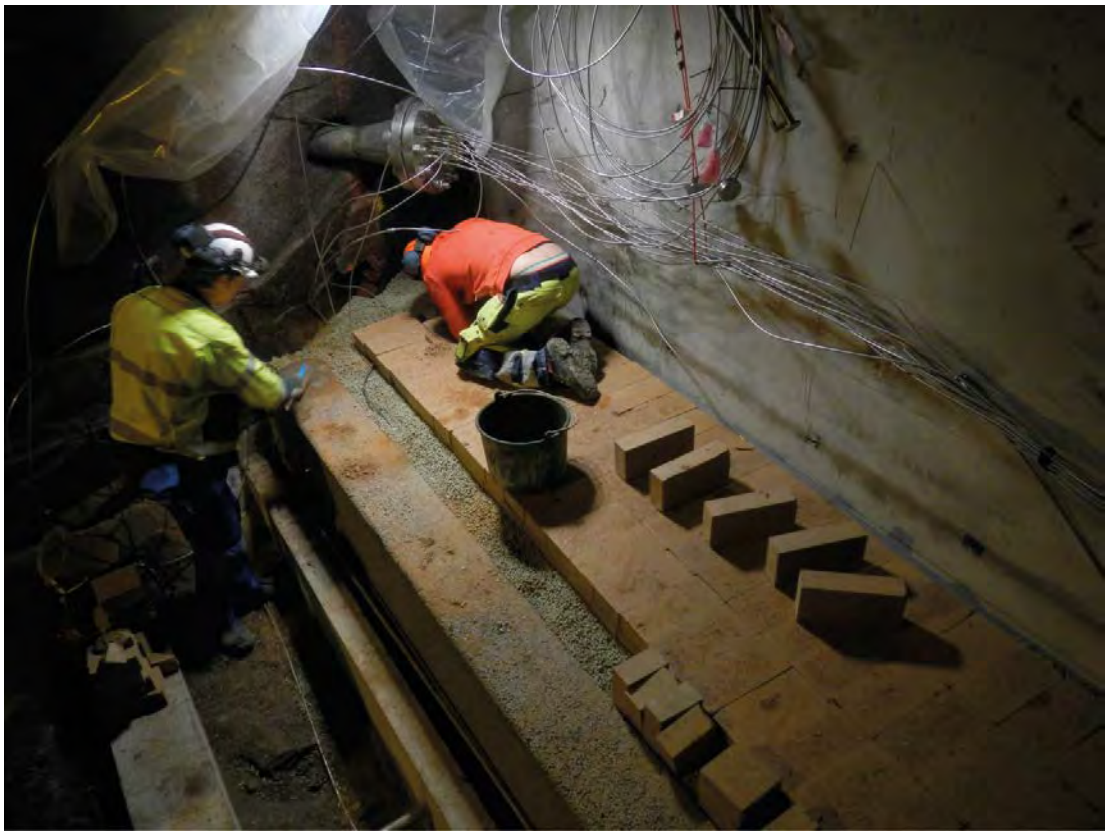

Figure 6-5. *View of the arrangement of bentonite blocks and pellets in the backfill transition zone for DOMPLU.*

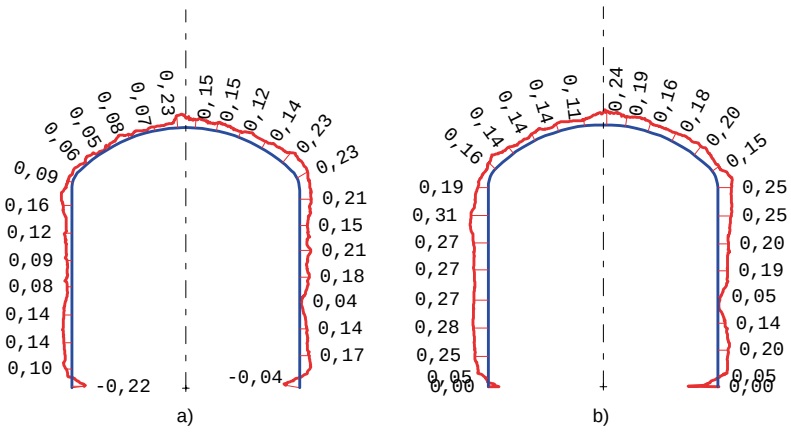

Figure 6-6. *Tunnel cross-section at the backfill, a) section 0/016.10 downstream face (i.e. near the filter), b) section 0/016.90 upstream section of backfill (i.e. near the concrete back-wall.*

6.2.1 Installation procedure

The installation started with emplacement of the first LECA beam. After this a 10 cm thick layer of bentonite pellets was placed on the tunnel floor. Subsequently the backfill bentonite blocks were stacked as illustrated by photos in Figure 6-5 and Figure 6-7. A band saw was placed close to the experiment location which was used to cut some of the blocks for optimal fitting in the horse-shoe shaped tunnel.

A slot with a thickness of 5 cm was left between the backfill blocks and the concrete back-wall, see Figure 6-7a. This slot was then filled with bentonite pellets but hosted also a gravel filled pocket as illustrated by Figure 4-6. The gravel filled pocket consists of a couple of hundred kg of gravel covered with geotextile wrapped around it. Three of the water injection pipes end up in this pocket, which enables it to be used for simulating a groundwater flow from the deposition tunnel.

The backfill blocks were assembled so that they ended at a distance of 15 cm before the LECA beams, see Figure 6-7b. This slot was filled with bentonite pellets subsequent to erection of a few LECA beams.

The installation of bentonite blocks and pellets for the backfill TZ was performed in parallel to installation of the LECA beam delimiter. Accordingly the installation was performed in stages where LECA beams were stacked up to a certain level, bentonite blocks were stacked to almost the same level and then the slots were filled with pellets, as shown by photos in Figure 6-8.

Temporary steel brackets were used to lock each LECA beam to the rock wall, to assure worker safety during ongoing installation. These brackets were later removed to allow some filter displacement to take place during pressurisation, due to the bentonite swelling.

a) b)

Figure 6-7. *Photos showing the installation process of bentonite backfill between the concrete back-wall and the LECA beams.*

a) b)

Figure 6-8. *Parallel installation of bentonite backfill blocks, pellets and LECA beams. In the photos, the installed displacement sensors are also shown together with some of the total pressure sensors.*

At the tunnel roof, the pellets were installed using a shotcrete equipment to fill the void between backfill blocks and the rock wall. In order to fill up the very last volume, a few liters with soaked pellets were used to prevent them from falling out.

Summary of the installed backfill transition zone:

- Total pellets: 10 862 kg.
- Total blocks: 29.5 pallets = 23.6 ton in 59 layers , where:
  - 50 full width layers (3885 mm),
  - 5 first instep layers (3285 mm) near tunnel roof,
  - 4 second instep layers (1800 mm) closest to tunnel roof.

6.3 Filter

The filter component of DOMPLU consists of two material layers; a stiff draining material of 30 cm thick LECA beams and a 30 cm layer of geological draining material, i.e. gravel (macadam 2–4 mm), as shown by Figure 6-1. The main reason for using a stiff draining material, i.e. the LECA beams, is that it also needs to act as a delimiter for the backfill transition zone and must carry the load from bentonite blocks/pellets during installation. Different alternatives for both geological and stiff draining materials were tested and evaluated by Börgesson et al. (2015a), as previously described in Section 4.1.2. In addition, two drainage pipes are installed from the gravel filter. These pipes pass through the bentonite seal and the concrete dome and drains groundwater during construction.

In Figure 6-9, a photo from installation of the LECA beams is shown.

The tunnel profile at the location of the filter is illustrated by Figure 6-10. The tunnel cross-section was measured with laser scanning, and is here shown for the two sections at the location of the filter. The nominal tunnel profile is illustrated with a blue line in the figure, while the actual tunnel geometry is shown with a red line. In Figure 6-10a, section 0/015.50 is presented. This is where the gravel filter is installed, which is the scanned section closest to bentonite sealing. Figure 6-10b shows section 0/015.90 where the LECA beams are installed (the filter section closest to the backfill), as seen in Figure 6-9.

Figure 6-9. *Installation of the LECA beams.*

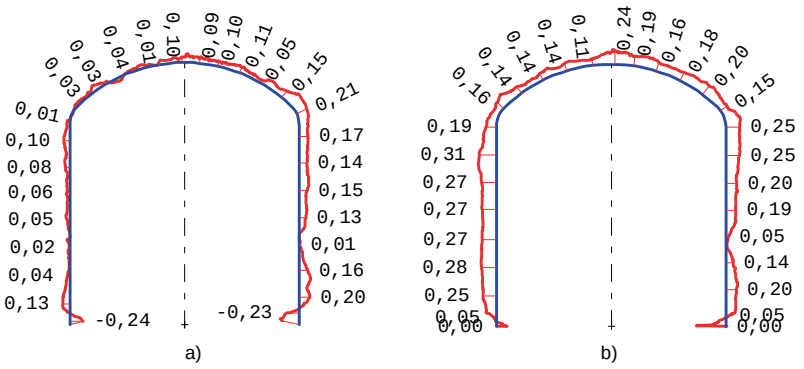

Figure 6-10. *Tunnel cross-section at the filter section, a) section 0/015.50 downstream side (i.e. near the bentonite seal), b) section 0/015.90 upstream section of the filter (i.e. near the backfill).*

6.3.1 Installation procedure

The installation of LECA beams was performed in parallel to the installation of bentonite backfill blocks and pellets, as described previously in Section 6.2.1. The prefabricated LECA beams (manufactured by Nyströms Cement AB) have a height of 600 mm and a thickness of 300 mm, which is consistent with dimension of the concrete beam delimiter.

The LECA beams were piled on each other and plastered together in order to prevent concentrated leakage of bentonite fines between them. The plaster was mixed using standard Portland based cement.

In addition, the beams were temporarily fixed to the rock with L-shaped steel brackets, and the voids between the rock wall and the edges of the LECA beams were caulked with fiberwool, as shown by Figure 6-11. The reason for using fiberwool as a material stopper is that the LECA delimiter should be able to move somewhat in a later stage, when the bentonite will start to apply a swelling pressure on the wall. Accordingly the steel brackets were removed one by one during installation of the further components downstream.

The installation of the geological draining material, i.e. 2–4 mm gravel, was performed in parallel to the installation of the bentonite seal (blocks and pellets) and the outermost delimiter (concrete beams) as shown by photo in Figure 6-12. The two drainage pipes had been prepared in advance during casting of the plinth for the concrete beam delimiter. The pipes' ends were provided with simplified bottom valves of fine wired copper mesh.

A needle felted geotextile delimiter was also installed to separate the gravel from the bentonite seal. The geotextile was wrapped underneath the gravel filter, i.e. in contact with the rock floor. After positioning the geotextile on the floor, a first layer of gravel was placed on the geotextile. On the other side of the geotextile, MX-80 bentonite pellet was placed on the floor to form an even surface for the bentonite seal blocks. The installation of bentonite blocks and gravel with geotextile in between was then performed as parallel activities, see Figure 6-12. The concrete beams, positioned on downstream side of the bentonite blocks, were also installed at the same time.

The general procedure was as follows; first a concrete beam was put in place followed by emplacement of one row of bentonite blocks behind the beam. Hence gravel was filled up to the blocks top surface. The geotextile was attached to the bentonite blocks with nail plugs, equipped with red plastic washers, and was after that pushed tight to the bentonite blocks by the weight of the gravel filling. When the bentonite blocks and the gravel had reached the upper level of the emplaced concrete beam, the next concrete beam was piled and the procedure repeated.

The geotextile carpet had a width of 2 m. When changing to a new geotextile, it was mounted with a large overlap (20–30 cm) to the already installed geotextile.

a) b)

Figure 6-11. *a) Fixing of LECA beams to the rock wall and tightening by fiberwool, b) Installation of LECA beams using plaster mix and temporary steel brackets.*

a) b)

Figure 6-12. *a) Simultaneous installation of gravel filter (macadam 2–4 mm), middle delimiter (geotextile), bentonite seal (blocks and pellets) and outer delimiter (concrete beams). b) Side-view of the drainage pipe used for de-airing, ending near the tunnel roof inside the gravel filter. The other drainage pipe ends at the bottom of the gravel filter (not visible in the photos).*

6.4 Bentonite seal

The bentonite seal consists of bentonite blocks composed of MX-80, compacted by uniaxial compression to a size of 500 × 571 × 300 mm. The design height 300 mm of a seal block was chosen to comply with the 600 mm height of a concrete beam. The total design depth of the bentonite seal for DOMPLU is 500 mm.

The bentonite blocks were compacted with a pressure of 27 MPa and had a water content of 17 % with a resulting dry density of about 1700 kg/m^3. A photo of a bentonite seal block is shown in Figure 6-13a.

The bentonite seal blocks were to be arranged in a design pattern provided by Figure 6-13b.

The cross-section of the tunnel, at the location of the bentonite seal was measured with laser scanning, and is illustrated in Figure 6-14, where the two sections closest to the beginning and end of the bentonite seal are shown. The excavated tunnel area was about 19.9 m^2 and is illustrated by the red line in the figure. In Figure 6-14a, section 0/015.10 is presented which is the downstream section of the bentonite seal (the section closest to the concrete beams). Figure 6-14b shows section 0/015.30, which is the upstream section of the backfill (the section closest to the geotextile delimiter and gravel filter).

6.4.1 Installation procedure

The installation of bentonite blocks was performed as a parallel activity to the installation of the gravel filter and concrete beams according to description in the previous Section 6.3.1.

The MX-80 bentonite blocks were stacked in accordance with the pattern illustrated by Figure 6-13b. A vacuum lifting tool was used to facilitate the manual work with block emplacement. Figure 6-15 provides a photo of the installation of bentonite blocks for the seal. Finally, the slots between the bentonite blocks and the rock were manually filled with bentonite pellets, similarly to the description of backfill pellets in Section 6.2.1.

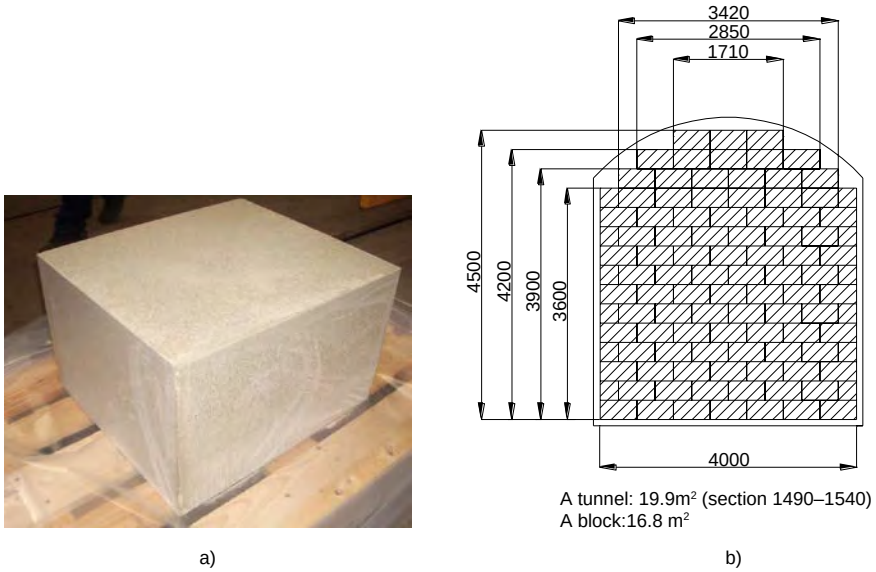

Figure 6-13. *a) MX-80 block for the bentonite seal. b) Schematic arrangement of bentonite blocks in the bentonite seal.*

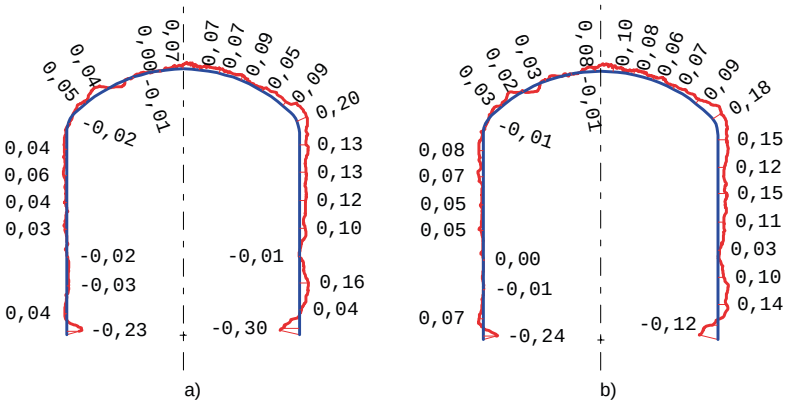

Figure 6-14. *Tunnel cross-section at the backfill, (a) section 0/015.10 downstream part of the seal (near the concrete beams), (b) section 0/015.30 upstream part of the seal (near the filter).*

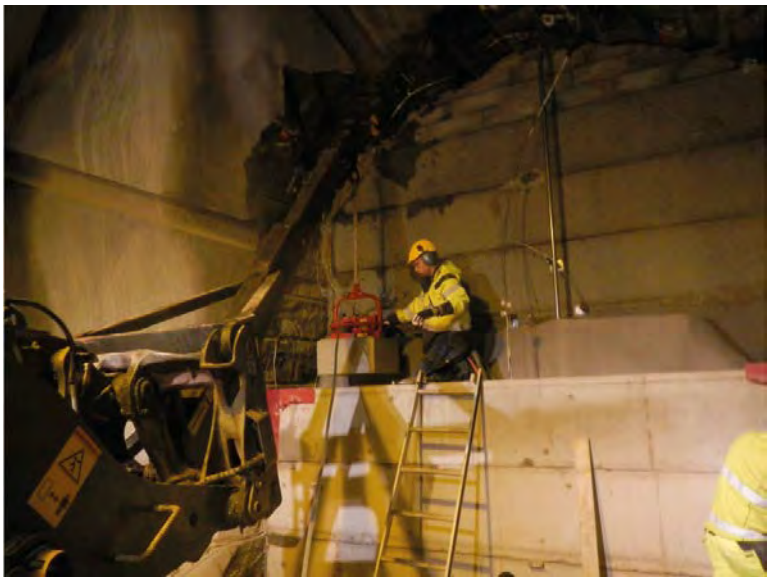

Figure 6-15. *Installation of bentonite blocks for the DOMPLU bentonite seal.*

Summary of the installed bentonite seal section:

- Mass of installed pellets: 2362 kg.
- Number and mass of installed blocks: 100.5 blocks at 160 kg each = 16.08 ton, in 15 layers:
  - 12 layers with 7 blocks,
  - 1 layer with 6.5 blocks,
  - 1 layer with 6 blocks,
  - 1 layer with 4 blocks.

6.5 Concrete delimiter

The concrete beams were prefabricated in the Äspö HRL, above ground. The beams consist of low-pH reinforced concrete. Their dimensions are 300 × 600 × 4160 mm ($w \times h \times l$). The concrete used for the beams was the B200 mix and pouring into the moulds was done in connection with casting of the concrete wall at the TAS01 tunnel face, as previously described in Section 6.1. The weight of one concrete beam is about 1800 kg. The beams were reinforced with six evenly distributed longitudinal bars ⌀16 mm with a spacing of 100 mm, on the upstream and downstream side respectively. In addition, the concrete beams were reinforced with shear reinforcement ⌀10 mm with a spacing of 200 mm. All reinforcement bars were of conventional steel, type B500B.

The tunnel geometry at the location of the installed concrete delimiter is shown in Figure 6-16. As this figure shows, the excavated tunnel geometry (red line) is very close to the theoretical shape (blue line). However, gaps between the concrete delimiter and the rock wall will always be present to allow for beam emplacement, which is especially intricate at the tunnel roof. These remaining gaps require additional concreting as described later in Section 6.5.1.

6.5.1 Installation procedure

The concrete beams were lifted into place by a crane on wheel as shown in Figure 6-17a. In order to fix the beams to each other, the beams had prefabricated vertical holes present, into which steel rods were inserted after mounting one beam on another. Steel fasteners were drilled into the rock wall at the two beam ends, i.e. at the position of its anchorage to the rock. In addition, mortar was filled in the remaining gap between the rock wall and the beam's ends as seen in Figure 6-17b. A liner of thick mortar (cement/water) was applied, and allowed to harden, before the more fluid mortar was poured. The filling at the ends was done to restrict possibilities for flow of bentonite (from the watertight seal) and concrete (from the concrete dome) respectively.

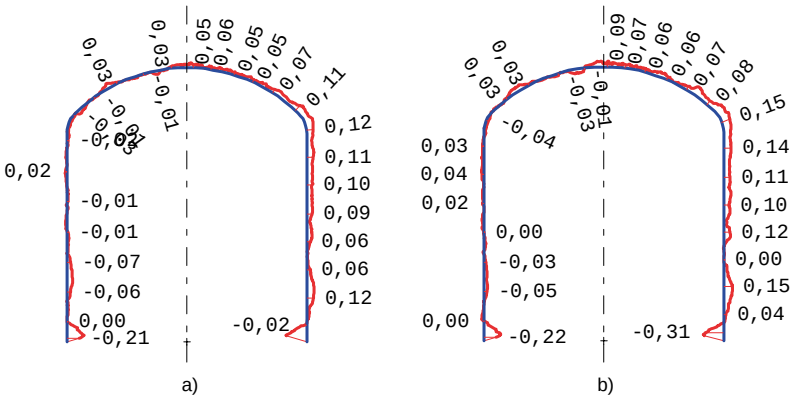

Figure 6-16. *Tunnel cross-section at the concrete delimiter position, a) section 0/014.70 downstream section (i.e. near the concrete dome), b) section 0/014.90 corresponds to the upstream delimiter face (adjacent to the bentonite seal).*

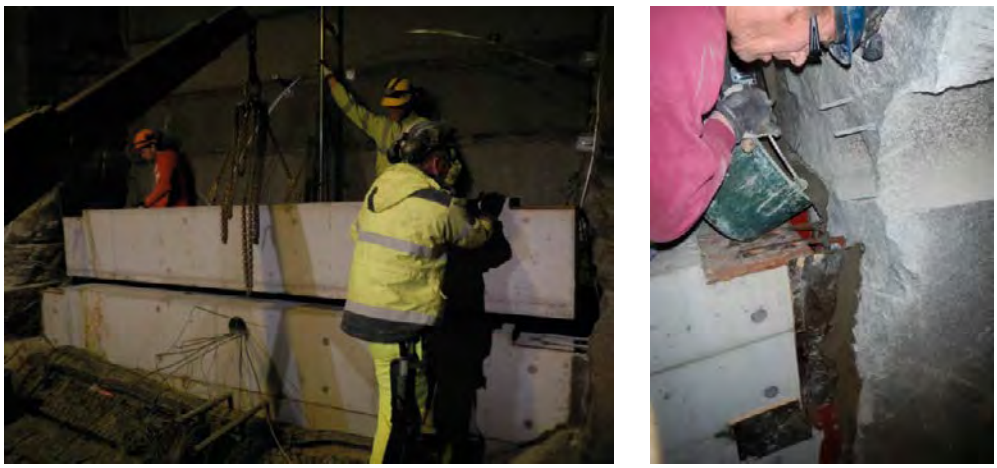

Figure 6-17. *Installation of a concrete beam, a) lifting it into place, b) filling of gap between beam end and the rock wall.*

A photo of the completed concrete delimiter is provided by Figure 6-18a.

Summary of the concrete delimiter component:

- A total of eight beams were installed:
  - 6 full length beams (BE1 in Figure 6-18b).
  - 1 beam with inclined sides at the rock interface (BE2 in Figure 6-18b).
  - 1 short beam with inclined sides at the rock and a height of 400 mm (BE3 in Figure 6-18b).

Finally, on the downstream face of the concrete delimiter, two layers of geotextile were installed in order to prevent a bond forming between the concrete dome and the concrete delimiter, as seen in Figure 6-19. This was made to allow the dome plug to detach from the delimiter during shrinkage associated with concrete curing.

As can be seen in Figure 6-19, the remaining half circular boreholes from wire sawing of the slot had been filled with concrete at an earlier stage. This is evident as the lighter-coloured rectangular segments in the photograph.

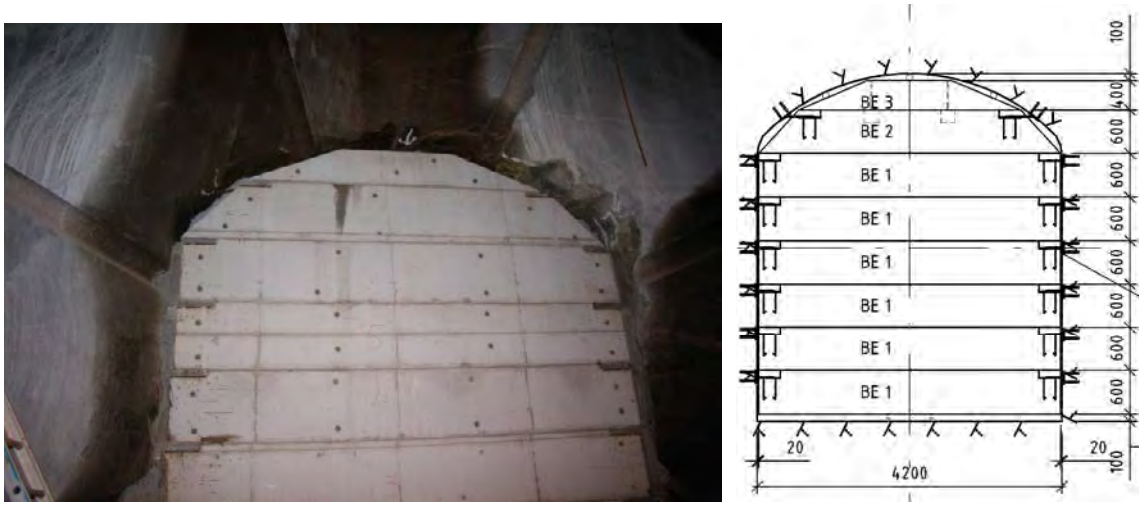

a) b)

Figure 6-18. *a) Installed concrete beams (the delimiter between bentonite seal and concrete dome. b) Sketch showing construction plan drawing of the concrete delimiter.*

Figure 6-19. *Geotextile fixed to the front of the concrete delimiter.*

6.6 Concrete dome

The concrete dome consists of self-compacting low-pH concrete without reinforcement and was cast-in-place on March 13, 2013. In this section, all main activities performed related to the casting of the concrete dome are presented.

First, the stages performed before casting the concrete dome are described. These are the installation of grouting tubes and cooling pipes, Section 6.6.1, and the installation of formwork, Section 6.6.2.

After this, the casting of the concrete dome is described in Section 6.6.3. In addition, a description of the contact grouting performed approximately three months after casting is provided by Section 6.6.4.

6.6.1 Grouting tubes and cooling system

The work began by installing grouting tubes in three circumferential sections of the excavated slot. The tubes used were made of cross-cut 50 mm plastic drainage pipes. A 10 cm wide cloth of geotextile was used to cover the pipes, to protect them from concrete clogging, and it was fastened to the rock with nails on the respective side of the tube. On each side of a circumferential grouting tube, approximately 30 cm away, bentonite bands (of type Volclay) were nailed to the rock to achieve a locker for the injection grout. Photos from installation of the grouting tubes can be seen in Figure 6-19 and Figure 9-42 and a drawing is provided by Appendix 1. The thinner grouting tubes, earlier installed in the moulded large-diameter boreholes, were connected to each grouting section by letting the wider tubes fully overlap them. Due to the height of the excavated slot, almost 9 m from bottom to top, a sky-lift was used by the staff during installations.

Subsequently, rock attachments for the framework to the cooling pipes were prepared by drilling 250 mm deep holes with flat bottoms in the inclined surface of the slot. The cooling pipes need a supporting steel frame, since they are not self-supporting.

The steel frame consisted of seven vertical steel profiles carrying fourteen horizontal profiles of pendulum rails. By anchoring the seven vertical steel profiles to the drill holes with surrounding sealing foam, both in the top and bottom holes, the design allows for some relative displacements between the rock and the frame with respect to the load of the concrete and its shrinkage. The pipes have a concrete coverage of at least 400 mm. The supporting steel frame and the mounted cooling pipes are shown in Figure 6-20. In the figure, some of the strain gauges, later described in Section 7.2, are also shown.

The purpose of the cooling pipes is to be able to control the temperature during different stages of the construction.

The cooling pipes were made of copper with a diameter of ⌀25 mm, and consist of three separate sections which had been pre-fabricated above ground. The three sections were divided in the vertical direction, and each section consists of about 80 m of copper pipes. An illustration of the placing of cooling pipes is illustrated in Figure 6-21. Larger size drawings are provided by Appendix 1.

An advanced cooling scheme was used to control the temperatures in the dome at different stages:

1. Stage A – To reduce the effect of hydration heat.
2. Stage B – Cooling of the dome in order to force it to release from the rock.
3. Stage C – Additional cooling of the dome prior to contact grouting.

Figure 6-20. *Installed cooling pipes with the supporting steel frame.*

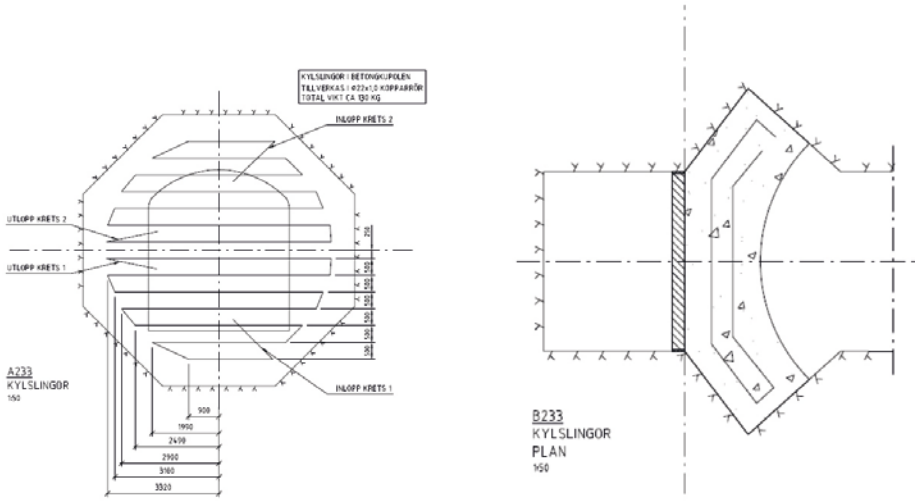

Figure 6-21. *Cutout from construction drawing for placement of cooling pipes in the concrete dome. Left: front view, Right: horizontal cross-sectional view. (Text in Swedish.)*

One machine, producing at least 20 kW, was used to cool the water before it was circulated within the cooling pipes. In addition, since the cooling is vital for the construction, a redundant (backup) machine was also placed on site, if the first one would fail for some reason. A photo of the two cooling machines is shown in Figure 6-22. The cooling media used consisted of water mixed with an anti-freeze fluid (propylene glycol), in the proportions of approximately 70 % water and 30 % propylene glycol. Temperatures were measured of the cooling media on both the inlet and outlet pipes respectively. The flow was controlled in the pipes with the target to maintain a temperature difference between these two less than 2°C. The temperature values given in Table 6-1 below refers to the average temperature of the inlet and outlet pipes.

In Table 6-1, the cooling sequence is presented, and further explanation of the cooling sequence is provided. The three different stages of cooling, described earlier, are seen in the table; starting after 13 hours, 151 hours and 78 days respectively. The ambient temperature in the tunnel varies slightly and is in general between 13–15°C, which is later shown in Section 9.2.2.

Table 6-1. Cooling sequence.

Time in hours (days)	Event	Temperature of cooling water
−1	The cooling system is started and running, but without cooling.	No cooling.
0–13 (0.5)	Casting of concrete starts, with a maximum casting rate of 1.0 m/hour. (target value is 0,75 m/hour).	No cooling.
13 (0.5)–126 (~ 5)	Cooling sequence to reduce heat generated by hydration (Stage A).	Minimum of +7°C
126 (~ 5)–151 (~ 6)	Cooling temperature is gradually increased, to allow for faster strength development.	+11°C
151 (~ 6)–484 (20)	Cooling sequence to force the concrete dome to release from the rock (Stage B).	+4°C
484 (20)	Cooling stopped, to allow for faster strength development.	No cooling.
500 (21)	The formwork is removed.	No cooling.
1861 (~ 78)	The cooling is started again gradually, in order to shrink the concrete dome prior to contact grouting. (Stage C).	+1°C
2477 (~ 103)	Contact grouting.	+1°C
After grouting	Cooling is stopped gradually.	No cooling.

Figure 6-22. *The two cooling machines placed in the main tunnel TASJ.*

The cooling system was not used for cooling the concrete in the beginning of casting. The cooling system was controlled so that cooling initiated when the bottom temperature sensor indicated an increased temperature of more than +1°C. This occurred after about 13 hours, i.e. almost at the same time as casting of the concrete was completed.

After this, the cooling system was turned on to lower the temperature inside the concrete during the hydration (Stage A). This cooling stage was carried out for about one week. During this period the cooling temperature was changed gradually to counteract the heat generated by hydration. The lowest temperature in the cooling pipes was +7°C. At the end of this cooling stage, the cooling was increased as much as possible without introducing a risk of cracking the concrete. The temperature in the cooling pipes at this stage (Stage B) was +4°C, and was kept constant for about 6 days. The reason for this second cooling step was to encourage the concrete dome plug to release from the rock (cause a bond failure between concrete and rock by cooling shrinkage). After this, the temperature in the cooling system was successively increased until it was finally shut off. At this point, the cooling system was turned off for almost two months. This allowed the concrete dome to increase in strength. Based on results from previous investigations, Vogt et al. (2009) and Malm (2012), it had been determined that the concrete dome requires about 3 months before contact grouting should be performed. The basis for this was to allow for sufficient strength development of the concrete and to make sure that a significant part of the autogenous shrinkage has occurred before initiation of the contact grouting procedure. Therefore, when estimated that sufficient strength had been developed, approximately 78 days after pouring, the cooling process began again (Stage C). This time the purpose of cooling was to create as large a gap as possible between the concrete dome and the rock in order to allow for effective contact grouting. By doing the contact grouting when the temperature in the concrete dome is much lower than the ambient temperature, a thermal pre-stressing of the dome is accomplished.

As mentioned previously, the ambient temperature in the tunnel was on average about +14°C, and the minimum temperature in the concrete during the thermal pre-stressing was almost the same as in the cooling pipes, i.e. +1°C. This results in a thermal compressive pre-stress of about 4.5 MPa, based on the following expression.

$$\sigma = E \cdot \alpha \cdot \Delta T \qquad (6\text{-}1)$$

where:

α is the thermal expansion of concrete, i.e. $10^{-5}\,°C^{-1}$.

E is the elastic modulus, i.e. 33.9 GPa according to Vogt et al. (2009).

ΔT is the temperature difference between cooling and the ambient temperature, i.e. –13°C.

However, the temperature in the concrete was not uniform, as later shown in Section 8.2.2 and 9.2.2 for the numerical analyses and measurements, respectively. This means that the thermal pre-stressing effect will be less than the value calculated above and also that the pre-stressing varies over the geometry of the concrete dome.

6.6.2 Formwork

The shape of the concrete dome is octagonal, while the tunnel normally is horse-shoe shaped. Therefore, the formwork used to cast the concrete dome has to adjust for the variations in shapes. The formwork was designed and delivered by Doka GmbH, and is illustrated in Figure 6-23 below. The formwork for the concrete dome consists of an outer frame that is adjusted to the contours of the excavated tunnel. In the centre, the formwork consists of four main pieces that are mounted directly to the outer frame. The main pieces are sealed together from the inside by fastening of plastic membranes. The remaining openings, mainly due to variations in theoretical and real tunnel shape, are thereafter adjusted and built on site by carefully sawn plywood moulds. The still remaining very small gaps were thereafter filled with sealing foam.

A photo of the outer frame for the concrete formwork is shown in Figure 6-24. The supporting struts, intended to transfer the hydrostatic pressure from the newly cast concrete to the surrounding rock is shown in Figure 6-25. To simplify anchoring of the supporting struts to the rock a thin layer of concrete was used to make the tunnel floor flat, as also seen in Figure 6-25.

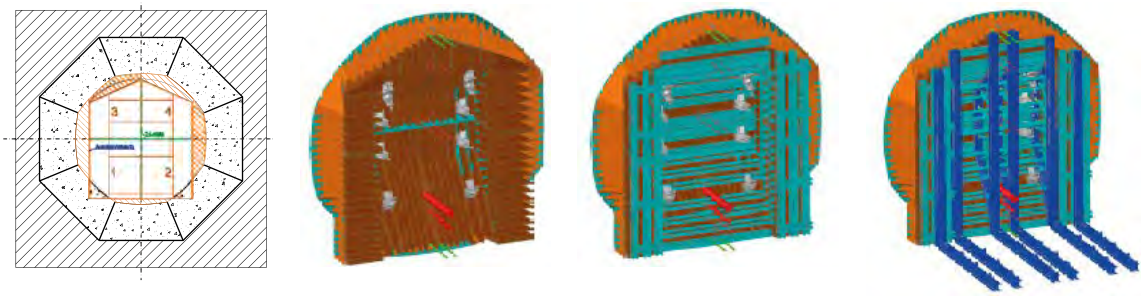

Figure 6-23. *Designed formwork used for casting the concrete dome plug.*

Figure 6-24. *Prefabricated outer frame of the concrete dome formwork.*

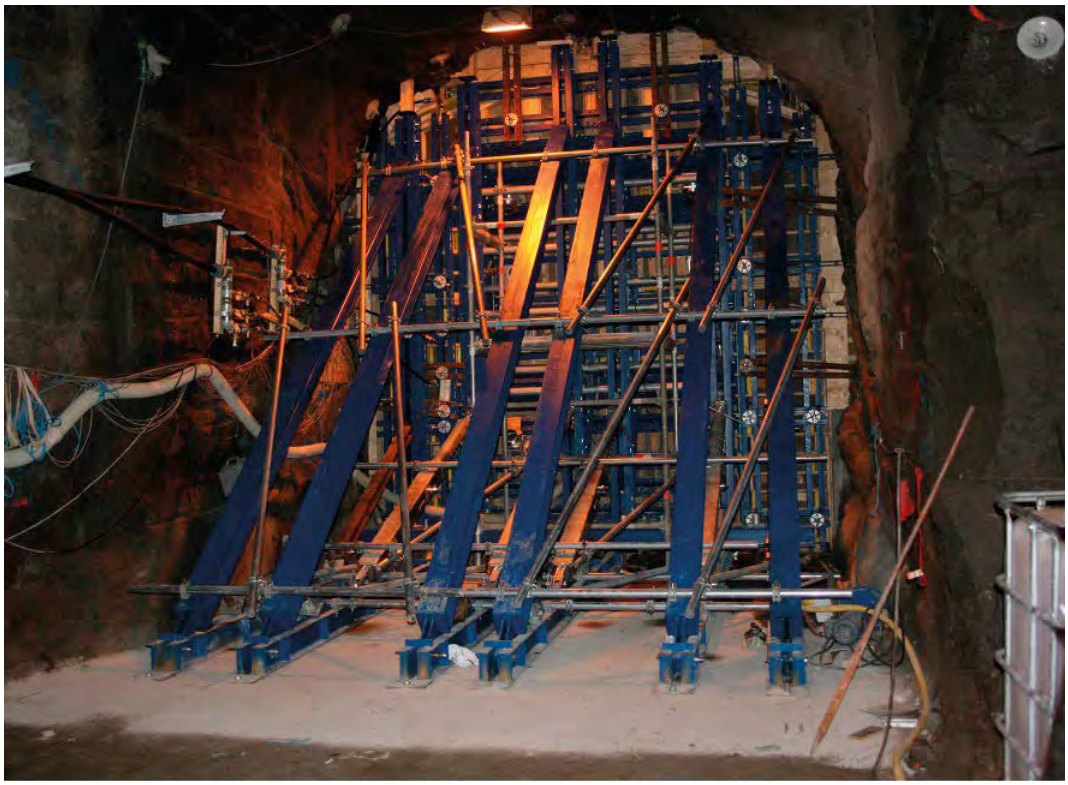

Figure 6-25. *Concrete formwork with supporting struts to transfer the hydrostatic pressure from the concrete slurry to the surrounding rock.*

The formwork is designed for a full hydrostatic concrete pressure. In design, the density of the concrete was assumed 2400 kg/m^3, which results in a maximum theoretical hydrostatic pressure (used in the ultimate limit state for the formwork) of 160 kN/m^2 at the bottom of the form (pressure height 6.8 m) and 30 kN/m^2 (pressure height 1.3 m) at the top of the formwork. The pressure distribution between these two levels is assumed linear, and is illustrated in Figure 6-26.

In the full-scale test, a low rate of casting was used, defined as less than one meter per hour. This will result in the concrete curing earlier in the bottom and thereby developing some strength by the time the last batch of concrete is cast in the top. This will contribute to a significantly reduced pressure on the formwork and it is also positive in the aspect of reduced concrete dome shrinkage.

The formwork was designed so that it could be mounted after the cooling pipes, instrumentation and drainage pipes had been installed. In addition, five pressure sensors were installed in the formwork as later described in Section 9.2.1. Several holes were also made in the formwork used to pump the concrete into the form.

This means that several perforations were made in the form, in order to lead cables and pipes out from the concrete dome plug to the downstream side of the plug.

6.6.3 Casting

The low-pH B200 concrete used for casting the concrete dome plug was delivered to Äspö HRL by lorries, see Figure 6-27a. In total, 13 lorries were used to transport the concrete from the factory in Kalmar to the site at Äspö. The estimated time needed for transport was about 2 hours from the factory to the site underground and then additionally 45 minutes were needed for the casting procedure. The concrete was pumped into the formwork by the help of a concrete pump as seen in Figure 6-27b. The casting of the dome is shown in Figure 6-27c and was made with a maximum casting rate of 100 cm per hour which resulted in a total time for the casting of approximately 10 hours. The arrival time and pumping time for each lorry is presented in Table 6-2.

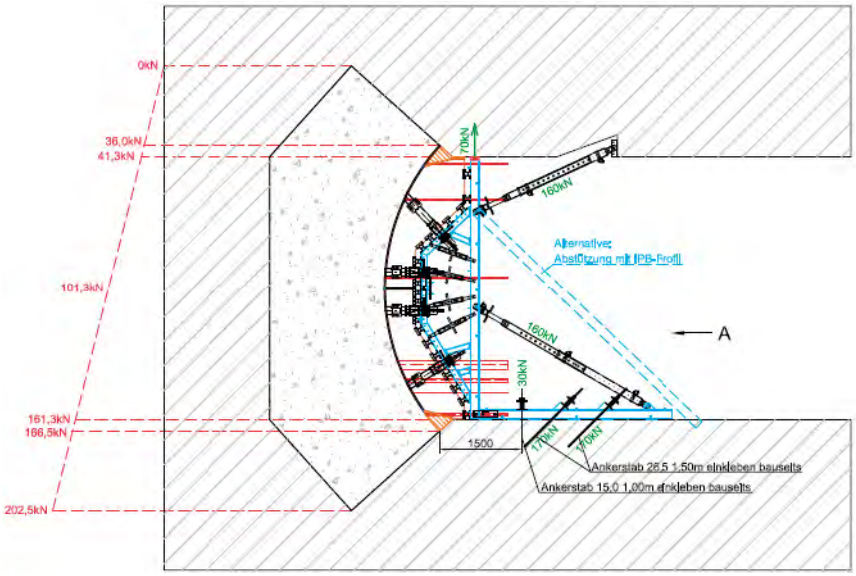

Figure 6-26. *Formwork and calculated hydrostatic pressure from poured concrete.*

a) b)

Figure 6-27. *Photos from the casting of the concrete dome, a) concrete lorry, b) casting the dome plug.*

Similarly to the cooling machine, a concrete pump breakdown would have been harmful to the concrete dome casting. Therefore, a backup concrete pump was kept on stand-by in the Äspö HRL during the dome casting.

Material tests were conducted at both the factory and at the site, as described in Chapter 5.

During pumping, there was no need to use all hatches in the formwork but 2 + 2 + 2 was used for pouring. The formwork was tight and not more than 2 dl of concrete escaped to the front.

Table 6-2. Casting of the concrete dome.

Lorry	Arrival time	Pump time
1	08:47	09:15
2	09:37	10:00
3	10:44	11:00
4	11:20	11:50
5	12:03	12:15
6	12:43	13:00
7	13:57	14:10
8	15:11	15:20
9	15:28	15:45
10	16:11	16:20
11	17:02	17:10
12	17:51	18:00
13	18:46	19:00

The formwork was detached three weeks subsequent to casting. A photo of the concrete dome is provided by Figure 6-28.

6.6.4 Contact grouting

The purpose of the contact grouting is to seal gaps that may have occurred between the concrete dome plug and the surrounding rock. During the first 90 days, significant autogenous shrinkage of concrete occurs. In addition, the thermal cooling of the concrete dome prior to contact grouting also results in contraction of the structure. Both of these effects force the concrete dome to release from the rock and should result in a gap forming between the concrete and the rock. According to Malm (2012), the estimated gap due to autogenous shrinkage at the time of grouting was estimated to be about 3.7 mm in the top of the dome plug and 1.8 mm on the sides (assuming that the plug has fully released from the rock), see Figure 6-29.

Figure 6-28. *Photo of the cast concrete dome. The steel bars in front of the dome were later used for positioning of displacement sensors.*

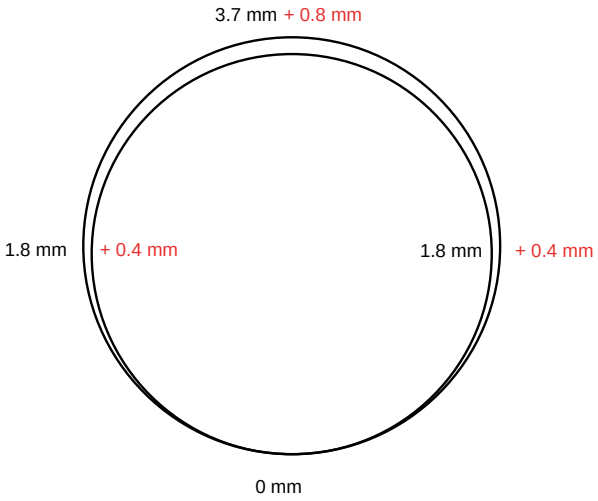

Figure 6-29. *Estimated slot after shrinkage and cooling, if the dome plug entirely releases from the rock.*

The cooling of the structure performed prior to contact grouting increases this gap further. As noted in Section 6.1.1 the temperature was decreased to + 1°C prior to grouting. In Malm (2012), it was assumed that the ambient temperature in the tunnel was +12°C, i.e. ΔT = 11°C, which results in a further increase of the gap in the top of the dome plug of 0.8 mm. The total gap in the top of the dome, prior to grouting, would according to this simplified estimation be approximately 4.5 mm.

Estimation of contact grouting needed

Based on the calculation in Malm (2012), the required amount of grout can be estimated. Due to the complex geometry of the dome plug, a few simplifications are made to estimate the amount of grout needed.

- The radius of the concrete dome plug is r = 4.05 m.
- Shrinkage strain 0.46 mm/m,
  - i.e. a constant reduction of the radius, equal to δ_{shr} = 1.8 m.
- Thermal strain 0.11 mm/m ($\Delta T \cdot \alpha$ = 11°C · 1e-5°C^{-1} = 0.1 mm/m),
  - i.e. a constant reduction of the radius, equal to $\delta_{\Delta T}$ = 0.4 m.

A rough estimate is that the amount of grout needed can then be calculated as:

$$V_{grout} = \pi \cdot r^2 - \pi \cdot (r - \delta_{shr} - \delta_{\Delta T})^2$$

This resulted in an estimate that approximately 260 litres of grout was needed to fill the gap between the rock and the concrete, of which about 210 litres are required to compensate for the shrinkage.

Contact grouting performed

The contact grouting was performed in three stages.

In the first stage, contact grouting was performed with the inner tube, located on the upstream side of the dome. After this, in the second stage, contact grouting was performed with the outer tube, located on the downstream side of the plug. Both of these groutings were performed on the same day, June 11th 2013. In the first stage, a total of 105 litres were used and the pressure was stable and ended at 10 bar. The grouting that was used was *Injektering 30* from Cementa with a water to cement ratio (vct) of 0.65.

During the second stage, i.e. grouting of the outer tube, grouting was performed with successively decreased water to cement ratio, starting from 0.65 to 0.60 and thereafter 0.5. The total amount of grout was 143 litres where the final injection pressure was 10.7 bar. At the time of this grouting, when about 42 litres of grout had been used, two smaller areas with leakage of grouting were

detected, which could indicate the presence of 2 m of bridging cracks past the dome. These leakage points corresponded with the locations where water leakage during pressurization was subsequently detected, see Section 9.3.1.

The third and final grouting stage was performed on June 19th, i.e. about one week after the first two. For this grouting stage, a grout product *Injektering30* with a water to cement ratio of 0.75 was used. In this stage, the centre tube was grouted. A total of 406 litres of grout was used. This grouting stage was performed with a pressure increase of 10 bar/min and ended with a final injection pressure of 61 bar (6 MPa). During the grouting of the last tube, no leakage was detected and the maximum pressure was maintained for 30 minutes until the grouting was stopped.

A total of 654 litres of grout was used, which is almost three times as much as needed to fill the gap between concrete dome and the rock according to the simplified estimation above. It is thereby likely that grout may have also have entered voids or fractures in the rock adjacent to the dome and/or gaps within the concrete dome (such as between cooling pipes and concrete dome). It is also possible that grout may have filled the region between the concrete dome and the concrete delimiter (i.e. the geotextile layers).

6.7 Weir for leakage measurement and plastic cover of dome

Subsequent to removal of the formwork, three weeks after casting, the weir for leakage water collection on the downstream side of the dome was constructed.

The weir consists of a reinforced concrete plinth (width 300 mm, height 300 mm) between the tunnel walls, cast by standard Portland cement (water cement ratio below 0,55). It had been prepared with injection tubes during moulding. The injection tubes (of type Fulko) were placed in two parallel lines with c/c distance 10 cm. Contact grouting of the cast weir was the performed to assure water tightness. A photo of the cast weir is provided by Figure 6-30.

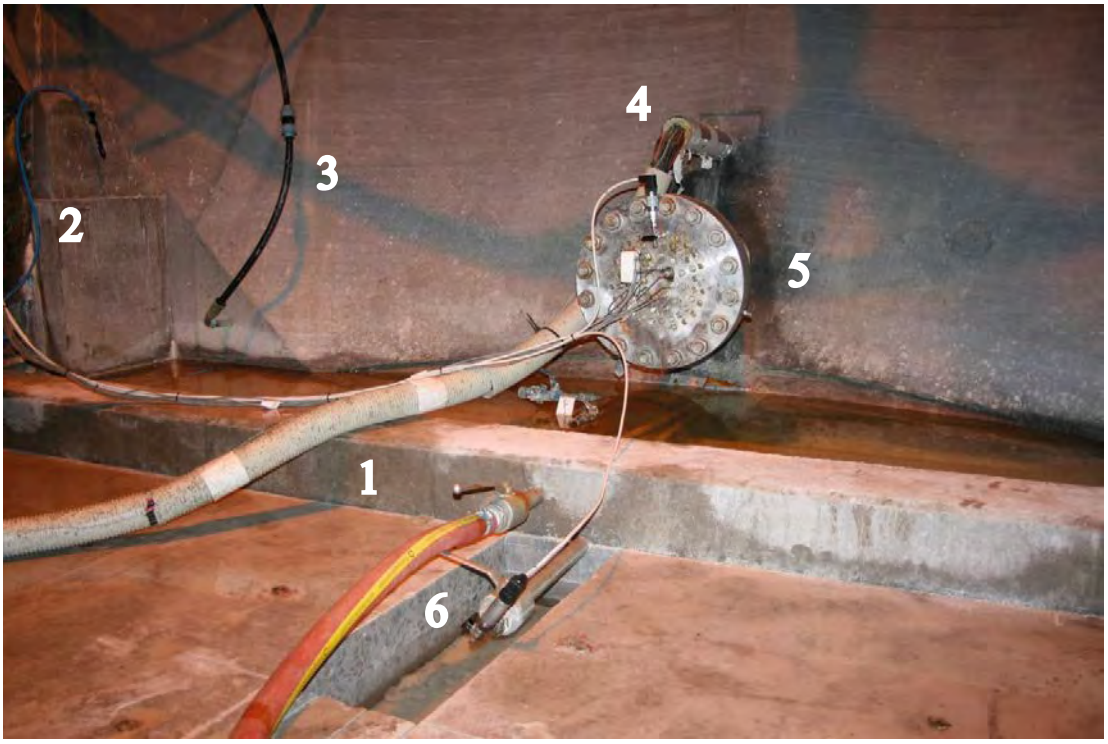

Figure 6-30. *Watertight weir for collection of leakage water. Legend:1) Weir, 2) Injection tube for the weir (blue tube), 3) Connection to the cooling system (black pipe). 4) Feed-out cables from sensors within the concrete dome, 5) Steel flange for lead-through of cables from sensors placed on the downstream side of the bentonite seal, 6) Drainage pipes with valves and one water pressure sensor.*

The final step in construction of the plug involved covering the downstream side of the concrete dome with a plastic sheet connected to the weir, see Figure 6-31. The plastic sheet encloses an area from the weir to the downstream side of the dome (corresponding to a distance of about one meter downstream of the concrete dome). This was installed in order for accurate leakage collection to be achieved. The sheet prevents water from evaporating from the test dome due to tunnel ventilation. Evaporative loss would have resulted in too low a measured leakage.

The tunnel ventilation system in the main tunnel TASJ was subsequently shut off as the monitoring phase began.

6.8 Important experiences from installation and field-work

The installation of DOMPLU required significant manual activity. This civil work presents an operational safety hazard during some activities. In this section a few important experiences are highlighted for certain work steps.

6.8.1 Installation of gravel and geotextile in the filter section close to the tunnel ceiling

Installation of gravel in the filter section and emplacement of geotextile close to the tunnel ceiling turned out to be very difficult. It was not possible to achieve a vertical wall of geotextile and gravel; instead it was decided to fold in the geotextile over the gravel which resulted in an empty space the last 0.5 meter, see Figure 6-32. This space was later filled with bentonite pellets that were blown in over the bentonite sealing blocks.

Figure 6-31. *Installed plastic sheet, which encloses the concrete dome plug to prevent evaporative water loss.*

Figure 6-32. *Photo showing the space left above the gravel section. The geotextile was folded in over the uppermost gravel surface.*

6.8.2 Installation of LECA and concrete beams close to the tunnel ceiling

The uppermost part of the LECA wall consists of small blocks instead of a beam. This facilitated the installation of the wall considerably. The demands on the concrete wall were higher regarding strength and included pre-fabricated beams that should be anchored to the rock wall. The installation of the last beam was difficult since it was not possible to lift it in place depending on the limited space. The method used was to place the beam on the outermost part of a platform that was lifted up to the right height by a wheel loader. The beam could thereafter be pushed into the final position, see Figure 6-33. The control of the beam was not total during this operation. It is recommended to instead develop special lifting brackets that are cast into the front side of the beam. With these it should be possible to lift also the final beam in position in a safe way.

6.8.3 Installation of bentonite pellets close to the tunnel ceiling

The installation of bentonite pellets above the sealing blocks was a bit complicated and solved in the following way:

1. A thin steel plate was fastened on the outside of the uppermost bentonite block row. The plate was manually cut to fit tight the rock surface (Figure 6-34, left).
2. An entrance was cut out in the steel plate, see photos provided in Figure 6-34. The entrance was possible to close by bending the steel plates back to original position.
3. Pellets were blown in through the hole until the volume was almost filled i.e. pellets were flowing out through the hole.
4. The last volume was filled up by using wetted pellets that could be pushed in manually through the hole until the gap was completely filled. The steel plates were then bent back to close the pellets volume.

6.8.4 Installation of the concrete dome

The installation of grouting tubes was time consuming and took almost two weeks. For the upper parts of the slot, work had to be performed from sky-lift. However, installation of grouting tubes in the lower part of the slot was even more difficult because the workers tend to slide down to the bottom.

Figure 6-33. *Photo showing the installation of the last concrete beam.*

Figure 6-34. *Left: Photo showing the steel plate fastened against the uppermost row of bentonite blocks Right: Close-up showing the opening through which the last pellets were installed.*

Installation of the prefabricated cooling system was successful but hard to accomplish in full accordance with the drawings. There was need for bigger tolerance (± 10 cm) near the intersection point of the slot since it was hard to reach these areas.

The dome formwork was perceived by the staff to be both solid and well designed. However, a modification with a man-hole was suggested by the workers for easier positioning of the larger upper parts. Possibly the upper part of the formwork could also be re-designed as one piece to facilitate fitting. The pressure measurements during casting showed that a future formwork can be built in thinner dimensions.

7 Monitoring of the full-scale test

In this section, the equipment used for monitoring the behaviour of the plug system is presented. The evaluation of the measurements and comparison with numerical analyses are later presented in Chapter 9.

In Section 7.1, the instrumentation used to measure the behaviour of the backfill transition zone and the bentonite seal is presented. Additional details regarding the instrumentation of the sensors in the backfill and the bentonite seal can be found in Appendix 3.

The instrumentation used to measure the behaviour of the concrete dome plug is presented in Section 7.2. More details regarding the instrumentation used to monitor the behaviour of the concrete dome can be found in Malm (2014).

One important aspect of planning the monitoring campaign of the plug system was to design the placement of cables and to design water-tight lead-through pipes in which the cables can be placed; this is further discussed in Section 7.4.

The leakage of the plug system was measured both automatically and manually; the leakage monitoring system is presented in Section 7.5.

7.1 Backfill and bentonite seal

The objectives of the measurements in the backfill and bentonite seal are to:

- Follow the saturation process of the bentonite.
- Monitor the development and distribution of swelling pressure.
- Evaluate the sealing function.
- Detect displacements between the material zones.

In order to monitor this, different types of sensors were installed in the backfill and bentonite seal. The instrumentation consists of:

- Total pressure (swelling pressure and waterpressure) – 20 sensors.
- Pore pressure – 6 sensors.
- Relative humidity – 16 sensors.
- Displacement – 3 sensors.

A sketch showing the instrumentation locations is shown in Figure 7-1. The sensors are installed in nine sections, where four are in the bentonite seal and five in the backfill. In addition, two pore pressure sensors are also installed in the excavated slot for the concrete dome. Photos of the different type of sensors used are presented in Figure 7-2 and Figure 7-3. More detailed information regarding the placement of these sensors can be found in Appendix 3.

All sensors that are installed in the bentonite backfill and in the bentonite seal are subjected to high water pressure. These sensors and cables were therefore designed to withstand a hydrostatic water pressure of at least 10 MPa. In Figure 7-3 the sensors used to measure the total pressure and pore-pressure are shown. The sensors used to measure relative humidity and the relative displacements are shown in Figure 7-3.

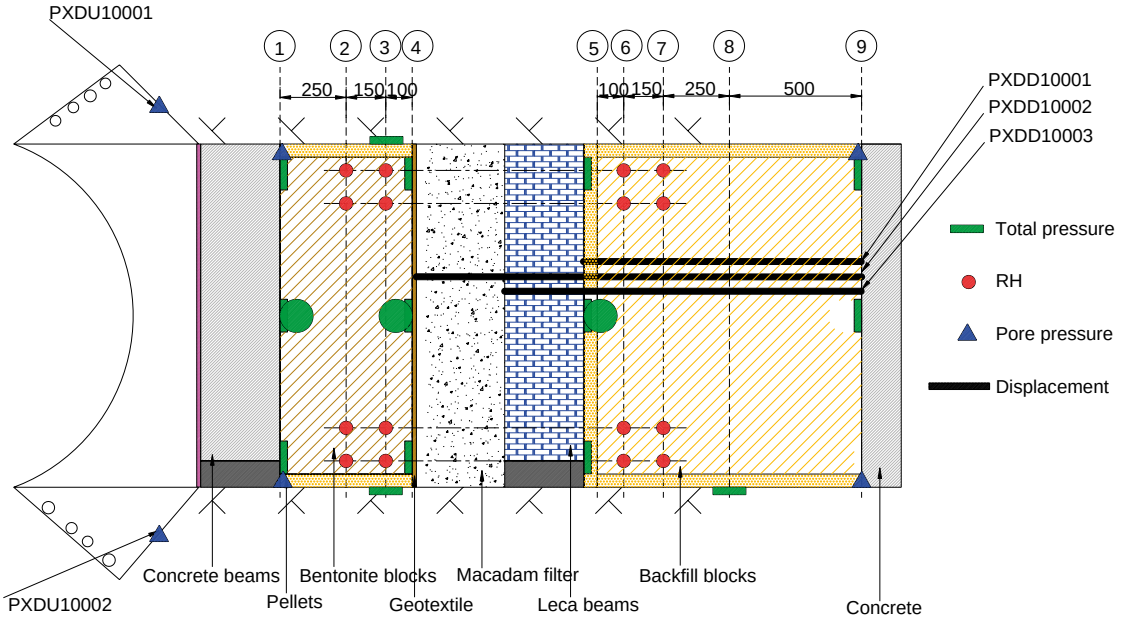

Figure 7-1. *Schematic drawing showing the sensor position in the bentonite seal and backfill.*

a) b)

Figure 7-2. *a) Total pressure sensor (Geokon 4800-1x-10 MPa), b) pore pressure sensor (Geokon 4500SH-3-10 MPa). Photographs are courtesy of Geokon Inc. (www.geokon.com).*

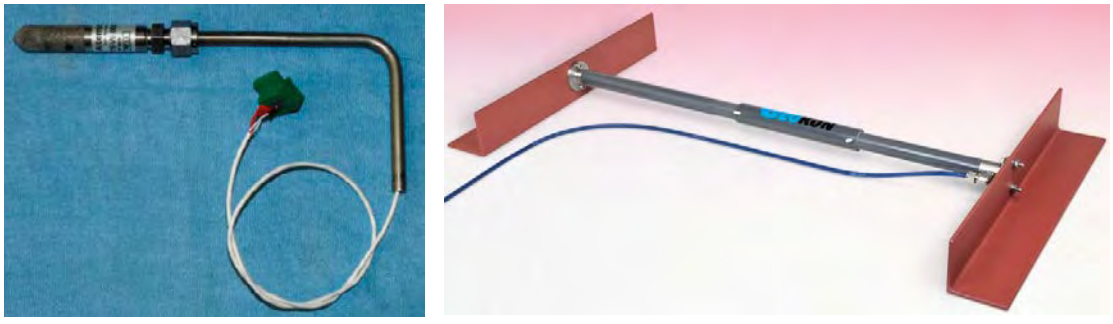

a) b)

Figure 7-3. *a) Relative humidity sensors (Aitemin SHT75 V3), b) Extensometer (Geokon 4435-1X-50). Photographs are courtesy of Geokon Inc. (www.geokon.com).*

7.2 Concrete dome

This information contained in this section is a summary of that provided by Malm (2014), where further information regarding the installation of sensors and details regarding their placement is presented.

In this section, the sensors used to monitor the performance of the concrete dome are presented. A temporary measuring system was used to measure the pressure on the formwork (Section 7.2.1). A permanent measurement system was used to monitor the concrete dome; it consisted of sensors cast in the concrete and sensors connected to the edge of the concrete dome.

7.2.1 Pressure on the formwork

Five pressure sensors were installed on the formwork, in order to measure the pressure on the formwork generated by the concrete dome. Wika S11 sensors were used. The sensors were located as illustrated in Figure 7-4. The pressure sensors were mounted on steel rings attached to the formwork, as seen in Figure 7-5. The membrane of the pressure sensor, on the upstream side of the formwork, was mounted to be placed in level with the formwork.

7.2.2 Long-term concrete measurements

The purposes of the instrumentation of the concrete dome are to:

- Measure the response of the concrete dome, from the point of casting the concrete up to the point where it is subjected to high loads due to water pressure.
- Determine if the concrete dome releases from the rock due to early age shrinkage.
- Measure the heat development and cooling of the concrete dome, and
- support comparison of the performance of the concrete dome with the predicted performance.

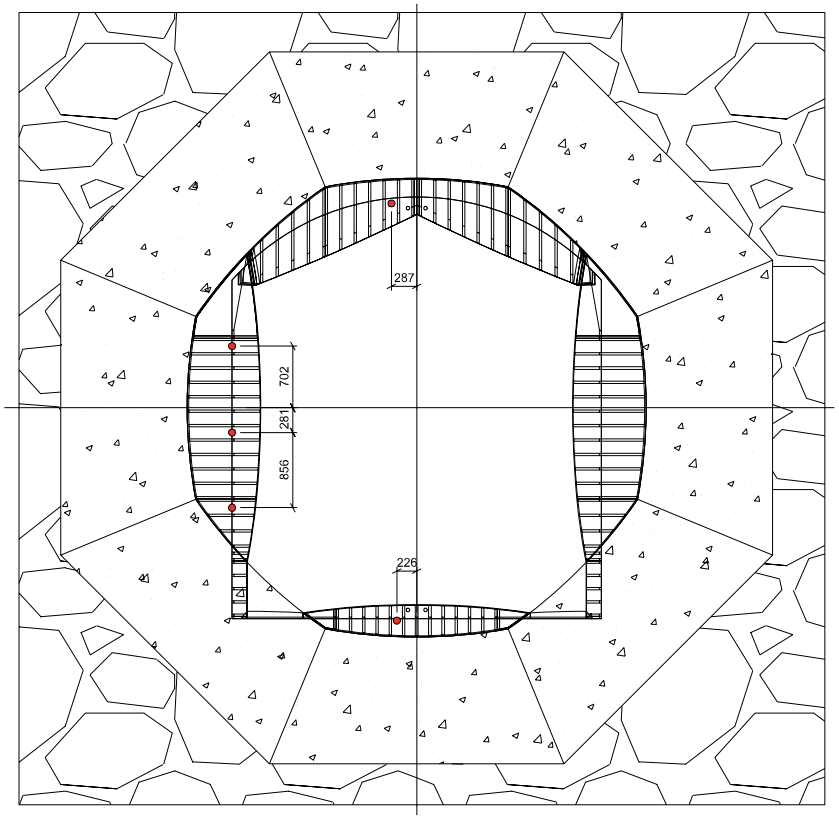

Figure 7-4. *Placement of sensors for measuring the pressure on the formwork.*

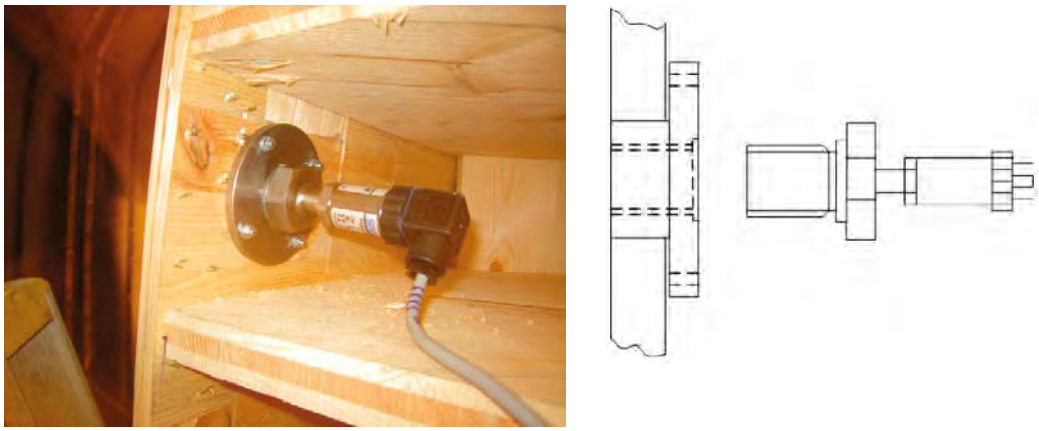

a) b)

Figure 7-5. *Installed pressure sensors (Wika S11) used to measure the pressure on the formwork.*

A sketch of the placement of sensors in the concrete dome is shown in Figure 7-6. To measure the response of the concrete dome, the following sensors are used:

- Joint meters (between concrete and rock) – 6 sensors.
- Embedded strain gauges – 27 sensors (18 of these also measure temperature).
- Displacement transducers (LVDT[1]) – 3 sensors.
- Ambient air temperature – 2 sensors.

Due to symmetry of the dome, effects from for instance shrinkage, water pressure etc. is expected to give the same results if they had been placed in any of the other quarters at the same depth and radius. However, due to the gravity force, largest stresses are expected in the upper half of the dome if bond between concrete and rock is present. Therefore, the instrumentation of the concrete dome is primarily made in one quarter (in the upper half) of the concrete dome. In order to obtain redundancy in the measuring set-up, sensors were placed at similar radius and depth and sensor from different manufacturers were used as seen in Figure 7-6.

Two different types of embedded strain gauges were used in the experiment, these are shown in Figure 7-7. The sensors used to measure the relative displacement between the concrete dome and the rock are shown in Figure 7-8 a), while the sensors used to measure the displacement of the concrete dome plug are shown in Figure 7-8 b). Further details' regarding the installed sensors is found in Malm (2014).

7.3 Pressurization system

The pressurization system was specifically developed for the purpose of injecting water to DOMPLU. It was prefabricated by standard components at the Äspö HRL, above ground. The pumps are redundant and each one was dimensioned to be able to reach 10 MPa pressure at 10 l/min. A flowcharter of the pressurization system is seen in Figure 7-9.

The pressurization of the plug system was performed by pumping water into the backfill and filter section through pipes installed in the lower-most lead-through borehole the experimental tunnel as shown in Figure 7-10.

In total, five pressurisation pipes with an outer diameter of 20 mm and a wall thickness of 0.75 mm were installed in this lead-through. Three of the installed pipes end in the layer of gravel located behind the bentonite backfill, while the last two pipes end in the gravel filter of the plug system. By using the three backfill pipes, the plan was to achieve a channel through the pellet filling to the filter section, from which the water then should be drained.

[1] Linear Variable Displacement Transducer

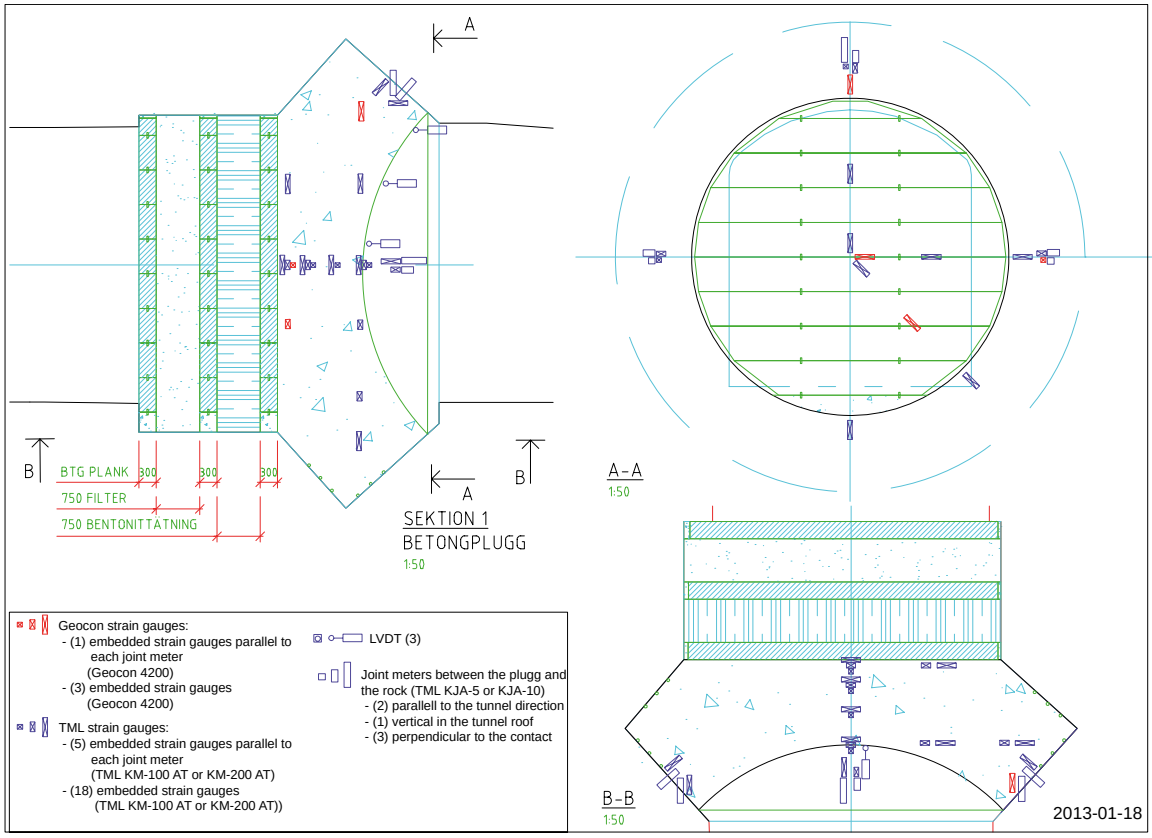

Figure 7-6. *Placement of sensors in the concrete dome.*

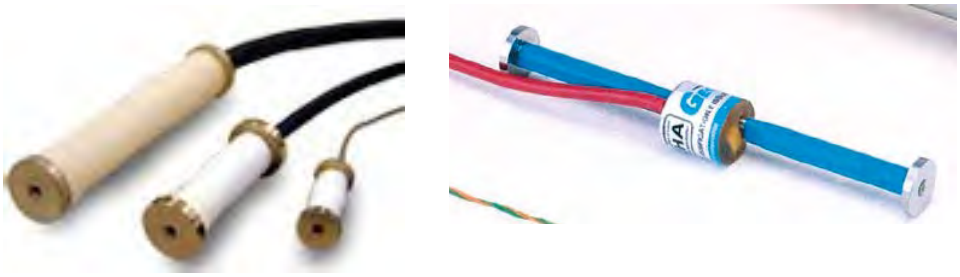

a) b)

Figure 7-7. *a) TML combined strain and temperature gauges (TML KM-100AT), b) Geokon combined strain and temperature gauge (Geokon 4200). Photographs are courtesy of Geokon Inc. (www.geokon.com).*

a) b)

Figure 7-8. *a) Joint meter (TML KJA-10A), b) LVDT sensor (HBM LVDT WA-10).*

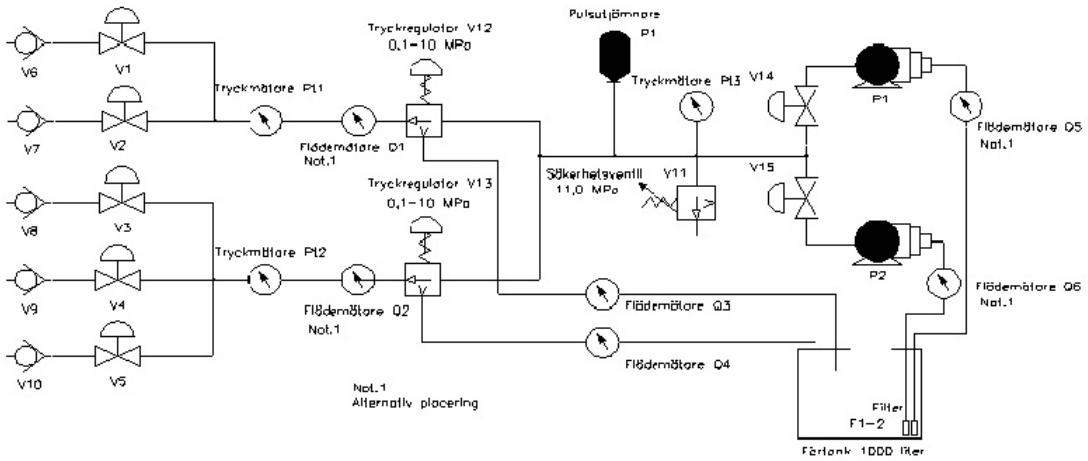

Figure 7-9. *Pressurization system flowcharter. (Text in Swedish.)*

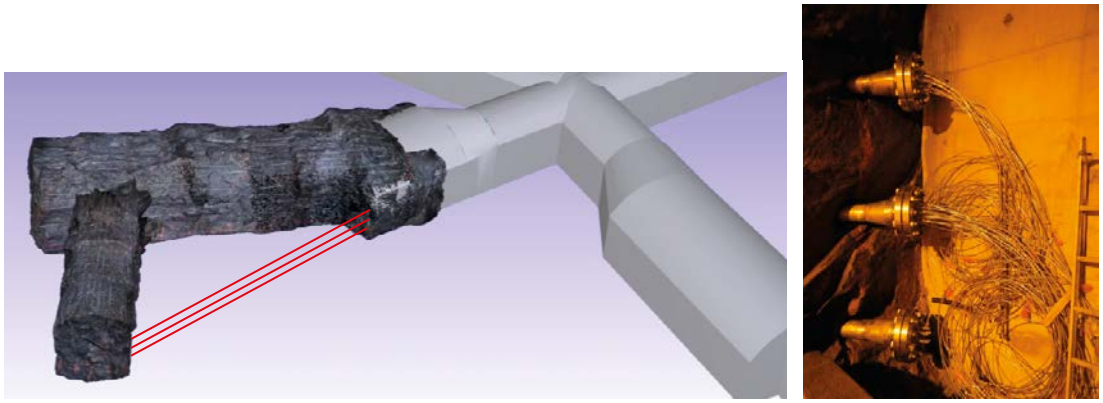

a) b)

Figure 7-10. *a) Sketch of the three lead-through pipes going from the experimental tunnel, b) photo of the lead-throughs.*

The two pipes ending in the filter section were only intended to be used for pressurization if any of the other pipes malfunctioned and also for reaching the pressure of 10 MPa in the final ultimate limit test of the concrete dome. However, during the test it became handy to use them also to fill up the filter in a very controlled way, in order to give the bentonite seal access to water and time to swell and seal.

The pressurization scheme developed for the plug during the preparations of the full-scale test was intended to simulate the real conditions in the future repository during both the construction and operation of the plug. Three milestones were included in the original scheme:

1. Reach a water pressure of 5 MPa in the plugged volume, which is equivalent to the expected maximum water pressure in the repository.
2. Reach a total pressure of 7 MPa, this could theoretically be obtained by a water pressure of 5 MPa in combination with a swelling pressure of 2 MPa in the bentonite.
3. Reach a total pressure of 10 MPa including both water and bentonite swelling pressure. The aim was to verify that the dome shaped concrete plug could meet this design target.

However, as described in the introduction to Chapter 9, the full water pressure of 7 MPa could never be reached due to conditions of the surrounding rock at the experimental site. The maximum pressure during this test period was limited to 4 MPa water pressure and the swelling pressure could not be fully developed due to the limited time before this first technical reporting.

The definite applied water pressurization scheme for DOMPLU is described in Section 9.1.1 (and made graphic by Figure 9-2).

7.4 Cable lead-through

Different approaches have been used to route the cables connected to the installed sensors to the measuring cabinets. The approach used for each sensor depended on where in the plug system the sensors are installed. The goal in routing selected was to disturb and affect the experiment as little as possible. All sensors installed on the upstream side of the bentonite seal (sensors that will be subjected to high water pressures), have stainless steel coatings to protect the sensors and the cables. These cables are routed from the experimental tunnel through two lead-through pipes that are installed in the rock. In total, three 200 mm diameter lead-through pipes for the sensor lines exit the experimental tunnel to the monitoring niche (Figure 7-10 a and b). As shown in Figure 7-10b, the two upper lead-throughs (not shown in Figure 7-10), are intended for cables of measurement equipment installed on the downstream side of the bentonite seal while the bottom lead-through pipe is used for the five water pressurization pipes, as described in Section 7.3.

In contrast, the sensors installed in the bentonite seal and against the rock in the slot for the concrete dome were drawn to the inside of the concrete dome in a steel pipe lead-through crossing the concrete dome. The reason for this was that it was preferred not to intersect the bentonite seal with cables, which could short-circuit the seal and cause a leakage path through it. The steel pipe lead-through used for this is shown in Figure 7-11 and in Figure 7-12.

The sensors that were embedded in the concrete (presented in Section 7.2), did not use any specific lead-through, instead the cables were routed directly out through the downstream side of the concrete dome. The reason why additional water-tightness measures were not used for these types of sensors was:

1. In previous full-scale tests in Äspö the same principle was used for sensors embedded in the concrete, without resulting in leakage.
2. Based on the planned behaviour of the concrete dome, these sensors were not expected to be subjected to water pressure. These sensors had in general a concrete cover of at least 400 mm and, based on the design specifications, the bentonite seal should prevent water pressure from acting on the concrete dome.

7.5 Leakage monitoring system

All leakage water passing the plug was collected in a watertight weir. This was previously illustrated in the schematic sketch of the full-scale test in Figure 6-1 and also shown in the photo provided as Figure 6-30.

Figure 7-11. *Lead-through in the concrete dome. The upper is for cables of measurement equipment installed inside the concrete dome and the bottom is for equipment installed in the bentonite seal and in the slot (i.e. not those cast inside the concrete dome).*

A plastic sheet cover, see Figure 6-31, was installed on the downstream side of the concrete dome in order to prevent leakage from evaporating and to allow condensation to drip into the weir. The water in the weir is transported via a steel pipe. The water is then collected into a basin, seen in Figure 7-13, where the water is automatically weighed, providing an on-line record of the leakage rate.

Other water escapes, e.g. via the cables and the rock, were measured manually and can be used to assist in evaluating plug performance.

The measured leakages are described in Section 9.3.

Figure 7-12. *Lead-through in the concrete dome, intended for cables of measurement equipment installed in the bentonite seal and in the slot (i.e. not those cast inside the concrete dome). Here also shown with the water tight connection.*

Figure 7-13. *Photo showing basin for weighing of leakage water from the weir.*

8 Numerical analyses

The following sections describe the analytical and numerical calculations performed within the project. In Section 8.1, the analyses and evaluation of the response of the bentonite seal and the filter are summarized. This section is based on Börgesson et al. (2015a), where these results are presented in more detail. Section 8.2 presents the numerical analyses performed intended to simulate the response of the concrete dome.

8.1 Hydro-mechanical modelling of the tunnel plug

The hydro-mechanical behaviour of the plug system has been studied extensively using both analytical and numerical methods. The calculations had two principal purposes:

1. Design calculations of the filter and bentonite seal as well as different configurations of the plug system. The aim with these calculations was to minimize the swelling pressure from the bentonite on the concrete plug. The pressure limit on the concrete was set to 2 MPa while the developed pressure in the backfill may reach significantly higher pressure levels. These calculations were primarily performed with analytical models.
2. Analyses of the hydro-mechanical behaviour for the full-scale test of the plug in order to predict the real behaviour. These analyses have mainly been based on numerical methods. However, before deciding the design of the full-scale test, analytical calculations were performed in order to decide the most suitable design of the test.

A thorough description of all analytical and numerical calculations can be found in Börgesson et al. (2015a). The discussion below covers the most relevant numerical model for the full-scale test and briefly presents the results from the analytical calculations directly related to full-scale test design.

8.1.1 Field test dimensioning calculations

Analytical calculations were performed before the final design of the field test was decided. These were based on the assumptions that all bentonite was completely homogenized and fully water saturated, that the swelling pressure of the bentonite was specified by a function of the dry density, and that the wall friction and the internal friction could be neglected. This would mean that the final density would be the same in the seal and the backfill.

A quite detailed description of the tunnel sections was adopted and the used tunnel area distribution is shown in Figure 8-1 together with the main components of the tunnel plug experiment. The dry density of pellets, the backfill blocks and the seal blocks were assumed to be 900, 1750 and 1682 kg/m^3, respectively. The block filling areas of the seal and the backfill was assumed to be 16.794 and 16.452 m^2, respectively. All block filling materials (seal and backfill) were assumed to be associated with a slot volume that was 2 % of the block volume. The length of the seal and the backfill was 0.5 m and 1.05 m, respectively, where the latter was composed of 0.15 m pellets and 0.9 m backfill blocks. This distribution between the lengths of blocks and pellets was the main variable in the final calculation.

The plug system was described as three major components in the calculation (seal, filter and backfill), and the change in length of these were defined as functions of the pressure at their interfaces (Figure 8-2). For the bentonite-based components, this was based on the installed dry mass, the tunnel area distribution and the position of the interfaces towards the filter. The corresponding function for the filter was based on the oedometer modulus values of the gravel and the LECA, and the initial lengths of these components. Finally, the sum of these changes in length should be zero and this was used as a condition for seeking the equilibration pressure. The method resulted in a final stress level of 2.48 MPa, and a change in the length of the seal of 0.034 m, and a corresponding change in length for the backfill of +0.005 m.

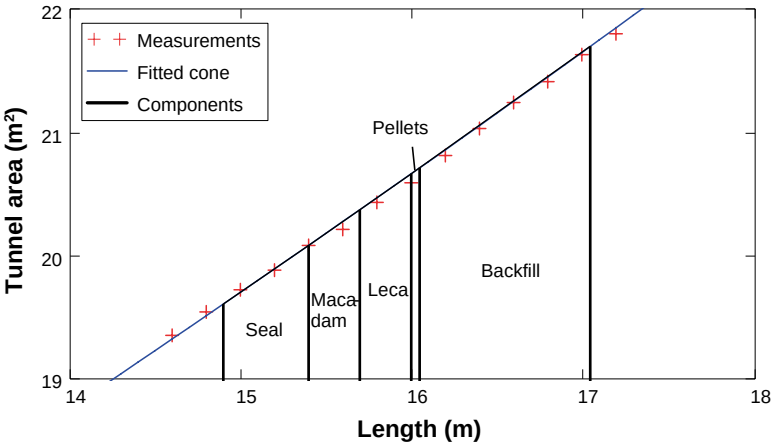

Figure 8-1. *Tunnel geometry used in the analytical calculations for the full-scale test, from Börgesson et al. (2015a).*

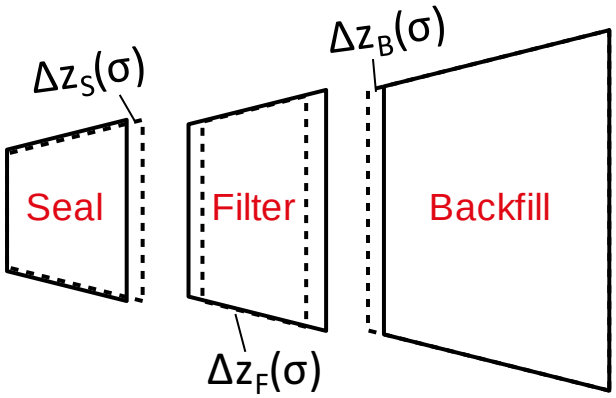

Figure 8-2. *Illustration of the length change for the different components of the plug system during homogenization of the bentonite, from Börgesson et al. (2015a).*

8.1.2 Predictions of the field test

All numerical analyses of the plug components, except the concrete dome, have been performed using the Code_Bright FEM code. The aims of the performed analyses have varied during the progress of the project. The initial analyses aimed to study the behaviour of different design concepts while the latter performed analyses aimed to predict the actual behaviour of the DOMPLU full-scale test. All aspects concerning the models and results are described and presented in Börgesson et al. (2015a). Only one model with the purpose to predict the real behaviour of the full-scale test is described in this report.

Model description and geometries

The geometry of the models was based on the real tunnel section measurements and the actual planned design of the test corresponding to the analytical calculation presented in Section 8.1.1. In total three different cases were analyzed: i) a *Base case*, which was supplied with water from the start but not pressurized*; ii) a Drained case*, which was intended to resemble the initial phase when the filter was drained; iii) a *Pressurized case*, which was intended to include the pressurization scheme which was planned at the time, but not implemented. The two latter cases are not described any further since these are less relevant for comparisons with the actual field test conditions.

The geometry and the mesh used for the base case model are shown in Figure 8-3. The quite coarse mesh used was selected since it was much harder to get convergence with a finer mesh.

Boundary and initial conditions

The same initial conditions were used for all materials in the analyzed models. The initial liquid pressure was set to −45.9 MPa while the total principal stresses were set to −0.11 MPa in all directions. A constant temperature and gas pressure of 20°C and 0.1 MPa, respectively, was defined in the models while gravity was neglected. The defined initial stresses correspond to a net mean stress of 0.01 MPa in the models.

The water was supplied to the bentonite through a hydraulic surface boundary in the model. The liquid pressure in this boundary was increased from −45.9 MPa to 0.1 MPa during the first 0.01 years of the analyses. The hydraulic boundary used for the base case model is shown in Figure 8-4.

The mechanical boundary conditions along the concrete dome plug and the rock wall were fixed while roller supports were used at the symmetry axis as well as at the back of the backfill.

A thoroughly description and presentation of the bentonite material model used in the analyses are given in Börgesson et al. (2015a) and is not further covered by this report.

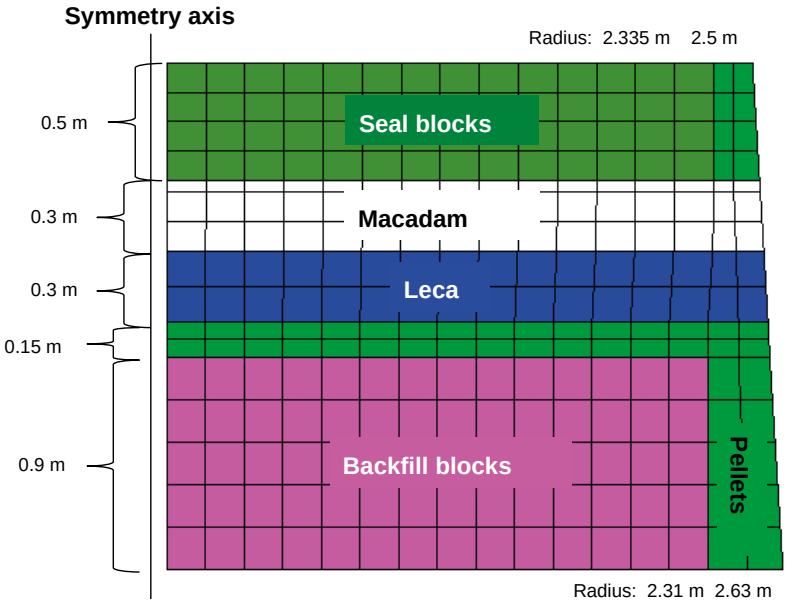

Figure 8-3. *Geometry and mesh used for the base case model, after Börgesson et al. (2015a).*

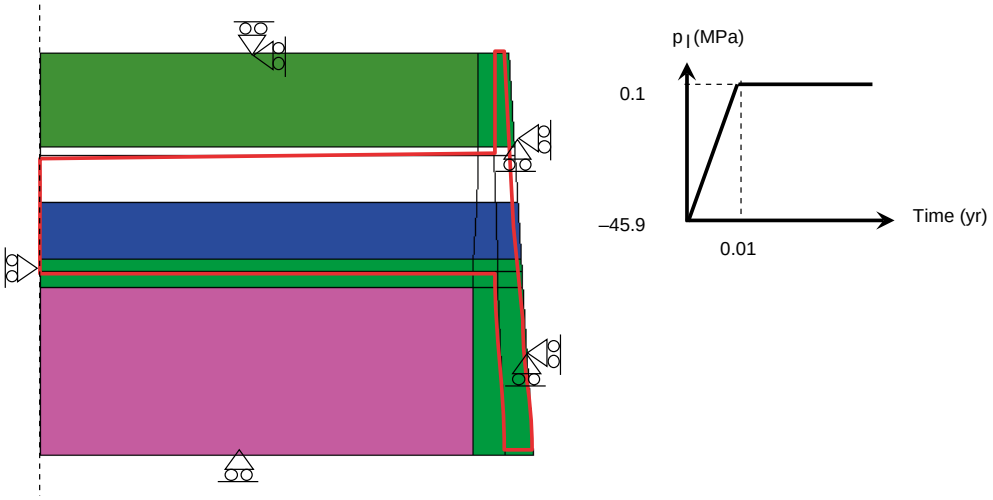

Figure 8-4. *Hydraulic surface boundary (red line) defined for the base case model, from Börgesson et al. (2015a).*

Results

The results obtained from the base case analysis are provided in Figure 8-5 and Figure 8-6 showing axial and radial stresses, axial displacements, void ratio and relative humidity. It should be noted that all stresses are given as total pressures relative to an atmospheric pressure of 0.1 MPa and that positive stresses correspond to compression.

The original plan was to dismantle the field test after day 415, i.e. after little more than one year. The axial stresses along the tunnel axis were expected to be approximately 0.7 MPa at that time according to the model, whereas the radial stresses at the seal towards the rock wall would be 0.2–0.5 MPa. The largest displacement along the tunnel axis would occur at the interface between the seal and the filter and would be approximately 4 cm. The inner part of the filter component will be pushed inwards by approximately 2 cm. The extent of hydration would be quite limited at day 415. For example, the relative humidity in the centre of the seal blocks (i.e. 0.25 m from the filter) would only have increased from 71 to 77 %.

Comparisons between the analysis results and the measurements performed during the full-scale test are presented in Section 9.1.

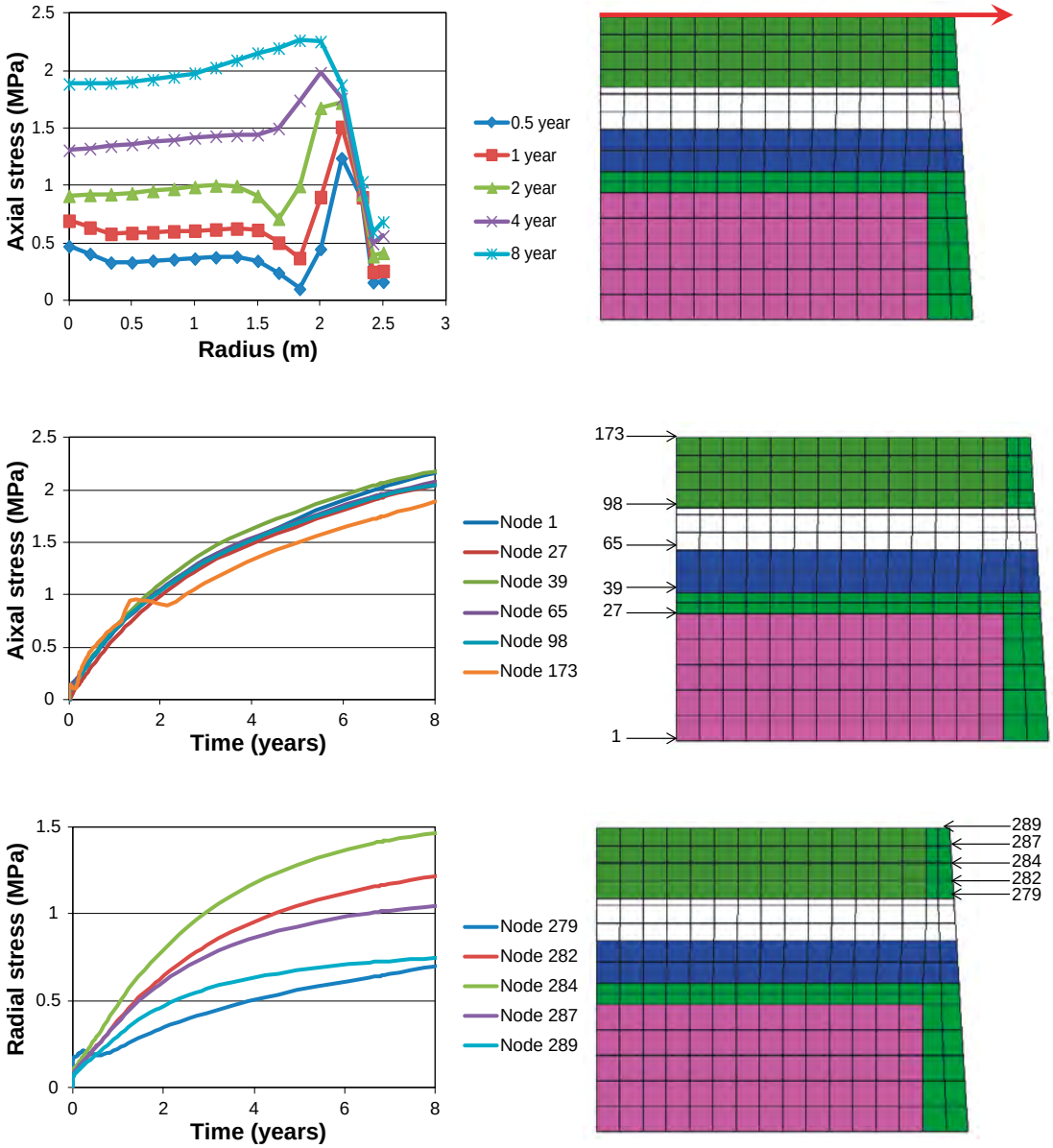

Figure 8-5. *Results from the base case analysis showing the axial stress (upper and middle) and the radial stress (lower). From Börgesson et al. (2015a).*

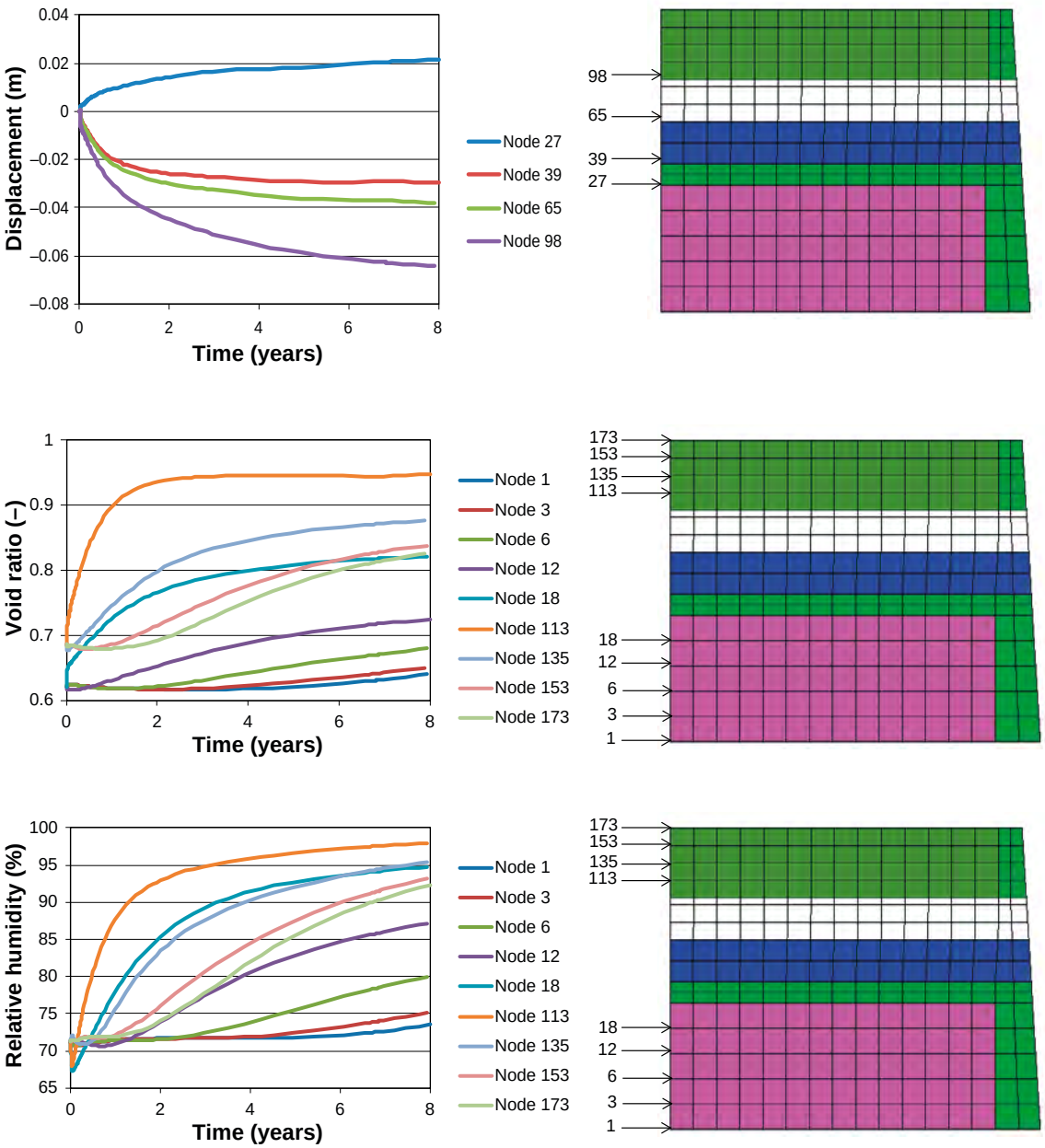

Figure 8-6. *Results from the base case analysis showing the axial displacements (upper), the void ratio (middle) and the relative humidity (lower). From Börgesson et al. (2015a).*

8.2 Predicting thermal and structural response of the concrete dome

A number of numerical models have been created and analysed during both the design of the concrete dome used in the full-scale test and in preparation for the actual test. The numerical analyses focused on the design of the concrete dome have previously been summarised and reported in Malm (2012). In this report, analyses focused on the actual test conditions at Äspö HRL are presented and the results are summarised. The focus of these analyses have been to get a better understanding of the response of the concrete dome, both in its early stages including casting, curing and other preparations before the full-scale test program and during the test program itself. It should be mentioned that unless otherwise mentioned, all analyses presented were performed prior to casting of the dome.

8.2.1 Models

The early age behaviour of concrete is difficult to describe both with analytical and numerical models as it contains many parameters that are dependent on both time and environmental conditions. In the material testing of the low-pH concrete conducted in Vogt et al. (2009), a significant number of material tests were included that focused on providing material parameters that could be used for numerical modelling of concrete at early ages. Material data were provided so as to fit with a numerical methodology for thermal and stress analysis of early age concrete developed at LTU (Luleå Technical University), see for example Ekerfors (1995) for a description of the methodology. It can also be noticed that that methodology also can be used to predict long-term material behaviour such as creep and strength growth of concrete.

All analyses of the concrete dome are made as one way coupled thermal-structural analyses. In such an analysis, a transient temperature field is calculated in a thermal analysis, which is then given as a predefined temperature field in the structural analysis with a resulting thermal expansion of the material.

Software

Analyses have been performed using two commercially available software packages:

- Abaqus 6.12 (Abaqus 2012).
- ConTeSt Pro 4.1 (ConTeSt 2012).

Of the analyses presented in this report, the majority are performed with the general multiphysics FE-package Abaqus. The ConTeSt program is a FE-program especially developed for modelling early-age temperature and stress development in concrete, and is based on the previously mentioned methodology developed at LTU.

Abaqus has been used both to model the early-age response and the response of the concrete dome during the test program. However, to implement all aspects of the early age behaviour of concrete that is described in Vogt et al. (2009) in Abaqus would require a lot of modifications and was therefore considered as out of scope for this project and some simplification was therefore made to the methodology, especially regarding the hydration process of the cement. All of these aspects of the proposed methodology are implemented in ConTeSt. However, it is only possible to perform 2D-analyses in ConTeSt and it also lacks some other features that are required for the stress analysis that are available in Abaqus. The results from ConTeSt will thus be used as a reference value for the heat development and strength growth during the early age behaviour of concrete and compared to the simplified method for calculating the early age behaviour of concrete in Abaqus.

The early-age response of concrete is a complicated and non-linear problem with many parameters that affect the response and also each other. In the methodology described above by Ekerfors (1995), the so called maturity concept is used in which the current temperature affects the current heat development, strength growth etc. Also the maturity function itself is affected by the temperature which results in a strongly coupled problem. To implement all of these aspects in general software's such as Abaqus would require a significant effort and is, as mentioned above, deemed out of scope of this project. The main simplification that has to be made in Abaqus is that a constant and predefined curing temperature has to be assumed when defining the hydration rate. This means that the maturity function is defined in advance. As a consequence the heat development during hydration of the cement and the growth of all strength parameters are also defined in advance and are not defined as a function of the current temperature in the concrete.

Thermal benchmark models

One aspect that is important when modelling the early age response of concrete is the heat development during the hydration process of the cement. To verify the proposed numerical method for modelling this heat development, two benchmark examples have been analysed. Both examples are from actual castings with the low-pH B200 concrete where temperature measurements are available.

Cylindrical mould

The first benchmark example is from a factory test casting performed during the development of the concrete mix and presented in Vogt et al. (2009). The aim of the test was to study the properties of a factory mixed version of the developed low-pH concrete compared to the properties from the laboratory environment. The test consisted of a concrete column cast in a cylindrical steel mould with a height of 3 m and a diameter of 0.85 m. Temperature sensors were placed at three points at the mid height of the column; in the centre, at half the radius and close to the outer edge of the column. Photos from the test set up can be seen in Figure 8-7.

An axisymmetric finite element model of the concrete cylinder was made in Abaqus for the analysis of temperature development in the cylinder during curing. The thermal material properties of the concrete are given in Table 8-2, while the parameters that define the heat development are defined according to Vogt et al. (2009). In the table, a constant curing temperature has been assumed based on an average temperature from the actual test, this is a simplification that affects the generated heat of the concrete. The initial concrete temperature is also based on the measurements. All outer surfaces are assumed to interact with the ambient air through a surface film condition, which describes the convective heat transfer at the surface. The ambient temperature is assumed to vary according to Figure 8-12. It should be noted that the steel mould is not included in the model.

Table 8-2. Thermal properties of the concrete (Vogt et al. 2009).

Property	Value
Density	2336 kg/m^3
Thermal conductivity	2.1 W/(m K)
Specific heat	1000 J/(kg K)
Constant curing temperature	21°C
Initial concrete temperature	15°C

Figure 8-8 shows the temperature variation from the numerical simulation as well as measured temperatures. The two measure points at the middle and half radius of the cylinder show very good agreement between the simulations and the measured results. For the measurement point at the surface of the cylinder, the simulation shows a lower peak temperature than the measured results. An explanation could be that the sensor is covered by a thin layer of concrete, and the steel mould, giving a slightly higher temperature as a result. The cooling of the column also agrees very well between the simulation and the measurements.

The temperature distribution obtained from the numerical simulation is shown in Figure 8-9 for three different time points; 6 h, 40 h and 100 h. In the figures, the locations of the three temperature sensors are also visible as red dots. Note that the geometry of the axisymmetric model is swept 180 degrees in the figure.

Figure 8-7. *Photo of the cylindrical mould, photo taken from Vogt et al. (2009).*

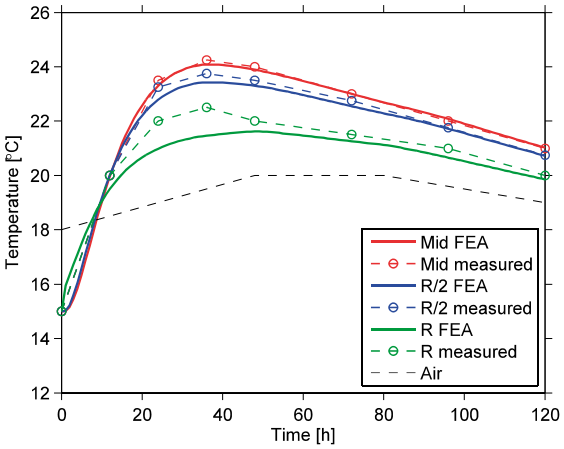

Figure 8-8. *Comparison of the results from the numerical simulations and the cylinder test's measurements.*

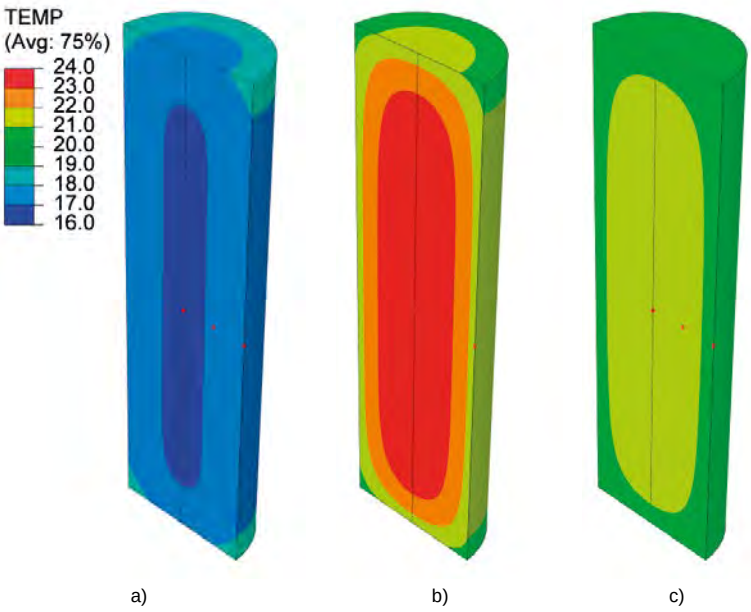

Figure 8-9. *Modelled temperature distribution in the concrete cylinder after a) 6 h, b) 40 h and c) 100 h.*

Concrete block test casting at Äspö HRL

The second benchmark test is taken from a test casting of a large cube with the B200 concrete at Äspö HRL, see Section 5.1.1. This test was done during the early spring of 2012, prior to the casting of the full-scale concrete dome. An unreinforced test specimen with dimension 4 × 2 × 2 m^3 was used during the test to evaluate the effects of casting in situ at Äspö, including the transport of concrete from the factory. Temperature sensors were installed in the test body. The twelve sensors were placed in the midsection of the test body and distributed as shown in Figure 8-10.

The thermal material properties of the concrete are the same as for the previous example and are therefore provided in Table 8-2. For the test casting, the concrete had a temperature of 11°C at arrival to Äspö HRL. In the numerical model, a portion of the ground is included to better simulate the actual boundary conditions from the rock, with assumed material properties according to Table 8-3. No measurements are available on the thermal properties of the ground material, thus its properties have been chosen based on engineering judgement given the assumption that the ground consists of gravel material. It should be noticed that the actual properties of the ground material only has a slight influence on the temperature distribution in the concrete. The surfaces towards the ambient air are modelled through a surface film condition, as in the previous example, with an air temperature of 13°C.

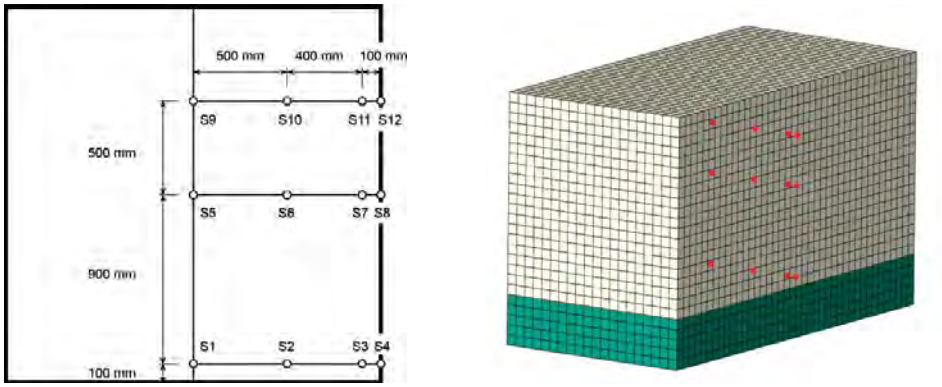

a) b)

Figure 8-10. *Distribution of temperature sensors shown in a) midsection of the test body and b) in the FE-model.*

Table 8-3. Thermal properties of the ground material.

Property	Value
Density	1700 kg/m^3
Thermal conductivity	2.1 W/(m K)
Specific heat	1800 J/(kg K)
Initial temperature	13°C

Readings from four of the twelve temperature sensors are shown in Figure 8-11 and are compared with results two different simulations in Abaqus. In Figure 8-11a, a constant temperature of 25°C was assumed in calculating the generated heat of the concrete, while in Figure 8-11b the heat development is taken from a separate analysis in ConTeSt which accounts for some of the non-linear effects mentioned in Section 8.2. Note that in the ConTeSt simulations the curing process does not start until approximately 10 h after casting.

From the figures it is evident that both simulations show lower peak temperatures than the measurements, for all temperature sensors. The peak temperature is, however, similar for the two simulations. Thereby, the simplification made in Abaqus where the generated heat is calculated based on a constant temperature seems to be a reasonable simplification. The results suggest that the condition at Äspö in combination with the long transportation from the concrete factory affects the curing properties of the B200 concrete mix to give a higher heat development. Some of the differences shown in Figure 8-11 might be attributed to uncertainties in boundary conditions, although the differences are too large to only be due to such modelling effects. The main reason for the difference is likely due to the fact that this concrete had much higher strength than according to the specifications as previously shown in Section 5.1.1. Thereby, the concrete used in this experiment was not representative for the B200 low-pH concrete. As seen in the previous analysis and the analysis on the concrete dome, much better correlation between numerical analyses and tests are obtained.

Modelling of the concrete dome plug

The thermal and structural models of the concrete dome are described in the following section, with focus on modelling of the early age response during casting of the dome. The design and geometry of the concrete dome is shown in Appendix 1, while this section describes the discretization of the actual geometry into a numerical model and other aspects of the numerical modelling.

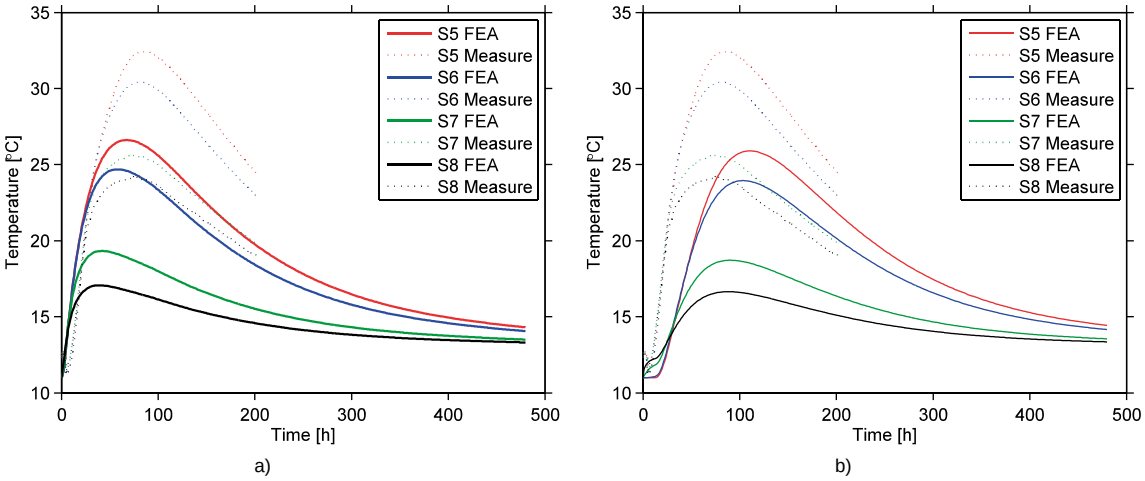

Figure 8-11. *Results from sensors S5-S8 for a) assumed constant curing temperature of 25°C and b) heat development from ConTeSt analysis.*

Temperature sequence

The temperature sequence applied within the thermal analysis is governed by the planned cooling sequence during curing of the concrete dome. The cooling sequence is described in detail in Section 6.6.1, with a summary of the different steps in the FE-analysis given below:

- **STEP 1** – First cooling sequence, most of the heat development, shrinkage and strength growth of the concrete occur and potential de-bonding of the concrete from the rock.
- **STEP 2** – Cooling pipes are turned off and the concrete strength continues to develop.
- **STEP 3** – Initiation of second cooling. This step continues until the temperature is raised in the cooling pipes. During this step, an increase of the gap between the concrete and the rock will occur.
- **STEP 4** – Temperature in the cooling pipes are increased until they reach the ambient temperature. Grouting of the gap between the concrete and the rock occurs.
- **STEP 5** – Cooling pipes are turned off. Pre-stressing of the concrete dome as the temperature increases.
- **STEP 6** – Pressurisation step.

Geometry and mesh

The same geometry and mesh are used for both the thermal and structural FE-model. This geometry is shown in Figure 8-12a, where it can be observed that a symmetry plane has been utilised in the numerical model. The figure shows the rock (dark grey), concrete dome (buff) and the cooling pipes (red); notice that the cooling pipes are only included in the thermal model. The geometry of the model has been defined so as to resemble the actual design of the concrete dome, shown in Appendix 1, as much as possible; however, the surrounding tunnel section used in the model is not the same as in the actual test. This assumption should not affect the results and the chosen tunnel section makes the FE-discretization much easier. Also, the 3D-model of the cooling pipes is based on the version of drawing M233 dated 2011-11-25, some revision have been made since that version. The mesh used for the concrete dome plug is shown in Figure 8-12b. A layer of elements close to the rock interface has been given an aspect ratio as close to one as possible and with quadratic shape functions to increase the accuracy at the interface, a similar layer is also modelled in the rock.

All solid bodies of the model are modelled with 8 noded brick elements while the cooling pipes in the thermal model are modelled with 2 noded truss elements. A summary of the two models are given in Table 8-4.

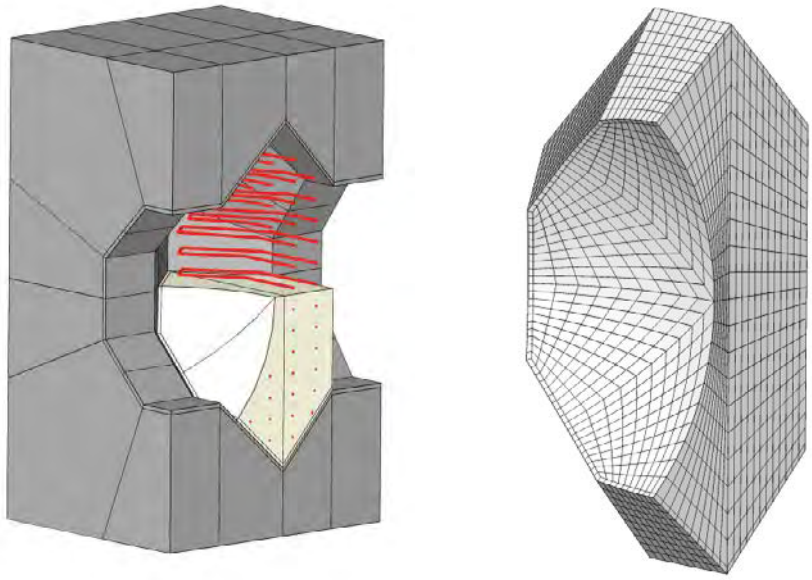

a) b)

Figure 8-12. *a) Geometry and b) mesh of the FE-model.*

Table 8-4. Summary of the thermal and structural models

	Thermal model		Structural model	
	Element type	**No. elements**	**Element type**	**No. elements**
Rock	DC3D8	18 944	C3D8 / C3D20	17 228 / 1716
Concrete	DC3D8	10 076	C3D8 / C3D20	8360 / 1716
Cooling pipes	DC1D2	710	–	–

Thermal boundary conditions and loads

The characteristics that are specific for the thermal model are described below. These mainly concern the applied boundary conditions and loads. A summary of the different boundary conditions and loads is given in Figure 8-13. It is assumed that the rock at Äspö has a constant temperature of 13°C, hence the boundaries towards the inner rock is prescribed as a constant temperature, see blue surfaces in Figure 8-13a. The surfaces towards the air and the bentonite seal are shown in Figure 8-13b, as red and blue respectively. Both the surfaces are modelled with a convective boundary condition with an ambient temperature of 13°C, but the surface towards the bentonite is given a different film coefficient than the surface towards the air to represent that heat transfer more accurately. In Figure 8-13c) the entire volume of the concrete dome is highlighted to indicate the volume that generates heat during the hydration of the cement. The surfaces of the rock that are perpendicular to the length axis of the tunnel are assumed to be adiabatic, i.e. no heat flux through the surfaces.

All materials in the model are given an initial temperature of 13°C and the transient variations are then given by the heat developed from the concrete dome and the cooling from the cooling pipes. The heat developed during the hydration process of the cement is given as a volume load and calculated according to Vogt et al. (2009). As earlier mentioned, the rate of hydration is a non-linear function of many variables including the temperature of the concrete during hydration and those effects are difficult to include in Abaqus where a predefined heat development needs to be specified. Furthermore, since the casting of the dome is expected to take around 10 hours, the heat development is assumed to start 5 hours after first casting as an average. In Figure 8-14a the heat development from three different assumed constant temperatures are shown together with the heat development obtained from a 2D simulation in ConTeSt which accounts for the non-linear effects. As a comparison the total heat of hydration for the four different curves in Figure 8-14a is shown in Figure 8-14b, as

expected the total heat development is almost identical and tends towards the same value with time. A constant curing temperature of 20°C, based on the measured test and modelling results is assumed in the analyses.

The cooling of the mass-poured concrete is modelled by assuming a prescribed temperature on the cooling pipes, this temperature is then transferred from the cooling pipe node to the closet node in the concrete dome by constraint equations. The temperature in the cooling pipes is defined to vary according to the cooling sequence used in the actual test, see Figure 8-15. The figure also shows the definitions of the different analysis steps in the simulation.

Structural boundary conditions and loads

The characteristics that are specific for the structural model are described below, these mainly concern the applied boundary conditions and loads. In Figure 8-16a the surfaces on which boundary conditions are applied in the structural model are highlighted. The red surface represents a symmetry plane and hence only constrains displacements in the normal direction of the surface. The blue surface represents the boundary to the surrounding rock mass, on these surface all degrees of freedom are constrained. Furthermore, the interface between the concrete dome and the rock is highlighted in Figure 8-16b. This interface is modelled differently depending on the model set up which is described later, but also contains one layer of elements that are used to model the grouting. How the grouting process is modelled is also described later. To be able to extract data from the numerical model at the same locations and directions as the sensors in the actual test, a number of truss elements are included in the model to represent the strain gauges; these are highlighted in Figure 8-16c.

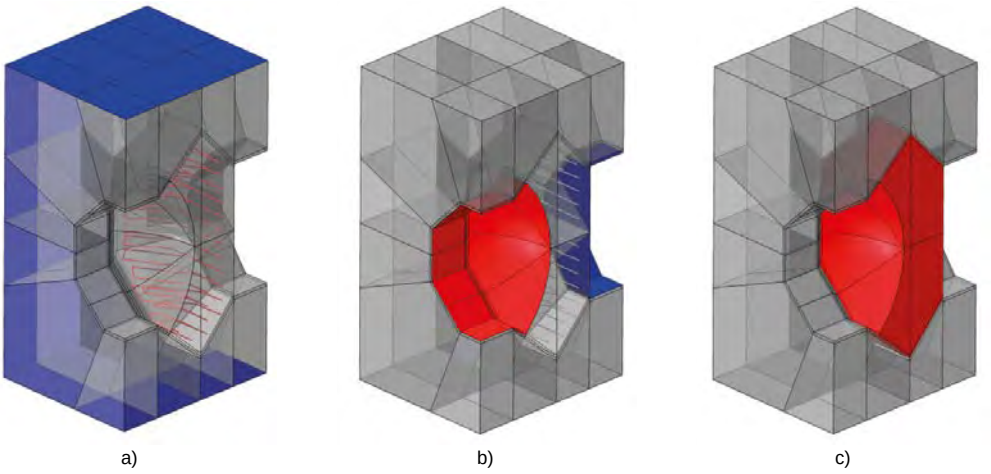

Figure 8-13. *Boundary conditions, a) shows regions with prescribed temperature, b) shows regions with convective boundaries and c) show regions which are assigned a temperature load.*

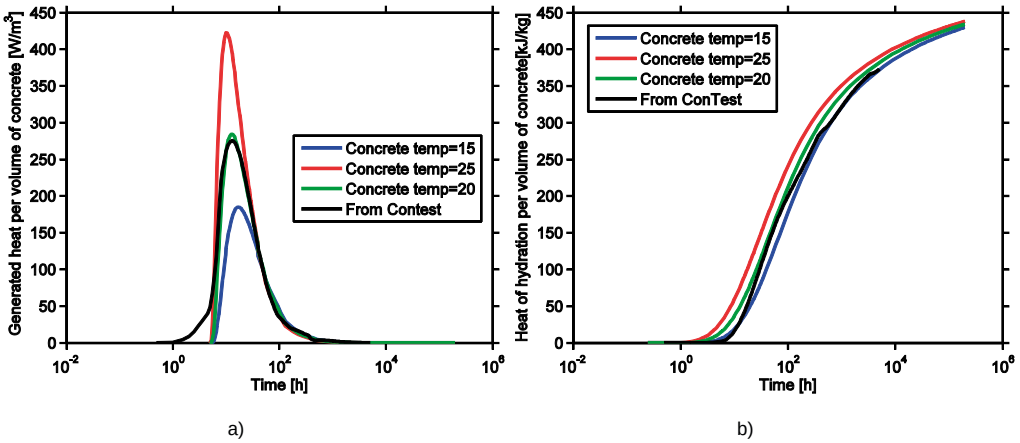

Figure 8-14. *Heat development of the concrete dome for different concrete temperatures.*

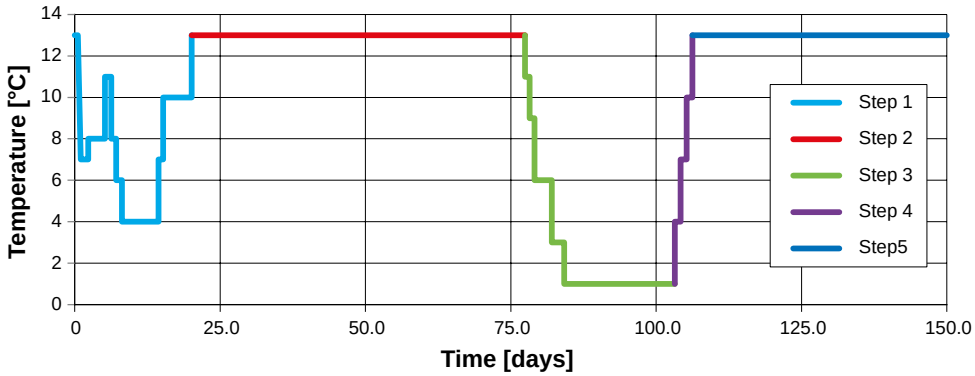

Figure 8-15. *Cooling sequence used in the simulations.*

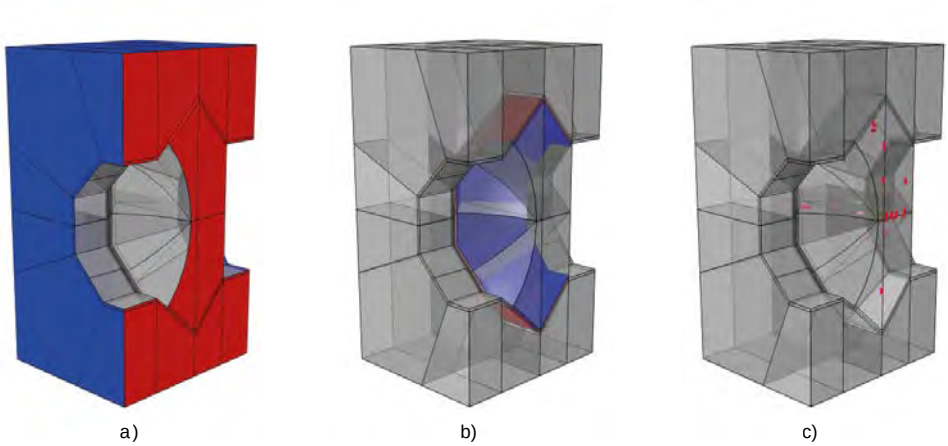

Figure 8-16. *Boundary conditions, a) show regions with mechanical boundary conditions, b) shows the location of the concrete-rock interface and c) shows the location of the embedded sensors.*

The main load in the structural model of the early-age behaviour is given by the temperature field, as calculated in the thermal model, which leads to thermal strains in both concrete and rock. Apart from the thermal strain, the structural model is subjected to gravity loading and some material effects such as strength growth and shrinkage as described below.

In the analysis of the pressurization, a pressure load is applied on the back surface of the concrete dome to represent the water pressure and swelling pressure from the bentonite.

Material properties

The material properties used in the numerical model of the concrete dome, both thermal and structural, are described below. For the thermal model, the material properties of all materials are given in Table 8-5. Note that the temperature of the cooling pipes is prescribed during the thermal analysis and its thermal properties therefore do not affect the temperature field. However, the cooling pipes are assumed to be made of steel when defining the material properties. The material properties used in the structural model are given in Table 8-6. Also, all materials are considered to be stress free at 13°C.

Table 8-5. Thermal material properties

	Density [kg/m^3]	Conductivity [W/(mK)]	Specific heat [J/(kgK)]
Concrete (Vogt et al. 2009)	2336	2.1	1000
Rock	2600	3.7	900
Cooling pipes	7800	287	276

Table 8-6. Structural material properties

	Density [kg/m^3]	Elastic modulus [GPa]	Poisson's ratio [-]	Thermal expansion [1/K]
Concrete (Vogt et al. 2009)	2336	Figure 8-21a	0.3	1.11×10^{-5}
Rock	2600	70	0.3	8×10^{-6}

The growth of the elastic modulus of the concrete is dependent on the rate of hydration, i.e. the temperature at which the concrete cures. An example of this is shown in Figure 8-17a where the blue curve corresponds to a constant curing temperature of 20°C and the red curve to a curing temperature as calculated with ConTeSt. A small difference is visible, where the assumption of 20°C slightly overestimates the strength growth. As mentioned earlier the assumption of a constant curing temperature of 20°C is used in the analyses performed in Abaqus.

Another material property of the concrete is the early-age chemical shrinkage, i.e. the autogenous shrinkage, which is high for the low-pH concrete if compared to conventional concrete qualities. The autogenous shrinkage of the low-pH concrete was measured in Vogt et al. (2009), those measurements are used to define a shrinkage in the numerical model. The shrinkage is defined according to Figure 8-17b, where the two different shrinkage curves shown are used to reduce the shrinkage due to the rate of casting as proposed in Malm (2012). This reduction is done due to the fact that the first poured concrete already has experienced the majority of its shrinkage when the last concrete is poured. Given that the last pour fills out the entire form it will also compensate for some of the earlier shrinkage in the lower parts of the plug. Hence, most parts of the concrete will not experience the majority of the shrinkage which occurs during the first 24 hours. It is further assumed in the analyses that no real shrinkage occurs until the last concrete is poured since new concrete will fill out the voids created by the shrinkage of the already poured concrete as long as concrete is poured into the form. Between these two extremes, the shrinkage is linearly interpolated with the height coordinate of the concrete dome. It should also be noticed that drying shrinkage is assumed to be zero, since the relative humidity at Äspö HRL is assumed to be close to 100 %.

It should be noticed that effect of creep is not included in the current models. This should not affect the results significantly for constrained full bond models when considering strains since only linear elastic material behaviour is assumed, however, any stress output from the model will predict to high stresses. For the no bond model, however, this simplification may cause the strains to be too small during its unconstrained early stages.

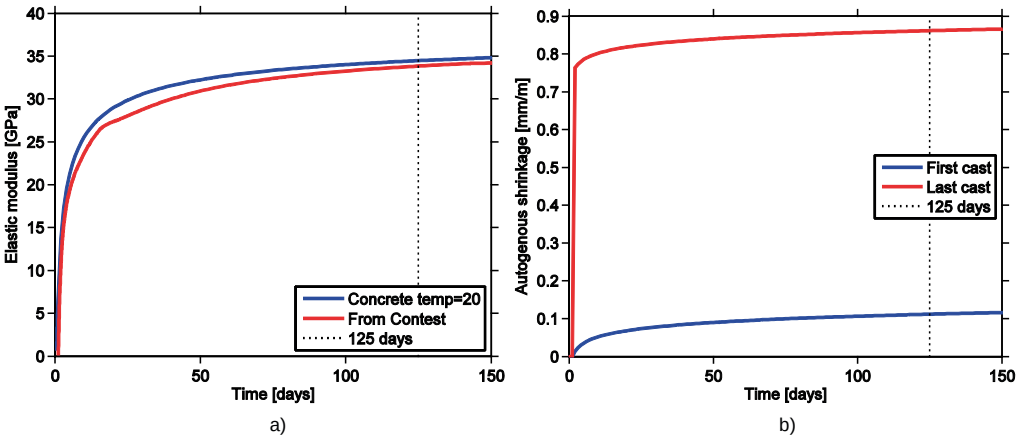

Figure 8-17. *Time dependent material properties, a) shows the growth of the elastic modulus and b) the autogenous shrinkage.*

Concrete-rock interface and contact grouting

To include the thermal pre-stressing of the concrete dome from the second cooling sequence in the numerical simulation, the behaviour of the concrete-rock interface and the contact grouting needs to be considered when defining the finite element model. Describing the concrete-rock interface as accurately as possible would require the use of a non-linear traction-separation law characterized by bond strength and fracture energy. Such material properties are available for the low pH concrete, see Section 5.2. However, such a de-bonding behaviour is very brittle and a release of the concrete dome from the rock would probably result in an unstable response of the model. To simulate such a de-bonding process could prove difficult and would come at a significant computational expense. Therefore, three different model approaches for the concrete-rock interface were proposed:

- **Non-linear:** A non-linear interaction of the interface based on a traction-separation law that also includes separation softening after the bond strength is reached is assumed.
- **Full bond:** Complete bond is assumed between the concrete and the rock throughout the entire simulation by equating the degrees of freedom on the respective surfaces.
- **No bond:** A frictional contact with no initial bond is assumed between the concrete and the rock.

During initial testing of the models, the use of the non-linear interface, as expected, gave major convergence difficulties with long simulation times as a result. Thus it was decided to exclude this model for further analysis and only continue with the two simplified models of the interface. The two simplified models could be considered as two extreme cases of the behaviour of the concrete rock interface and should therefore bound the response of the actual non-linear behaviour.

To account for the pre-stressing of the contact grouting, a methodology was developed to include this effect in the numerical simulations. The basic idea is to add and remove certain elements at appropriate times of the simulation and thus introduce the pre-stressing. At the creation of the model, the outer layer of elements of the concrete dome adjacent to the rock surface is duplicated. The duplicate elements, now called grout elements, are constrained to both the rock and the concrete dome. During the initiation of the model, the grout elements are deactivated and the interaction between the concrete and the rock is only determined from the chosen interface model as described above. Later, during the second cooling cycle (Step 4), the outer layer of concrete dome elements are replaced by the grout elements, which are now introduced to the model without any strains, even though they are in a deformed state. Since the grout elements are constrained to the rock, any gap introduced during the earlier stages of the simulation will be closed by the grout elements. In particular, the change in the gap during the second cooling will lead to a pre-stressing of the concrete dome as the temperature increases after the cooling is turned off. It should be noticed that the grout elements are given the same material properties as the rest of the concrete dome.

Pressurization

The pressure sequence used in the analyses is shown in Figure 8-18 and is based on measured values from pressure sensors in the bentonite seal during the full-scale test. The mean value of the pressure sensors closest to the dome plug is shown as a reference curve in Figure 8-18. During the pressure step of the analysis, step 6, the temperature and other effects analysed during step 1–5 are assumed to be constant. The pressure is applied as a number of discrete values shown as dots in Figure 8-18 fitted to the measured values. Note also that the analysis in this step is semi-transient since the state of the model is only solved as these discrete time points.

The pressure is applied to the downstream surface of the dome plug. To represent a realistic load case during pressurisation no bond is assumed between the rock and the concrete on the upstream side, i.e. no tensile forces can be transferred at this part of the interface. Also, pressure is assumed to act on the upstream part of the rock slot to simulate a gap in the interface, as indicated in Figure 8-19.

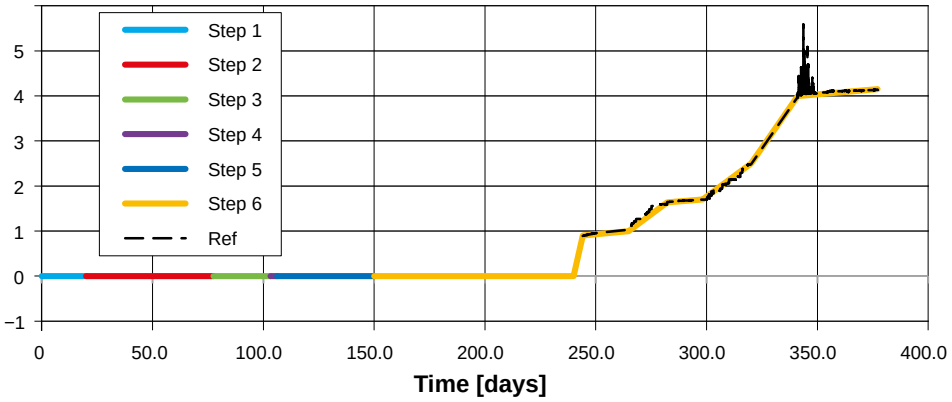

Figure 8-18. *Pressure sequence used in the simulations and comparison with measured values in the bentonite seal.*

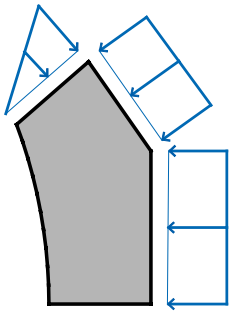

Figure 8-19. *Schematic figure of the surfaces that are assumed to be subjected to the applied pressure load.*

In the full bond concrete-rock interface model, the applied pressure load would be directly transferred to the rock since no deformations are allowed in the interface. This will lead to very small deformations and changes in strain in the concrete dome. To overcome this issue some modification needs to be made to the interface of the full bond model when the pressure load is applied. In the analyses of the full bond case the upstream surface of the rock slot is assumed to loose bond before or when the pressure load is applied, two cases of the full bond model have thus been assumed.

- Bond of the upstream rock slot is lost during the second cooling.
- Bond of the upstream rock slot is lost during the first application of the pressure load.

Result extraction at sensor locations

To compare the results from the numerical simulation to the data collected from the field measurements, it is important to extract results from the model at the approximate locations and at the same directions as the sensors installed in the full-scale test. Since these do not coincide with the mesh, truss elements are used to represent the sensors which are placed in the location and direction of the actual sensors and are assumed to be fully embedded in the concrete elements. Each sensor is represented by a single truss element and is given fictitious mechanical material properties, since the strain is given by the deformation of the concrete. However, to account for the thermal strains, a thermal expansion coefficient of 1.11×10^{-5} [1/K] is given to the sensor elements.

8.2.2 Predicted thermal response of the concrete dome

In the following section results from the thermal simulations are presented. Note that only a single thermal analysis is performed in Abaqus since the mechanical concrete-rock interface is assumed to not affect the temperature field.

The changes in temperature during the initial 150 days from casting as predicted by the Abaqus simulations are shown in Figure 8-20 for a selected number of sensors. Predicted results from all installed sensors can be found in Appendix 4. Note that some of the sensors shown do not measure temperature in the actual test. The temperature sensors shown in Figure 8-20a corresponds to the sensors in the middle of the dome plug, with ST01 closest to the upstream surface. As expected, the temperature variations are largest for the two sensors located in the mid sections of the dome plug, both during high temperature from the heat of hydration and also for the low temperatures during cooling. In Figure 8-20b sensors that show representative results for the remaining sensor locations are shown, including the high and low bounds of temperature for these sensors.

To illustrate the predicted distribution of temperatures in the concrete dome, contour plots of the nodal temperatures are shown in Figure 8-21 for different times. The temperature field in Figure 8-21a corresponds to a time of 42 hours from the casting which is when the maximum temperature value due heat from the hydration process is observed. In Figure 8-21b and Figure 8-21c the temperature field at the minimum observed temperatures during the two cooling sequences are shown.

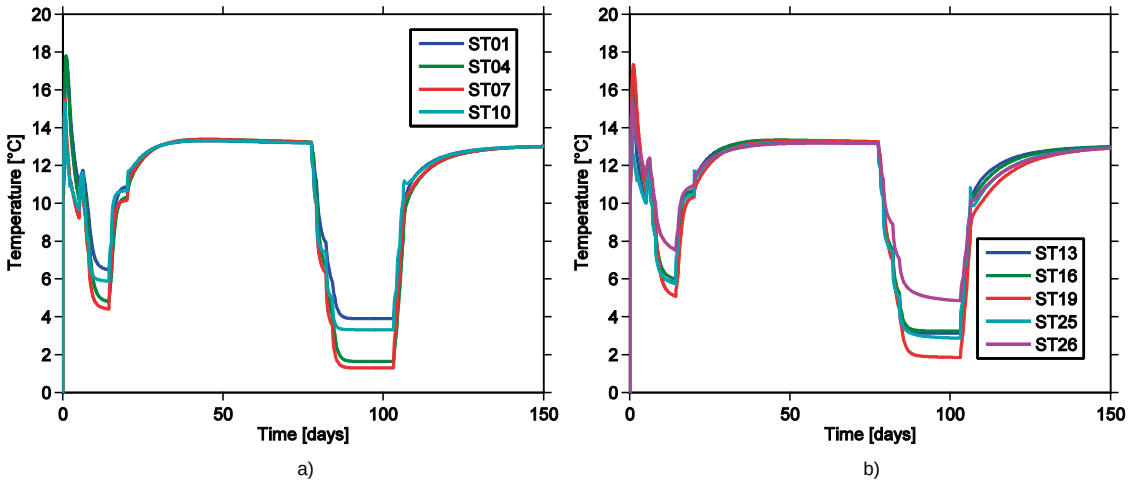

Figure 8-20. *Temperature output from simulations at sensors locations.*

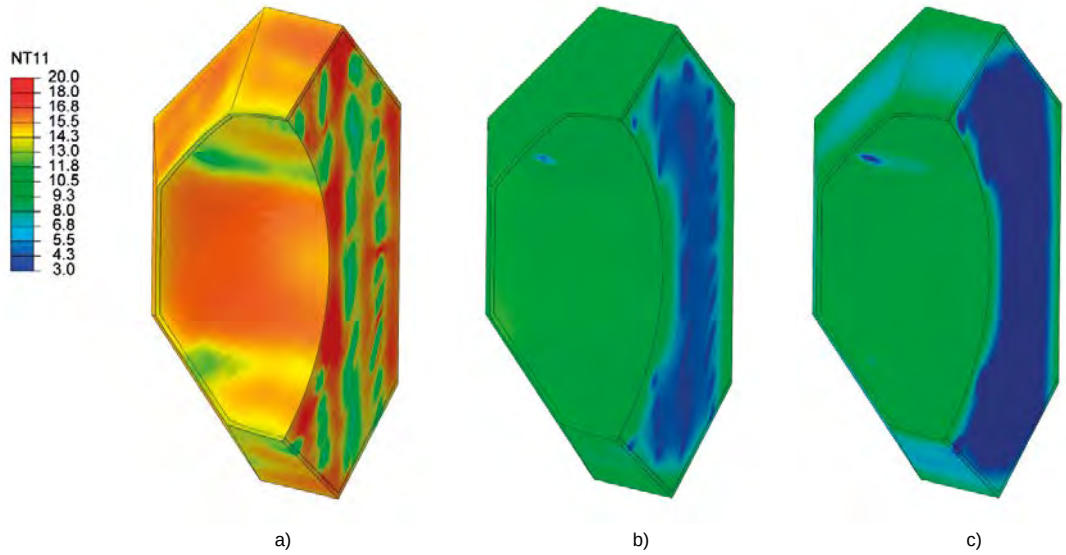

Figure 8-21. *Simulated temperature fields in the concrete dome at a) 42 hours, b) 14 days and c) 100 days from casting.*

8.2.3 Predicted structural response of the concrete dome

In the following section the mechanical response of the concrete dome plug as predicted by simulations in Abaqus is presented. The first part of the section is focused on predicting the early age response, up to 150 days from casting, including initial heat development and the two cooling sequences. In the second part, the response due to the pressurization during the test procedure is also included.

Early age behaviour

The strain output from the simulations during the initial 150 days from casting for a selected number of sensors is shown in Figure 8-22. Results from all installed sensors can be found in Appendix 4.

As expected, the largest strains appear for the no bond model (solid lines) since it is free to deform due to the shrinkage and temperature changes. It can be noticed that there is a predicted difference in strain level before and after the second cooling which indicates that a pre-stressing of the dome is achieved from the simulated cooling and grouting sequence. Also it can be observed the all sensors indicate that the dome is contracting, i.e. no tensile stresses occur. For the two full bond cases, significantly smaller strains are observed. Both cases indicate that tensile stresses occur in some sections of the dome. After approximately 100 days, the bond of the upstream rock slot is assumed to be lost for one of the models (dashed lines) which results in a sudden and significant change in the strain level. This is due to the release of all built in energy in the dome due the shrinkage and temperature decrease when the boundaries of the dome are changed. This phenomenon, although probably not as sudden, would also be observed in reality when and if the dome completely or partially releases from the rock. The other case with no change in boundary condition (dotted lines), shows only small change in the strain level during the second cooling and the contact grouting.

The predicted response of the joint meters is shown in Figure 8-23a for the first 150 days. Note that since a vertical symmetry plane is used in the model, joint meters JM01 and JM02 are not included in the simulations; however, they should show similar results as JM05 and JM06 due to the symmetry. The simulations predict that a maximum gap between the concrete and the rock of approximately 4.3 mm is obtained at the top of the dome for the no bond concrete-rock interface model (solid lines). This value is close to the estimated gap of 4.5 mm obtained from the simplified method in Section 6.6.4. The main reason for the discrepancy is the assumed thermal strain in Section 6.6.4 is higher than the due to the more detailed calculated temperature obtained from the finite element model, see Figure 8-21. For the two full bond models (dashed and dotted lines) the gap is below 0.5 mm due to elastic deformations in the interface. In Figure 8-23b the graph is zoomed in at the full bond models to better see the change in gap distance for these two models.

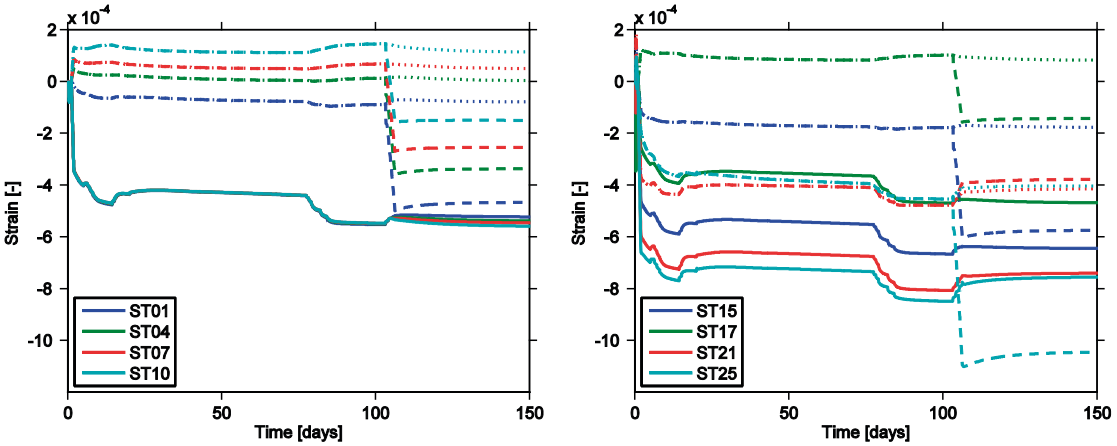

Figure 8-22. *Strain output from simulations at sensors locations during the early age of the concrete. Solid lines shows the case of no bond while dashed and dotted lines show the two cases of full bond for the concrete rock interface.*

The predicted horizontal displacement at the location of the LVTDs mounted to the dome surface is shown in Figure 8-24a for the first 150 days. Due to the unconstrained volumetric shrinkage of the concrete, the no bond model (solid lines) shows a large negative displacement at early stages. Negative displacements are defined towards the bentonite seal. During the cooling sequences further negative displacement is predicted with a maximum value of −3 mm at 150 days. For the full bond models (dashed and dotted lines) the displacement are recorded as positive with a magnitude below 1 mm. For the full bond model with a release of the bond at the upstream rock surface during the second cooling sequence (dashed lines), a large drop in displacement is shown due to the built in stresses in the concrete. In Figure 8-24b the graph is zoomed in at the full bond models to better see the change in displacement for these two models.

Pressurization

The strain output from the simulations including the pressure step for a selected number of sensors is shown in Figure 8-25. Results from all installed sensors can be found in Appendix 4.

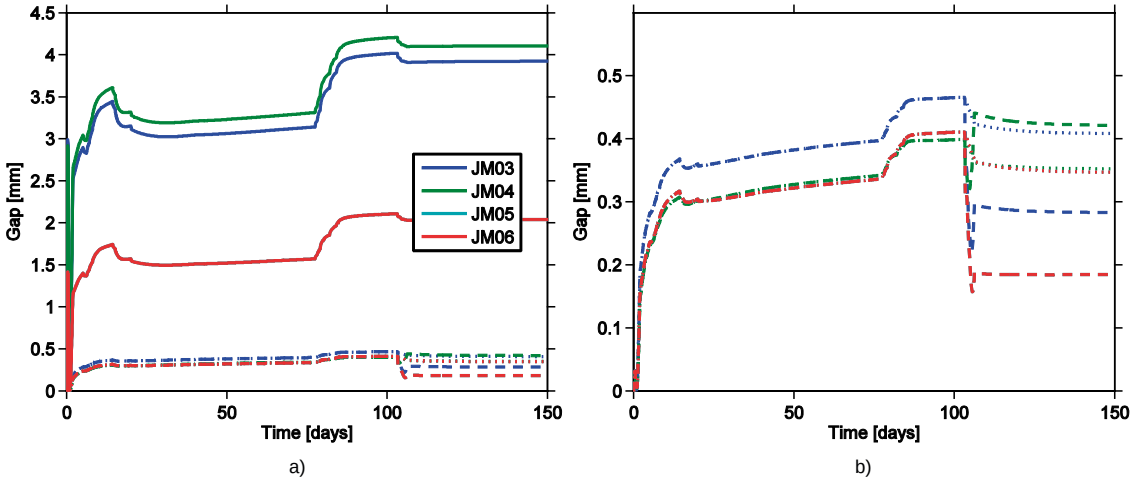

Figure 8-23. *Displacement output from simulations at joint meter locations during the first 150 days from casting. Solid lines shows the case of no bond while dashed and dotted lines show the two cases of full bond for the concrete rock interface.*

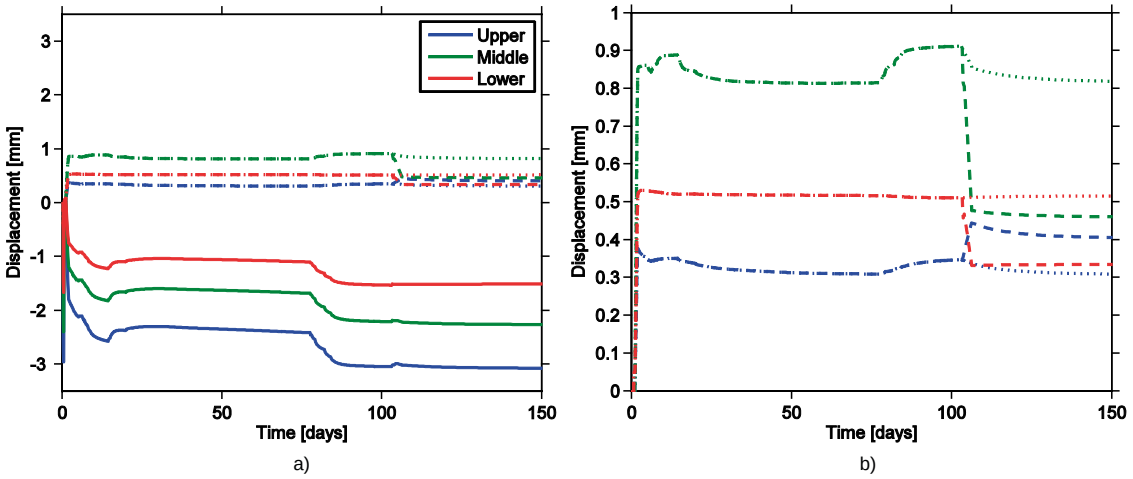

Figure 8-24. *Model output for horizontal displacement from the LVDTs during the early age of the concrete. Solid lines shows the case of no bond while dashed and dotted lines show the two cases of full bond for the concrete rock interface.*

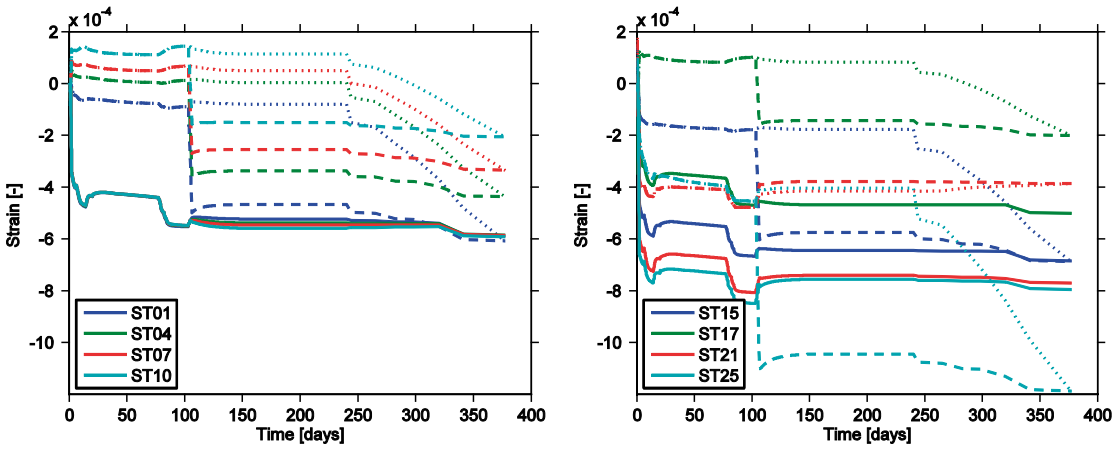

Figure 8-25. *Strain output from simulations at sensors locations including pressurisation. Solid lines shows the case of no bond while dashed and dotted lines show the two different cases of full bond for the concrete rock interface.*

For the case of no bond (solid lines) the change is in the region of −100 micro strain (μs) due to the applied water pressure for all sensors. This small change can probably be explained by the pre-stressing of the concrete dome. For the full bond case, where bond of the upstream rock slot is lost during the second cooling (dashed lines) a slightly higher change in strain is observed during the pressure phase. However, the largest change still occurs during the second cooling (~ 100 days). Due to the temperature increase after the second cooling there is still some pre-stressing of the dome which might explain the small change in strain. For the second case of full bond (dotted lines), where bond of the upstream rock slot is lost at the application of water pressure, the change in strain is significantly higher for most sensors. The highest change in strain, −800 microstrain, due to the pressure load is observed in ST25 located close to the downstream rock slot. The significant increase in strain response due to the pressure load can probably be explained by the lack of pre-stress in the concrete dome for this case. It is also interesting to notice that the strain levels of the two full bond cases converge at the last pressure step.

The predicted response of the joint meters is shown in Figure 8-26a the entire analysis, including the pressure step. As can be observed, the change in gap due to the water pressure is small for all models. Compared to the magnitude of early age gap, the two full bond models, however, show a significant change in gap due to the water pressure, which can be seen in Figure 8-26b.

The predicted response of the LVDTs from all three models is shown in Figure 8-27a for the entire analysis, including the pressure step. As for the joint meters, the displacements due to the pressure load are small for all three models, below 0.5 mm. The largest displacements due the pressure load occurs in the full bond model where the bond of the upstream rock surface is released at the application of pressure (dotted line), as can be observed in Figure 8-27b.

In Figure 8-28, Figure 8-29 and Figure 8-30 the contour fields of the displacement component in the direction of the tunnel are shown for all three models prior to the application of the pressure load in figures (a) and at the end of the analysis at approximately 4 MPa water pressure in figures (b). As can be observed, the deformation due to the water pressure is small for the no bond model, Figure 8-28, smaller than 1 mm. For the two full bond models, the deformation is larger and in the order of a couple of millimeters.

The stress state predicted to be present prior to the application of the water pressure is shown in Figure 8-31 for all three models. In the figures, the hydrostatic stress is shown where positive values indicate compression and negative values indicate tension. Only for the no bond model, Figure 8-31a, the entire dome is under compressive stress. The magnitude of the hydrostatic stress for this case varies between 2–5 MPa. For the two full bond cases, most part of the dome are subjected to tensile hydrostatic stresses, only for the case with release of the upstream rock interface bond during the second cooling cycle, Figure 8-31b some parts are subjected to compressive stress. For the other full bond case, Figure 8-31c, the entire dome is subjected to large tensile stresses. The large tensile stresses in the two full bond models are largely due to the restrained shrinkage strains that occur during the early age of the concrete.

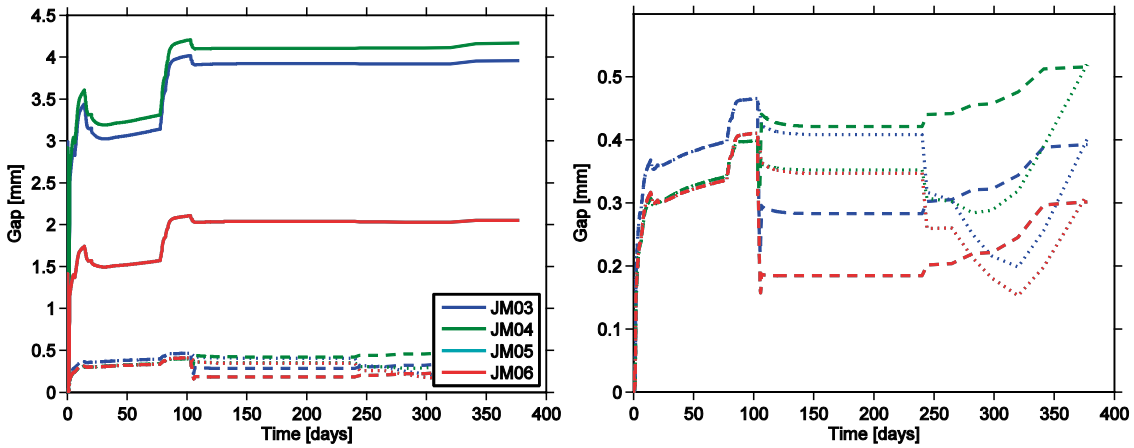

Figure 8-26. *Displacement output from simulations at joint meter locations. Solid lines shows the case of no bond while dashed and dotted lines show the two different cases of full bond for the concrete rock interface.*

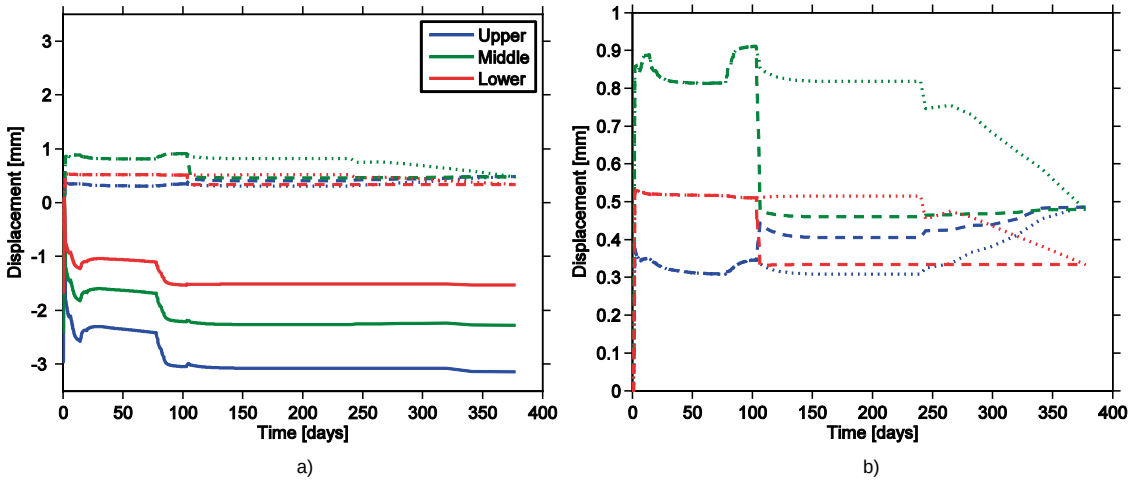

Figure 8-27. *Horizontal displacement prediction for the LVDTs. Solid lines shows the case of no bond while dashed and dotted lines show the two different cases of full bond for the concrete rock interface.*

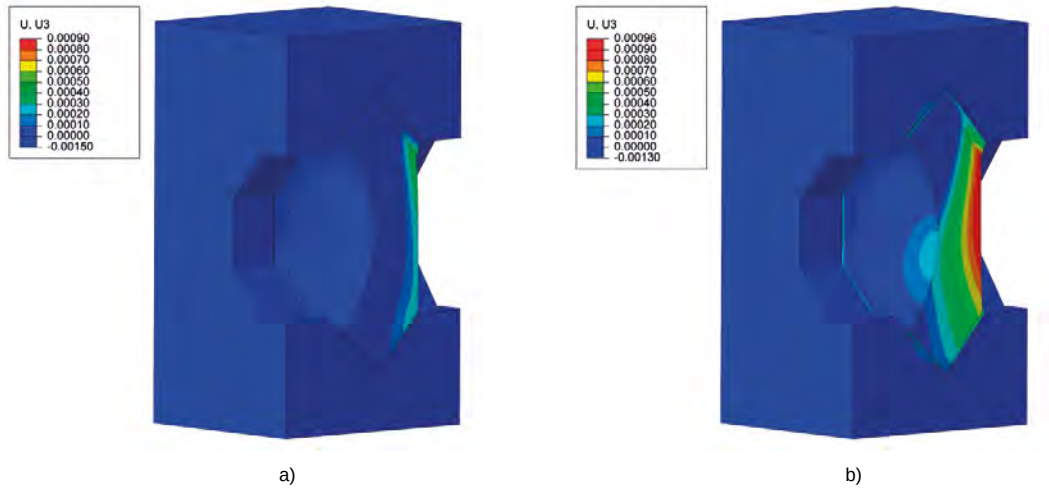

Figure 8-28. *Contour of displacement component in the tunnel direction for the no bond model, a) prior to the pressure load and b) at 4 MPa water pressure.*

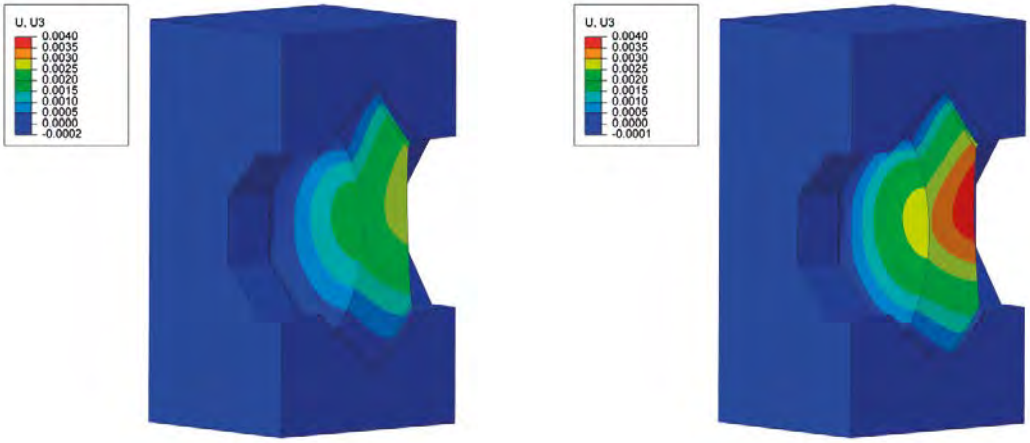

a) b)

Figure 8-29. *Contour of displacement component in the tunnel direction for the full bond model with release of bond during the second cooling cycle, a) prior to the pressure load and b) at 4 MPa water pressure.*

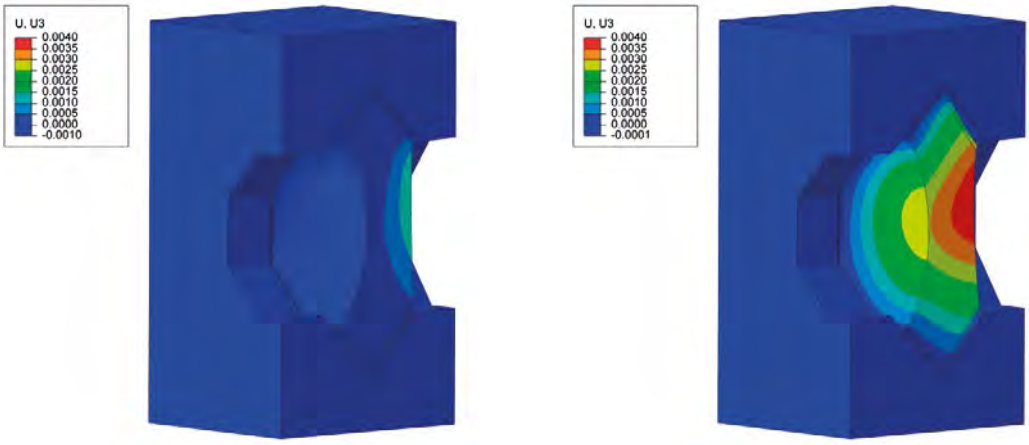

a) b)

Figure 8-30. *Contour of displacement component in the tunnel direction for the full bond model with release of bond at the application of water pressure, a) prior to the pressure load and b) at 4 MPa water pressure.*

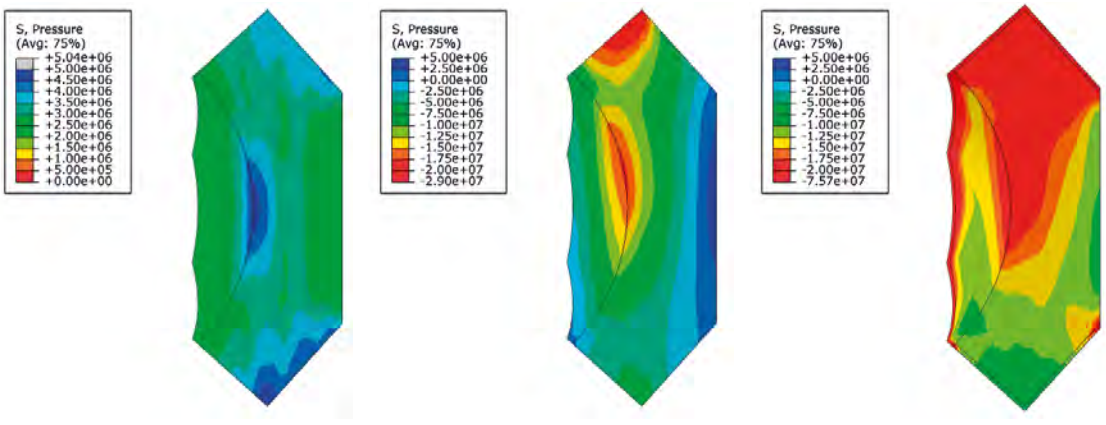

a) b) c)

Figure 8-31. *Stress field showing the hydrostatic pressure in the concrete dome prior to application of the water pressure for a) no bond, b) full bond with release during the second cooling cycle and c) full bond with release at the application of the water pressure.*

8.2.4 Comments on the FE-modelling

The most difficult part of modelling the mechanical state of the concrete dome proved to be an accurate description of the concrete-rock interface. Ideally a non-linear description of the interface with de-bonding should have been used. However, as mentioned above, this proved to be difficult due to the brittle behaviour of concrete and rock interfaces in general. This was further complicated by the large mass of the dome and a sudden release of large amounts of mechanical energy when interface rupture occurs. This behaviour makes the model unstable with slow or non-converging solutions. To solve the model stability problem, if at all possible, the run-time of the model would be very long and it was therefore use a non-linear interface in the model was deemed to be beyond the scope of this project.

One of the most important aspects regarding the behaviour of the dome seems to be the large early age autogenous shrinkage of the low-pH concrete. It gives rise to large volumetric changes of the dome, which if restrained causes major tensile stresses and possibly cracking of the concrete. One difficulty of modelling this type of early age shrinkage is to define when during hydration that the concrete starts to behave as a homogenous elastic medium, since prior to that point, the autogenous shrinkage does not cause any significant volume changes.

A possible improvement of the current model would be to also include creep deformations. This could both improve the stress predictions and also the response during the water pressurization step. This would allow for inclusion of the relaxation of the built-in pressure in the dome during the second cooling cycle, especially for the no bond model.

Comparison between the analysis results and the performed measurements is made in Section 9.2.

9 Results of from the full-scale test

The instrumentation used to monitor the full-scale test was previously described in Chapter 7 and numerical modelling of the dome plug performance was presented in Chapter 8. In this chapter, the results from monitoring of the performance of the full-scale test are presented together with comparisons of the performance with the predictions based on the numerical modelling.

The two key influences on system behaviour are the cooling sequence following casting of the dome and the subsequent water pressure application to the volume upstream of the dome. The temperature in the cooling pipes is illustrated in Figure 9-1and the water pressurization process is provided in Figure 9-2.

In Figure 9-1, red vertical lines have been included to illustrate the three stages of cooling.

1. Stage A – To reduce the effect of hydration heat.
2. Stage B – Cooling of the dome in order to force it to release from the rock.
3. Stage C – Additional cooling of the dome prior to contact grouting.

About the pressurization scheme, it had been shown in the laboratory scale-model tests (Section 4.2.6) that the bentonite seal gives reliable sealing function when a swelling pressure of about 500 kPa has been reached in all its parts. Since this process takes at least one year in full-scale, it was recommended to let the bentonite seal access water from the filter as soon as possible. Consequently, during summer of 2013, the two drainage pipes were connected to a simple water supply system and the filter section was slowly flooded. The water pressure inside the filter was controlled at low level (7 m head) to provide possibility for the bentonite seal to gently initiate saturation (from day 117 and forward).

After four months flooding of the filter, at the end of September 2013 (day 243), the drainage valves from the filter section were closed. Thus the pressure inside the plugged volume slowly increased (about 15 kPa/day) by the natural groundwater inflow. The rate of the groundwater inflow had been estimated according to description in Section 3.5. On December 2, 2013 (day 306), the water injection system was started to allow pressure build up at a higher rate (250 kPa /week).

The artificial pressurization was stepwise increased to 4 MPa during the period from December 2013 (day 306) to the mid of February 2014 (day 383), see Figure 9-2.

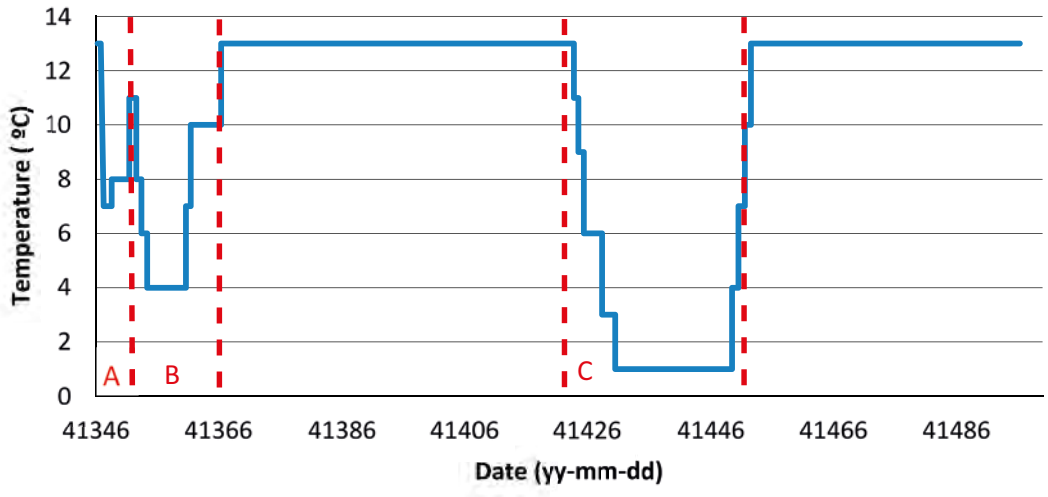

Figure 9-1. *Illustration of the temperature in the cooling pipes during the cooling scheme. (T = 14°C corresponds to no cooling.)*

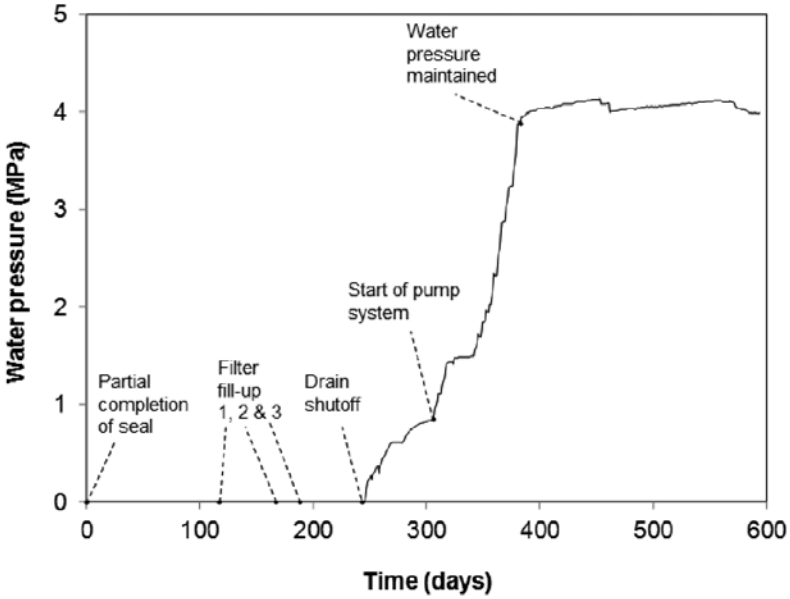

Figure 9-2. *Applied water pressure for DOMPLU, measured at the pump outlet.*

One of the test objectives (as described in Section 1.3) was to test the plug at the reference load case value of 7 MPa. The load case is a combination of the hydrostatic pressure from the groundwater (up to 5 MPa) and the swelling pressure from the backfill transition zone (approximately 2 MPa), acting together on the plug system. Since the development of a full swelling pressure in the seal is predicted to take many years, the plan was to achieve this load for DOMPLU by injecting water from the pressurization system described in Section 7.3.

However, the full water pressure of 7 MPa could never be reached due to conditions of the surrounding rock at the experimental site. Shortly after the injected water pressure having exceeded the prevailing groundwater pressure at the experimental site (approximately 3 MPa), a main water escape was discovered in a fracture by-passing the plug to the main tunnel. Despite the promising results from the hydro-tests in the pilot-borehole of the experiment tunnel, water escaping into the rock had been recognized as one major project risk since the rock at Äspö HRL is much fractured in general. Due to the encountered rock fracture, by-passing the plug, it was decided to limit the water pressure in the plug to 4 MPa and perform continuous measurements of the observed leakages at this level. This pressure could successfully be maintained by the water pressurization system until the date for data freeze for technical reporting on September 30, 2014 (day 608).

The water escapes related to the experimental site is further described in Section 9.3 while more details about the pressurization scheme are provided in Section 9.1.1 here below.

9.1 Bentonite seal and backfill measurements

In order to analyse the behaviour of the bentonite seal, filter and backfill these sections have total and pore pressure sensors, relative humidity sensors and displacement gauges installed in them. The results presented in this section are based on the report by Börgesson et al. (2015a). The installation of sensors has previously been presented in Section 7.1 and a description of the detailed positions of the instruments is located in Appendix 3.

9.1.1 Water pressurization scheme

Monitoring results have responded to the pressurization of the system by injection of water into the filter and backfill, followed by saturation and development of swelling pressure in the watertight seal and backfill transition zone. The details of the pressurization sequence is described below and illustrated in Figure 9-2. These activities have been marked in the graphs shown in this section for clarity and to aid understanding of the system responses:

- **January 30, 2013 (day 1).** All sensors on the inside of the concrete delimiter have been positioned and connected to the data acquisition system. The last concrete beam was put in place two days later.
- **May 27 (day 117). Draining test and filter fill-up 1.** In order to give the bentonite seal access to water as soon as possible and also to simulate the worst groundwater case in the final repository, it was decided to apply a flow rate from the inside of the backfill. The plan was to achieve a channel through the pellet filling to the filter section, from which the water then should be drained. At the same time it was important to not erode any bentonite into the gap between the concrete dome and the rock since this gap should be grouted with cement. Initially a constant water inflow of 5.0 l/min was applied. A large outflow of bentonite slurry through the lead-through pipe in the concrete dome occurred the next day (the cone and flange were still not mounted) and the inflow was stopped. A new attempt was performed with an inflow rate of 1.0 l/min but the system failed again to drain also this flow rate. The filter section was believed to have been partly filled during this procedure. It was subsequently decided to postpone further activities until the grouting of the plug had been performed.
- **June 11 and 19, 2013 (days 132 and 140).** Contact grouting of the plug.
- **July 16 (day 167). Draining test and filter fill-up 2.** After having back-flushed the drainage pipe, a constant flow of 1.4 l/min was applied from the inside of the backfill. The draining then functioned well during one day. The next day the draining pipe had clogged and the flow was mainly running through the de-airing pipe i.e. the filter section was full of water. The inflow was thereafter kept constant but after about 12 days it was discovered that also the de-airing pipe had clogged. A leakage was then observed through the sensor cable lead through pipe (through the dome) and the flow was stopped. Approximately 240 kg bentonite was lost. It is believed that the finely meshed copper net placed over the drainage tube endings inside the gravel filling is the reason for the problem with clogging.
- **August 6 (day 188). Filter fill-up 3.** The draining- and de-airing pipes were back flushed and the filter was completely water filled from the outside, by water injection via the drainage pipes. The water pressure in the filter was slowly raised to 7 m head and then maintained at that level. No draining test was done in this procedure and no water flow rate was applied through the backfill.
- **August 26, 2013 (day 208).** A lid was mounted on the lead through tube in the plug. In addition, an extra pipe is installed inside in order to measure the water pressure inside the lead through.
- **September 30 (day 243). Shutoff of the drain.** The valves on the draining and de-airing pipes from the filter section were closed. Natural pressure increase was allowed to occur as water entered from the surrounding rock.
- **October 7 (day 250).** Installation of safety valve (6 bar). The natural water pressure increase is now allowed to increase up to 6 bar.
- **November 6 (day 280).** Installation of safety valve (10 bar). The natural water pressure increase is now allowed to increase up to 10 bar.
- **December 2, 2013 (day 306).** Start of pump system. The water pressure is artificially increased in steps (See Figure 9-2).
- **February 17, 2014 (day 383).** The water pressure inside the plug has reached 4 MPa. The pressure was kept at this level for the remainder of the testing
- **September 30, 2014 (day 608).** Defined date for data freeze of this technical reporting. The DOMPLU experiment will be in continued operation at 4 MPa water pressure until October 2016. That period will be separately reported.

Day 117, 167, 188, 243, 250 and 280 are all indicated in the graphs provided in the following sections.

9.1.2 Relative humidity and temperature

The water retention curve for a material is a relation between the water content and the potential of the soil water expressed as relative humidity. This means that by measuring the relative humidity in the bentonite it is possible to estimate the water content and the degree of saturation. In total 16

relative humidity sensors were installed, 8 in the backfill and 8 in the bentonite seal. In addition, the temperature is registered in each of these sensors. The results from measurements of relative humidity (RH) and the temperature are presented in Figure 9-3 through 9-5. Locations of each measuring section of sensors are provided in Appendix 3.

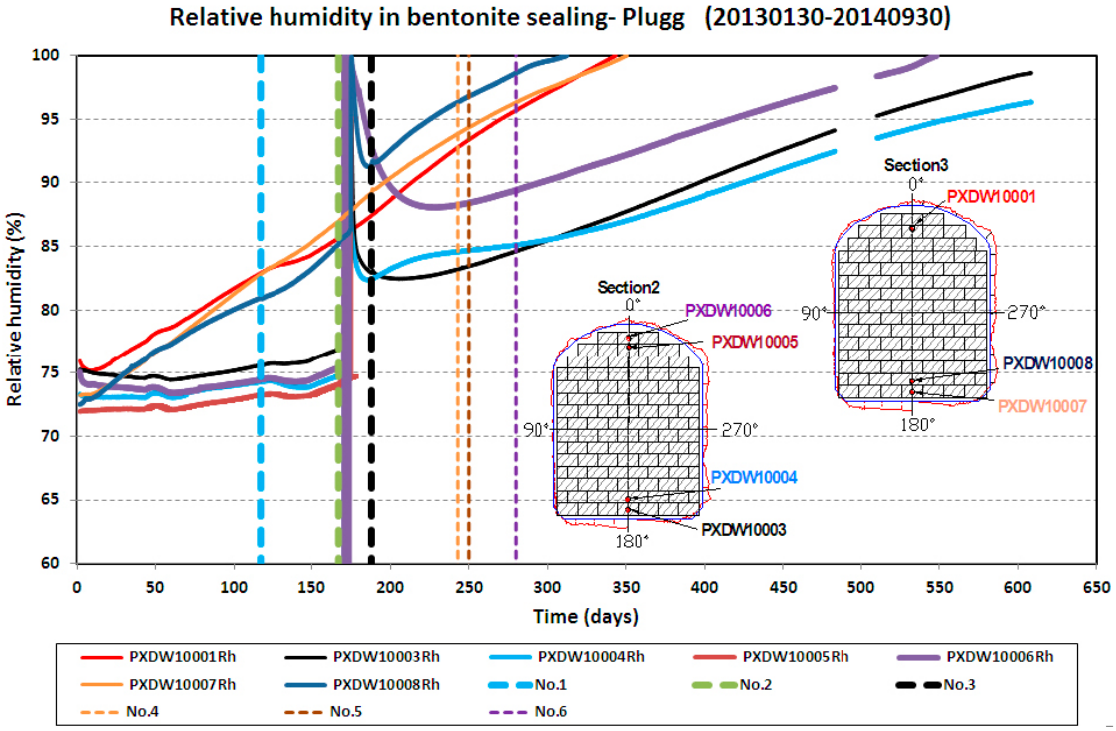

Figure 9-3. *Relative humidity recordings in the bentonite seal. Activities associated with testing (see section 9.1.1) are identified as "No.1 through No.6".*

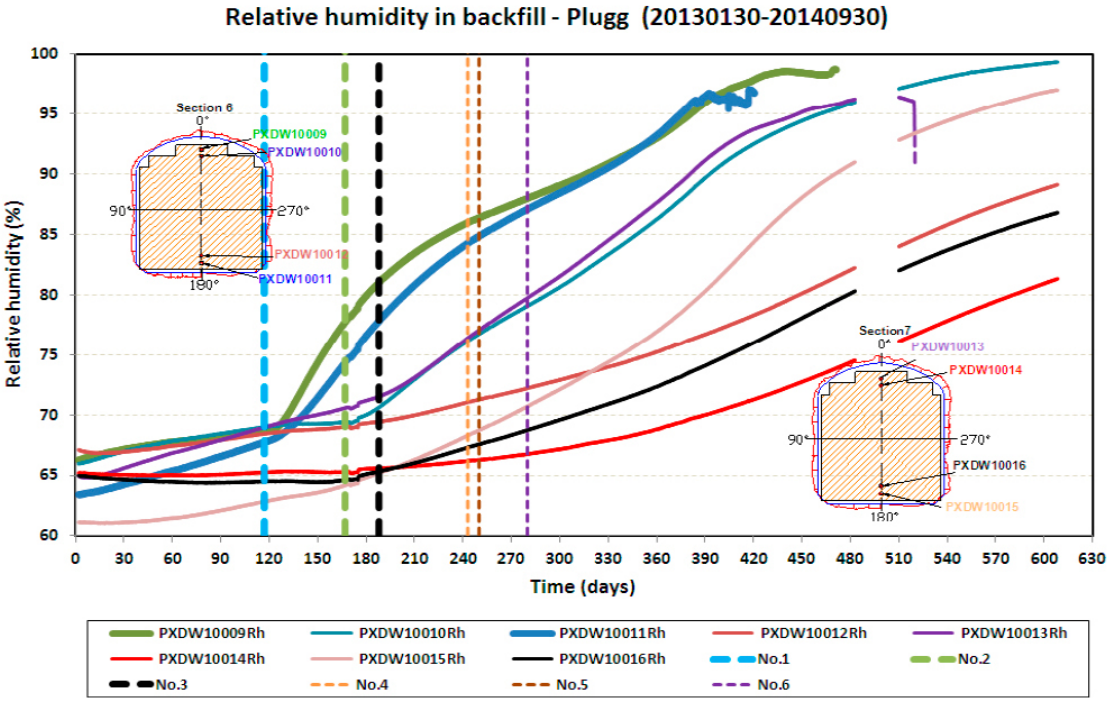

Figure 9-4. *Relative humidity recordings in the backfill. Activities associated with testing (see section 9.1.1) are identified as "No.1 through No.6".*

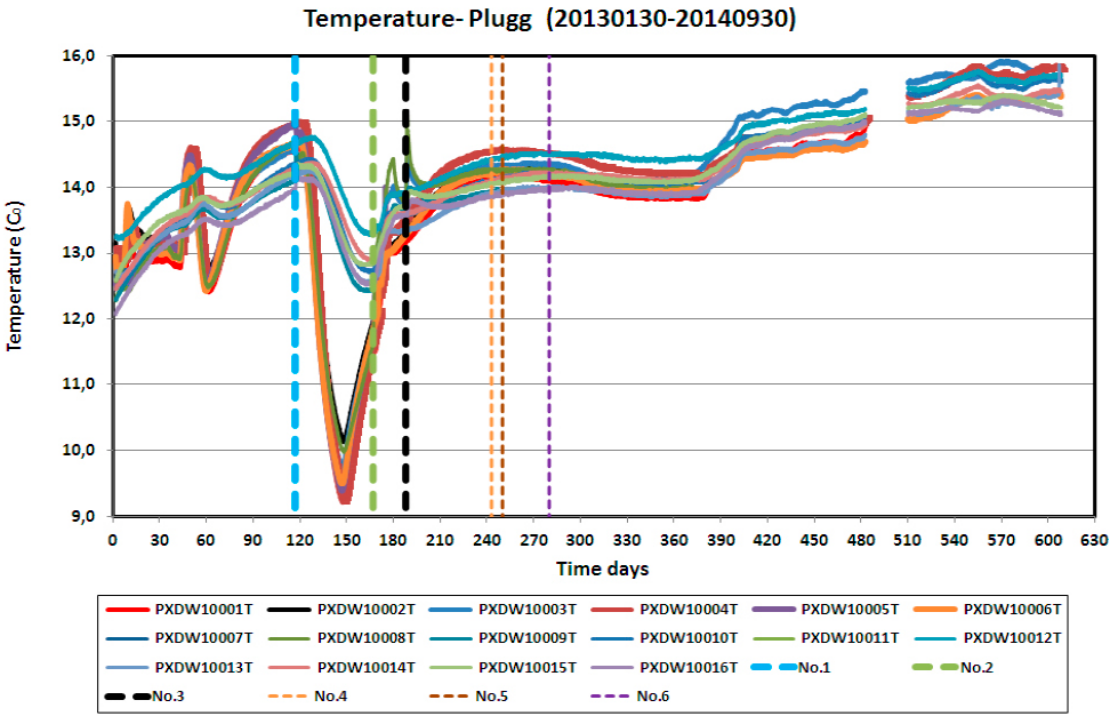

Figure 9-5. *Temperature recordings in the bentonite seal and backfill. Activities associated with testing (see section 9.1.1) are identified as "No.1 through No.6".*

- Eight sensors are positioned in the bentonite seal, where one of the sensors has failed to function. The measured relative humidity after installation was between 72 and 77 % compared to the initial water content in the blocks of 17 %.
- Eight sensors are positioned in the backfill section. The measured relative humidity after installation was between 63 and 67 %. The retention curve for the Asha material gives that the measured relative humidity well corresponds to the current water content of the backfill blocks i.e. 15–16 %, see Johannesson et al. (2008).
- Directly after installation, the relative humidity started to increase in some positions in the bentonite seal e.g. sensor 1 (top in measuring Section 2) and sensor 7 and 8 (bottom in measuring Section 3). There was also a tendency for increasing relative humidity directly after installation at some positions in the backfill e.g. sensor number 9 to 12 (top and bottom in measuring Section 6) and 13 (top in measuring Section 7).
- The first draining test and filter fill-up (day 117) significantly affected two RH sensors in the backfill, No.9 and 11 (Section 6). After this test, the RH in these positions has continued to increase.
- At the second draining test and filter fill up (day 167), the main part of the RH sensors (5 out of 7) placed in the bentonite seal, initially showed a significant increase in RH and five of the sensors reaches 100 % RH. One sensor (PXDW1005) is after that lost but four of these sensors (PXDW1003, PXDW1004, PXDW1006 and PXDW1008) recover. Further measurement shows a dropping in measured RH probably depending in that the injected water has been absorbed by the surrounding bentonite. If these types of sensors are exposed to free water they often stop working, especially if the water contains salt. These four sensors continue, however, further on to show realistic values. This indicates that they have been exposed to very high RH in the form of gas and not as free water.
- The influence of the activities with water filling of the filter can also be observed in the temperature recordings, as seen in Figure 9-5. The influence of cooling the concrete dome can also be seen in the graph.
- The increasing water pressure in the filter (from day 243 and forward) has not affected the RH sensors in the backfill and the bentonite seal.

- By approximately day 550 the relative humidity throughout the bentonite seal had reached 95–100 %, at some positions e.g. in measuring Section 2 (at the top) and in measuring Section 3 (at the bottom). When the relative humidity reaches 95–100 %, the readings provided by the sensors are very difficult to interpret and if the sensors are exposed to free water they will stop working.

Comparison with numerical analyses

The predictions of the seal's components and overall evolution produced through numerical analyses were previously presented in Section 8.1.2. In this section, comparisons are made for the sensors in the bentonite seal and the backfill respectively. In Figure 9-6, the location of the sensors used for comparison is shown; the arrows in the figure are colour coded to correspond to the colour of the graphs comparing the data and predictions, i.e. in Figure 9-7 and Figure 9-8 respectively. In Figure 9-7 and Figure 9-8, the measured and calculated development of relative humidity is shown for the bentonite seal and backfill section respectively. In the measured response of the sensors, the flooding event during the drainage test and second filter filling (day 243 listed in Section 9.1.1 and also shown in Figure 9-3 through Figure 9-5), is clearly shown. The numerical analyses were performed in advance to the full-scale test and therefore this originally unplanned event is not included in the numerical analysis.

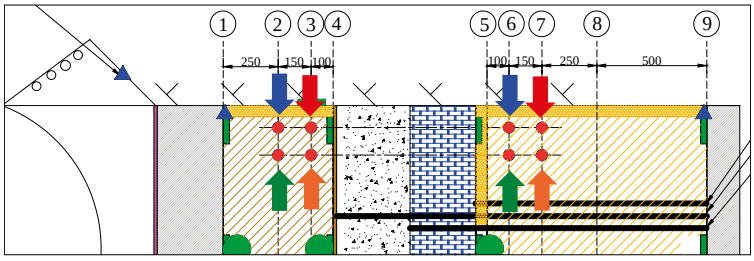

Figure 9-6. *Location of the sensors in the bentonite seal and backfill respectively, which are used for comparison of relative humidity.*

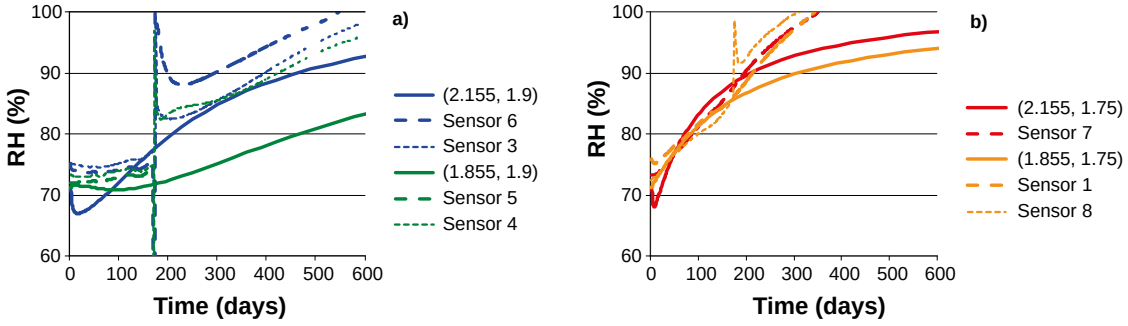

Figure 9-7. *Comparison between numerical and measured relative humidity (RH) for the bentonite seal.*

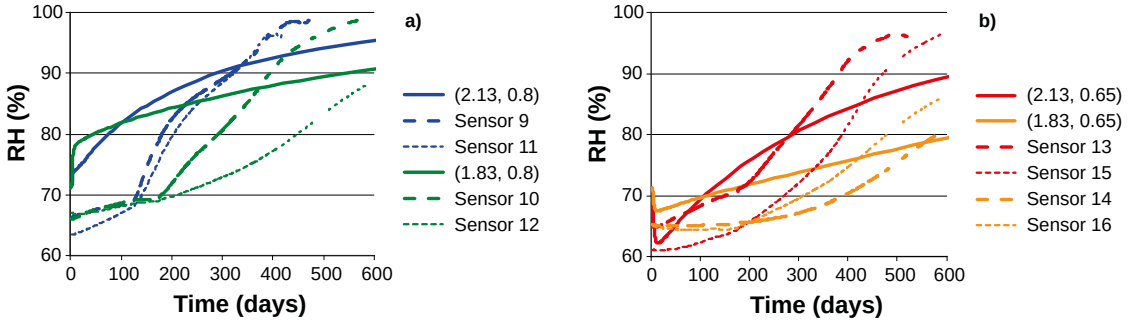

Figure 9-8. *Comparison between numerical and measured relative humidity (RH) for the backfill.*

For the numerical prediction, it was assumed that the filter would be filled with water immediately after installation, whereas this occurred after day 188 in the full-scale test. Still, the prediction showed a fairly good agreement with data from the RH sensors, and an explanation for this may be that the bentonite had access to some groundwater before the filling of the filter.

9.1.3 Total pressure and pore pressure

In order to monitor the development of swelling pressure and pore pressure, sensors have been positioned in the bentonite seal and in the backfill. The results from the total pressure measurements (swelling pressure and pore pressure) are provided in Figure 9-9, Figure 9-10 and Figure 9-11. The results from the pore pressure measurements are provided in Figure 9-12.

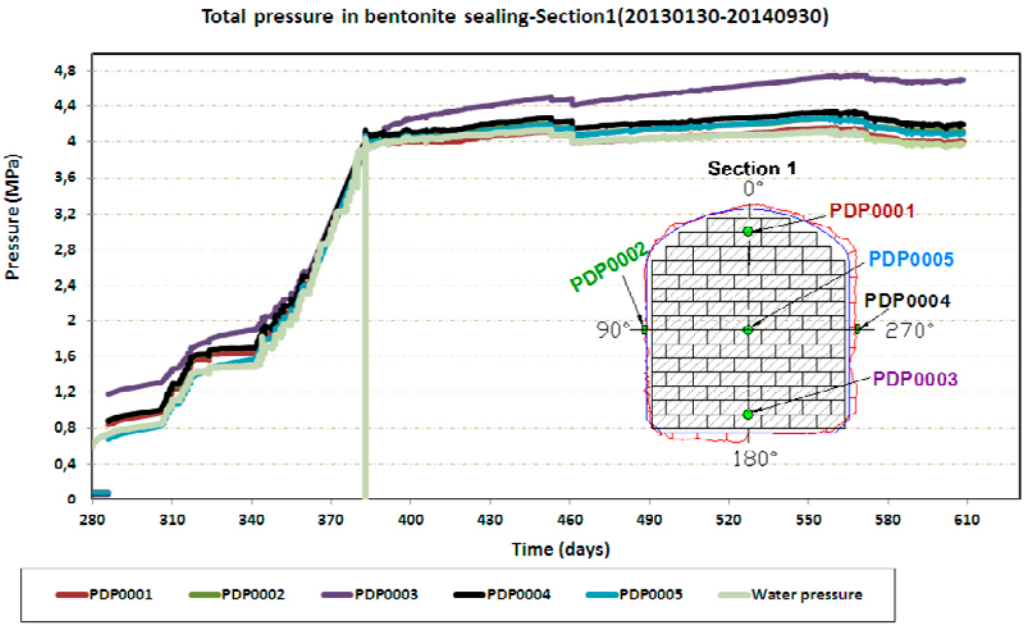

Figure 9-9. *Total pressure in Section 1 in the bentonite seal.*

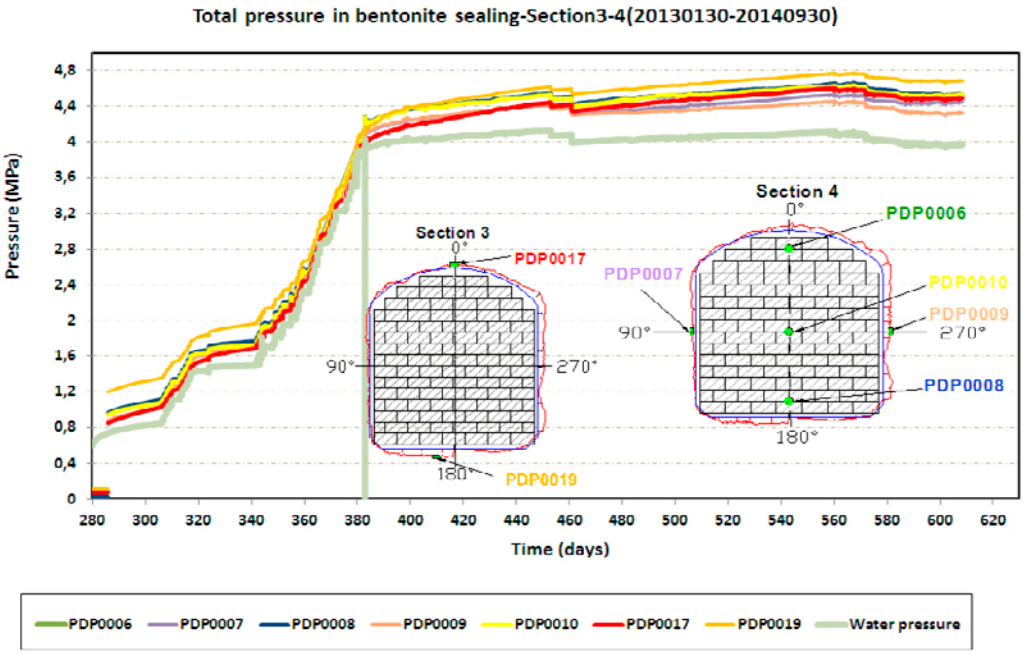

Figure 9-10. *Total pressure in Sections 3 and 4 in the bentonite seal.*

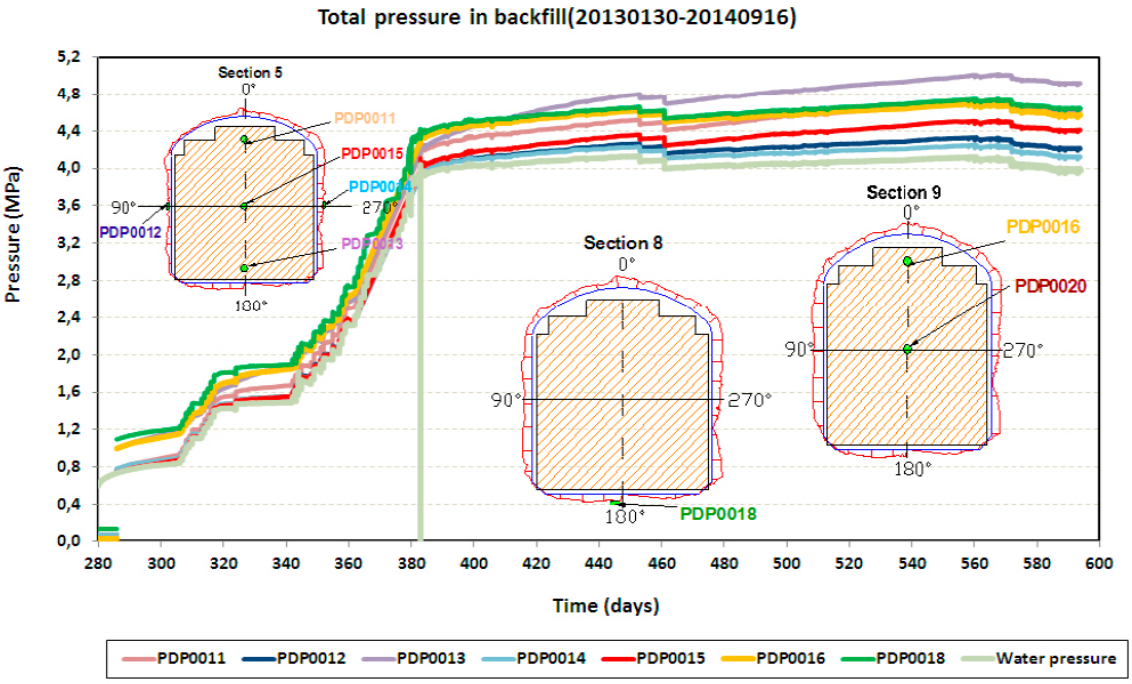

Figure 9-11. *Recorded total pressure in the backfill Sections 5, 8 and 9.*

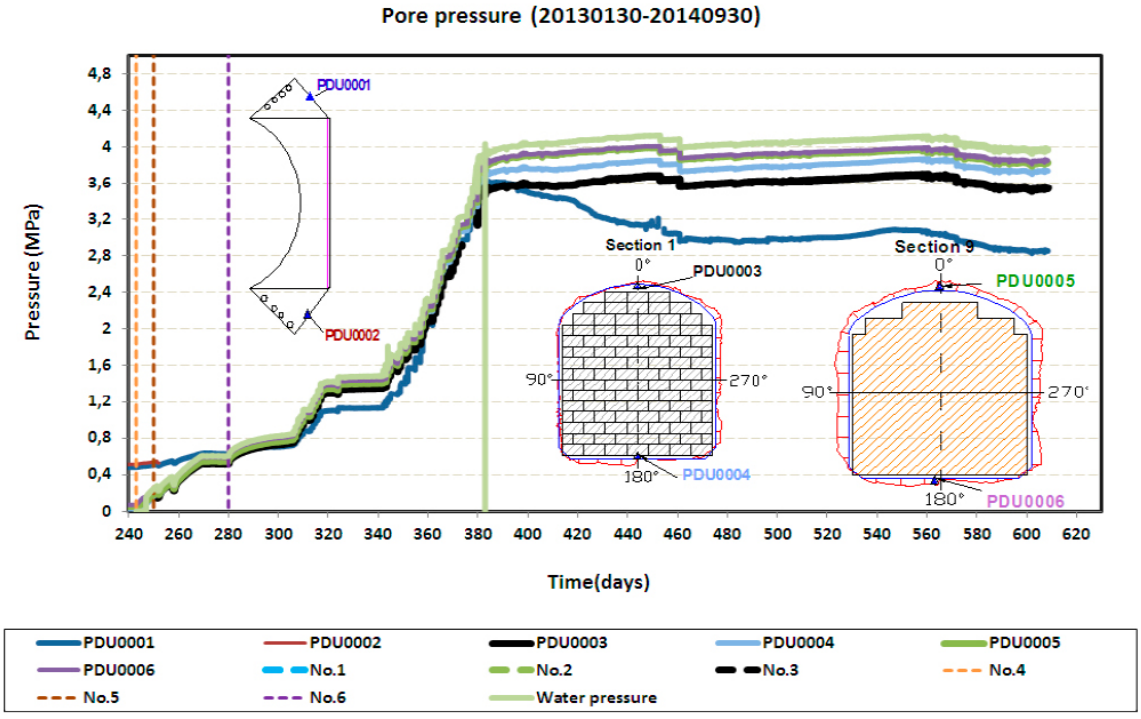

Figure 9-12. *Recorded pore pressure between concrete and rock, between the bentonite seal and the rock (Section 1), and between the backfill transition zone and the rock (Section 9).*

It was unfortunately after long time discovered that the total pressure cells had been evaluated in a wrong way in the logger. In the software it is possible to choose between linear or polynomial evaluation and since the accuracy was higher with polynomial evaluation according to the calibration certificates it was decided to use this. The registered values of the total pressure had since the installation been very low which was quite logical since it will take time to build up a swelling pressure in this rather inhomogeneous volume. However, when the pore pressure started to increase day 243

and it was not possible to see any reaction on the total pressure measurements we became suspicious and started to investigate if something was wrong. After having contacted the instrument supplier it was discovered that with the actual combination of sensor and logger it was not possible to perform a polynomial evaluation, only a linear. After having changed this, all sensors started to show realistic values (from day 285). Work has been going on to recreate the values registered earlier but it was unfortunately not possible. Below some comments are given to the graphs provided in Figure 9-9 to Figure 9-12:

- The monitored swelling pressure (total pressure-pore pressure) in the bentonite seal has increased with time and, by 30 September 2014, the swelling pressure was between 100 and 700 kPa.
- The monitored swelling pressure (total pressure-pore pressure) in the backfill has increased with time and, by 2014-09-30, the swelling pressure was between 100 and 1000 kPa.
- The two pore pressure sensors positioned in the slot between rock and concrete dome initially showed a pressure of 450 to 500 kPa prior to closing the drainage. One of the pore pressure sensors positioned in the plug between rock and concrete started to leak (after more than eight months of testing) through the steel tube. In order to seal this leakage, it was necessary to cut the cable and plug the steel tube (this was done on day 252, sensor no. PXDU10002). The sensor on the opposite side (PXDU10001) is still in operation. Up to the point when the water pressure increased up to 4 MPa it could be seen that this sensor showed about the same pore pressure as the other pore pressure sensors. This shows that the bentonite seal was not water tight at this time. However, whilst the water pressure in the bentonite seal was maintained at a constant value of 4 MPa, the pore pressure in the slot has successively decreased implying that the bentonite seal is starting to seal and is restricting water access to this location.
- An evident influence of the drainage test and filter filling at day 167, on the water pressure in Section 9, was registered by pore pressure sensors 5 and 6. The pressure increase is likely an effect of the clogging of the drainage and de-airing pipes and so when leakage through the lead-through pipe occurred, the pressure instantly dropped.
- The shutoff of the drainage on day 243, has affected all pore pressure sensors i.e. the two sensors in the backfill, two sensors on the other side of the sealing and also the two sensors placed in the concrete-rock slot. This means that the bentonite is not yet providing a tight seal.
- One of the total pressure sensors (PDP0020) located in the centre of the cross-section at Section 9 i.e. near the concrete back wall showed after day 285 (the day when the evaluation was changed to linear) a rather high pressure; 3 MPa. The pressure continued to increase and had after 380 days reached 15 MPa. The measured pressure is assessed to be unrealistic and is not presented in the graphs.

Comparison with numerical analyses

In order to compare the measured results with those obtained from the numerical analyses, the measured total pressure is reduced by the applied water pressure, i.e. hence obtaining the mechanical stress. Thereby, it is the effective stress in the radial and axial direction that can be compared between numerical and measured results.

In Figure 9-13, the locations of the sensors used for comparison are shown, the arrows in the figure are colour coded to correspond to the colour in each graph in the two figures showing measured results, i.e. in Figure 9-14 and Figure 9-15 respectively. In Figure 9-14 and Figure 9-15, the measured and calculated development of stresses is shown for the bentonite seal (i.e. on the concrete beams) and backfill section (i.e. on the concrete back-wall) respectively.

The results show large discrepancies in the modelled versus field results in drier sections, i.e. Section 1 and Section 9. The results also show that the numerical analysis overestimates the pressure on the concrete beams quite significantly. In the numerical analyses, the pressurization starts at time zero and was defined to occur more or less instantaneously, after 0.01 year. However, in the full-scale test the drain was not closed until day 188 (August 6th) and thereafter full water pressure of 4 MPa was obtained about 6 months later. As can be seen in the results, a better match of prediction to measured stress build up would be obtained if the numerical analyses were to be translated 188 days so that the pressurization occurred at the same time as in the full-scale test. However, the results from

comparison of the relative humidity measurements, and simulations, see Section 9.1.2, shows that shifting the timescale used would cause worse agreement than obtained for the relative humidity. One explanation for why there is a difference in the time it takes for the increase in relative humidity and stress could be that some gaps exist between the bentonite block in the full-scale test. These gaps would need to be closed before a stress can build up within the bentonite sections, which could explain why stresses build up more slowly than the relative humidity.

In the same way, the radial stresses have been compared between measurements and numerical analyses. The location of the points studied for comparison is shown in Figure 9-16 for the bentonite seal and backfill. The comparison of simulation and measured radial stress is then shown in Figure 9-17 and Figure 9-18.

Similar to the evolution of axial stresses, the predicted radial stresses showed a more rapid evolution than the corresponding data from the full-scale test, especially before the water filling of the filter. The reason for this may be that the gaps between the blocks, which were not represented in the model, had to be closed before any stresses could build up.

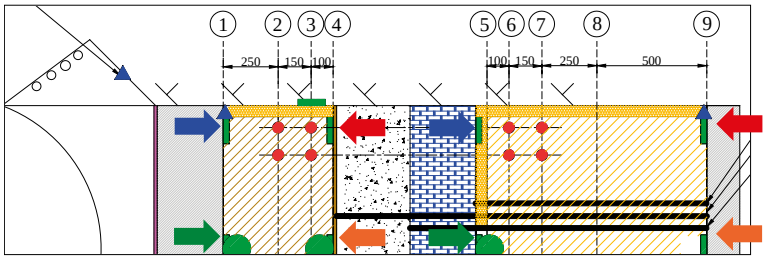

Figure 9-13. *Location of the sensors in the bentonite seal and backfill respectively, which are used for comparison of axial stresses.*

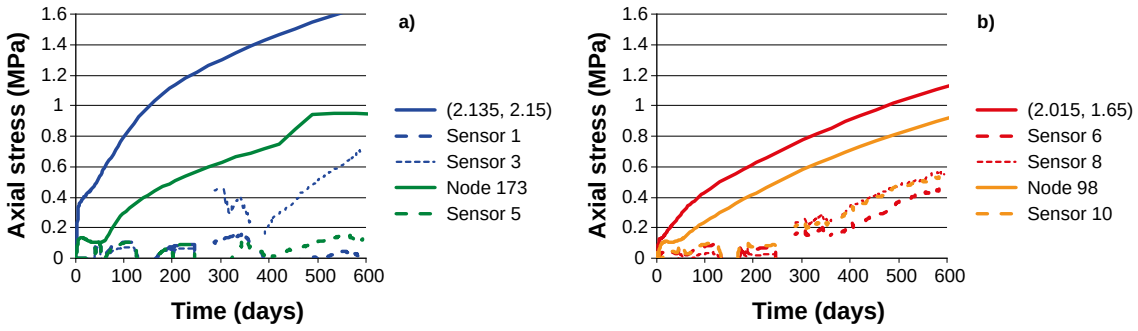

Figure 9-14. *Comparison between numerical and measured axial stress in the bentonite seal.*

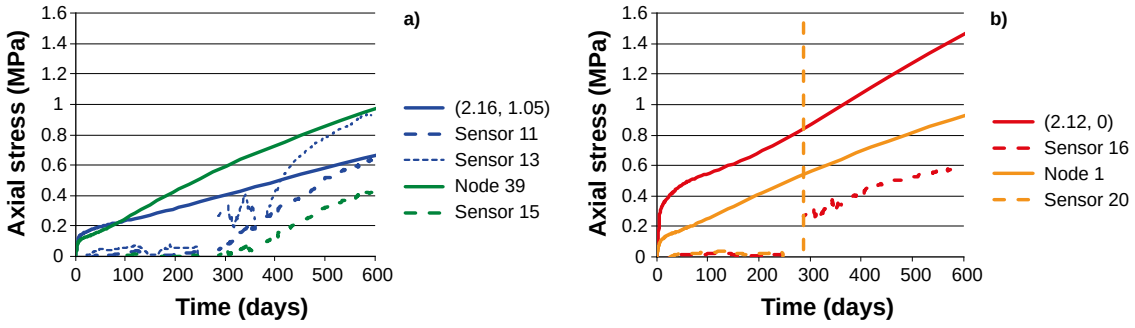

Figure 9-15. *Comparison between numerical and measured axial stress in the backfill.*

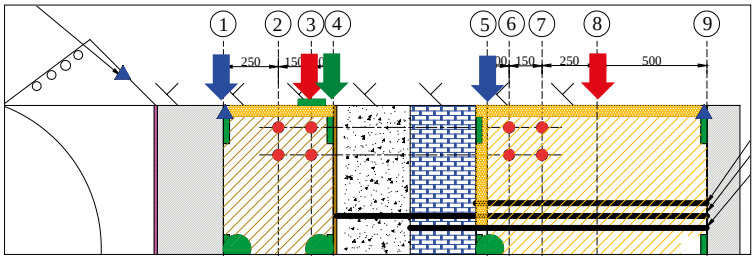

Figure 9-16. *Location of the sensors in the bentonite seal and backfill, which are used for comparison of radial stresses.*

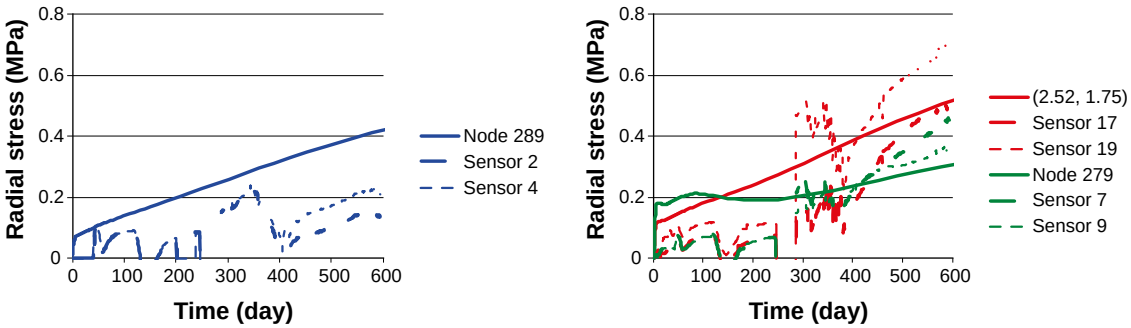

Figure 9-17. *Comparison between numerical and measured radial stress in the bentonite seal.*

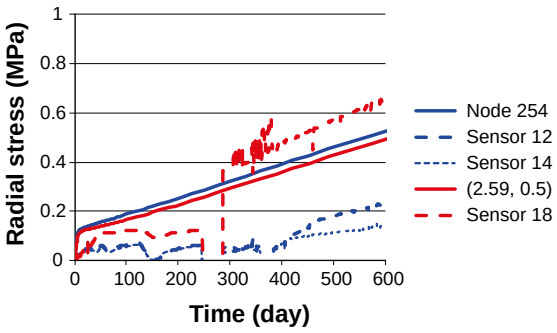

Figure 9-18. *Comparison between numerical and measured radial stress in the backfill.*

9.1.4 Displacements

The results from the measurements of displacement are shown in Figure 9-19. In Figure 9-19 it can be seen that all three displacement sensors have registered a movement inwards i.e. the bentonite sealing has swelled and compressed the gravel filter and the pellet filled slot inside the LECA wall. In total a movement of approximately 30 mm was registered from test start until day 385. After this date, no reliable data has been registered by these sensors as all three sensors probably had exceeded their measuring range which is the explanation for why they have failed. As a result subsequent displacements cannot be determined.

In detail:

- During some periods, there were problems with sensor no. 2, measuring the distance between the innermost concrete wall and the bentonite sealing blocks. The sensor seems to have worked properly most of the time but after day 235 it has not been possible to get any values.
- Sensor no. 3, measuring the distance between the outside of the LECA wall and the inner concrete wall failed on day 325.
- After day 385, Sensor no. 1 no longer provided useable output as it had exceeded its operating range.

Comparison with numerical analyses

The measured displacements have been compared with the displacements obtained from the hydro-mechanical model presented in Section 8.1.2. In Figure 9-20, the location of the sensors used for comparison is shown, where the arrows are colour coded to correspond with the colour of each graph in the Figure 9-21. In the figure, the dashed lines represent the measured behaviour that was previously shown in Figure 9-19 and the solid lines represent the results from the numerical analyses.

In general the comparison is satisfactory. The predicted displacements had; i) the same direction (i.e. upstream); ii) basically the same order of precedence (with the largest displacements at the seal/gravel interface); and iii) approximately the same magnitude, as the measurements. Some differences could however be noted regarding the rates of the displacements. The sensors data showed initially lower displacement rates than the prediction, but after the water-filling of the filter (day 188) the relation was the opposite with higher measured displacement rates.

It can be noted that both the modelled and the measured displacements at the sensor positions were directed upstream. In contrast, the initial analytical calculation showed that the length of the backfill would increase with 5 mm, i.e. a minor displacement downstream. This discrepancy is due to the 15 cm pellets-filled slot adjacent to the LECA beams, see Figure 6-8. This low density component was initially highly compressible and this caused the upstream movements. With time, however, the backfill block will swell and displace the pellets-filled slot downstream.

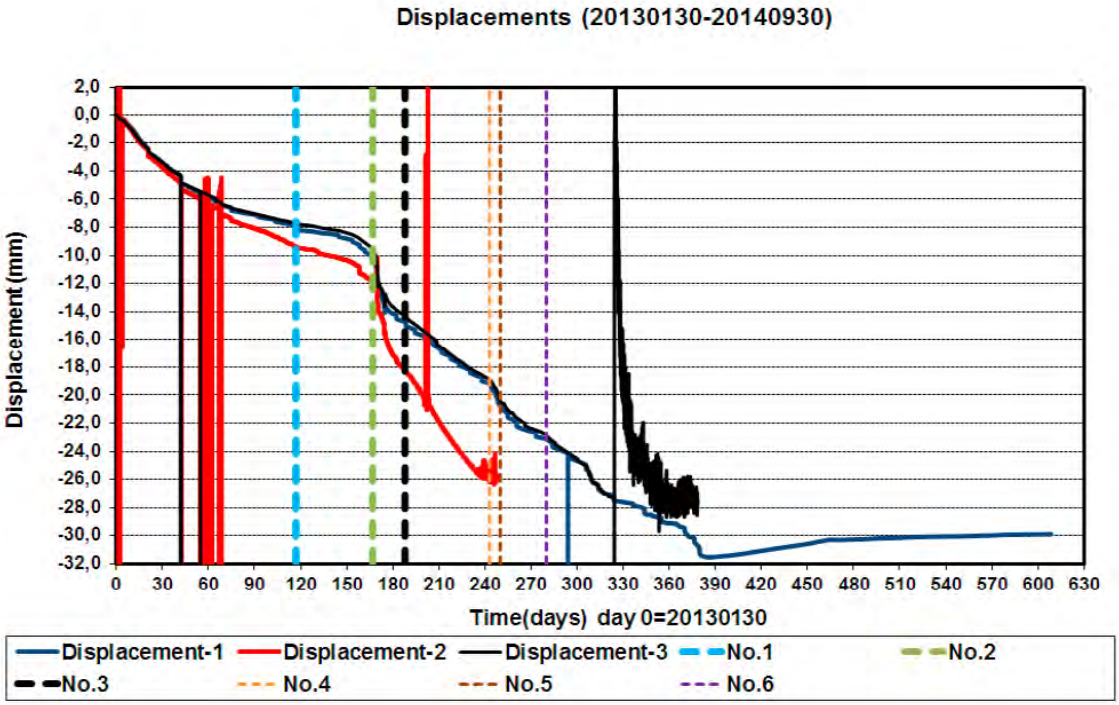

Figure 9-19. *Measured displacement of the seal (2) and LECA (1 and 3) respectively compared to the concrete back wall.*

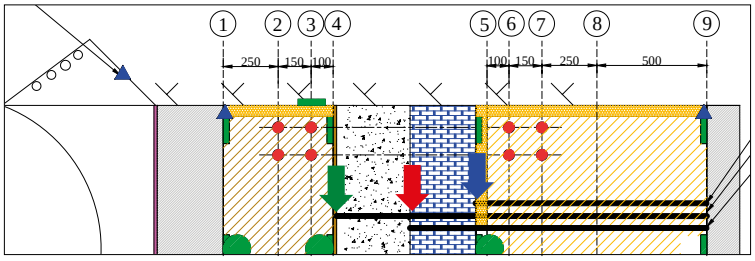

Figure 9-20. *Location of the sensors in the bentonite seal, filter and backfill respectively, which are used for comparison of the displacements.*

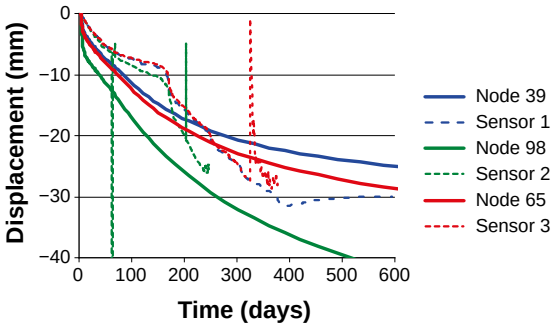

Figure 9-21. *Comparison between numerical and measured displacements in the bentonite seal, filter and backfill respectively.*

9.2 Concrete dome measurements

The measured response summarized and presented here is based on the results presented in Malm (2014).

9.2.1 Pressure on the formwork

The total contact pressure is measured at five locations over the height of the formwork/dome, as presented earlier in Section 7.2.1. These sensors are numbered from 1 to 5 based on their height above the ground, meaning that sensor no 1 is at the bottom and sensor no 5 is close to the top. In Figure 9-22a, the pressure as a function of time is plotted for a 30-hour period after the onset of concrete pouring. The sampling rate in these measurements is one reading each minute.

The maximum pressure at each location of the sensors develops rapidly, just a few hours after the concrete has been poured into the formwork and it reached the location of the sensors. This means that the hardening of concrete in the bottom has started even before the whole plug is cast. This means that the maximum theoretical hydrostatic pressure of 160 kN/m^2 (in the bottom) will not occur. Instead the maximum form pressure was typically less than 35 kN/m^2 measured at all sensor positions. However, there is a spike in the results where the pressure at the topmost sensor reaches 80 kN/m^2 for a period of four minutes. According to the staff at site during casting, the contact grouting tubes were pressurized at the end of casting in order to ensure they were clear. This pressure spike may be a result of this action. Alternatively, the spike may have been caused by a pressure increase from the concrete pumps at the final stage of casting the concrete dome plug. The pressure was increased to make sure that the whole volume was filled with concrete and to prevent air voids inside the formwork. It can be seen in the zoomed Figure 9-22b that all the sensors experienced a change in pressure at this time, but to a smaller extent than measured by sensor 5.

9.2.2 Temperature

The temperature of the concrete dome was measured with 18 embedded sensors that were combined to measure both temperature and strain. In addition, two ambient air temperature sensors were also used. In Figure 9-23, the measured temperature variation is shown. The measured curves for each sensor are presented individually in Malm (2014). It can be seen from the figure, that the cooling sequence was successful in limiting the maximum temperature in the concrete during hydration. The maximum temperature that occurred was just below 18°C and according to the specifications for the casting and cooling, the maximum allowed temperature was 20°C.

During the second cooling stage (stage B in the cooling sequence) where the temperature in the cooling pipes was reduced to 4°C, the corresponding temperature in the concrete dome varied between 6–10°C depending on the location of the sensor.

In the final cooling stage (stage C in the cooling sequence) which was performed prior to contact grouting, the temperature in the cooling pipes was reduced to 1°C. This resulted in a temperature in the concrete dome of approximately 3–8°C depending on the location of the sensor.

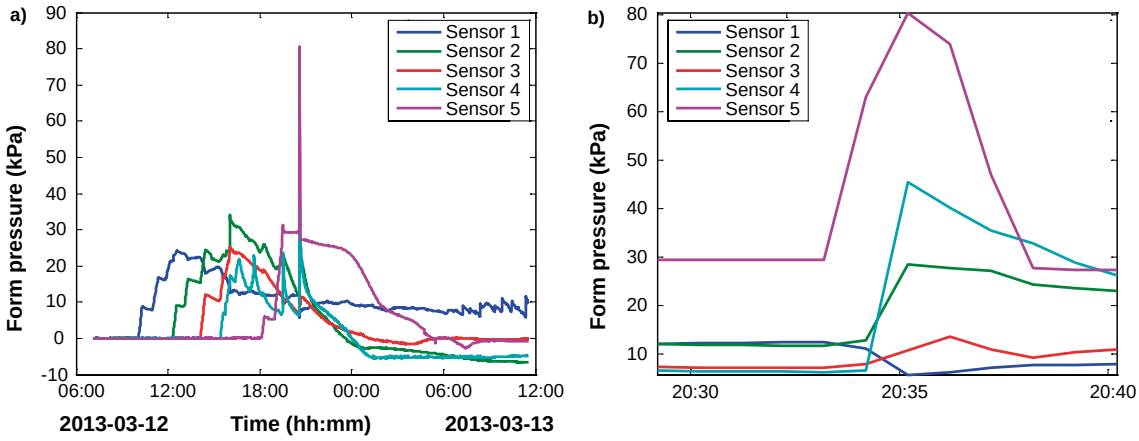

Figure 9-22. *Measured form pressures for the five pressure sensors on formwork. a) during the whole time period and b) zoomed in on the pressure spike.*

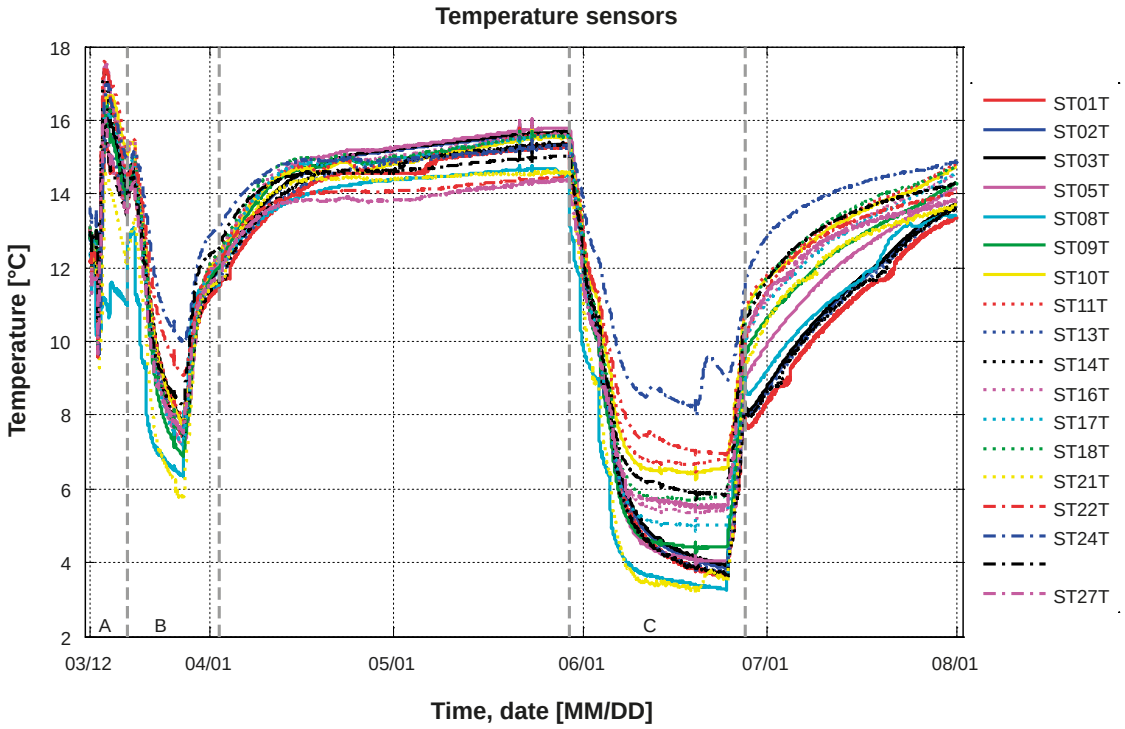

Figure 9-23. *Measured temperatures in the concrete dome from casting until the cooling system was turned off after contact grouting. From Malm (2014).*

In the numerical analyses, the ambient temperature has been assumed to be constant at 14°C. This is a simplification, since the actual ambient temperature varies due to seasonal effects. As it can be seen in Figure 9-24, the temperature varies quite significantly, over the measuring period. Especially during the cooling period prior to contact grouting (denoted as bullet C above), i.e. between June and July, a high increase in ambient temperature is observed. The reason for this high increase in ambient temperature is mainly due to the fact that the ambient temperature sensors were initially placed close to the cooling machines and they were therefore affected by the heat generated by the pumps. When these sensors were moved to their permanent location a significant decrease in temperature was observed. A seasonal variation in ambient temperature is also seen in the results; the temperature in the Äspö HRL during August and September is about 3–4°C warmer than during January to March.

Comparison with numerical analyses

The simplification of the ambient temperature conditions present will naturally have some effect when comparing the numerical analyses with the measured data. This is mainly seen in the portion of the temperature data where cooling system is turned off and a constant temperature of 14°C is obtained in the analyses while slightly higher temperature are recorded from the measurements. The numerical analyses correspond well with the measured results (Figure 9-25 and Figure 9-26). In general the numerical results follow the measured variations in temperature very well where the curves have the same shapes. The difference in temperature is in general less than 2°C, mainly occurring when the cooling system is turned off and thereby is an effect of the assumed ambient air temperature. Typical behaviour of some of the representative sensors are shown in Figure 9-25 and Figure 9-26.

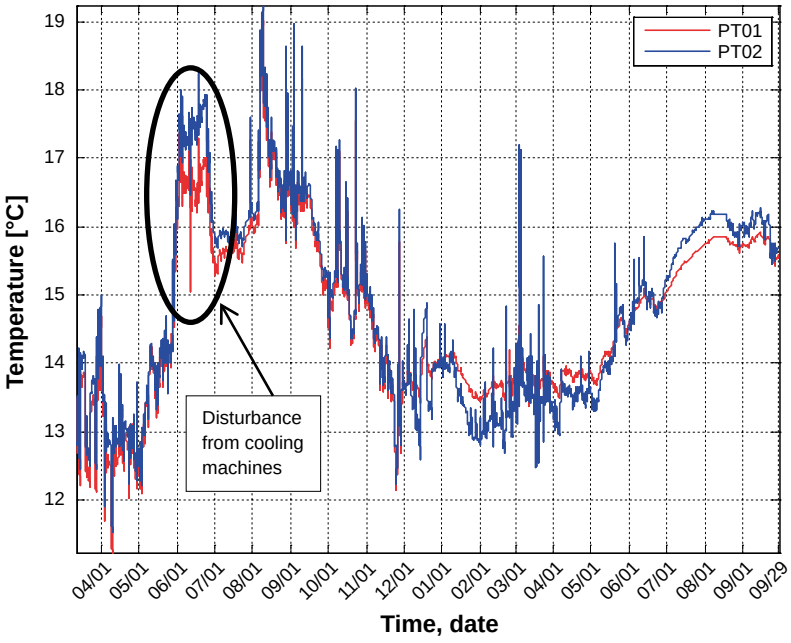

Figure 9-24. *Measured variation in ambient air temperature in the tunnel TAS01. From Malm (2014).*

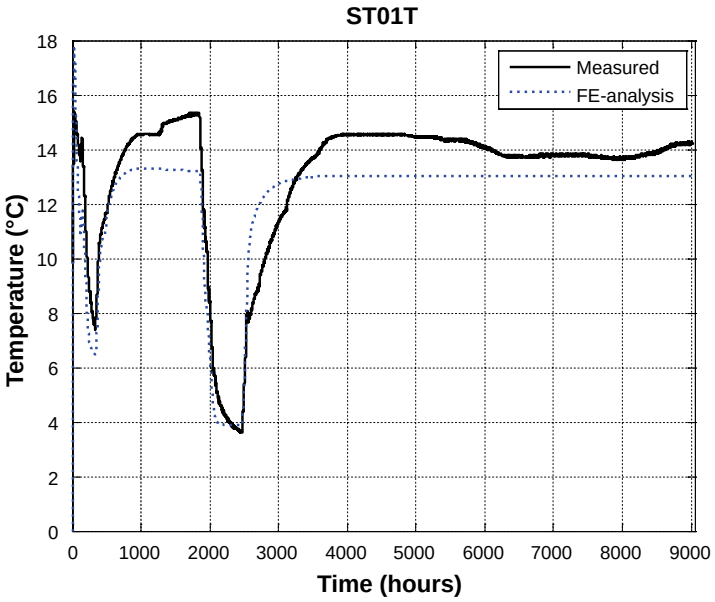

Figure 9-25. *Numerical and measured variation in temperature at the location of ST01T.*

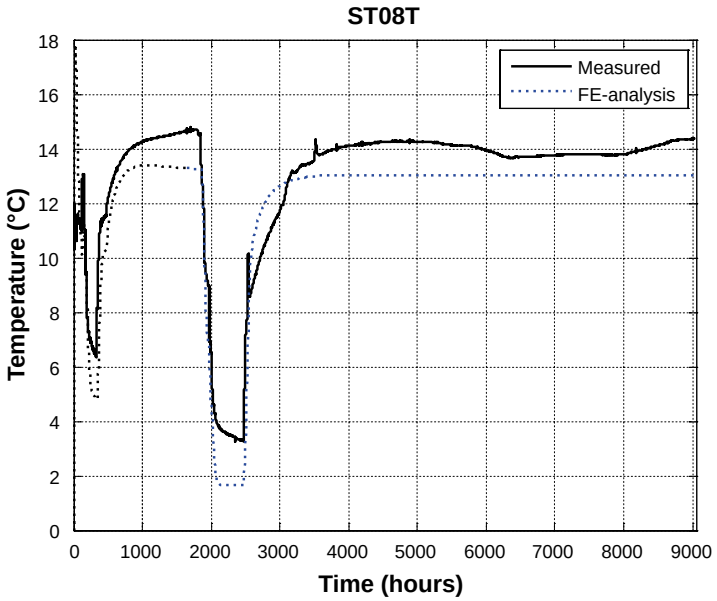

Figure 9-26. *Numerical and measured variation in temperature at the location of ST08T.*

The sensor that gives the best agreement between measured and predicted temperature is sensor ST21 which is located near the top of the dome (Figure 9-27). The sensor that gives the worst agreement, ST24, is located quite close by (2.8 m). ST24 is also located in the top of the dome, but closer to the rock and is mounted on a reinforcing bar that has been drilled into the rock. The result for this sensor is shown in Figure 9-28. One explanation why this sensor gives poorer agreement than some others may be that since the ambient air temperature is underestimated in the model, so also is the temperature of the rock. Additionally, since this sensor is located only 15 cm from the rock, larger discrepancies are expected due to thermal interactions between the concrete and rock.

Evaluation of the measurement system

According to Malm (2014), the measuring system has worked reliably during the whole experiment and especially during the first stages, showed in Figure 9-29, all sensors worked perfectly. In addition, the results show that the different types of sensors used (Geokon and TML) gave very similar results (the difference between the sensors is less than 0.5°C), as seen in Figure 9-29. The three sensors installed close to each other in the centre of the dome are shown in Figure 9-29. Two of these sensors, ST02T and ST03T are of TML type while ST01T is from Geokon. According to Malm (2014), the Geokon sensors occasionally experienced output voltage spikes that had to be filtered out of the database to allow plotting.

In total, three of the temperature sensors, denoted ST08T, ST13T and ST22T have failed during the full-scale test. About one month after the contact grouting, the temperature sensor associated with a displacement instrument (ST08T), started to have problems with its output. After a short while the displacement sensor failed completely with no obvious explanation. Two other sensors failed during the increase of water pressure, where ST13T failed at a water pressure equal to about 1.5 MPa and the sensor ST22T failed when the water pressure was about 4 MPa. Both these sensors failed completely, i.e. they also failed regarding recording the variation in strain. These sensors failed at the following dates:

- ST08T – August 5th 2013.
- ST13T – December 19th 2013.
- ST22T – August 8th 2014.

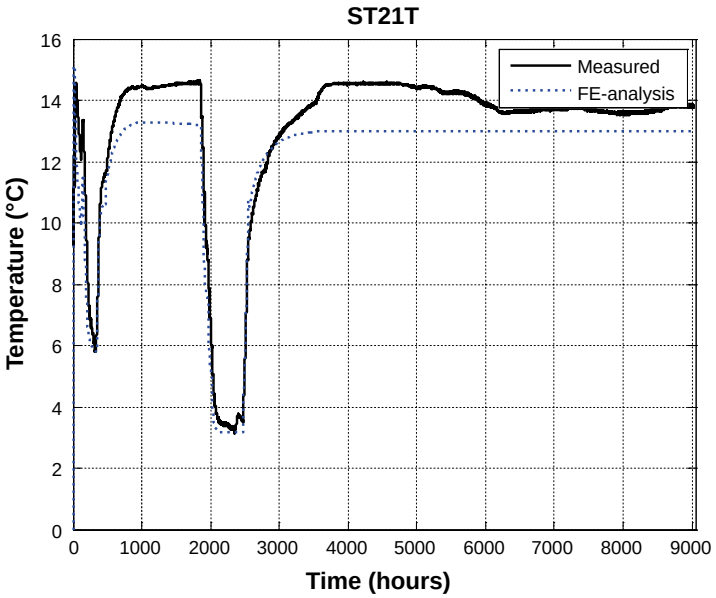

Figure 9-27. *Numerical and measured variation in temperature at the location of ST21T.*

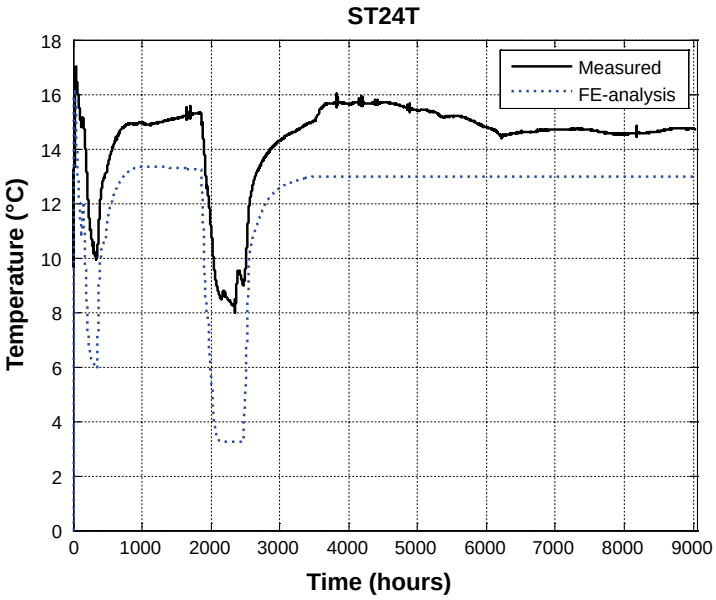

Figure 9-28. *Numerical and measured variation in temperature at the location of ST24T.*

9.2.3 Strain

In total, 27 strain gauges measuring the variation in strain were embedded in the concrete dome. The measured strain for the embedded strain gauges is shown in Figure 9-30 from approximately the time of casting until the cooling equipment is turned off. In the figure, the three cooling stages are also illustrated. In this figure, it can be seen that all sensors show the same type of behaviour, where the variation in measured strain is clearly dependent on the variation in temperature. This indicates that the concrete dome has released from the rock at least partially. If the concrete dome were completely bonded to the rock, then there would only be small variations in strain due to the cooling. On the other hand, if it had released completely from the rock in the upper part of the dome, then a significant decrease in strain would be visible at the time of release of the restraining forces. No such drop can however be found in the results for the strain gauges. Based on this observation, it can be concluded that the concrete dome had at least partially released from the rock.

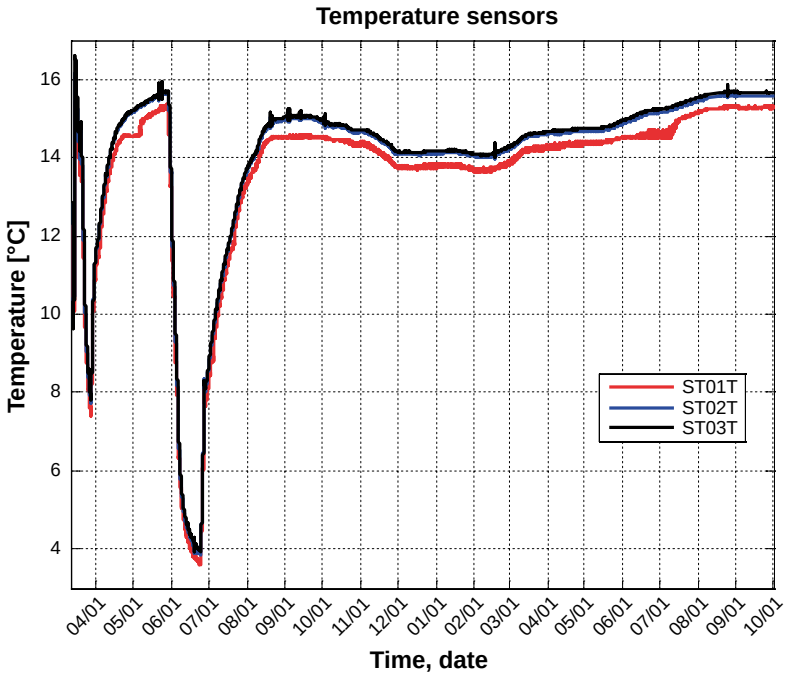

Figure 9-29. *Comparison of different types of sensors. ST01T is from Geokon, while ST02T and ST03T are from TML, from Malm (2014).*

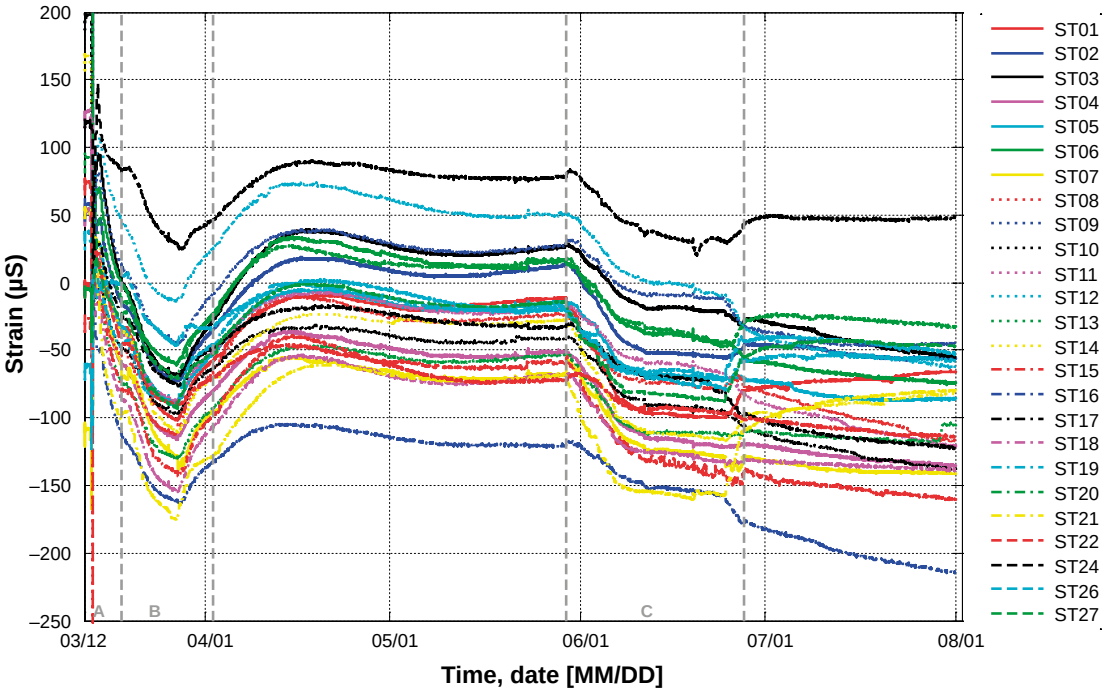

Figure 9-30. *Variation in strain according to the embedded strain gauges from casting until the cooling system was turned off after contact grouting. From Malm (2014).*

The measured strain for the complete period of evaluation of the full-scale test is shown in Figure 9-31. In this figure, only the sensors that worked for the full period are shown. In the figure, it can be seen that a significant decrease in strain occurs, owing to the applied water pressure, starting from about October 2013, but the main decrease occurs from the beginning of January 2014 to mid-February 2014. The sequencing of applied water pressure change was previously shown in Figure 9-2, with an increase to 1.5 MPa during the period of October to December (2013), and during the period from January to February (2014) the water pressure was increased to 4 MPa.

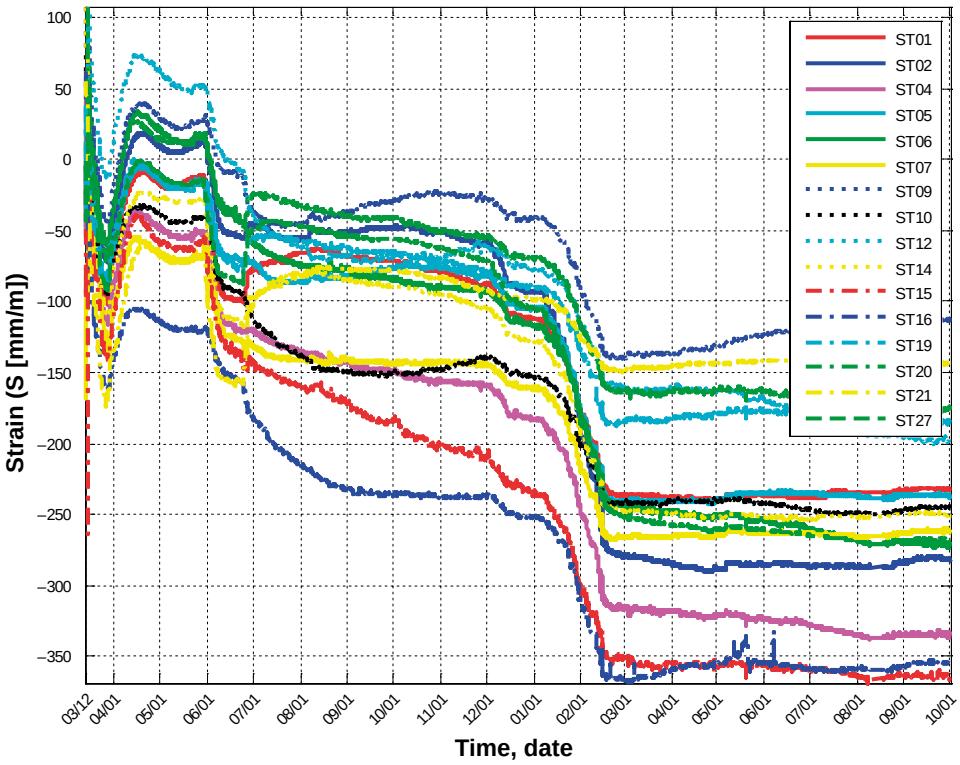

Figure 9-31. *Variation in strain for the full measuring period. From Malm (2014).*

Because all strain gauges show a decrease in strain, all sensors thereby indicate increasing compressive stresses in the concrete dome. From mid-February, the water pressure had been maintained constant at 4 MPa, and it can be seen that the variation in strain after this is relatively constant. The small variations that are visible after this change are due to variations in ambient temperature in the tunnel.

Effect of thermal pre-stressing

Another method to determine if the concrete dome has released from the rock is to study the pre-stressing that occurs by analysing the behaviour of the strain gauges before and after the cooling period when the contact grouting is performed. If the concrete dome has released from the rock prior to contact grouting then there would be a difference in strain just before the cooling period and when the cooling period has stopped. This difference in strain corresponds to the thermal pre-stressing that occurs. In a case where the dome had released from the rock, the difference in strain would be equal to the sum of the temperature difference multiplied with the thermal expansion coefficient ($\alpha = 10^{-5}\,C^{-1}$).

In order to study the influence of pre-stressing and to thereby determine if the concrete dome had released from the rock, Malm (2014) calculated the difference in strain between the period prior to grouting and the period after grouting for each sensor. The strain prior to contact grouting was chosen as the average strain during May and the strain after contact grouting was chosen as the average strain during July. The compressive pre-stress was obtained by multiplying the difference in strain was with the elastic modulus of concrete (33.9 GPa according to Vogt et al. 2009). The result is shown in Figure 9-32a. As seen in the figure the pre-stress varies from about 0.5 MPa to 3.5 MPa.

In order to be able to determine if the concrete dome has released from the rock, this pre-stressing has to be compared to the maximum pre-stress that could occur. The maximum thermal pre-stress was therefore calculated based on the difference in temperature between maximum temperature during hydration, about 18°C, and the minimum temperature during cooling prior to contact grouting. This result is shown in Figure 9-32b. As can be seen, the maximum theoretical pre-stress varies from about 3 MPa to 4.5 MPa for the different locations of the strain gauges.

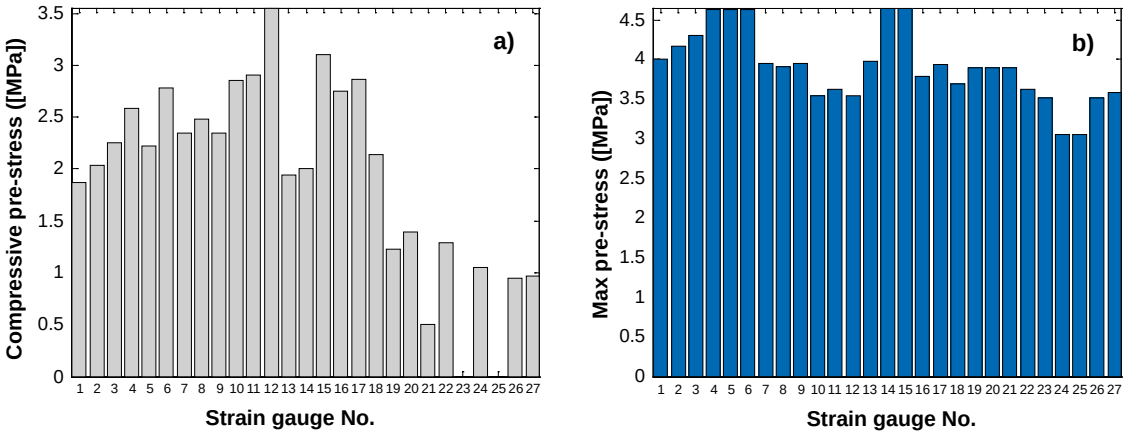

Figure 9-32. *Calculated pre-stress in the concrete dome due to cooling and contact grouting. a) Obtained pre-stress based on the strain gauges, b) Max pre-stress based on the temperature variation. From Malm (2014).*

As seen, there is a significant difference in the amount of pre-stressing that has occurred in the concrete dome (Figure 9-32a) compared to the thermal pre-stress that would occur if the dome was free to deform. To calculate the utilization of the pre-stress, the ratio of the obtained pre-stress compared to the maximum pre-stress is calculated and is shown in Figure 9-33. Based on this evaluation it can be seen that the dome is on average pre-stressed to approximately 53 % of the value that would be obtained if it had released prior to contact grouting. Only one of the sensors, ST12, shows that it has been pre-stressed to its maximum value. Two sensors close to this one, ST10 and ST11, also show high utilization of the pre-stress (80 % of the maximum theoretical value). In common for the five sensors showing highest pre-stress compared to the theoretical is that they all are mounted on the downstream side of the dome. Based on this evaluation it can be concluded that the dome plug had partially released from the rock and it is likely that the downstream side of the slot has released to a greater extent than the upstream side.

Comparison with numerical results

The previous evaluations regarding the strain gauges are all based on relative values at different times for each sensor. Therefore, these evaluations are not dependent on the definition of the zero level of the strain gauges. However, in order to be able to calculate the variation of stress from the strain gauges and to be able to compare the measured strain with the result from the numerical analyses, the zero level has to be determined. In Malm (2014) and Kristiansson (2014**)** different approaches to determine the measurement reference point (i.e. the time when the strain gauges should be defined as zero) were analysed. The reason why this is important is that the strain gauges will not be bonded to the concrete initially, and hence the recordings up to the point when the concrete has reached sufficient strength are not relevant. In this report, the findings of Malm (2014) are used and, hence, it is assumed that the concrete bonds to the strain gauges at 22:00 on the day of casting, i.e. about 2.5–3 hours after the casting is completed.

The results from the numerical models are presented for three different cases, according to Section 8.2. Two cases were based on that full bond (i.e. no relative displacements) was assumed between concrete and rock during the initial time period after casting the concrete dome. In the first of these models, it was assumed that the bond breaks at the moment when the water pressure (denoted as Full bond – release at WP) is applied while the second model is performed under the assumption that the bond breaks during cooling stage C, i.e. cooling prior to contact grouting (denoted as Full bond – release at grouting). In the third model, it is assumed that the concrete dome had released initially after casting and hence was allowed to deform due to shrinkage more or less stress free (denoted as No bond).

In Figure 9-34 to Figure 9-39 comparisons between calculated and measured strain is shown for some of the strain gauges.

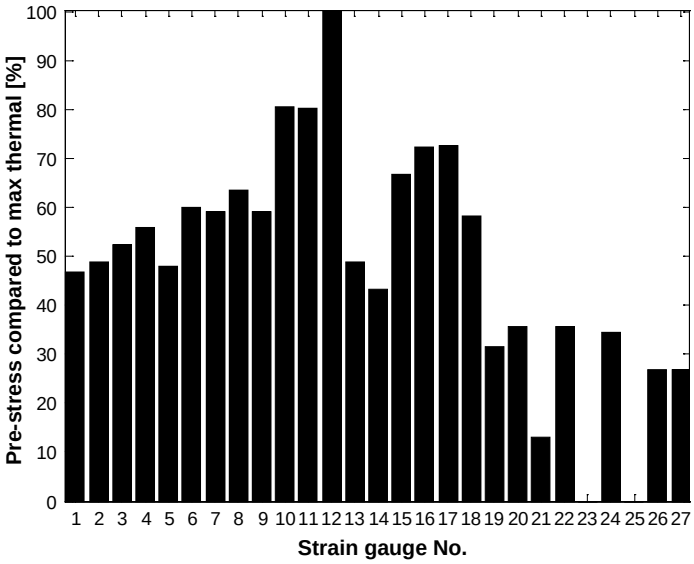

Figure 9-33. *Ratio of obtained pre-stress and the maximum theoretical pre-stress. From Malm (2014).*

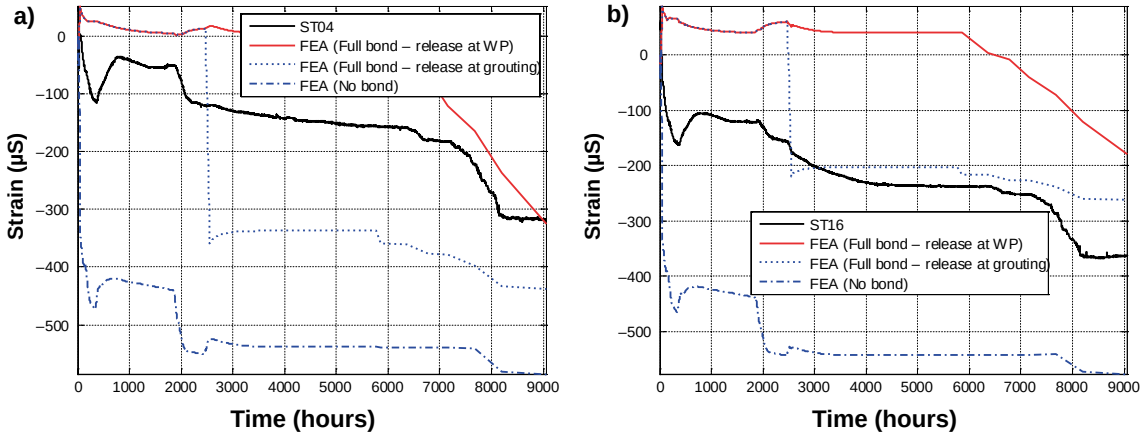

Figure 9-34. *Comparison of strain from measurements and numerical analyses for a) ST04 and b) ST16. These represent typical behaviour of the horizontal strain gauges.*

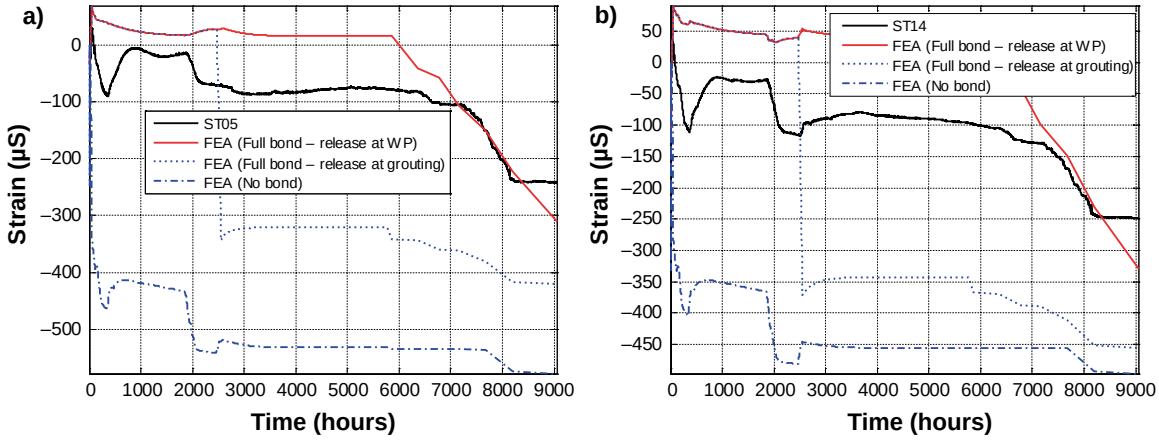

Figure 9-35. *Comparison of strain from measurements and numerical analyses for a) ST05 and b) ST14. These represent typical behaviour of the inclined strain gauges.*

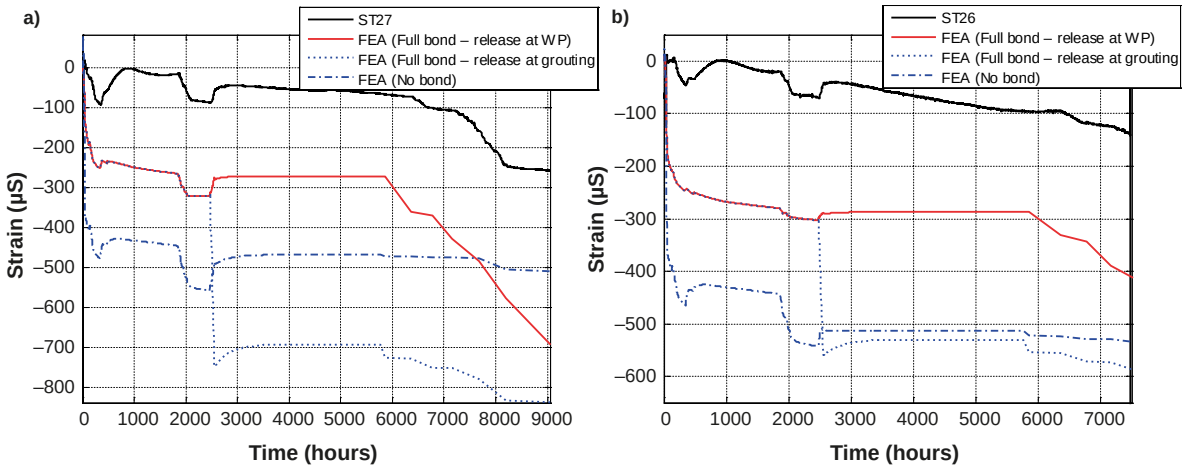

Figure 9-36. *Comparison of strain from measurements and numerical analyses for a) ST27 and b) ST26. These represent typical behaviour of the strain gauges close to the slot.*

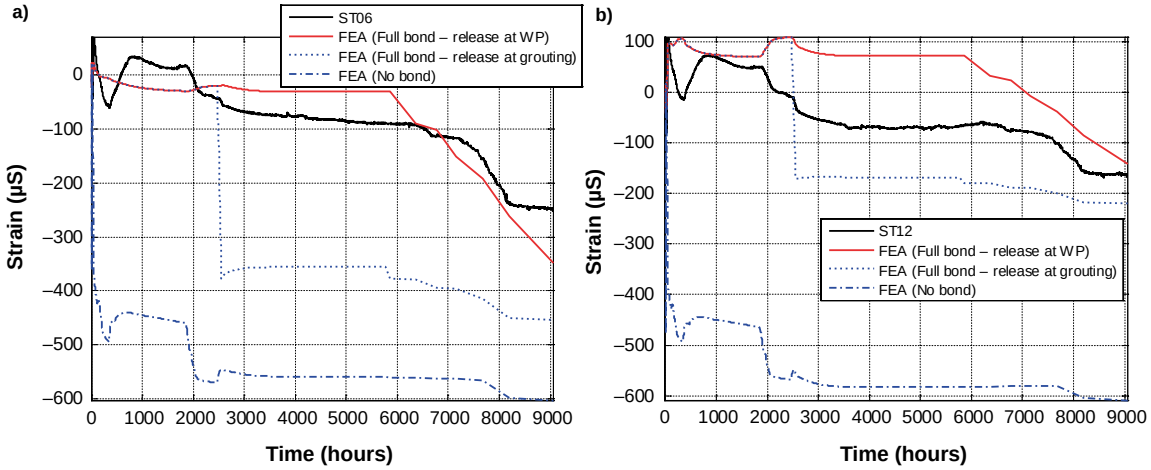

Figure 9-37. *Comparison of strain from measurements and numerical analyses for a) ST06 and b) ST12.*

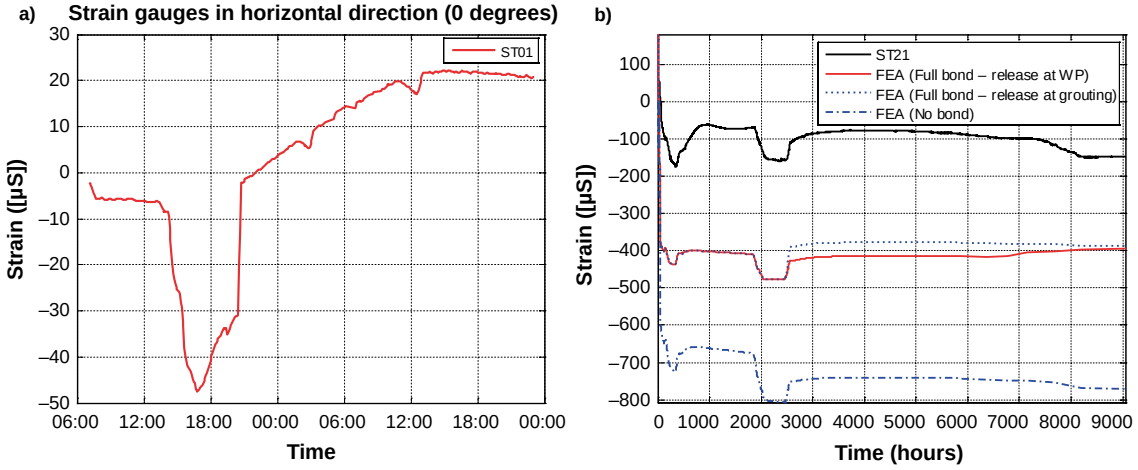

Figure 9-38. *Behaviour of Geokon strain gauges. a) early age behaviour of ST01, b) variations in strain of ST21.*

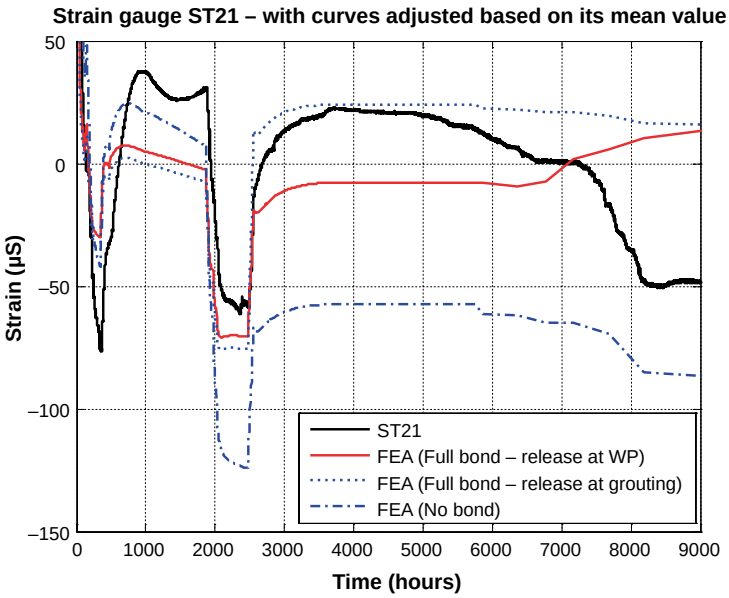

Figure 9-39. *Variation in strain for ST21 if all curves are adjusted to have the same mean value, i.e. the influence of the early behaviour is removed.*

The horizontal strain gauges (ST1, ST4, ST7, ST10, ST13, ST16, ST19) generally show a behaviour that is in between the curves from the FEA models with full bond and without bond, respectively. An example of this is shown in Figure 9-34.

The inclined strain gauges (ST25, ST11, ST14, ST17, ST20) typically show the same type of behaviour as the horizontal strain gauges. However, their measured behaviour is closer to the result of the numerical models with full bond. This is shown in Figure 9-35.

The strain gauges near the slot (ST22, ST23, ST24, ST25, ST26, ST27) all showed smaller compressive strains (or even in some cases tensile strains) than any of the numerical analyses. This is illustrated in Figure 9-36. The reason for this is discussed later in this section.

The vertical strain gauges (ST3, ST6, ST8, ST9, ST12, ST15, ST18, ST21) typically show a behaviour that is close to the case from the numerical analyses where full bond is assumed. As described in Malm (2014), strain gauge ST08 was inadvertently placed on the upstream side of the concrete dome instead of the downstream side. The numerical model is based on this sensor in its planned position; therefore, no comparisons will be made for this sensor.

Example of the similarity between the strain measurements and the predictions based on the full bond model are shown in Figure 9-37, which illustrates typical behaviour of vertical strain gauges. All sensors except one, ST21, showed this behaviour. Strain gauge ST21, showed the same type of variations as the other sensors, but with the difference that the level of strain was less. This sensor is discussed later in this section. One difference between the measured behaviour of the vertical sensors and the numerical result for the full bond case is that the measurements show significant influence of the temperature variation during the cooling stages. No such influence is seen in the result from the FE model. It can also be seen that these sensors show a clear effect of the pre-stressing, hence, some gap between concrete and rock must have been present.

Possible explanations for the vertical strain gauges measuring similar strains to those predicted by the full bond models, while the measurements of strain up to the point of contact grouting are more similar to the no bond model, could be:

1. Incorrect estimation of the zero (reference) value for the strain gauges.
2. The large reduction in strain (due to autogenous shrinkage) shown in the FE analysis occurs before the strain gauges bonded to the concrete.
3. The autogenous shrinkage is smaller for the real concrete dome plug than assumed in the numerical analyses.

The first point, i.e. that this could be a result of incorrect selection of zero (reference) value is unlikely. The reason for this is that most sensors do not show as significant drops initially as the numerical analyses predict. Some measurements even show increasing strain for the entire period before they stabilized. In addition, the drop that occurs in the numerical analyses is due to the autogenous shrinkage which is quite significant the first 24 hours. In the numerical analyses, where the autogenous shrinkage is taken from the experimental tests, these drops last for about 24 hours. In the measurements, these drops occur for a maximum period of 3 hours, when the casting is still on-going. Finally, the Geokon strain gauges, which bond quickly to the concrete and are able to measure reliable strain values almost immediately, show no such large drops at all.

The second point, i.e. that the large autogenous shrinkage happened prior to bonding between the concrete and the strain gauges is also considered highly unlikely. The reason for this is that the definition of autogenous shrinkage is that it starts during the stiffening phase of concrete (Holt 2001). During the liquid phase, only chemical shrinkage occurs. According to Vogt et al. (2009) and also seen in Section 5.2.2, a large part of the autogenous shrinkage occurs within the first 24 hours after casting and the sensors bond quite rapidly to the concrete, only a few hours after casting. In addition, the Geokon strain gauges bond very quickly to the concrete as shown in Malm (2014) and that so captures both the development of compressive stresses due to the hydration heat and its transition to tensile strains as the temperature decreases, as shown in Figure 9-38a.

As seen in Figure 9-38b, the measured strain is much less than the numerical analyses predicted. The mean value for the measured curve is almost 25 % of the two full bond models and 15 % of the no bond model. If the early behaviour, occurring < 50 hours, is removed from the curves, by adjusting the plots so that all curves have the same average value, it can be seen in Figure 9-39 that the behaviour of the measured curve corresponds quite well with the full bond models.

Based on these observations, the most likely explanation is that the autogenous shrinkage is lower for the concrete mix used in the full scale test than what previous material tests have shown.

Estimation of induced stresses

Based on the time dependent curve for the elastic modulus presented in Vogt et al. (2009) for concrete mix B200, the stress has been calculated directly from the strain gauges by the use of Hook's Law ($\sigma = \varepsilon E$). The calculated stress is shown in Figure 9-40, and it shows as expected that the strain gauge located near the top of the concrete dome, ST24 (it is attached perpendicular to the rock on the downstream side of the slot), is the one with highest tensile stresses. The strain gauge, ST12, which is located in the centre of the dome, on the downstream side, is another sensor that also shows high tensile stresses. According to Malm (2012), high tensile stresses are also expected in this region. Both these sensors show that the induced stresses are above about 1.5 MPa during the first cooling stage, i.e. cooling to reduce the temperature from hydration, as seen in Figure 9-41. During this stage, all vertical strain gauges located in the centre of the dome (ST03, ST06, ST09) show relatively high tensile stresses, about 1.0 MPa. This shows that the whole cross-section is subjected to tensile stresses in the vertical direction, which indicates that the concrete dome has not released (completely) in the top. This peak value occurs about 24 hours after the casting was completed.

According to Table 5-5, the tensile splitting strength is about 2.2 MPa after 7 days, i.e. the tensile strength is about 1.8 MPa (80 % of the splitting strength). The bond strength between concrete and rock, as presented previously in Table 5-13, is even lower than this. Therefor, since the tensile stress in the concrete after about 1 day is higher than both expected bond and tensile strength and the highest tensile stresses are found close to the interface between concrete and rock, it is reasonable to assume that either cracks occurred near the interface between concrete and rock or may even have occurred as sub-horizontal cracks inside the concrete dome.

Evaluation of the measurement system

According to Malm (2014), the measuring system has worked reliably during the whole experiment and in the first stages of monitoring all sensors were operational, as shown in Figure 9-30. There has only been a single, short period of power loss and missed recordings.

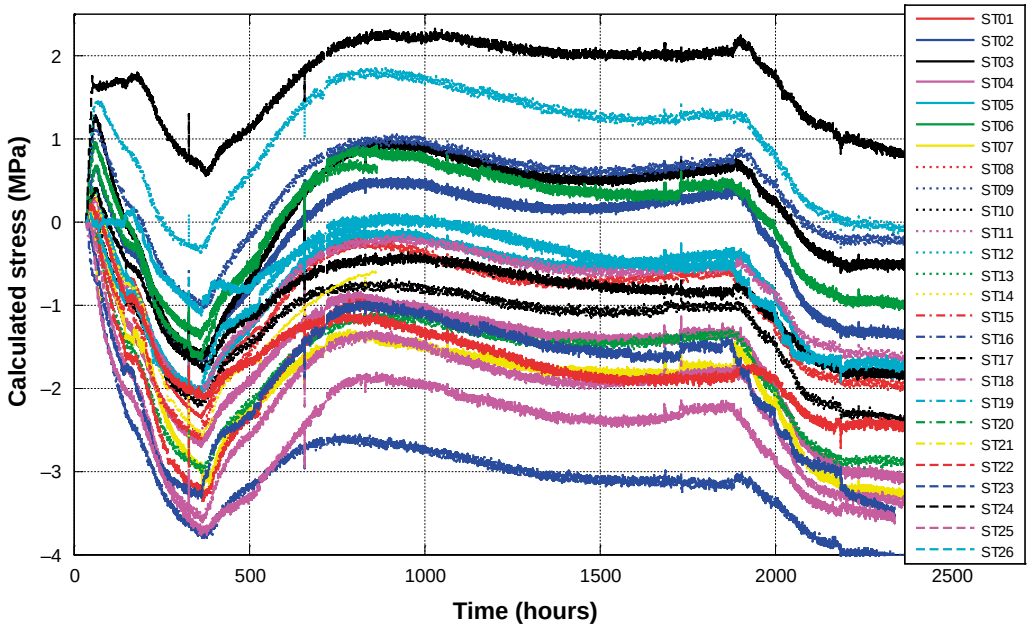

Figure 9-40. *Calculated stress based on the measured strains. From Malm (2014).*

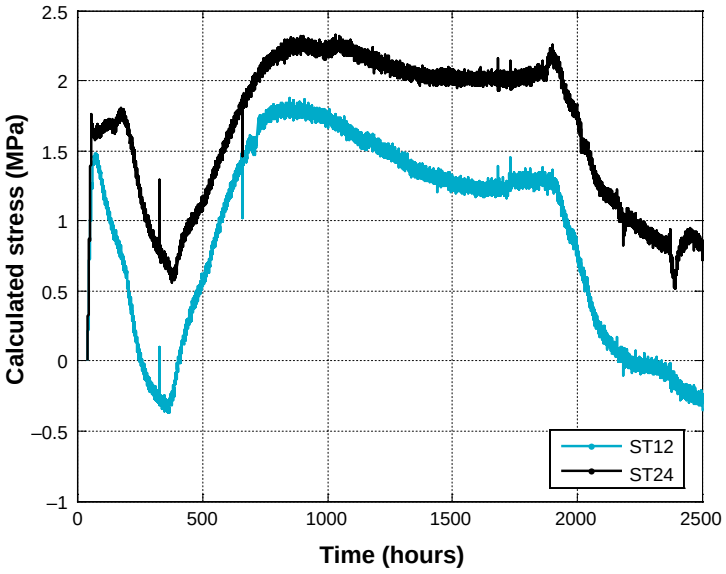

Figure 9-41. *Calculated stress for two strain gauges, ST12 and ST24, close to the top.*

As mentioned above, one difficulty regarding interpretation of embedded strain gauges is to define the zero reference point, i.e. when the sensor is bonded to the concrete and actually gives reliable readings. The Geokon sensors had large flanges which improved the bond between sensor and concrete (Figure 7-3b), which resulted in early stable readings. The zero point on the other sensor type used, TML, was more difficult to define as it lacks the flange feature. The approach used in Malm (2014) where the starting point was defined when the signal was stable after some early significant changes in the signal, seems to give a reliable zero reference value for the different sensors. With this approach, similar results are obtained for sensors located in similar locations. One downside with the Geokon sensors was that occasional output voltage spikes occurred which had to be filtered out in order to observe the behaviour.

Several of the strain gauges (11 in total) have malfunctioned during the full-scale test. Two of these failed early, during the contact grouting of the concrete dome. The term failure is here used to describe a situation where a sensor no longer can fulfil its intended performance. The sensor may still give recordings, but these may either be constant (for instance equal to zero) or giving results for

other reasons are unreliable (for instance showing results that are not physically possible typically occurring after a voltage impulse). The reason for these early failures is that the grouting tube was adjacent to the reinforcement bar used to mount these sensors, as seen in Figure 9-42. Hence, the grout may have been pushed along the reinforcement bar towards the sensor, resulting in sensor damage.

The remaining nine strain gauges that failed in the course of monitoring started to malfunction during the water pressurization phase. A summary regarding the failure sequence and related activities is provided in Table 9-1. One conclusion that can be drawn from this information is that the bentonite seal was not watertight initially and because of this, the concrete dome had to sustain the water pressure and the strain gauges also had contact with pressurized water. The manner in which the impacted sensors responded to water pressure varied substantially with readings that were not consistent with the physical reality of the structure's response. Therefore, despite these sensors continuing to provide changing readings, they are considered to be malfunctioning and hence not used for evaluation.

Table 9-1. Malfunctioning strain gauges.

Strain gauge	Date of failure	Failure cause
ST23	June 19th 2013	contact grouting
ST25	June 19th 2013	contact grouting
ST08	August 5th 2013	unknown reason for failure
ST13	December 19th 2013	water pressure 1.4 MPa
ST26	January 18th 2014	water pressure 2.0 MPa
ST24	January 28th 2014	water pressure 2.5 MPa
ST18	January 29th 2014	water pressure 2.5 MPa
ST17	February 12th 2014	water pressure 3.5 MPa
ST03	April 9th 2014	water pressure 4 MPa
ST11	April 25th 2014	water pressure 4 MPa
ST22	August 8th 2014	water pressure 4 MPa

9.2.4 Relative displacement between concrete and rock

The result for the first five months of measurements, i.e. from casting up to about one month after contact grouting, is shown in Figure 9-43. All joint-meters show a limited crack opening during this period, with a maximum crack opening displacement of 0.1 mm. This measured crack opening displacement is far lower than the analytically calculated displacement of about 4.5 mm which was presented in Section 6.6.4. As discussed previously, it is likely that the concrete used in the full-scale tests yields lower autogenous shrinkage than the previous lab tests showed. However, according to Section 6.6.4, if the concrete dome had released from the rock prior to grouting then the thermal expansion of the cooling alone would result in larger crack opening displacements than observed in the test.

a) b)

Figure 9-42. *Photo of the two strain gauges ST23, (Figure (a)) and ST25 (Figure (b)) that failed during contact grouting.*

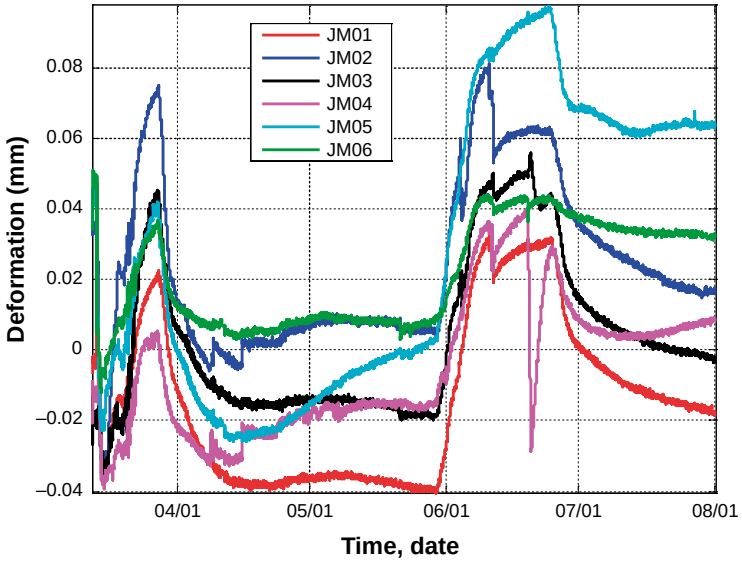

Figure 9-43. *Variation in relative displacement between concrete dome and rock. From Malm (2014).*

Considering that the joint-meters measure movements at a location where the dome is still attached to the rock, then an elastic behaviour would be visible, i.e. the crack opening displacement would be the same before and after one cooling period and be constant in between. The results show that there is a small difference in relative displacement before and after the contact grouting for most of the sensors. The crack opening displacement just before cooling (i.e. on May 29th) and after cooling (i.e. August 1st) is presented in Table 9-2.

As seen in the table, all joint-meters except one shows differences that are about 0.02 mm or less. One sensor (JM05) shows a larger difference than this, but it is also rather small, about 0.06 mm. Another difference when comparing the sensors is that two of them, JM05 and JM06, show much less relative unloading, i.e. larger plastic deformations, than the others after the contact grouting. Both these sensors are placed at the same location, which is about 3 o'clock i.e. on the right hand side when observed from the downstream surface. Sensor JM05 measures the horizontal displacement perpendicular to the rock and JM06 measures the horizontal displacement in the tunnel axis. It is likely that there was a crack between the concrete and rock at this location. As mentioned in Section 6.6.4, observations during contact grouting confirm that significant use of grout was observed in this area.

Table 9-2. Relative crack opening displacement before and after contact grouting.

Joint-meter	Relative opening before and after grouting [mm]
JM01	0.022
JM02	0.011
JM03	0.016
JM04	0.024
JM05	0.062
JM06	0.024

The measurements from the joint-meters for the full period of the experiment are shown in Figure 9-44. As seen in the figure, the two joint-meters, JM03-04, located in the top, i.e. at 12 o'clock, shows significant negative displacements, which implies that the top of the dome was pushed downstream and thereby the joint-meters more or less act like displacement gauges. It can also be noted that movement started abruptly, at February 12th. At this point, the water pressure was continuously increasing and was about 3.5 MPa. Only a few days after this, significant leakage was observed and after this the pressure was maintained at 4 MPa. This abrupt change in behaviour for these joint-meters is probably a result of to the top of the concrete dome being released from the rock on the upstream side of the slot. This would cause significantly increased pressure on the downstream side of the slot.

Comparison with numerical results

The experimental results have also been compared with the results from the numerical analyses which are shown for JM03 and JM06 in Figure 9-45 and Figure 9-46 respectively. The numerical results are only shown for the two models with full bond. The reason why the case with no bond is not shown in these graphs is that its displacement is significantly higher (4.1–4.2 mm) than measurements and the simulation results for full bond conditions.

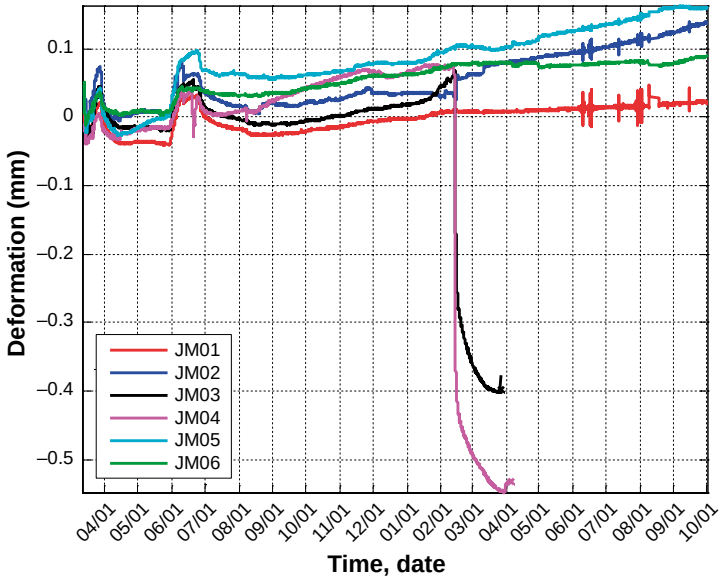

Figure 9-44. *Variation in relative displacement between concrete and rock, for the full measuring period. From Malm (2014).*

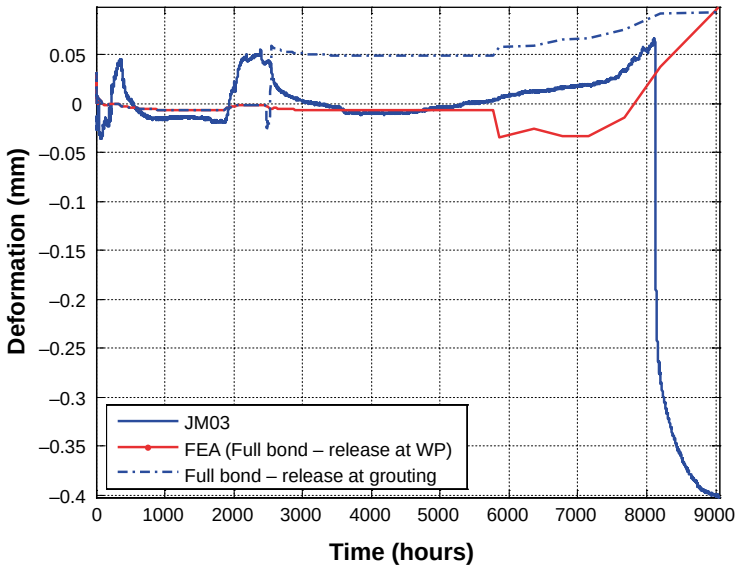

Figure 9-45. *Comparison of measured and calculated relative displacement for the joint-meter JM03 (located in the top of the dome).*

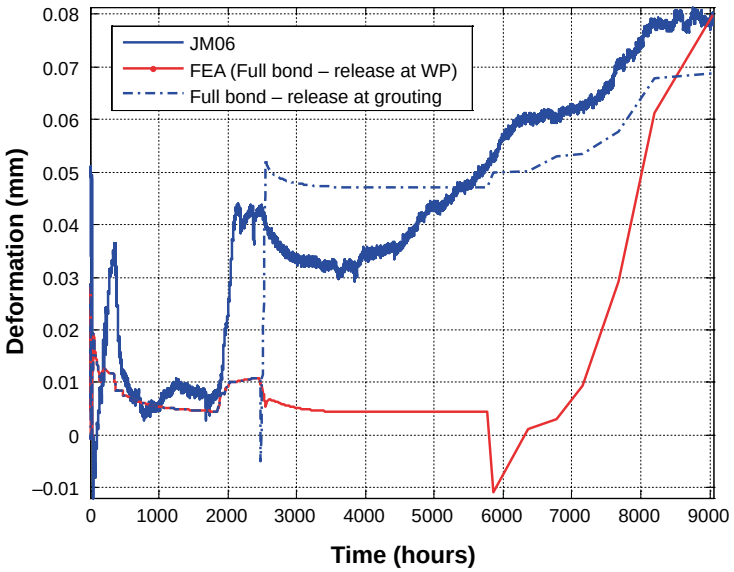

Figure 9-46. *Comparison of measured and calculated relative displacement for the joint-meter JM06 (located on the left side of the dome, i.e. 9 o'clock).*

Evaluation of the measurement system

The joint-meters show a relatively high level of background noise. The reason for this is that the measured relative displacement between concrete and rock is much less than anticipated, which is due to the fact that the concrete dome did not release completely from the rock. Two of the joint-meters also started to malfunction during the pressurization, which was shown earlier in Figure 9-44. The reason for this is that these sensors were completely compressed and so no longer provided useful information, which likely is due to the concrete dome losing contact with the rock on the upstream side of the slot, near its crest.

9.2.5 Horizontal displacement of the dome plug

The horizontal displacement of the concrete dome plug is measured with three LVDTs, as described in Section 7.2.2. The result from the three LVDTs is shown in Figure 9-47.

As can be seen from the results, there are discontinuities in the measured behaviour. These discontinuities are not realistic, since no real load situation could have caused these large instantaneous displacements. Both the LVDTs in the centre of the dome and the one closest to the top of the dome, LVDT01 and LVDT03 respectively, give constant values in-between these apparently instantaneous displacements. This behaviour is not consistent with the expectation that the pressure load should cause a significant increase in displacement measured, as shown for LVDT02. These instantaneous discontinuities are likely caused by an external event such as inadvertent contact during the installation of the plastic sheet, which is installed on the steel frame supporting the LVDT sensors. With these sensors reaching their maximum displacement due to disturbance, subsequent displacements, caused by the water pressure would not be measured. This is considered to be the most likely reason since both malfunctioning LVDTs are subjected to these jumps on the same days. One other possible explanation for the behaviour of these two LSVDT sensors might be that particles and leakage water may have dripped on the sensors and thereby obstructing the sensor tip's ability to move freely and thereby clogging the sensor and restraining the recorded displacement. If this is the cause, then it is not expected that these jumps should occur for both sensors at the same time. There is just one event, in December 2013, where only one of the sensors is affected by a jump and thereby, this may be explained by clogging of the sensor.

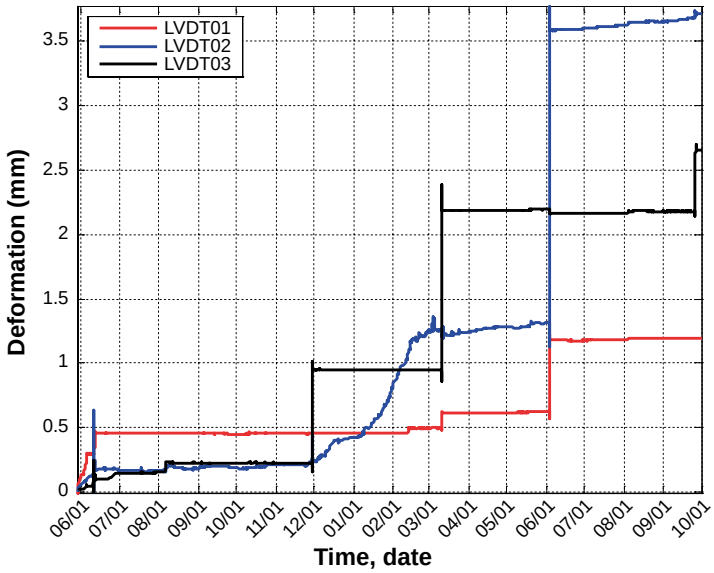

Figure 9-47. *Measured variation in horizontal displacement.*

LVDT02 measures reliable values for the period when the pressure is being increased up to 4 MPa. However, during the period of constant pressure, this sensor also showed an instantaneous jump in its response (this occurred during June 2014). At the same time, one of the other LVDTs also experienced a jump in its recorded signal, which indicates that some work was on-going at site which may have disturbed the measurements. One important difference is however, that despite this jump LVDT02 still seems to give reliable values since the direction of the measured displacement is the same before and after this event. In Malm (2014) the behaviour of the sensors is shown if these instantaneous jumps are removed. Based on these results it can be concluded that only LVDT02 gives reliable recordings and that the jump this sensor experienced has not influenced its capability to continue to measure the displacements. The displacement of the dome plug is, according to the experimental results, about 1.25 mm in the domes quarter point during the period when a constant water pressure of 4 MPa is applied.

Comparison with numerical results

A comparison between the measurements provided by LVDT02 and the three cases of numerical analyses is shown in Figure 9-48. As can be seen from the results, the horizontal displacement from the experimental results is similar to the displacement obtained from the model with full bond that releases when the hydrostatic water pressure is applied.

Evaluation of the measurement system

As shown earlier, only one of the LVDT sensors has provided reliable displacement readings. The reason for this may have been disturbance of them due to parallel work activities. One other possible explanation for the behaviour of these two LVDT sensors might be that particles and leakage water may have dripped on the sensors and thereby clogged the sensors but as noted earlier this was deemed to be unlikely.

9.3 Leakage measurements

The measurement of leakage across the plug has been made using several different methods. The primary method automatically transfers seepage water from the weir to a scale that weighs the leakage mass for on-line recording, as described in Section 7.5. In addition to this, manual measurements were introduced to record the experiment-related leakages that started to occur at high pressure; a water escape via the sensor cable bundle within the concrete dome and a water escape via a rock fracture. Further information on these leakages is provided below.

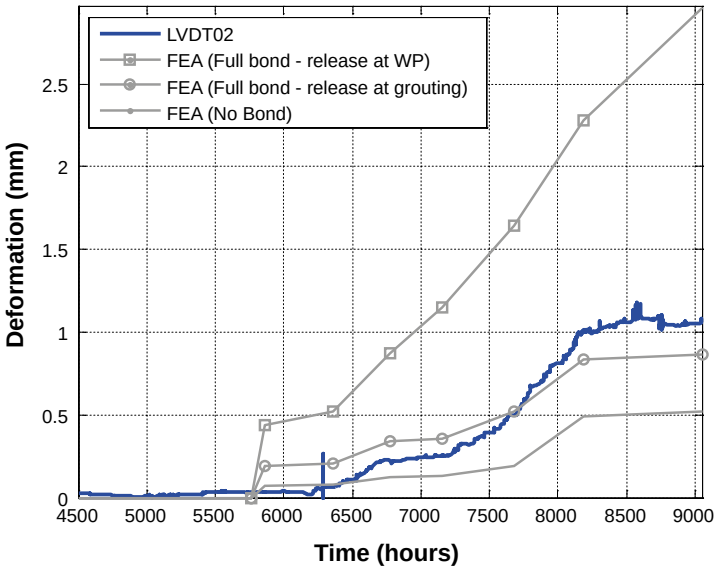

Figure 9-48. *Comparison between experimental results and the results from the numerical models.*

9.3.1 Measured leakage across the plug, collected in the weir

The drainage from the filter section was closed on September 30th 2013 (day 243). A safety valve (6 bar) was mounted on the drainage tube and the water pressure was then allowed to increase naturally by groundwater inflow up to this level. A water pressure of six bars was reached after about 26 days and this pressure was then maintained for about eleven days.

In the next step, a new safety valve (10 bar) was mounted on November 6th 2013 (day 280) and after this the pressure was again allowed to increase "naturally". One of the reasons for the high initial leakage rate values observed during this time is that one of the pore pressure sensors was leaking through the steel pipe, see Section 9.1.

The pressurization system was started on Dec 2, 2013 (day 306). The pressure was increased by up to 2.5 bar every week with a somewhat slower rate in the beginning.

When water pressure exceeded about 31 bar, two major water escapes were recorded. According to Figure 9-49, which shows the recorded leakage rate and water pressure build-up, the plug system had been almost watertight during pressure increments up to about 31 bar. After this, water bearing fractures opened in the rock and also in the concrete dome via the main cable bundle. These experiment-related water escapes were recorded separately and are thus not included in the monitoring of leakage past the plug collected in the weir.

Since the water pressure has been held stable at about 4.0 MPa, the leakage rate collected from the weir stabilized at about 4 litres per hour (0.066 l/min). During the eight month follow up of the leakage rate it has been steadily reduced. On the date for data freeze for this project on September 30, 2014 (day 608), the recorded leakage rate collected in the weir was about 2.6 litres per hour (0.043 l/min).

Initially, about 1.0 l/min injection water was needed to keep the 4.0 MPa water pressure in the filter. After eight months of plug system operation, just about 0.4 l/min was needed to maintain the same pressure.

The results from the leakage measurements have varied during the period but seem to have stabilized on a low level, and still with a decreasing trend. The monitored data from the applied water pressure (from the pump), the measured leakages and the pore pressure measured in the lead-through pipe in the concrete dome is provided in Figure 9-49. The water pressure inside the lead-through pipe (blue line) has increased with time indicating a water connection, possibly via sensor cabling to the concrete–rock contact surface or via the inside of the concrete delimiter.

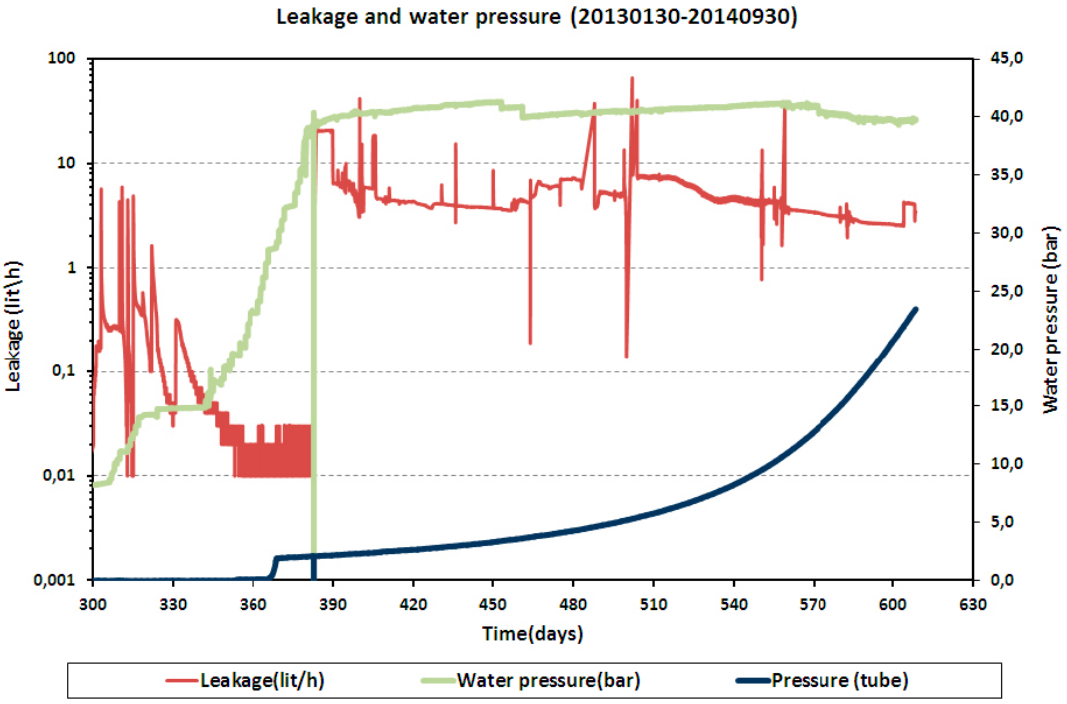

Figure 9-49. *Measured leakage from the weir and the applied water pressure.*

Visual observation of the surroundings of the concrete dome shows one apparent leak as seen in Figure 9-50. Moist and small drips can also be seen from the tunnel roof just outside the concrete dome left side. These leaks are included by the leakage measurement recordings.

9.3.2 Salt in the weir

A metal filter was installed in the weir to prevent particles from being transported to the basin. The outlet from the weir could otherwise clog affecting the leakage measurements. Therefore, this filter has to be cleaned on a regular basis (every week). Raman spectroscopy analysis shows that the salt found in the water mainly is calcium carbonate (calcite; $CaCO_3$) as illustrated in Figure 9-51.

Further testing of the contents of the salt using XRF showed that the elemental composition is consistent with calcite with minor traces of chloride from the salt water, and minor sulphate possibly as gypsum, as seen in Table 9-3.

Table 9-3. Elemental composition of the salt in the weir.

Compound	Concentration
Na_2O	0.000 %
MgO	0.002 %
Al_2O_3	0.070 %
SiO_2	0.252 %
P_2O_5	0.035 %
SO_3	1.254 %
Cl	2.120 %
K_2O	0.052 %
CaO	96.150 %
TiO_2	0.018 %
MnO	0.001 %
Fe_2O_3	0.046 %

Figure 9-50. *Observed water leakage in the interface between the concrete dome and the rock, in the top of the slot (at 13 o'clock). Note that the dark line on the face of the dome is water not a crack in concrete.*

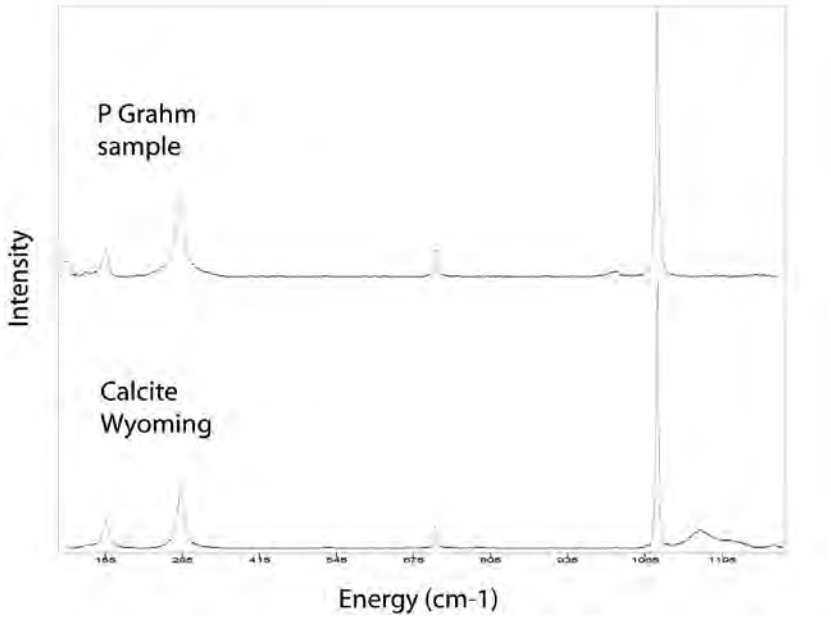

Figure 9-51. *Raman spectroscopy results showing calcium carbonate content in the weir.*

The source of calcite is calcium-leachate from the concrete dome combined with the ambient carbon dioxide. This quick appearance of salt on the water surface accentuates a need for regular cleaning of the weirs in a repository.

9.3.3 Experimentally related leakage during increase of water pressure

As stated in Section 9.1, the original ambition was to pressurize the DOMPLU experiment with water up to 7 MPa during 2014 and thereafter keep the water pressure constant. However, when pressure increased above 3.1 MPa, it was observed that the water was escaping through a fracture in the rock, shown in Figure 9-52. Apparently, this fracture has connection with the plug location and is thereby to some extent by-passing the plug and transports water out from the filter section. Before plug installation began, the fracture had been mapped as a small and dry fracture.

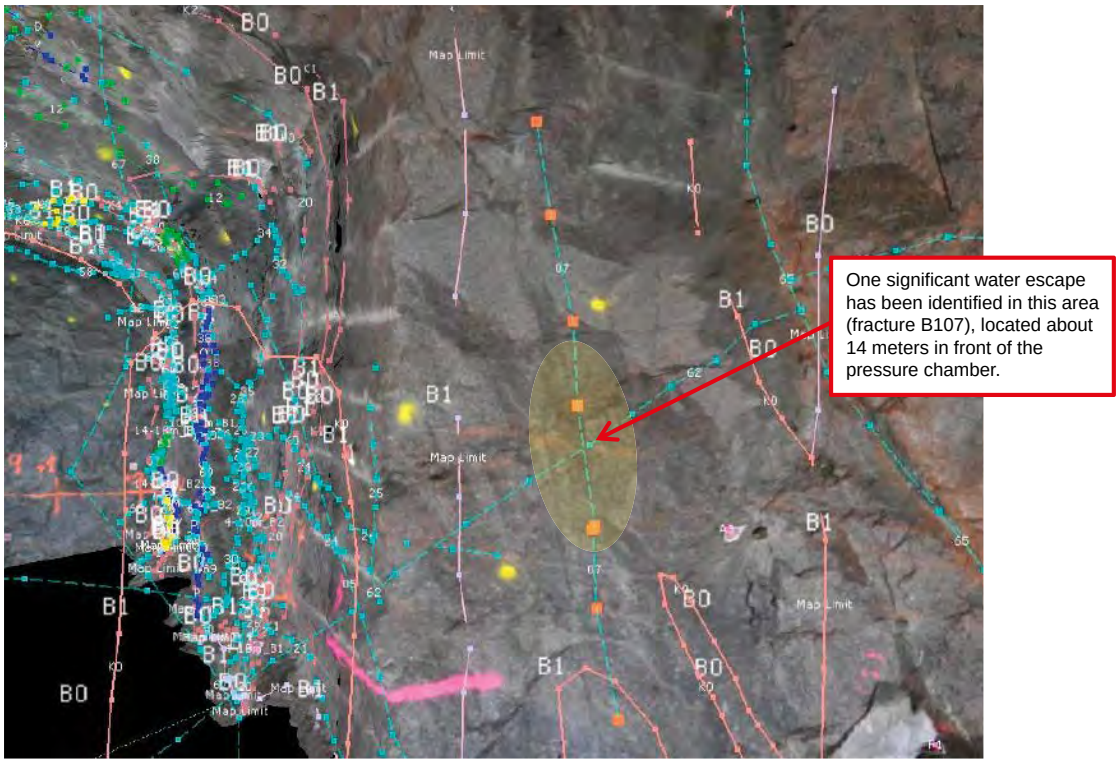

Figure 9-52. *Area where leakage was detected in the rock for a water pressure of 3 MPa.*

Another experiment- related leakage was short after observed through the cable bundle from the sensor cables from the concrete dome, as shown in Figure 9-53.

The experimentally related leakages were measured manually every week. They increased exponentially when increasing the water pressure (i.e. hydraulic jacking). Consequently, it was decided to continue operation and monitoring at a stable pressure.

Leakage past or around the plug were recognized project risks but do not compromise the basic goals of DOMPLU. A project change was incorporated and the original plan for a water pressure up to 7 MPa was abandoned. Running the test at 4 MPa is a realistic worst-case scenario for a groundwater pressure during operation of the Spent Fuel Repository since it approximates the natural hydraulic head at repository depth and thus is a reasonable pressure target for the DOMPLU test.

It should again be noted that the rock at the DOMPLU site in Äspö HRL is of lower quality with respect to its hydraulic integrity than the rock at the site for the Spent Fuel Repository in Forsmark. It would therefore be reasonable to consider the DOMPLU test to have been completed in a less favourable location than would occur at a repository.

The leakage from both the fracture in the rock and from the cable bundles was diverted in order not to be collected in the weir and was measured manually. The results from the manual leakage measurements are shown as a complement to the results from the on-line recordings from the weir. By comparing the results, an estimate can be made of the leakage distribution between the different leakage paths. Figure 9-54 shows the measured leakage through the rock fractures, the cables and the weir. The water pressure is also shown as is the water volume that is pumped into the plug system in order to maintain a constant water pressure of 4 MPa.

As can be seen in Figure 9-54, the volume of water (Total inflow) needed to maintain the upstream pressure increased significantly from 900 to 1640 ml/min as the water pressure increased from about 3.1 MPa to 4.0 MPa. At the same time the leakage from the rock fracture increased from 445 ml/min to 810 ml/min, which corresponds to 49 % of the increased total inflow. At this time, the weir was showing almost zero seepage entering it. The reason for this lack of outflow to the weir was that the outlet pipe had clogged and after it was cleaned a leakage rate of about 108 ml/min was measured.

a) b)

Figure 9-53. *Located leakage through the cable bundle for sensors installed in the concrete dome.*

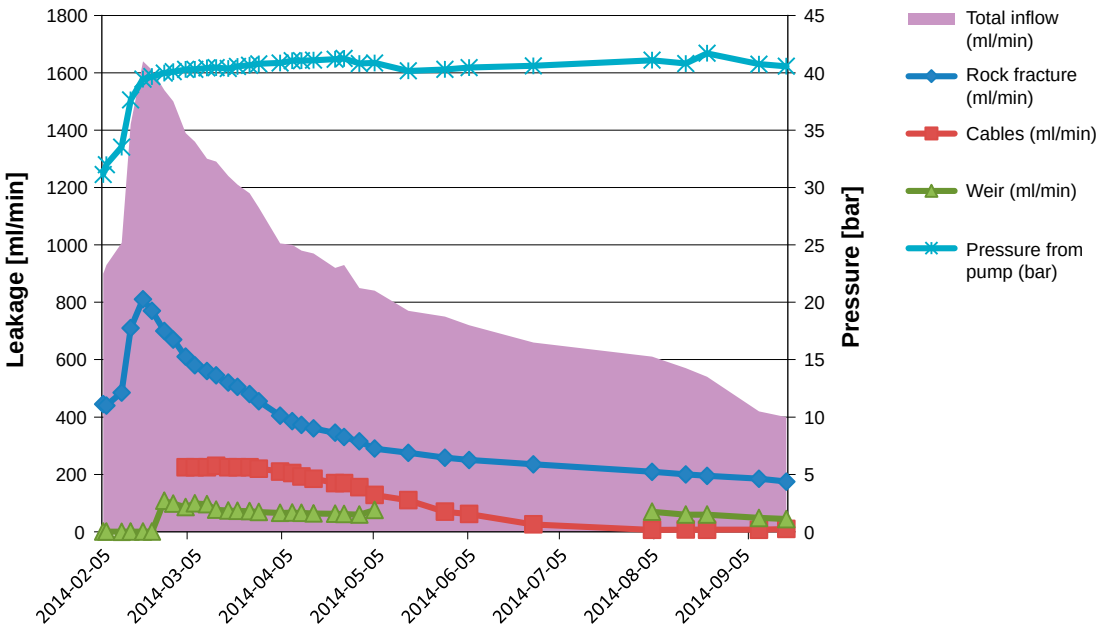

Figure 9-54. *Measurements of leakage together with total water injection flow needed to keep the water pressure stable near at 4 MPa (about 40 bar).*

This early-stage measurement included the experimentally related leak from the cable bundle which began increasing in the same time period. One week after the identification of the cable leakage, a separate flow collection system was arranged for the cable bundle. A leakage rate of 225 ml/min was observed from the cables at that time. This leak has gradually decreased and was almost zero at the end of the monitoring period.

As seen in Figure 9-54, all leakages have decreased substantially and seem to be relatively stable, slight downward trend, by the end of monitoring. The total inflow to keep 4 MPa water pressure was about 400 ml/min on September 30, 2014. The measured leakage was distributed as follows (note that leakage is expressed as percentage of inflow in the brackets):

- Rock fracture 169 ml/min (42 % of inflow).
- Weir 43 ml/min (11 % of inflow).
- Cable bundle 8.5 ml/min (2 % of inflow).
- Remaining rock mass 178.5 ml/min (45 % of inflow).

A continuously decreasing leakage with time can be observed in Figure 9-54. The reduction of leakage through the cables and into the weir is probably due to saturation of the bentonite seal, resulting in an increased swelling pressure and thus better sealing capability at the rock interface.

However, a large part of the leakage seems to take place through the “intact rock” either into the test-drift outside the plug or to other cavities nearby. The reduction of this leakage and the leakage through the fracture is probably caused by clogging, but this is uncertain since it is not clear where this leakage originates.

10 Conclusions and experiences

10.1 Summary of Results

This report summarizes four years of system design development for the deposition tunnel end plugs, carried out in cooperation between SKB and Posiva Oy, according to the KBS-3V reference disposal concept. In addition, the research leading to these results has received funding from the European Union's European Atomic Energy Community's (Euratom) Seventh Framework Programme FP7/2007-2013 under grant agreement no 323273, the DOPAS project.

The system design development has included verification of the dome plug design by analytical and numerical calculations, laboratory examinations and scale tests. The main activity though, has been to test a dome plug system in full scale (The DOMPLU test) at the Äspö HRL. The rock conditions at Äspö HRL are not as good as found in Forsmark, the site for the Spent Fuel repository, but nevertheless the experiment has been carried out at similar depth in crystalline rock with comparable overburden pressure.

In a general summary, the system design phase for the deposition tunnel end plug was successful. The full-scale test of the plug system (DOMPLU) has given promising results until September 30, 2014, and the trial is still operating at the depth of 450 meters in the Äspö HRL. The monitoring is planned to continue for at least two more years after which the plug should be breached and examined, see further information in Section 10.3 Future activities. Furthermore, some important lessons learned from the full-scale test have been obtained. These experiences are described in Section 10.2.

Below, summarized assessments and discussions of the results are addressed to each of the objectives stated in Section 1.3.

10.1.1 Finalize the details of the reference design

The DOMPLU experiment is based closely on the SKB reference conceptual design of the deposition tunnel plug. In contrast to the earlier plug experiments undertaken by SKB, DOMPLU therefore represents a more detailed iteration of the design rather than a fundamental change. The current SKB reference design and DOMPLU design are broadly similar, with the exception of a few modifications intended to test the performance of new materials planned to be introduced as the reference design in the future. Such modifications include:

- The use of unreinforced concrete instead of reinforced concrete for the concrete dome. Measurement specifications have also been suggested for the dome geometry and the associated slot excavation.
- In DOMPLU, the backfill end zone has been redefined as a backfill transition zone where the pressure on the plug due to the swelling pressure from backfill is reduced to a level that is similar to the resulting swelling pressure of the bentonite seal (approximately 2 MPa). The purpose of introducing a transition zone was to reduce the displacement of the plug system components. A backfill transition zone of 100 cm was included in DOMPLU, however the length of the zone for a future plug system is dependent on the specification of bentonite components, either a combination of blocks and pellets or merely pellets.
- In DOMPLU, the innermost delimiter was considered to be part of the filter. Instead of concrete beams, porous LECA beams with high permeability were used.
- The filter thickness was 60 cm, made up of 30 cm of gravel (with an aggregate size of 2–4 mm) and 30 cm of LECA beams, compared to a thickness of 700 mm, which is specified in the reference design for the filter. The DOMPLU filter was well-designed, but the inlets of the drainage pipes clogged due to the use of too fine copper mesh. It is suggested that customized bottom valves for the pipes inside the gravel filter are introduced during detailed design.
- The middle delimiter between the filter and the bentonite seal was composed of a geotextile instead of concrete beams. This simplified installation and provided good conditions for the bentonite seal to become saturated by water from the filter.

- The outer delimiter was composed of prefabricated low-pH concrete beams as for the reference design. There was also a double geotextile layer introduced between this delimiter and the concrete dome to prevent adhesion of the delimiter to the concrete dome, and therefore avoid potential cracking of the concrete dome during shrinkage. However, for DOMPLU there is a question raised whether the double geotextile layer introduced a vertical path for the water on the inside of the dome. Therefore it should be studied during breaching of the plug if injection grout filled this path or not.
- Cooling pipes were made of copper and was delivered to the site in three prefabricated sections to streamline the installation. The cooling pipes need a supporting framework, which for DOMPLU consisted of seven vertical steel beams carrying 14 horizontal bars. It should be studied further during the detailed design phase whether it is possible to arrange the supporting structure without continuous vertical connections. The cooling procedure used during casting and contact grouting was feasible and predictable, as shown by both sensors data and modelling.
- Grouting tubes were made of cross-cut 50 mm plastic drainage tubes, installed in three circumferential sections of the excavated slot. Bentonite bands were used to create lockers for the grout. It is the first time these cross-cut tubes were used for a similar application. Nevertheless, the results of the performed contact grouting were promising. Sensors data from DOMPLU show that the water tightness of the plug has been maintained by the contact grouting in the initial stage. However, the interface between the concrete dome and the rock should be visually examined by drilling cores during a future breaching of the plug in order to verify the results of this design, i.e. the distribution of grout.
- The thickness of the bentonite seal was 500 mm in DOMPLU, which was practical and considered sufficient for the timescale of the experiment. It is suggested that the final seal thickness should correspond to the thickness of reference backfill blocks, thus the same production tools can be used. The same clay material for the seal as for the buffer system is recommended and therefore MX-80 material was used in DOMPLU.
- The installed dry density of the filter was 1400 kg/m^3 in DOMPLU while a value of 1900 kg/m^3 is considered in the reference design. In the reference design compaction of the filter was presumed, but this turned out to be impractical and not useful for the grading chosen of the filter material. The result is of course a larger compression of the filter by the swelling pressure, which has to be taken into account in the design of the backfill transition zone.

Until this date, the DOMPLU design has performed well. Based on this, it can be assumed that new potential materials, such as LECA, geotextiles, fiberwool and cross-cut plastic drainage pipes, can be implemented in the modified reference design. It is though suggested that these materials, and the interfaces between materials, are further examined during a future retrieval of DOMPLU. Undertaking getting the new component materials approved for use in a final repository has not been a part of the project. Consequently, this must be checked from post-closure safety point of view at latest during the detailed design phase.

10.1.2 Demonstrate the feasibility of plug installation

One of the main outcomes from the full-scale test is showing that it is possible to build the dome plug system. This includes practical aspects of logistics and arranging of parallel construction activities in a tunnel system etc.

Subsequent to rock excavation of the slot and other experimental preparations, the installation of DOMPLU took about two months. It started January 7th 2013 with installations of backfill blocks and was finished in March 13th 2013 with casting of the concrete dome. After this, formwork was dismantled and the concrete dome was contact grouted in June 2013, 11th and 19th respectively. In the full-scale test all installations were made manually while the installation of bentonite blocks is planned to be performed with an automated system in the repository. DOMPLU also included experimental items such as approximately 100 sensors and a water injection system connected to in total four lead-though pipes. The time required for installation of a plug in the Spent Fuel Repository will therefore most likely be shorter than in the full-scale test. A further discussion about such scheduling is provided in Section 10.2.

The civil work for DOMPLU was in general successful with a few important experiences gained from construction, highlighted below:

Rock excavation of the slot

The excavation of the slot by wire-sawing was a bit more problematic than expected. The method with blind cuts was however feasible and resulted in smooth surfaces but with unwanted deviations in planarity for a few cuts. Further practical improvements can be introduced for future excavations and there is also a need for site-specific testing of excavation at the Forsmark site, where rock stresses will be even higher than in Äspö HRL. There is a need to define new requirements on fracture-free rock and flat surfaces, potentially free from continuous EDZ. Safety aspects, to protect workers from the risk of falling stones, will need continued focus.

Installation method

To begin with, the remaining semi-circular boreholes used for the wire-sawing were moulded, prepared with thin grouting tubes and filled with mortar. Water inflow to two of the holes made the work complicated and thus water bearing fractures should always be avoided for the plug locations. Furthermore, plinths were moulded and cast for the delimiters and the drainage collection in the bottom of the filter.

Subsequently, the plug components of DOMPLU were emplaced by manpower using vacuum lifting tool, sky-lift and crane support from a wheel loader. Firstly, LECA beams and backfill transition zone was emplaced. Secondly, gravel filter, geotextile, bentonite seal and concrete delimiter was emplaced in a simultaneous sequence. It was difficult to install beams, filter and seal-pellets near the tunnel ceiling. For instance it was not possible to achieve a vertical wall of geotextile and gravel; instead it was decided to fold in the geotextile over the gravel which resulted in an empty space the uppermost 0.5 meter. This space was later filled with bentonite pellets that were blown in over the bentonite seal blocks. The sensors were installed in parallel to installation of each component.

Temporary attachments to the rock were used for the LECA delimiter beams. Those were removed in connection with installation of the following components.

Detailed methods and instructions for installation should be produced during detailed design. The workers safety aspect of working at heights, for instance during installation of cooling pipes where a sky-lift could not easily be used, should also be studied further.

Formwork

Based on 3D-visualization, the formwork had been manufactured by Doka GmbH and documentation consists of more than 50 drawings. The formwork was perceived by the staff to be both solid and well designed. A modification with a man-hole was suggested by the workers for easier positioning of the larger upper parts. Possibly the upper part of the formwork could also be re-designed as one piece to facilitate fitting. The pressure measurements during casting showed that a future formwork can be built in thinner dimensions. An improved routine should also be developed for positioning of the frame of the formwork, especially regarding the extension with fitting pieces to the rock.

Casting of the concrete dome

The concrete control station and the organization at the test site functioned well. During pumping, there was no need to use all hatches in the formwork but 2 + 2 + 2 was used for pouring. The formwork was tight and not more than 2 dl of concrete escaped to the front. For the purpose of risk mitigation, a redundant concrete pump was available at site but it was never needed.

The concrete used was good quality and its behaviour was as expected of the B200 concrete. An exception to the initial expectations was that it was found to be high air content (6–9 %) at delivery which is probably related to the mixing of additives and the long transport. Another exception was the lower amount of autogenous shrinkage, which likely was caused by the higher air content. The exact relation of air content and autogenous shrinkage is not clear, but according to Tazawa (1999) it is likely that the air content has the similar influence as the cement paste on the autogenous shrinkage (increased cement content results in increased autogenous shrinkage). Studies have shown that the autogenous shrinkage is not significantly affected by lower values of air content. However, when the air content is relatively high, studies from e.g. Bentz et al. (2012) have showed a significant reduction of autogenous shrinkage. Further studies on this are discussed in Section 10.2.

Cooling

Installation of the prefabricated parts of the cooling system was successful but hard to accomplish in full accordance with the drawings. There was need for bigger tolerance (± 10 cm) near the intersection points of the slot since it was hard for the technicians to reach these areas.

The cooling procedure was successful and can be specified in detail for future plugs. The redundant cooling machine was never needed but it is considered important to have a spare cooler on site if failure would occur on the operating machine.

Contact grouting

The installation of grouting tubes was time consuming and took almost two weeks. For the upper parts of the slot, work had to be performed from sky-lift. However, installation of grouting tubes in the lower part of the slot was even more difficult because the workers tend to slide downward on the steep and smooth rock surface.

The contact grouting procedure, in combination with cooling, worked as intended and the leakage monitoring indicate that the injection grout made the plug watertight enough for the initial pressure increments.

10.1.3 Validate requirements on construction methods

About the concrete dome, it was shown that it is possible to use an unreinforced dome consisting of low-pH concrete mix B200. Due to the lack of reinforcement, the tensile stresses in the concrete dome have to be limited in order to prevent it from cracking. High tensile stresses may occur during hydration and due to shrinkage if the concrete dome is subjected to restraint, i.e. bonded to the rock in the slot. The previous design calculations, for instance presented in Malm (2012), were all based on the fact that the induced stresses were limited prior to contact grouting, i.e. it was assumed the concrete dome would release from the rock. As seen in the numerical analyses presented in Section 8.2.3 the stresses are small if the concrete dome releases. For the two cases where it is not assumed to release during the early response, high tensile stresses occur mainly due to the large shrinkage. In order to reduce the induced stresses in the concrete dome, an advanced cooling scheme was used to:

A. reduce the temperature rise due to heat from hydration,

B. force the concrete dome to release from the rock, and

C. create a gap between concrete and rock before contact grouting.

The cooling procedure in combination with the contact grouting results in a thermal pre-stress of the concrete dome plug.

The full-scale test showed that tensile stresses were induced in the concrete dome as the heat from the hydration reduced. These stresses are high enough to have forced the concrete dome to at least partially release from the rock, but may also have caused some cracks in the concrete dome. Based on the evaluation of the measurements, it can be concluded that the dome did not release fully and remained at least locally bonded to the rock. This conclusion is based on the following observations:

i. High tensile stresses occur in the concrete dome during the first three months, which could cause cracking in the concrete dome.

ii. The obtained thermal pre-stress is lower than what would have been obtained if it had released from the rock (about 53 % of the theoretical value).

iii. The relative displacements between concrete and rock was significantly lower than the expected displacements that would occur if it released.

One important finding from analyses of the measured response and the results from the numerical model is that the autogenous shrinkage of the concrete dome is less than the observations in the material tests. This may be the primary reason why the concrete dome did not release fully from the rock. However, the high autogenous shrinkage was the main reason for the decision to force the dome to release from the rock. Thereby, if the shrinkage is less than used in the design calculations it may no longer be a requirement that the concrete dome releases from the rock.

10.1.4 Demonstrate that the plug works as intended under realistic conditions, up to the reference design total pressure of 7 MPa

Since the hydrostatic pressure at Äspö HRL level 450 m is approximately 3 MPa, a pressurization system was needed for DOMPLU to inject water at high pressure in the backfill section. The relatively rapid rate at which the experiment has been pressurized may have affected some of the results from the experiment.

In addition, it should be noted that the introduction of sensors can have affected the performance of some plug components. For instance an experimentally related water escape across the plug occurred via sensor cabling from inside of the concrete dome. Undoubtedly water at high pressure found a leakage path from sensors in the dome near the rock interface.

The experimentally related water escape, especially via the rock fracture to the main tunnel, was the main factor in deciding not to raise the hydraulic head above the approximately 4 MPa level. It should again be noted that the rock at the DOMPLU site in Äspö HRL is of lower quality with respect to its hydraulic integrity than the rock at the site for the Spent Fuel Repository in Forsmark. It would therefore be reasonable to consider the DOMPLU test to have been completed in a less favourable location than would occur at a repository.

Monitoring of the concrete dome

During the increasing of water pressure to 4 MPa, the following responses were observed for the concrete dome:

- The joint-meters located in the top of the dome showed a rapid decrease in displacement as the water pressure reached 3.5 MPa. This was likely caused by a release in bond between concrete and rock on the upstream side of the slot.
- Leakage was also detected in the region where joint meters showed release during pressurization, which further implies a loss of bond on the upstream side of the slot.
- All strain gauges showed decreasing strain during increasing water pressure, which means that all sensors showed a compressive state of stress as expected.

The results show that almost all installed sensors in the concrete dome have worked successfully and captured the behaviour from a few hours after casting up to the point of contact grouting the concrete dome, which occurred about 3 months after casting. However, after this, several of the sensors failed. Most of the sensors failed due to the increasing water pressure, since none of these concrete-related sensors were designed to withstand the water pressure and contact with water was not anticipated.

Monitoring of the seal, filter and backfill

The sensors installed in the bentonite sections were all known in advance to be subjected to high water pressures and therefore these were all designed to withstand a water pressure of at least 10 MPa. However, a few of the sensors in the bentonite sections have also failed during the full-scale test.

During the increasing of water pressure to 4 MPa, the following responses were observed for the bentonite seal and filter components:

- The shutoff of the drainage did as expected affect all pore pressure sensors i.e. the two sensors in the backfill, the two sensors on the other side of the sealing and also the two sensors placed in the concrete-rock slot. This means that the bentonite seal was not yet providing enough water tightness at that point. However, since the measured leakage rate across the plug was very low at this time, it is evident that the performed contact grouting provided a watertight seal.
- As expected, the monitored swelling pressure (total pressure minus pore pressure) in the bentonite seal increased slowly with time and, by 30 September 2014, the swelling pressure was between 100 and 700 kPa. Based on experience from the scale-model tests, the bentonite seal should provide water tightness when the swelling pressure reaches more than approximately 500 kPa in all its parts. Thus the bentonite seal was still not fully functional at the time for data freeze of this first technical reporting of DOMPLU.

- The displacement sensors have registered a movement inwards, i.e. the bentonite seal has swelled and compressed the gravel filter and the pellet filled slot inside the LECA wall. In total a movement of approximately 30 mm was registered which was in accordance with the predictions.

10.1.5 Develop a method for leakage measurement

An appropriate prototype of a water collection system was developed for DOMPLU. The system records, with reliable on-line updates, the water leakage rate out of the pressurized region. However, the system is sensitive to evaporation and a plastic sheet was used to cover the concrete dome to reduce these effects. The sheet was connected to the weir.

The plug system has been almost watertight during pressure increments up to approximately 3 MPa, which corresponds to the ambient hydrostatic pressure at the test site. When pressure was raised further, water began escaping from the pressurized volume, especially via a rock fracture to the main tunnel. It was thus decided to continue the test at a stable water pressure of 4 MPa (400 m head), which is still a representative value for operational repository conditions.

After 8 months (to September 30, 2014), of subjecting the dome plug a water pressure of 4 MPa, the leakage across the plug was about 0.043 l/min (2.6 l/h). This is well below the desired level of a leakage past the plug of less than 0.1 l/min.

Based on the appearance of the measured leakage versus time plots, this rate is expected to decrease further. The results show that the water pressure next to the concrete dome is decreasing while the water pressure on the upstream side of the bentonite seal is being maintained. Thereby, it can be concluded that the bentonite seal is becoming more and more watertight with the slot between concrete and rock gradually becoming less water conductive.

Another evidence for DOMPLU being a tight plug system is that no eroded bentonite has been seen through visual inspections of the weir subsequent to closing the drainage.

10.1.6 Improve testing and quality control during repository construction

The plugs have no long-term barrier function and thus the requirements on quality control are lower than for the canister, buffer and backfill. However, a basic design condition for the deposition tunnel end plug is that it shall be manufactured, installed and controlled based on proven technology. The installation must be made with high reliability, i.e. without risk for failure, and it should be possible to control the installation in relation to predetermined acceptance criteria.

It is suggested that relevant acceptance criteria for the choice of plug location should be determined. Important experience is available from DOMPLU where the design criteria on fracture-free rock could not fully be achieved. This resulted for instance in that water escaped from the pressurized volume to the main tunnel, via a fracture in the rock.

The exact positions of the components, i.e. the boreholes in the slot for casing of the concrete dome and plinths for the material delimiters, will be determined by geodetic survey. This can be done already in connection with positioning of deposition holes in a newly excavated tunnel.

As for the areas of the deposition tunnels, the actual geometry of an excavated slot can be determined by laser scanning etc. This will be helpful in planning the formwork installations and determining the amounts of concrete and grout. It also provide basis for 3D-visualization of the plug system.

In general, installation of the backfill transition zone and the bentonite seal will be done according to the established principles for bentonite installations in the deposition tunnel. Installed densities for both the bentonite components and the gravel filter will be registered. Laboratory examinations of new sealing and draining components have been carried out by Börgesson et al. (2015a). The suggested new materials, such as LECA and geotextile, need to be approved for use in the Spent Fuel repository.

Dimensions of prefabricated components will be checked before emplacement and positioned on site by geodetic survey. In addition, the positions of grouting tubes, cooling system support structure and concrete dome formwork will be determined by geodetic survey according to construction drawings.

The B200 low-pH concrete recipe has been further studied by Magnusson and Mathern (2015). Despite fact that the concrete recipe has been specifically developed by SKB for this application, conventional control methods can be used to check quality of the fresh concrete during casting of the dome. Following standards were used for DOMPLU:

- Slump flow according to SS-EN 206-9.
- t_{500} according to SS-EN 206-9.
- Air content according to SS-EN 12350-7.
- Density according to SS-EN 12350-7.
- Temperatures.

Temperatures of the cooling water, in and out, will be measured during the processes of concrete hydration and contact grouting. The amounts of grout and pressures applied during contact grouting will as well be registered.

Drainage of groundwater past the plug, and the content of bentonite fines in the water, should be checked during plug construction until the drainage valves are closed.

Finally, a continuous control of the leakage rate across the plug, together with control of the water pressure inside the filter, can be implemented to validate construction of the plug system. See further information below.

10.2 Lessons learned

Lessons learned from the full-scale test show that the modified reference design of the plug can be built with the required tightness to restrict the axial flow of water in the deposition tunnel. From constructional point of view it was hard to force the unreinforced concrete dome to completely release from the rock during cooling before contact grouting. Reasons for this were partly due to that the low-pH concrete bonds strongly even against a smooth rock surface, and partly due to fact that the B200 concrete self-shrinkage was lower than expected in the full-scale casting. Additional calculations and tests may be needed in the detailed design phase to validate these processes. Also for the concrete recipe further studies are needed to assure that the recipe has enough robustness and flexibility for future use in the Spent Fuel Repository.

It is suggested, by the system design project, that each plug should be a vital monitoring point in the Spent Fuel Repository, where both water pressure inside the tunnel (in a drainage pipe from the filter) and the groundwater outflow on the downstream side of the concrete dome can be measured. This has been confirmed by DOMPLU to give functional results and provide relevant understanding of some important processes in a repository. These types of measurements do not introduce a threat to any of the engineered barriers since the equipment can be removed before closure of the repository. In addition, the sensors are easily exchangeable during the service life of up to 100 years.

To measure the leakage water past the plug, an appropriate prototype of a water collection system was developed for DOMPLU. Furthermore, DOMPLU has given important experience regarding the starting point from the achieved initial state of the deposition tunnel. The plugs can then be commissioned by closing of the drain valves to the filter after which the water pressure is allowed to build up inside the plugged deposition tunnel. Commissioning of DOMPLU showed that it is possible to use a simple water system on the outside of the plug to provide a very controlled filling of the filter, via the drainage valves, so that the bentonite seal obtains quick and gentle access to water. This will be of utmost importance for all dry tunnels since this procedure ensures that the requirements on certain water tightness and gas tightness can be fulfilled in the shortest possible time (within a few years). To cope with the tightness requirements also in the initial stage, the proven technology method with contact grouting has once again shown to be a functional approach to seal the concrete-rock interface.

Installation aspects

The rock excavations are done well in advance, about two years, before start of canister depositions. Consequently it is believed that both the decisions on plug location and the rock excavations of the slots can be made without critical time pressure to achieve good enough quality. Based on DOMPLU experience a successful procedure with core drilling and subsequent wire sawing should be able to complete slot excavation within approximately 40 days working in single shift.

For effective logistics during plug installation, prefabricated components should be used to possible extent. The cooling system pipes can be pre-assembled in large sections, the delimiter beams are cast in advance and the bentonite blocks and pellets are as well produced and prepared above ground.

Major manual work activities for a plug installation are listed in Table 10-1 below.

Unlike DOMPLU, installation of a repository plug system will be done without inclusion of experimental sensors. Nevertheless, the basic installation sequence used in DOMPLU has been captured as a construction procedure which can be used for the reference deposition tunnel plug. A future installation could therefore be planned according to the suggested schedule in Table 10-1. The civil work of the plug system starts when the final section of backfill blocks has been emplaced.

Table 10-1. Experience-based planning schedule for installation of a plug system.

Activity	Time (days)	Resources
Civil work preparations such as casting plinths for delimiters and drainage pipes.	2	Manpower (2), concrete, moulds, drainage pipes, supplies.
Start of controlled drainage. Installation of backfill transition zone and stiff filter (LECA delimiter beams).	5	Manpower (2), wheel loader, pellets, prefabricated LECA beams anchored on the plinth. Filling gaps towards the rock.
Installation of gravel filter, geotextile delimiter, bentonite seal and concrete delimiter beams. Double geotextile layers on the concrete delimiter wall towards the dome.	5	Manpower (3), wheel loader, gravel 2–4 mm, bentonite blocks and pellets, prefabricated concrete beams anchored on plinth. Geotextiles.
Installation of grouting tubes in the slot (3 sections).	5	Manpower (3), sky-lift, grouting tubes, bentonite bands, supplies.
Mounting of frame for the formwork and, in parallel, erection of the supporting framework for the cooling system.	7	Manpower (5), wheel loader crane, sky-lift, prefabricated formwork, prefabricated frame, supplies.
Installation of cooling system including proofing.	5	Manpower (4), sky-lift, prefabricated cooling pipes, cooling machine + 1 spare, supplies.
Erection of formwork for the concrete dome.	4	Manpower (4), sky-lift, wheel loader crane, prefabricated formwork, supplies.
Anchoring of formwork struts.	1	Manpower (3), supplies.
Preparations before casting.	1	Manpower (3).
Casting.	1	Manpower (8), concrete trucks delivering low-pH concrete, concrete pump + 1 spare, test equipment, supplies.
Dismantling and cleaning of formwork, approximately 28 days subsequent to casting.	5	Manpower (3), wheel loader crane, supplies.
Moulding and casting of weir for the leakage control.	2	Manpower (2), low pH concrete.
Contact grouting, begins 3 months after casting.	7	Manpower (2), injection grout mixer and pump equipment.
Covering of the dome.	1	Manpower (2), sky-lift, plastic sheet, supplies.

As understood from Table 10-1, approximately 35 days are needed to install the plug components to prepare casting of the concrete dome. The planned schedule can probably be shortened if double work shifts are introduced for certain activities.

The installation of DOMPLU required significant manual activity. In the Spent Fuel Repository, this civil work must be thoroughly coordinated with the automated deposition sequence ongoing in neighbouring tunnels of the deposition area. Heavy vehicles and equipment like cooling machines and contact grouting device need enough space. Staff will be working in the plug area and consequently radioactive transports cannot use the same schedule. During the day of casting, repository operation may need to cease due to frequent transports of concrete batches. Rock excavations in neighbouring tunnel system should as well be avoided for one day due to the desire for low vibrations during initial curing of the concrete. In general, manual activity in the deposition area also presents an operational safety hazard. Stricter procedures may be enforced in the Spent Fuel Repository compared to the provisional routines used in Äspö HRL.

Quality control aspects during installation have been discussed in Section 10.1.6 above.

Maintenance aspects

The quick formation of salt (calcite) in the weir for leakage collection accentuates a need for visual inspections and regular cleaning on a weekly basis.

The leakage measurement system is foreseen to be controlled on-line and the basket for water collection can be emptied automatically. However, this leakage control system will also need regular cleaning and service. Moreover the weight sensors (or alternative solution) used for recording of the flow rate will need to be exchanged during the operational period.

Safety valves and shut-off valves are needed for the drainage pipes and these will need regular service as well as the potential pore pressure sensors inside the pipe.

The cover of the dome should be regularly inspected and exchanged when necessary.

10.3 Future Activities

Results produced by this project will be used to modify the reference design of the plug system for use in the PSAR. Subsequently all information is handed over to the detailed design phase. It is foreseen that a few more iterations will be needed in this stage. The detailed design of the plug system will for instance include further structural calculations and update of construction drawings. It is intended that examination results, from opening and retrieval of the DOMPLU experiment in a few years, will be used as a further basis to the detailed design of the plug system.

Important aspects to study in connection with retrieval of the experimental set-up are all the interfaces between rock, concrete, delimiters and bentonite. Actual displacements of the plug components should be determined. In addition, material samples will be examined and some sensors checked for validity. Consideration could also be given to excavating the EDZ when DOMPLU is decommissioned. Similarly, tracer could be added to the water injected into the filter zone in case future studies could exploit its presence.

The plug system is now being subjected to a water pressure of 4 MPa at its upstream end and this pressure is intended to be maintained for a period of at least two years. During that time, measurement of the behaviour of the plug system and the leakage will continue. After two more years of monitoring, a decision is made as to whether a loading test, planned to be potentially up to 10 MPa of total pressure, will be performed.

The load test would be an important aspect in the full-scale test since it will show the response of the concrete dome when subjected to loads close to the design load (the design load is the sum of 5 MPa water pressure and 4 MPa swelling pressure, whereof 2 MPa is a safety margin). This load test would be a unique opportunity to verify the design of the concrete dome and the numerical models used.

The full-scale test showed that it is difficult to force the concrete dome to release completely from the rock; instead all evaluations indicate that the concrete dome was partly bonded to the rock. The results also showed that the concrete dome released on the upstream surface of the slot during the increasing of water pressure. Further investigations are needed to study the stresses in the concrete

dome depending on if it releases from the rock or not. In this study, alternative methods to evaluate means to reduce the initial stresses in the concrete should also be studied.

The results from the full-scale tests also showed that the autogenous shrinkage may be less in the full-scale than compared to what has been observed in the material tests. This must be studied further since a low amount of shrinkage will introduce much smaller tensile stresses in the dome. In addition, further work regarding defining suitable target values for the fresh concrete properties is required. For instance, the target value for slump flow was initially defined as 700 ± 30 mm but during the full-scale casting slump flow values such as 660 mm showed sufficient flowability. Further investigations are also required regarding the cause of high content in the concrete used for the dome plug and procedures to reduce the risk of obtaining material behaviour that deviates from expected.

A development program for low-pH concrete has already been started by SKB and will endure a couple of years. The continued development of the concrete monolith properties, cast at the same time as the concrete dome, will be followed-up and reported within this program. The continued studies will also focus on aggregates available at the Forsmark site and additives that are available in the future.

Low-pH injection grout was not used for DOMPLU. The amount of cement used for the contact grouting was about 500 kg compared to approximately 13 000 kg included in the concrete dome and delimiters. However, there should be a requirement on using a low-pH injection grout in the Spent Fuel Repository and therefore a further study on the grout recipe is needed.

New plug component materials used in DOMPLU, such as LECA, geotextiles, plastic tubes and fiberwool, must be checked from post-closure safety point of view at latest during the detailed design phase. There were also several steel materials used in DOMPLU, including framework for the cooling system, the reinforcement in the concrete blocks and the steel pins used to lock the concrete beams together. The quantities of steel are likely to be insignificant with respect to repository performance (e.g. to cause disruption owing to gas generation or to affect backfill performance through iron-bentonite interaction). Nonetheless, this should be demonstrated by simple scoping calculations included in a future iteration of the deposition tunnel plug design.

The full-scale test showed that the homogenization of the bentonite seal did not progress rapidly enough to produce a water-tight seal during initial pressurization. This was experimentally related due to the short schedule of the project. Nevertheless, the simple water injection system used for DOMPLU, to fill the filter via the drainage pipes, was helpful to initiate a gentle saturation of the bentonite seal. The filter was flooded slowly up to 7 m head (the roof of the main tunnel) and this pressure was maintained for eight weeks. It is suggested that the full procedure to commission a plug system, including the water injection components and relevant monitoring equipment, is further investigated. As discussed in Section 10.2, water injection equipment connected to the drainage pipes would be beneficial to fulfil requirements on certain water tightness and gas tightness in the shortest possible time.

The prototype system for measuring leakage water past the plug system needs to be slightly refined before the operation and monitoring of plugs in the Spent Fuel Repository.

Demonstration in the Forsmark bedrock is needed for proofing of the slot excavation method by wire-sawing. A recommendation for future development of slot excavation is to find a way to release rock tensions before cutting begins. It will also be possible to implement more productive ways to drill the large-diameter holes and emplace the guide pulleys for the diamond wire. Moreover the productivity can be increased with improved methods for drill rig positioning and use of specifically adapted platforms.

Full-scale demonstration of the reference deposition tunnel plug will be done again in the future, potentially in connection to integrate testing of buffer and backfill installations.

References

SKB's (Svensk Kärnbränslehantering AB) publications can be found at www.skb.se/publications.

Abaqus, 2012. Abaqus 6.12. Abaqus/CAE User's manual. Providence, RI: Dassault Systemes Simulia Corp. Available at: http://things.maths.cam.ac.uk/computing/software/abaqus_docs/docs/v6.12/pdf_books/CAE.pdf

Andersson L, Sandén T, 2012. Optimization of backfill pellet properties. ÅSKAR DP2. Laboratory tests. SKB R-12-18, Svensk Kärnbränslehantering AB.

ASTM C512-02. Standard test method for creep of concrete in compression. West Conshohocken, PA: ASTM International.

Bentz D P, Stutzman P E, Sakulich A R, Weiss W J, 2012. Study of early-age bridge deck cracking in Nevada and Wyoming. NISTIR 7841, National Institute of Standards and Technology.

Börgesson L, Sandén T, Andersson L, Johannesson L-E, Goudarzi R, Åkesson M, 2015a. System design of Dome Plug. Preparatory modelling and tests of the sealing and draining components. Clay Technology. SKB R-14-25, Svensk Kärnbränslehantering AB.

Börgesson L, Sandén T, Dueck A, Andersson L, Jensen V, Nilsson U, Olsson S, Åkesson M, Kristensson O, Svensson U, 2015b. Consequences of water inflow and early water uptake in deposition holes. SKB TR-14-22, Svensk Kärnbränslehantering AB.

ConTeSt, 2012. Concrete Temperatures & Stresses, ConTeSt R&D Version 4.1. Luleå, Sweden: JEJMS Concrete AB.

Dahlström L-O, 2009. Experiences from the design and concstruction of plug II in the Prototype Repository. Prototype Repository. SKB R-09-49, Svensk Kärnbränslehantering AB.

Dixon D, Sandén T, Jonsson E, Hansen J, 2011. Backfilling of deposition tunnels: Use of bentonite pellets. SKB P-11-44, Svensk Kärnbränslehantering AB.

Dixon D A, Priyanto D G, Martino J B, 2012. Enhanced Sealing Project (ESP): Project status and data report for period ending 31 December 2011. APM-REP-01601-0005, Nuclear Waste Management Organization, Canada.

Ekerfors K, 1995. Mognadsutveckling i ung betong: temperaturkänslighet hållfasthet och värmeutveckling. Lic. thesis. Luleå tekniska universitet. (In Swedish.)

Flansbjer M, Magnusson J, 2014a. System design of Dome Plug. Creep properties at high stress levels of concrete for deposition tunnel plugs. SKB P-13-37, Svensk Kärnbränslehantering AB.

Flansbjer M, Magnusson J, 2014b. System design of Dome Plug. Mechanical properties of rock–concrete interface. SKB P-13-38, Svensk Kärnbränslehantering AB.

Grahm P, Karlzén R, 2015. System design of Dome Plug. Experiences from full-scale wire sawing of a slot abutment for the KBS-3V deposition tunnel plug. SKB R-14-24, Svensk Kärnbränslehantering AB.

Holt E E, 2001. Early age autogenous shrinkage of concrete. Espoo: VTT Technical Research Centre of Finland. (VTT Publication 446)

ISO 1920-2:2009. Testing of concrete – Part 9: Determination of creep of concrete cylinders in compression. Geneva: International Organization for Standardization.

Johannesson L-E, Sandén T, Dueck A, 2008. Deep repository – engineered barrier system. Wetting and homogenization processes in backfill materials. Laboratory tests for evaluating modeling parameters. SKB R-08-136, Svensk Kärnbränslehantering AB.

Kristiansson A, 2014. Evaluation of a concrete plug – From the Dome Plug Experiment at Äspö HRL. Master thesis. Royal Institute of Technology, Stockholm, Sweden.

Magnusson J, Mathern A, 2015. System design of Dome plug. Experience of low-pH concrete mix B200. Material properties from laboratory tests and full-scale castings. SKB P-14-26, Svensk Kärnbränslehantering AB.

Malm R, 2012. Low-pH concrete plug for sealing the KBS-3V deposition tunnels. SKB R-11-04, Svensk Kärnbränslehantering AB.

Malm R, 2014. Instrumentation and evaluation of the concrete dome plug DOMPLU. TRITA-BKN Report 147, Royal Institute of Technology, Stockholm, Sweden.

Martino J B, Dixon D A, Vignal B, Fujita T, 2006. A full-scale tunnel sealing demonstration using concrete and clay bulkheads exposed to elevated temperatures and pressures. WM'06 Conference, Tucson, Arizona, 26 February – 2 March 2006. Available at: http://www.wmsym.org/archives/2006/pdfs/6089.pdf

Sandén T, Börgesson L, 2010. Early effects of water inflow into a deposition hole. Laboratory tests results. SKB R-10-70, Svensk Kärnbränslehantering AB.

Sandén T, Börgesson L, Dueck A, Goudarzi R, Lönnqvist, 2008. Deep repository –Engineered barrier system. Erosion and sealing processes in tunnel backfill materials investigated in laboratory. SKB R-08-135, Svensk Kärnbränslehantering AB.

Sandén T, Olsson S, Andersson L, Dueck A, Jensen V, Hansen E, Johnsson A, 2014. Investigation of backfill candidate materials. SKB R-13-08, Svensk Kärnbränslehantering AB.

SIS, 2005. SS 137232:2005: Concrete testing – Hardened concrete – Modulus of elasticity in compression. Stockholm: Swedish Standards Institute.

SIS, 2008. SS-EN 1992-1-1:2005: Eurocode 2: Design of concrete structures – Part 1-1: general rules and rules for buidlings. Stockholm: Swedish Standards Institute.

SIS, 2009. SS-EN 12390-3:2009: Testing hardened concrete – Part 3: Compressive strength of test specimens. Stockholm: Swedish Standards Institute.

SKB, 2010a. Design and production of the KBS-3 repository. SKB TR-10-12, Svensk Kärnbränslehantering AB.

SKB, 2010b. Design, production and initial state of the backfill and plug in deposition tunnels. SKB TR-10-16, Svensk Kärnbränslehantering AB.

SKB, 2010c. Design, construction and initial state of the underground openings. SKB TR-10-18, Svensk Kärnbränslehantering AB.

Tazawa E (ed), 1999. Autogenous shrinkage of concrete: proceedings of the international workshop, organised by the JCI (Japan Concrete Institute), Hiroshima, 13–14 June, 1998. New York: Routledge.

Vogt C, Lagerblad B, Wallin K, Baldy F, Jonasson J-E, 2009. Low pH self compacting concrete for deposition tunnel plugs. SKB R-09-07, Svensk Kärnbränslehantering AB.

Cut-outs from design drawings of the Dome plug

M210 – Side view detail of the full-scale experimental set-up DOMPLU

(Text in Swedish.)

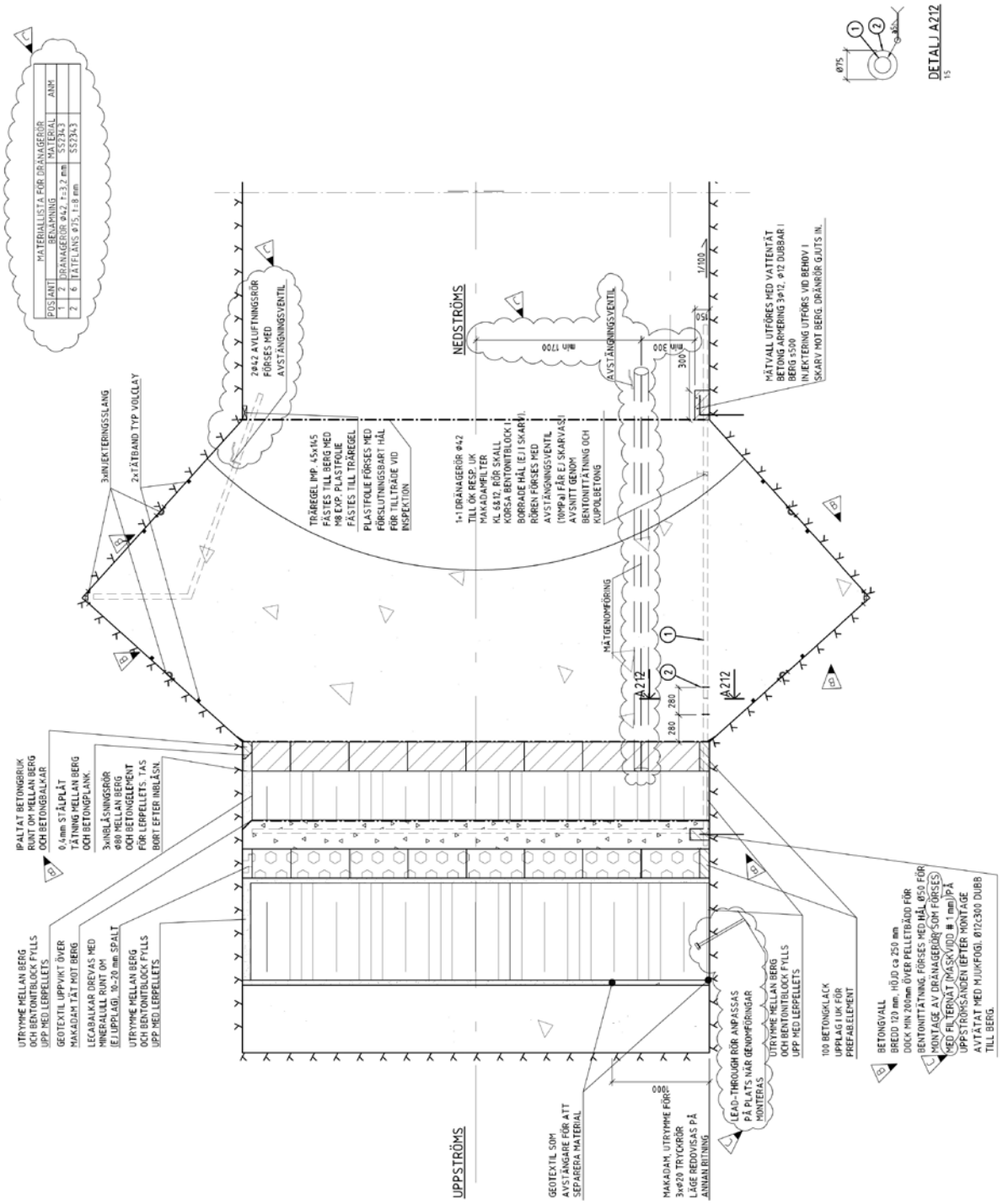

M222 – Concrete dome geometry for rock excavation

(Text in Swedish.)

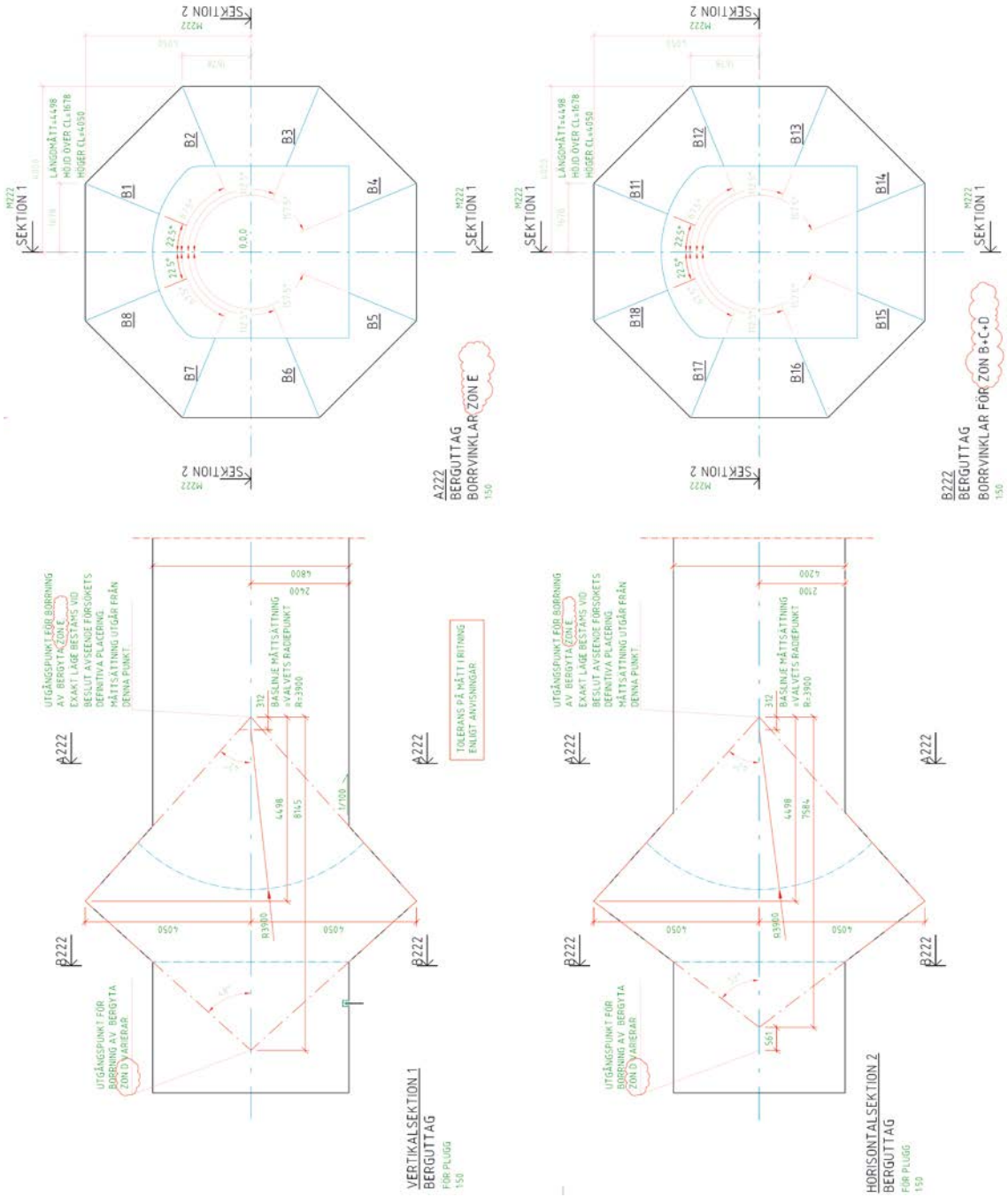

M231 – Concrete dome geometry, vertical and horizontal sections

(Text in Swedish.)

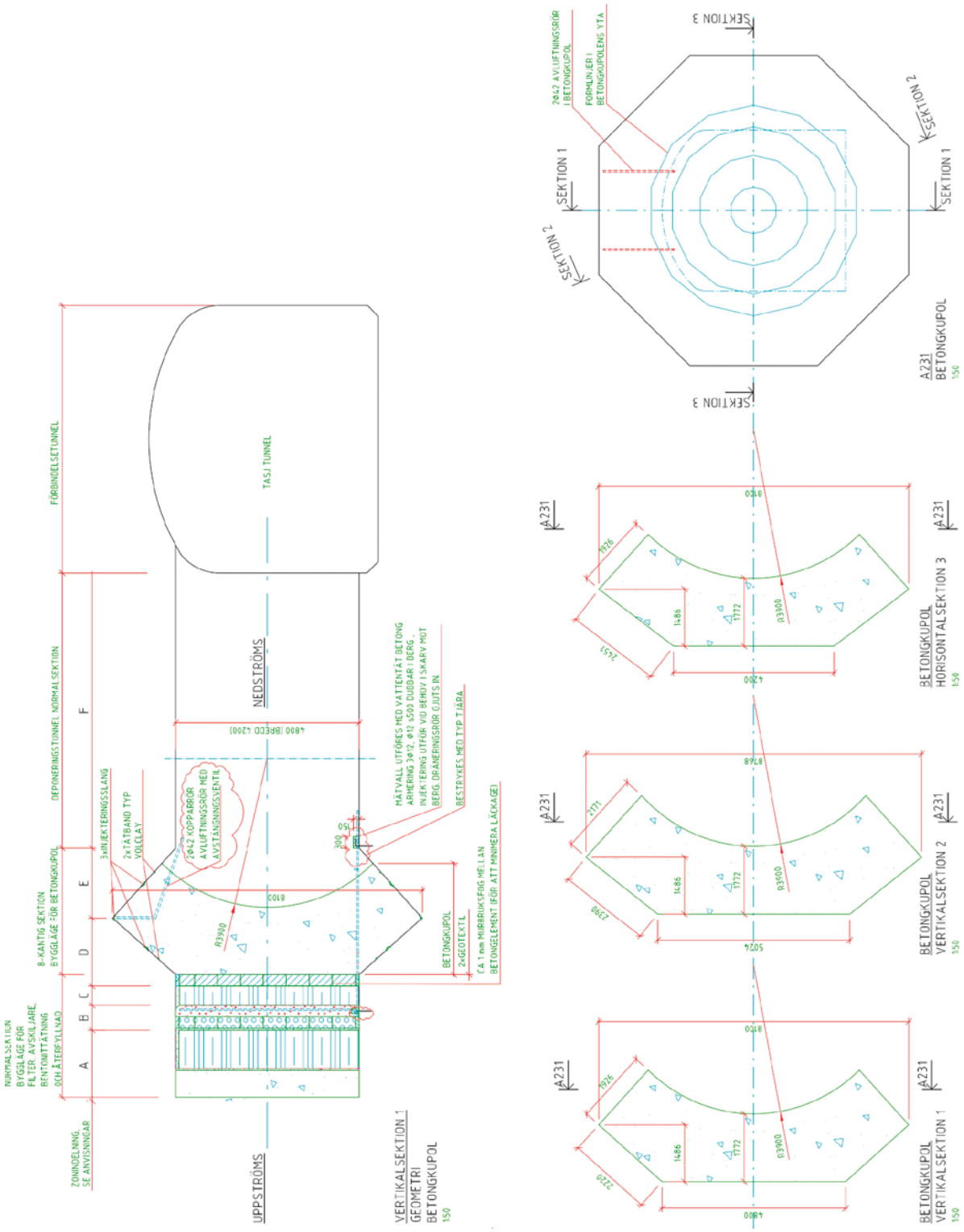

M232 – Concrete dome, injection grout sections

(Text in Swedish.)

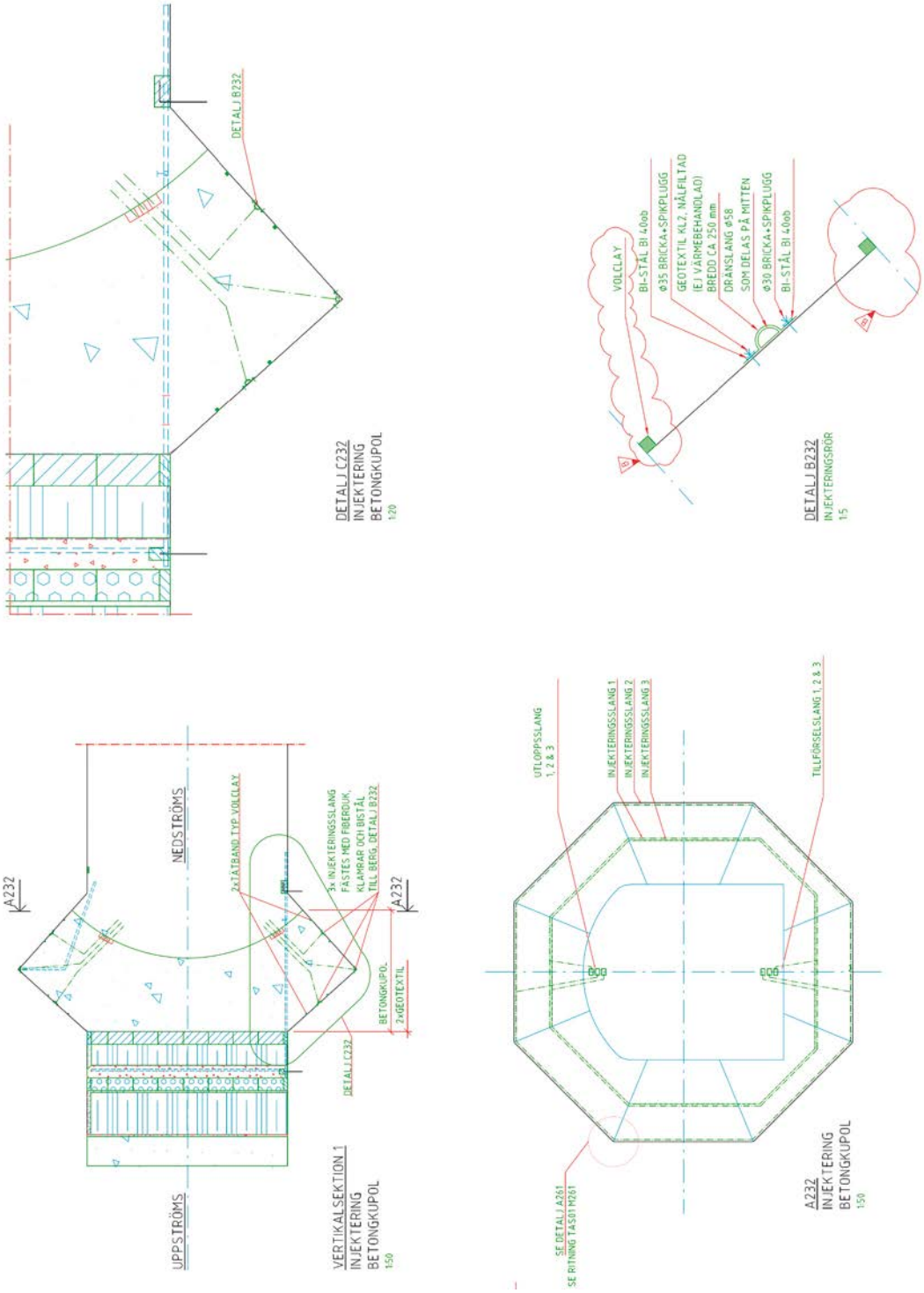

M233 – Concrete dome, cooling system

(Text in Swedish.)

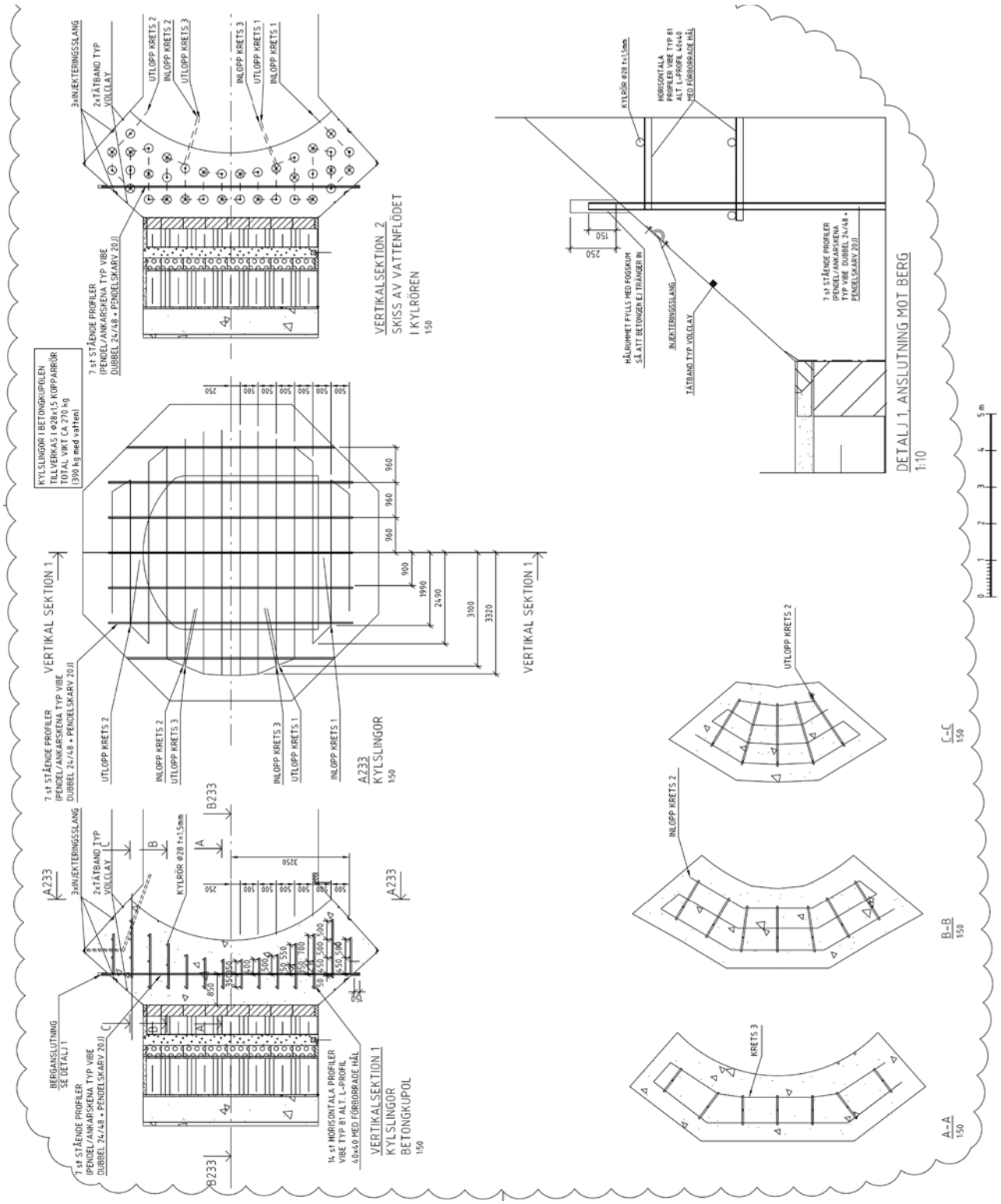

M241 – Concrete delimiter, geometry

(Text in Swedish.)

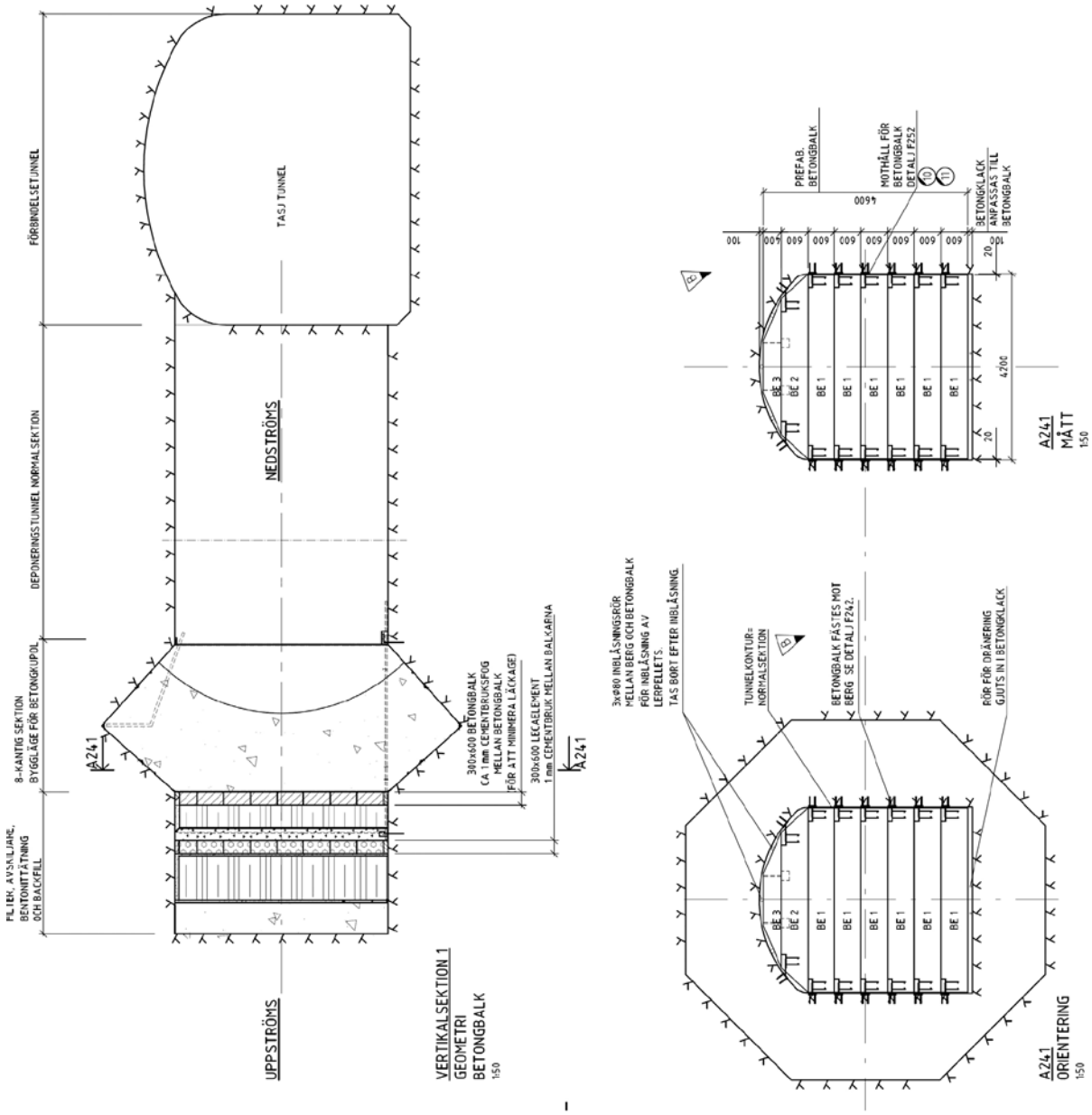

M251 – LECA delimiter (part of the filter), geometry

(Text in Swedish.)

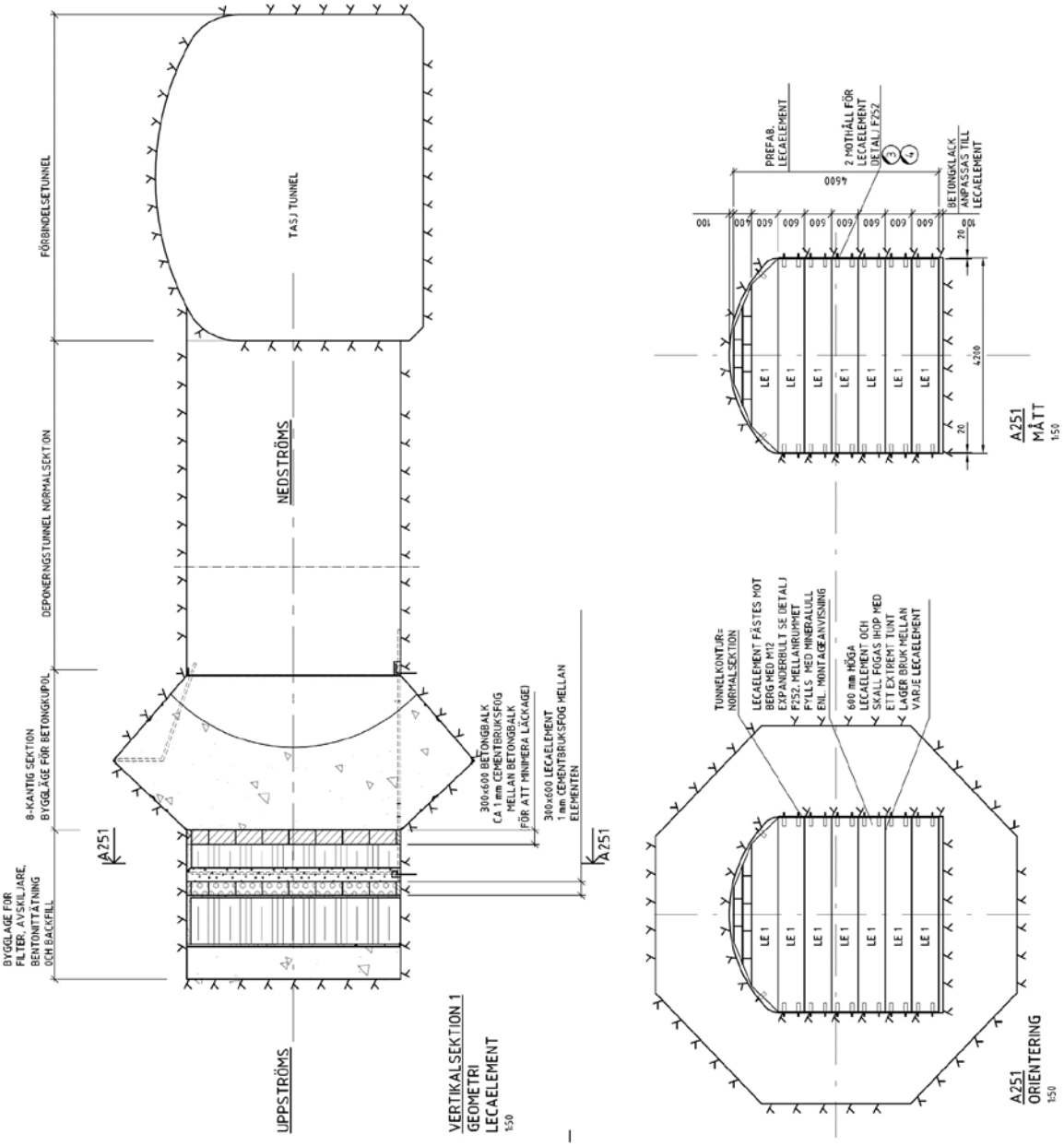

Appendix 2

Concrete material testing

Batch no.	Arrival time	Pump time	At arrival/after 1st/2nd/3rd adjustment/half batch pumped						Comment
			Temperature, °C	Slump flow, mm	t_{500} , sec	Air, %	Density, kg/m^3	Added admixture, liter	
1	08:47	09:15	9,2	570 680	3,3 2,2	8,5	n.a.	 2,0	
2	09:37	10:00	9,1	660	3	6,4	2225		
3	10:44	11:00	9,3	630 660	2,5 2,6	7,8	2210	 1,5	
4	11:20	11:50	9,7	610 540 560 620 720	2,9 4,2 4,8 3,6	6	2240	 1,5 1,5 1,0 0	
5	12:03	12:15	9,7	670	5,7	9	2180		
6	12:43	13:00	9,7	570 700	3,6 2,3	8	2170	 2,0	
7	13:57	14:10	9,1	650 670	4 2,1	6,6	2210	 0	After half the batch was pumped
8	15:11	15:20	9,3	670	3,7	7,2	2190		
9	15:28	15:45	9,5	680	2,2	7,8	2210		
10	16:11	16:20	9,4	690	2,3	5,8	2260		
11	17:02	17:10	9,5	620 680	2,7 2,0	7,2	2180	 1,5	
12	17:51	18:00	8,9	660 700	2,8 2,0	7,8	2190	 0	After half the batch was pumped
13	18:46	19:00	8,9	640 720	2,5 2,1	7,1	2240	 1,0	
14	19:35	n.a.		680	3	5,5	2240		

Appendix 3

Measurements – Bentonite sealing and backfill

The placement of the installed sensors are shown in Figure A3-1 and Figure A3-2 for the bentonite seal and backfill sections respectively.

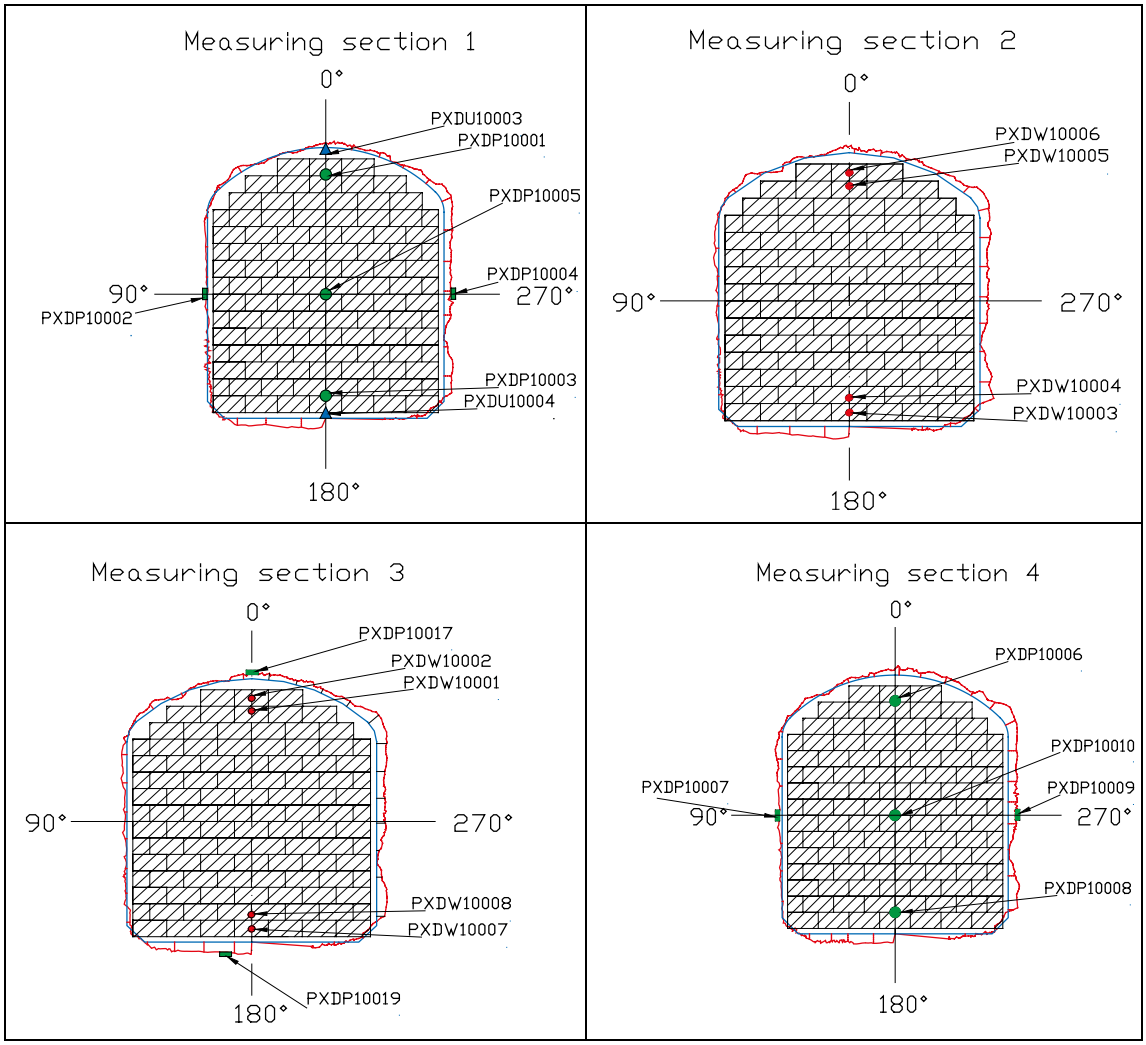

Figure A3-1. *Placement of sensors in the bentonite seal.*

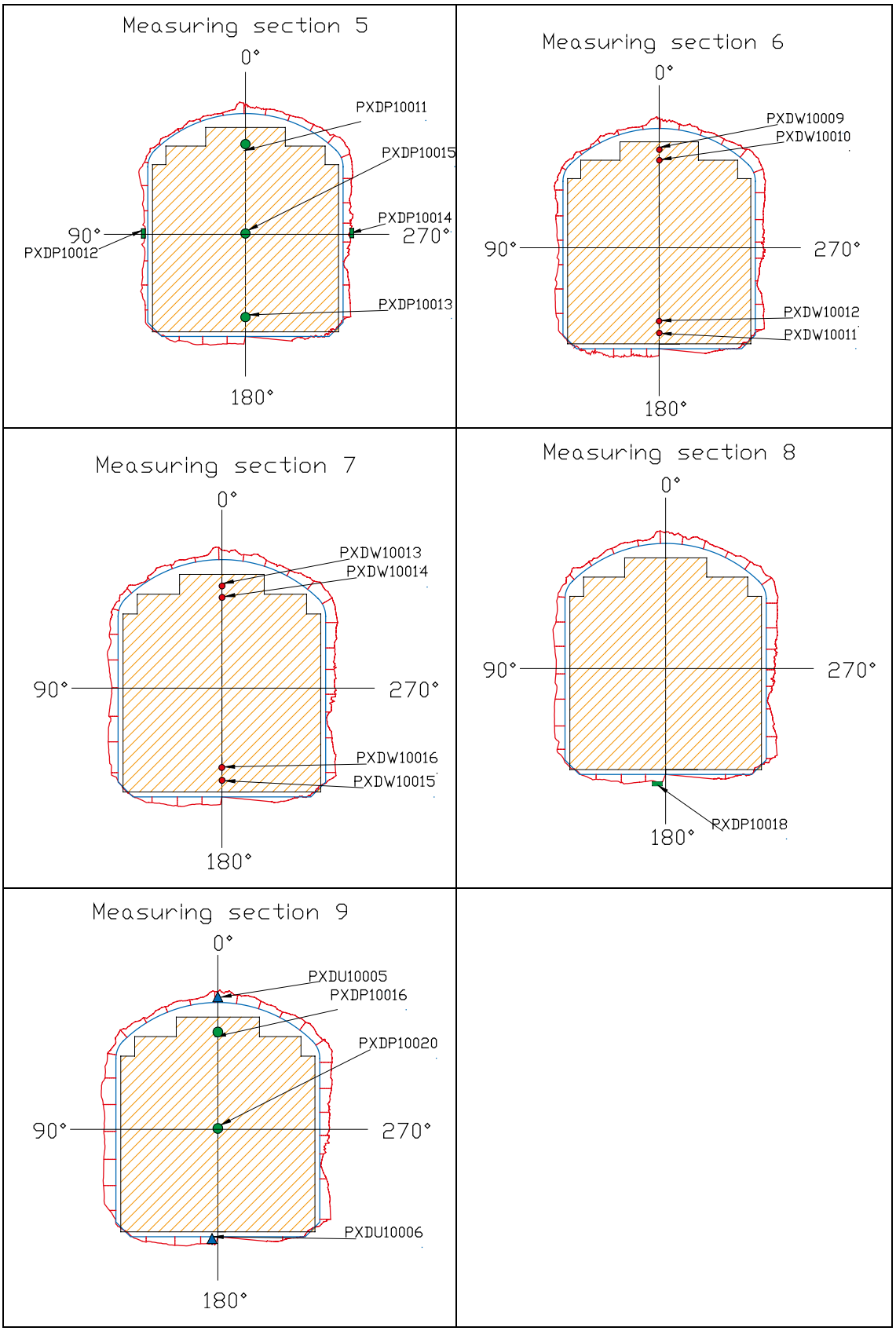

Figure A3-2. *Placement of sensors in the backfill.*

Appendix 4

Numerical simulations

Thermal response

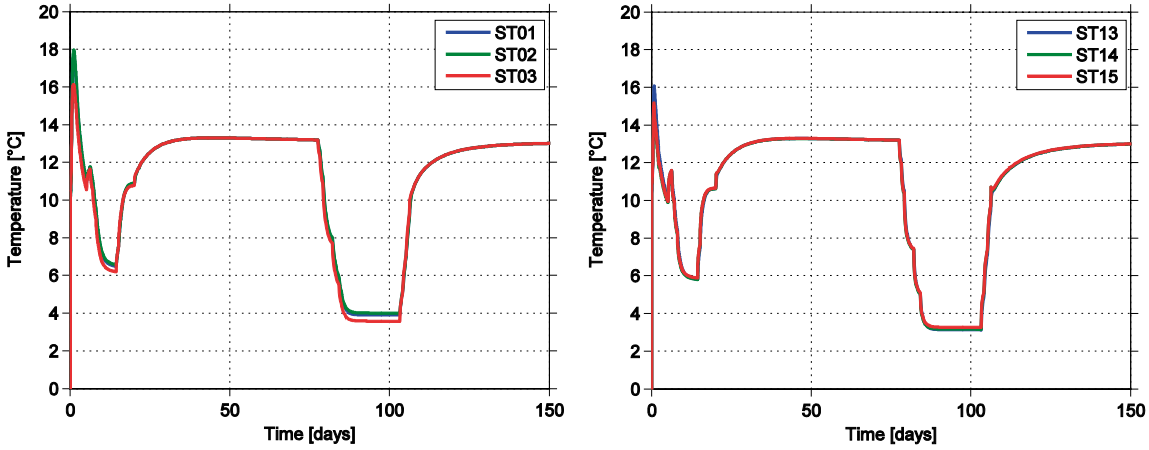

Figure A4-1. *Temperature output from simulations at sensors in section 1.*

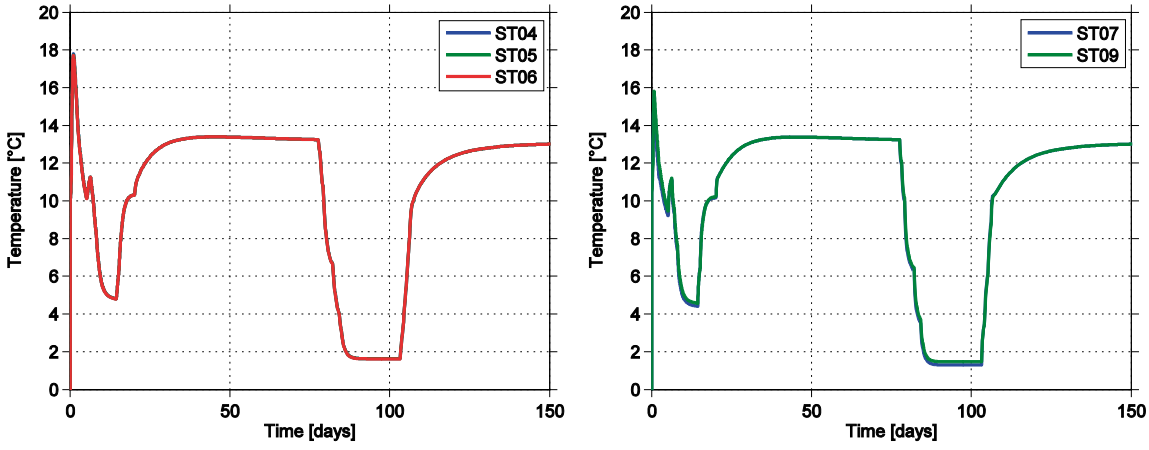

Figure A4-2. *Temperature output from simulations at sensors in section 2 and 3.*

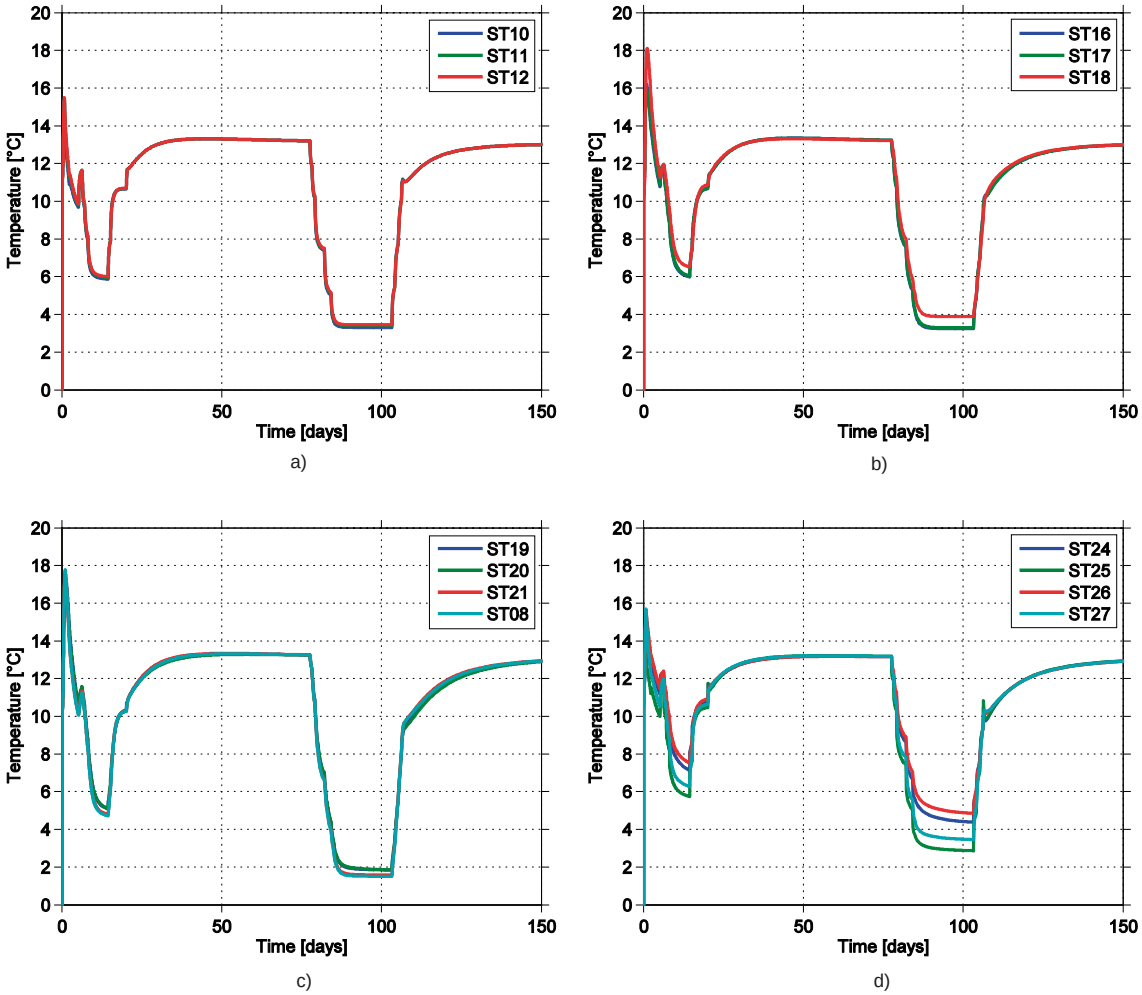

Figure A4-3. *Temperature output from simulations at sensors in section 4 and other sensors.*

Strain gauges – No bond

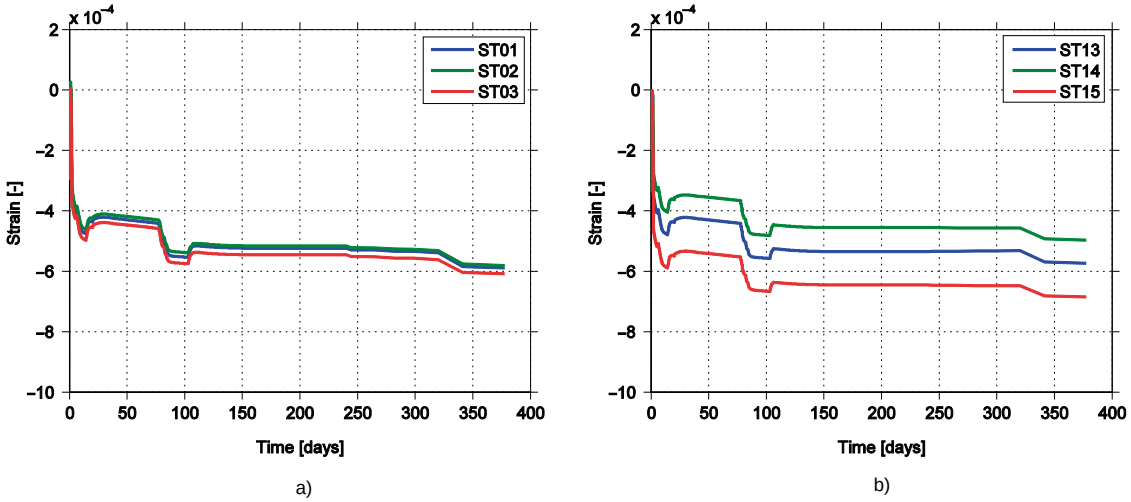

Figure A4-4. *Strain output from simulations with no bond at sensors in section 1 including the pressure step.*

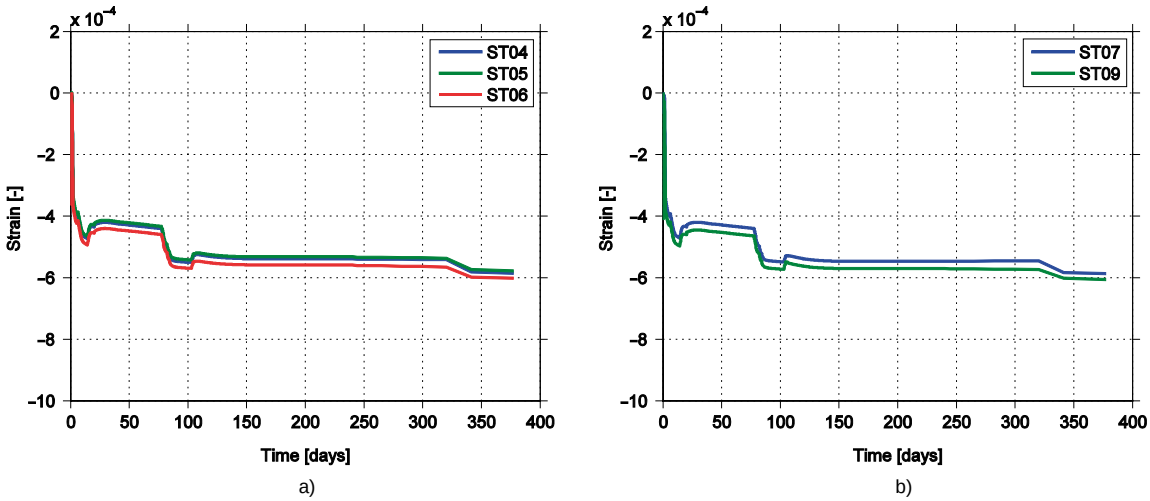

Figure A4-5. *Strain output from simulations with no bond at sensors in section 2 and 3 including the pressure step.*

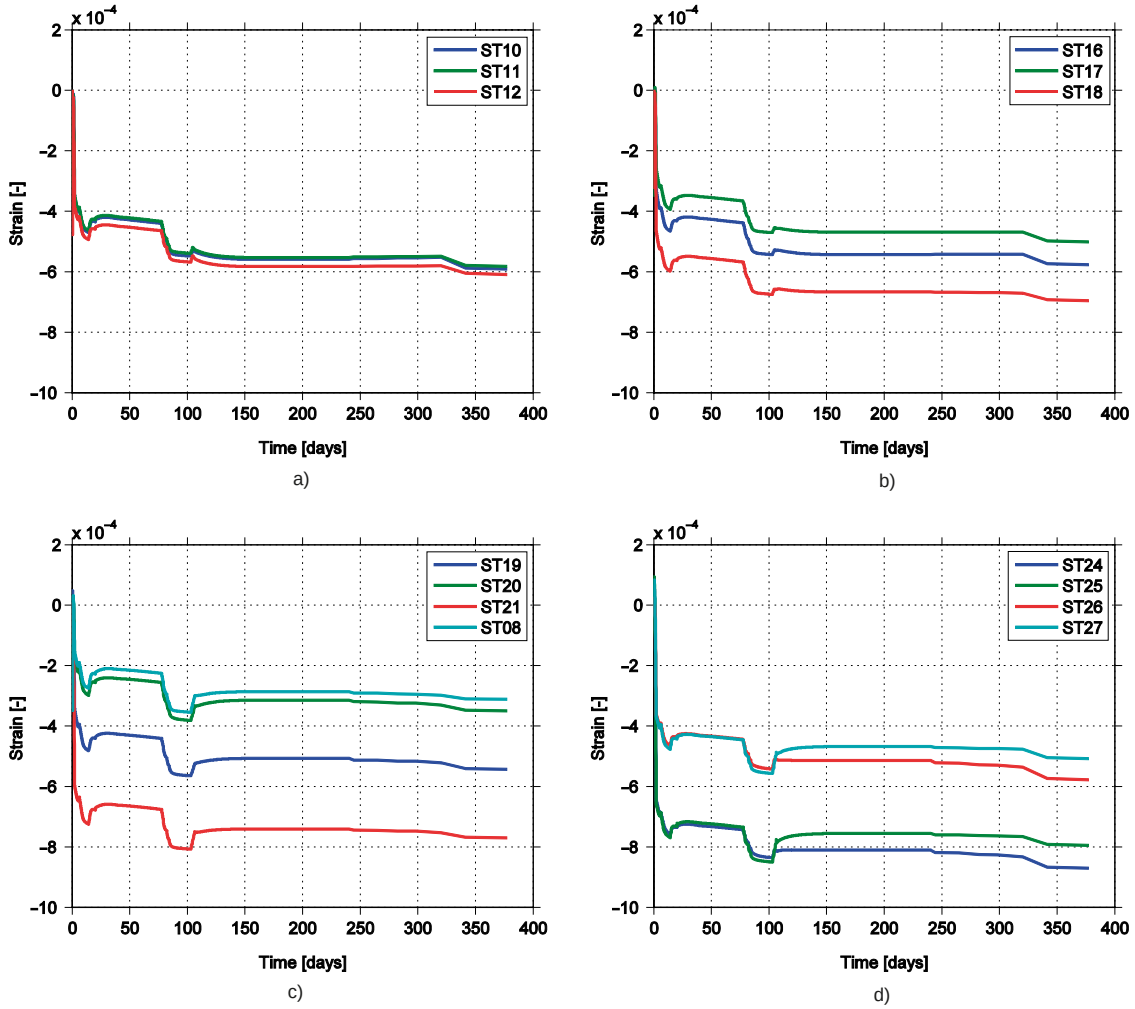

Figure A4-6. *Strain output from simulations with no bond at sensors in section 4 and other sensors including the pressure step.*

Strain gauges – Full bond 1

Model with release of bond for the upstream slot rock surface during the second cooling.

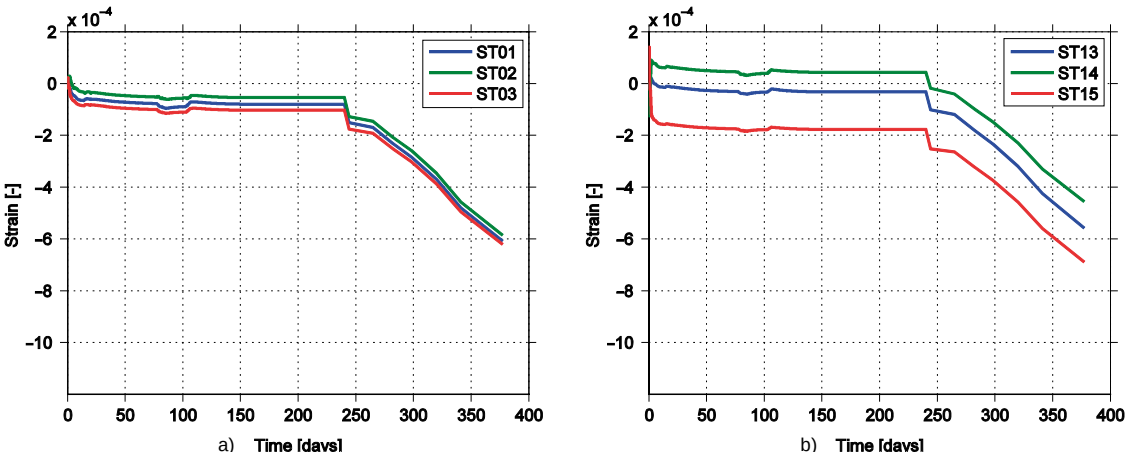

Figure A4-7. *Strain output from simulations of the full bond 1 model at sensors in section 1 including the pressure step.*

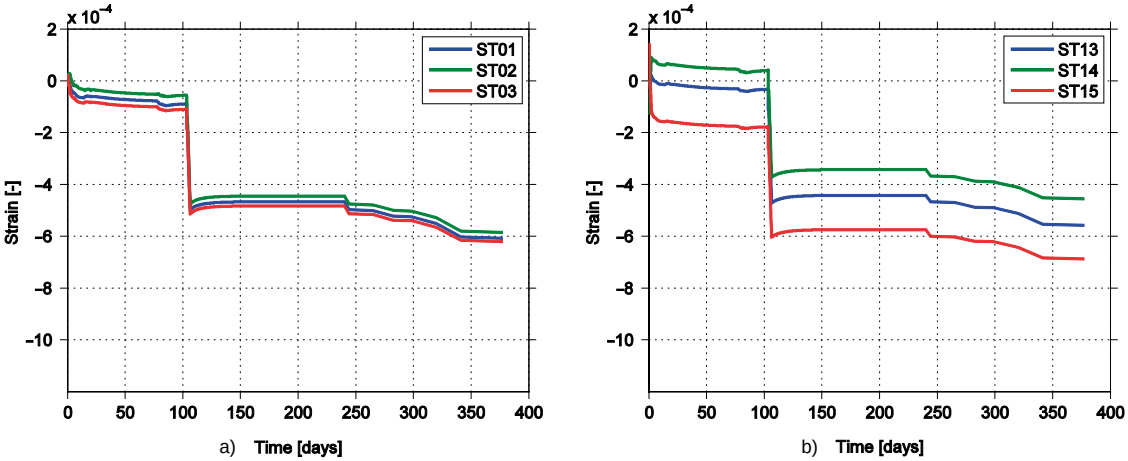

Figure A4-8. *Strain output from simulations of the full bond 1 model at sensors in section 2 and 3 including the pressure step.*

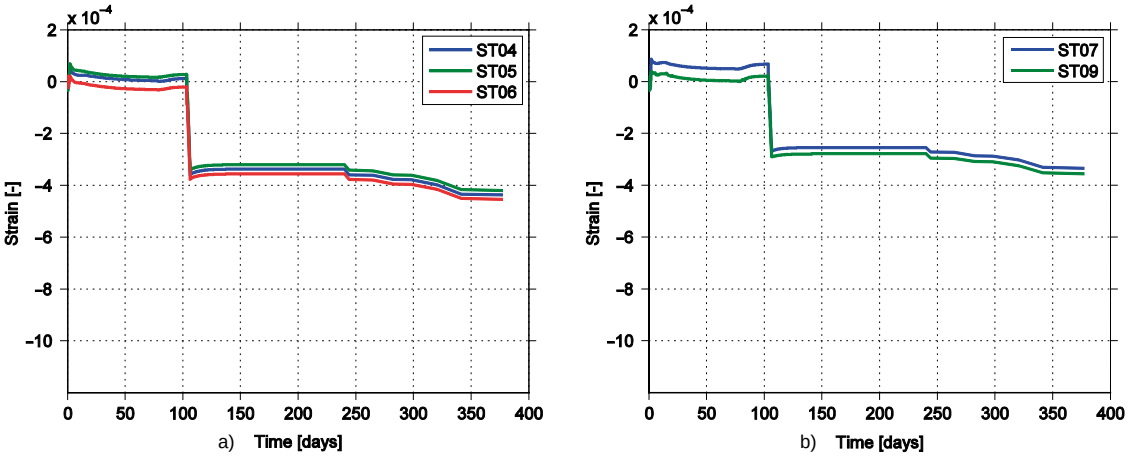

Figure A4-9. *Strain output from simulations of the full bond 1 model at sensors in section 4 and other sensors including the pressure step.*

Strain gauges – Full bond 2

Model with release of bond for the upstream slot rock surface at the pressure load application.

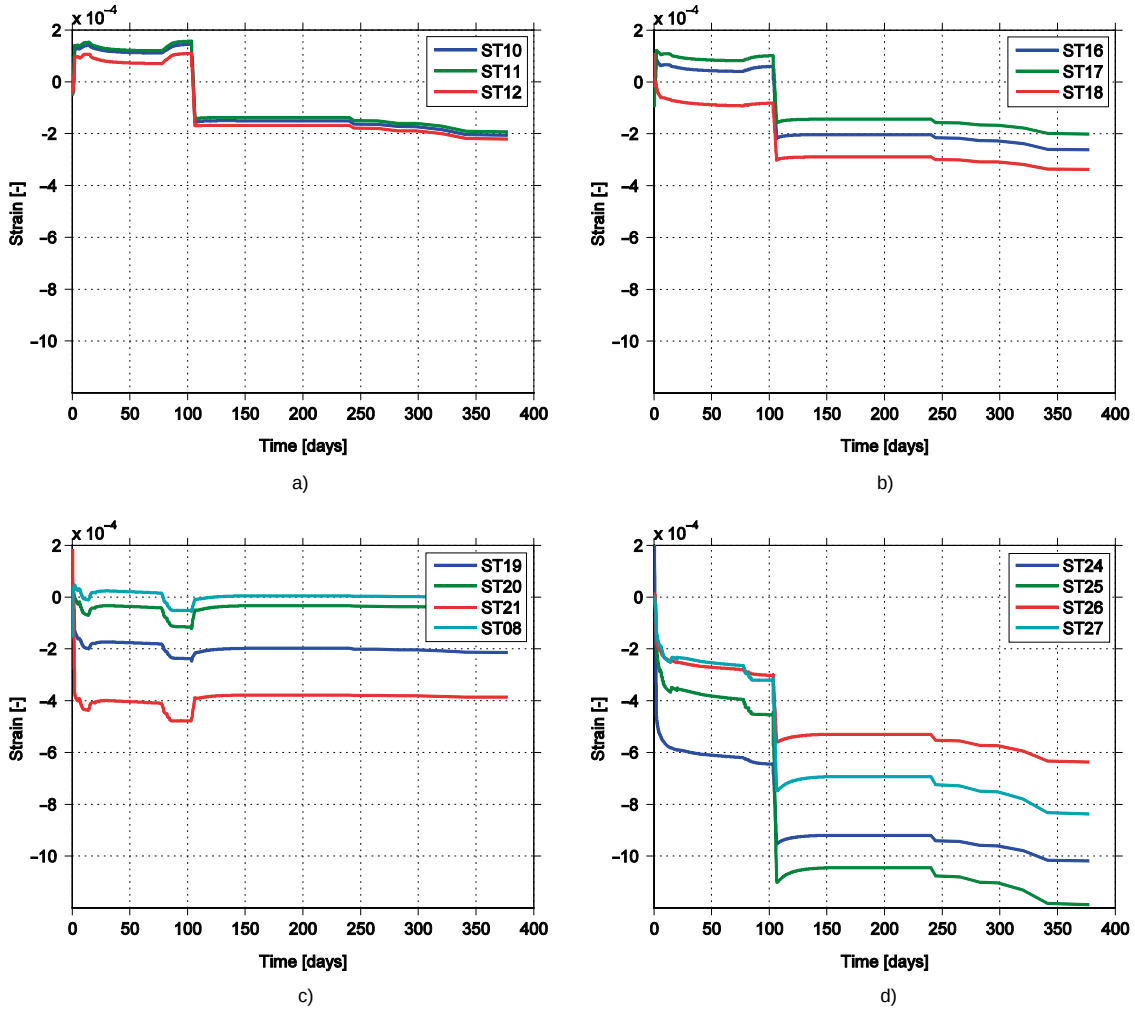

Figure A4-10. *Strain output from simulations of the full bond 2 model at sensors in section 1 including the pressure step.*

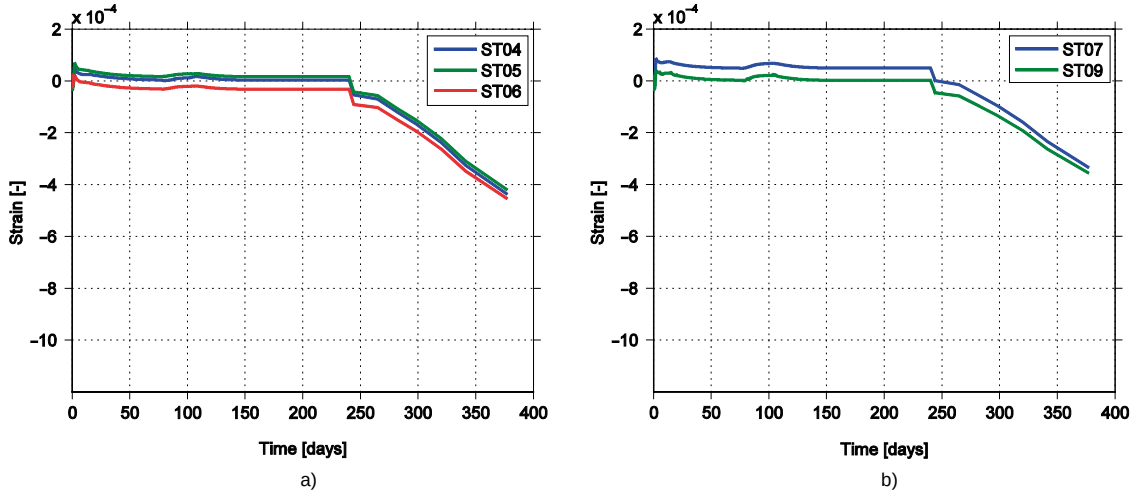

Figure A4-11. *Strain output from simulations of the full bond 2 model at sensors in section 2 and 3 including the pressure step.*

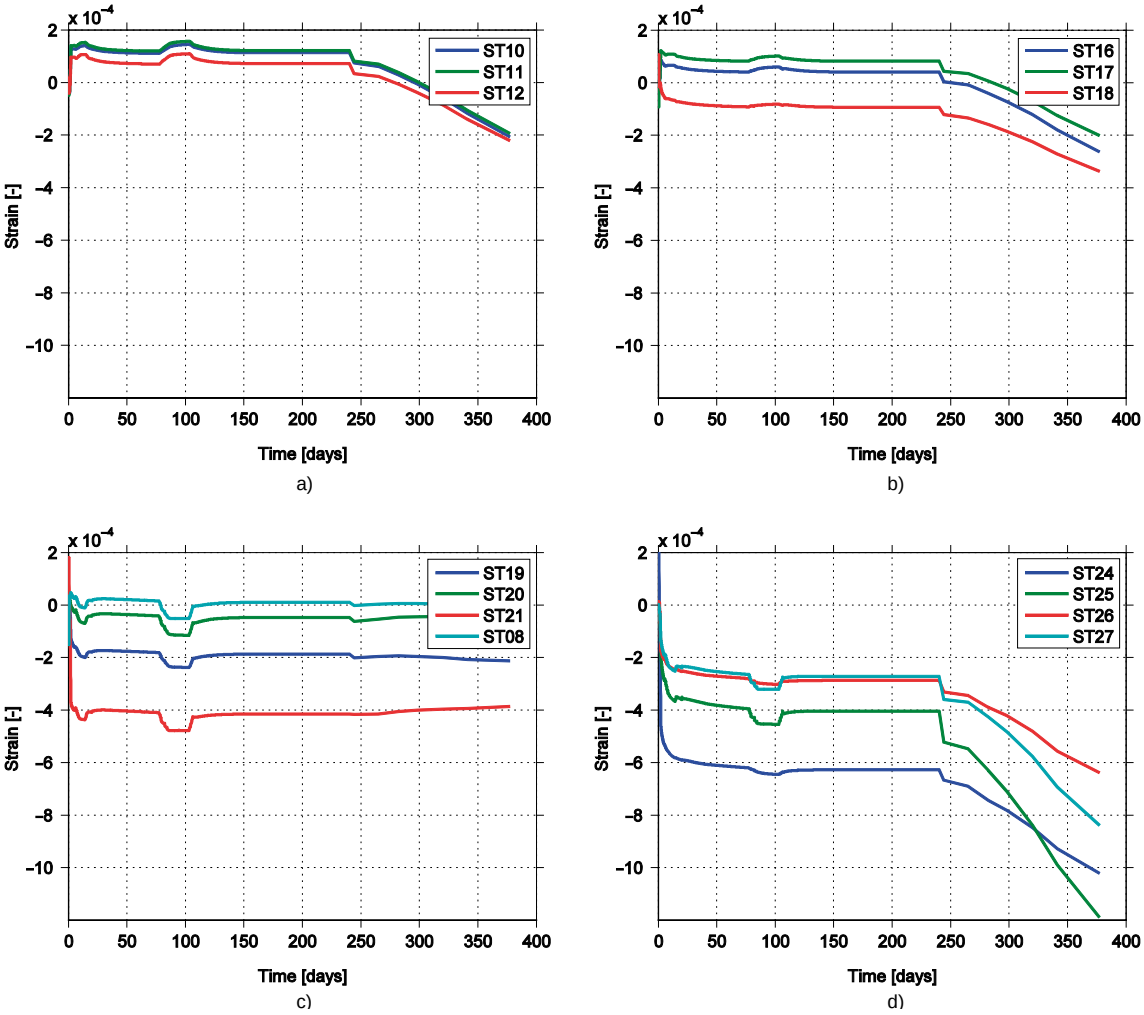

Figure A4-12. *Strain output from simulations of the full bond 2 model at sensors in section 4 and other sensors including the pressure step.*